Oxygen Transfer
in a Fluctuating Capillary Fringe

Dissertation

der Mathematisch-Naturwissenschaftlichen Fakultät

der Eberhard Karls Universität Tübingen

zur Erlangung des Grades eines

Doktors der Naturwissenschaften

(Dr. rer. nat.)

vorgelegt von

Dipl.-Ing. Christina M. Haberer

aus Wolfach

Tübingen

2012

Tag der mündlichen Qualifikation:	27.11.2012
Dekan:	Prof. Dr. Wolfgang Rosenstiel
1. Berichterstatter:	Prof. Dr. Peter Grathwohl
2. Berichterstatter:	Prof. Dr.-Ing. Olaf A. Cirpka

Abstract

Mass transfer processes across and within the capillary fringe affect the transport behavior of volatile compounds and, thus, the natural attenuation of contaminants present in this region. We studied the mass transfer of oxygen in the fluctuating capillary fringe since oxygen is the most relevant electron acceptor for many biogeochemical processes. Cyclic fluctuations in water table elevation are important in the supply of oxygen to oxygen-depleted groundwater and, thus, can significantly affect the groundwater geochemistry, but also the effective hydraulic properties of the porous medium due to gas entrapment. We performed a series of quasi two-dimensional flow-through experiments at the laboratory bench-scale (i) to directly compare oxygen transfer across the capillary fringe with mass transport within the saturated zone at steady state; (ii) to gain an improved understanding of the processes governing oxygen transfer in a fluctuating capillary fringe; (iii) to study the influence of different flow conditions and porous medium properties on oxygen transfer in the capillary fringe following an imbibition event; and (iv) to investigate the effect of a coarse-material inclusion, present in the vicinity of the water table, on flow and oxygen transfer. High-resolution vertical profiles of oxygen concentration were measured at distinct positions along the horizontal groundwater flow direction, applying a non-invasive technique that is based on optode technology. The effectiveness of oxygen transfer under varying experimental conditions was evaluated by additional mass flux measurements in the effluent of the flow-through chamber. Modeling of flow and transport was performed for selected experiments to fully understand the processes involved. Under steady-state conditions, we found that transverse vertical dispersion in the water-saturated part of the capillary fringe is the process limiting oxygen transfer. Gas partitioning between the aqueous and gaseous phases plays a significant role in the medium-term supply of oxygen to oxygen-depleted groundwater following an imbibition event. In case of a fast decreasing water table, the effect of specific yield has to be considered. We also observed that the characteristic of the water table fluctuations determines a specific system's dynamic response and, therefore, the amount of oxygen that is transferred to the aqueous phase. Furthermore, the magnitude of the water table fluctuation and the grain size of the porous medium are particularly relevant for effective oxygen supply from entrapped gas to oxygen-depleted groundwater. In the presence of a coarse-material inclusion, steady-state oxygen flux across the unsaturated/saturated interface may be considerably enhanced. In case of increasing water levels, we hypothesize that the amount of oxygen supplied to the groundwater depends on the spatial distribution, the geometry, and the hydraulic properties of the coarse-material inclusion(s).

Kurzfassung

Stofftransportprozesse über und innerhalb des Kapillarsaums beeinflussen das Transportverhalten flüchtiger Substanzen und somit den natürlichen Schadstoffabbau in dieser Zone. Wir untersuchten den Transport von Sauerstoff im Kapillarsaum, da Sauerstoff für viele biogeochemische Prozesse der wichtigste Elektronakzeptor ist. Periodische Fluktuationen der Wasserspiegelhöhe sind dabei wesentlich für die Zufuhr von Sauerstoff zu sauerstoffarmem Grundwasser und können somit maßgeblich die Grundwassergeochemie, aber auch die effektiven hydraulischen Eigenschaften des porösen Mediums aufgrund von Gaseinschlüssen beeinflussen. Wir führten eine Reihe quasi zwei-dimensionaler Durchflussexperimente im Labormaßstab durch, (i) um den Sauerstofftransport über den Kapillarsaum und innerhalb der gesättigten Zone direkt miteinander zu vergleichen; (ii) um ein verbessertes Verständnis der Prozesse zu erlangen, welche den Transport von Sauerstoff in einem fluktuierenden Kapillarsaum bestimmen; (iii) um den Einfluss unterschiedlicher Strömungsbedingungen und Eigenschaften des porösen Mediums auf den Sauerstofftransport im Kapillarsaum nach Anstieg des Wasserspiegels zu untersuchen; und (iv) um die Auswirkung eines grobkörnigen Einschlusses in der Nähe des fluktuierenden Wasserspiegels auf die Strömung und den Sauerstofftransport im Kapillarsaum zu studieren. Räumlich hochaufgelöste vertikale Sauerstoffprofile wurden durch Anwendung einer nicht-invasiven Methode, basierend auf der Optoden-Technologie, an unterschiedlichen Positionen entlang der horizontalen Grundwasserfließrichtung gemessen. Die Effektivität des Sauerstofftransports unter variierenden Versuchsbedingungen wurde durch zusätzliche Massenflussmessungen am Auslass der Durchflusskammer ermittelt. Strömungs- und Transportmodellierungen wurden für ausgesuchte Experimente durchgeführt, um ein vollständiges Prozessverständnis zu erlangen. Unter stationären Bedingungen beobachteten wir, dass die transversal vertikale Dispersion im wassergesättigten Teil des Kapillarsaums der transportlimitierende Prozess ist. Nach Anhebung des Grundwasserspiegels spielt die Gasverteilung zwischen wässriger und gasförmiger Phase eine bedeutende Rolle für die mittelfristige Sauerstoffzufuhr ins Grundwasser. Im Falle eines schnell abfallenden Wasserspiegels muss der Einfluss des Speicherkoeffizienten mit berücksichtigt werden. Wir beobachteten außerdem, dass die Charakteristik der Wasserspiegelfluktuationen die dynamische Antwort eines spezifischen Systems bestimmt und somit die Sauerstoffmenge, welche in das sauerstoffarme Grundwasser überführt wird. Darüber hinaus sind das Maß der Auslenkung der Wasserspiegelfluktuation sowie die Korngröße des porösen Mediums besonders relevant für die effektive Sauerstoffzufuhr von eingeschlossenem Gas zu sauerstoffungesättigtem Grundwasser. Bei Vorhandensein eines grobkörnigen Einschlusses kann der Sauerstoffmassenfluss über die Grenzfläche zwischen ungesättigter und gesättigter Zone unter stationären Bedingungen deutlich erhöht sein. Im Falle steigender Was-

serstände nehmen wir an, dass die Sauerstoffmenge, die dem Grundwassersystem zugeführt wird, von der räumlichen Verteilung, der Geometrie sowie den hydraulischen Eigenschaften des/r grobkörnigen Einschlusses/-schlüsse abhängt.

Acknowledgements

This dissertation would not have been possible without the guidance and the help of several individuals, who, in one way or another, contributed to the preparation and completion of this work. First of all, I would like to thank my supervisor, Prof. Dr. Peter Grathwohl, for giving me the opportunity to write this thesis, the interesting and revealing discussions we had, and his constant support, ideas, and inspiration. I also would like to express my gratitude to Prof. Dr.-Ing. Olaf A. Cirpka, who introduced me into the field of 'excess air'. I am very grateful for everything I have learned from him and his surprisingly kind and honest character. Special thanks go to Sanheng Liu, who was there during the first months of my Ph.D., answering all my questions regarding transverse dispersion and supporting me throughout the years. He motivated me to follow a small idea, which finally ended up in our first joint paper. Besides, I owe a great deal to Christina Eberhardt. She helped me in conducting the flow-through experiments by giving suggestions and sharing her knowledge with me. For helping hands and a great time, I also want to thank the people working in the hydrogeochemistry lab, especially Thomas Wendel. When it got late working in the lab and the stomach started rumbling, Ilka would spend evenings with me in the lab to have dinner together. Farhana often brightened up my life, e.g., when she called me at 1 a.m. in the lab. Besides, I thank the night watchmen, for keeping an eye on me during the scariest times of my Ph.D. I also want to appreciate the excellent work of Wolfgang Kürner on the experimental setup as well as the numerous support of Manuela Hoch and Willi Kappler in the remorseless fight against Worms and Trojans. Thanks to Uli Maier, Uli Mayer, and Rich Amos, who supported me in my work with MIN3P. Massimo Rolle and I share the memory of an unforgettable trip to San Francisco. He spent hours and days with me in his little office, where we pored over my data with smouldering heads and where we had many fruitful and inspiring discussions. His continuous help and suggestions, when preparing reports and manuscripts, were great. My acknowledgement is also directed to all the colleagues from the DyCap Research group, especially Daniel Jost, for the enjoyable working environment and the constant encouragement to look beyond the rim of my teacup. Also, my time in Tübingen would definitely not have been the same without the people I got to know there and I want to thank them for everything: Ahmed, Anna, Diana, Dietmar, Gabriele, Kinza, Mira, Patricia, Prasesh, Sebastian, Stefan, Stéphane … Manu, Marc, and Martina helped me out from occasional downs, and last, but not the least, I would also like to thank my family and Jens for their patience and steadfast encouragement to complete this work.

The study was funded by the German Research Foundation (DFG), which is, hereby, gratefully acknowledged.

Contents

List of Figures

List of Tables

Notation

The following table shows the significant symbols used in this work. Local notations are explained in the text.

Symbol	Definition	Dimension
Greek Letters:		
α	van Genuchten model: capillary pressure parameter	$[L^{-1}]$
θ_{aq}	volumetric water content	[-]
θ_g	volumetric gas content	[-]
θ_r	residual water content	[-]
θ_s	saturated water content	[-]
λ	Brooks-Corey model: pore size distribution index	[-]
μ_i	chemical potential of compound *i*	$[L^2\ T^{-2}]$
Φ	total porosity	[-]
Φ_{aq}	water-filled porosity	[-]
Φ_g	gas-filled porosity	[-]
Latin Letters:		
A	interfacial area between the unsaturated and the saturated zone	$[L^2]$
$cum_{O2\text{-}mass}$	cumulative oxygen mass supplied across the unsaturated/saturated interface	[M]
C	concentration of the diffusing compound	$[M\ L^{-3}]$
C_0	aqueous concentration at the source, unsaturated/saturated interface	$[M\ L^{-3}]$
C_{bg}	aqueous concentration of the background	$[M\ L^{-3}]$
C_{norm}	normalized equivalent aqueous concentration	[-]
CF	capillary fringe	[-]
d	average grain diameter	[L]
D_{aq}	diffusion coefficient in the free aqueous phase	$[L^2\ T^{-1}]$
$\mathbf{D}_{aq}$	diffusion tensor in the free aqueous phase	$[L^2\ T^{-1}]$
D_g	diffusion coefficient in the free gaseous phase	$[L^2\ T^{-1}]$
D_{mech}	mechanical dispersion coefficient	$[L^2\ T^{-1}]$
$\mathbf{D}_{mech}$	mechanical dispersion tensor	$[L^2\ T^{-1}]$
D_p	pore diffusion coefficient	$[L^2\ T^{-1}]$
D_t	transverse hydrodynamic dispersion coefficient	$[L^2\ T^{-1}]$
$\mathbf{D}_{tot}$	total effective dispersion tensor	$[L^2\ T^{-1}]$
EM_{O2}	excess mass of oxygen	[M]
F	mass flux density across the unsaturated/saturated interface	$[M\ L^{-2}\ T^{-1}]$
h	matric head/hydraulic head	[L]
h_b	Brooks-Corey model: air-entry pressure head or bubbling pressure head	[L]
h_c	capillary pressure head	[L]
h_{CF}	height of the capillary fringe's upper limit	[L]
H	height of the flow-through chamber	[L]

ΔH_{CF}	difference in the height of the capillary fringe's upper limit	[L]
ΔH_{WT}	difference in pressure head	[L]
k_r	relative permeability	[-]
k^{sat}	permeability at full saturation	[L^2]
K	saturated hydraulic conductivity	[L T^{-1}]
K_H	compound-specific Henry's law coefficient	[-]
L	length of the flow-through chamber	[L]
m	van Genuchten model: shape parameter	[-]
$\dot{m}$	total mass flux across the unsaturated/saturated interface	[M T^{-1}]
$\dot{m}_{out}$	total mass flux in the effluent of the flow-through chamber	[M T^{-1}]
n	van Genuchten model: shape parameter	[-]
$NRMSE$	normalized root mean squared error	[-]
p	total pressure	[M L^{-1} T^{-2}]
p_i	partial pressure	[M L^{-1} T^{-2}]
Pe	Péclet number	[-]
PV	pore volume	[-]
q	specific discharge	[L T^{-1}]
$\mathbf{q}$	specific-discharge vector	[L T^{-1}]
Q_{in}	average flow-rate used in horizontal direction	[L^3 T^{-1}]
R	retardation factor	[-]
S_e	effective water saturation	[-]
S_g	gas saturation	[-]
t	time	[T]
Δt	time taken to fluctuate the water table	[T]
T	temperature	[t]
v_a	horizontal seepage velocity	[L T^{-1}]
W	gap width of the flow-through chamber	[L]
WT	water table	[-]
x	horizontal coordinate, in average groundwater flow direction	[L]
y	horizontal coordinate, transverse to the groundwater flow direction	[L]
z	vertical coordinate	[L]
Z	source-width	[L]

Subscripts:

BC	Brooks and Corey model	[-]
vG	van Genuchten model	[-]

Additional Symbols Used:

∇	Nabla operator, $\left(\frac{\partial}{\partial x}, \frac{\partial}{\partial y}, \frac{\partial}{\partial z}\right)$	[L^{-1}]
$\Re$	ideal gas constant, 8.314 J mol^{-1} K^{-1}	[L^2 t^{-1} T^{-2}]

1. Introduction

1.1 Motivation

Mass transfer of a contaminant plume usually takes place by diffusion, advection, and dispersion, where under stationary conditions transverse dispersion is seen as the main process that mixes dissolved terminal electron acceptors (TEAs), such as oxygen, across the plume's fringes (Thornton et al., 2001; Schürmann et al., 2003; Rahman et al., 2005; Cirpka et al., 2006). Mixing plays a role when assessing degradation rates as well as plume lengths (e.g., Olsson, 2005; Liedl et al., 2005; Maier and Grathwohl, 2006; Bauer et al., 2008). In experiments performed at the laboratory bench-scale (Klenk and Grathwohl, 2002; Liu, 2008), transverse vertical dispersion was also found to be essential with regard to mass transfer of volatile compounds across the capillary fringe. Since, owing to their physico-chemical properties, many contaminant (LNAPL) plumes are located near the water table and in the capillary fringe region, the role of existing gas pockets (e.g., as result of a fluctuating water table) to hydrodynamic dispersion is of interest to many researchers (Orlob and Radhakrishna, 1958; Maraqa et al., 1997; Nützmann, et al., 2002; Vanderborght and Vereecken, 2007; Mayer et al., 2008). The presence of a gaseous phase may lead to a change in mixing behavior, which, thus, also impacts natural attenuation of a contaminant plume.

Transfer of volatile organic contaminants (VOC) and soil gases (e.g., O_2, CO_2) across the unsaturated/saturated interface is an important mechanism for a variety of natural subsurface processes and engineered applications, including groundwater contamination, natural attenuation, waste management, and in situ remediation. Mass transfer, hereby, depends on the morphology of the transition zone (Caron et al., 1998; Maier et al., 2007) and the dynamics of the groundwater table (Lappala and Thompson, 1983; Russo et al., 1989; Hinz, 1998). In addition to natural factors like infiltration of rain water and evaporation, fluctuations in the height of the water table may arise from human activities, such as extensive groundwater pumping for irrigation, process water supply for industry, and preparation of potable water from groundwater resources. Because of the water table's dynamic nature, air may be entrapped in the transition region between the unsaturated and the saturated zone. As a consequence, volatile compounds partition across the gas/water interfaces until steady state is reached.

In 1-D column experiments, Werner and Höhener (2002) studied the mass transfer of volatile contaminants (CFC-113, CFC-114, CFC-21, and cis-dichloroethene) from the saturated into the unsaturated zone. The authors observed that the contaminant concentrations in the gaseous phase decreased above a stagnant or rising water table, whereas a lowering of the phreatic surface resulted in a significant increase in the measured gas concentrations. These results also agree to those derived by McCarthy and Johnson (1993), who performed experiments on an

aquifer model with underlying horizontal groundwater flow. Furthermore, by conducting a laboratory experiment in a flow-cell, Williams and Oostrom (2000) found that water table fluctuations increased the oxygen transfer from the unsaturated zone to anoxic groundwater.

The supply of oxygen possibly enhances all biogeochemical processes within the upper, quasi-saturated zone for which oxygen is the rate-limiting factor (Holocher et al., 2003). In fact, it is widely hypothesized that the capillary fringe, combined with the region immediately below the water table, is a highly active zone in terms of physico-chemical processes and microbiology (Dunn and Silliman, 2003; Berkowitz et al., 2004; Maier and Grathwohl, 2005; Barth et al., 2005). The coexistence of aqueous and gaseous phases in the capillary fringe has important consequences to microbial processes since both too much water and too little water will depress microbial processes (Chapelle, 2001; Jost et al., 2010, 2011). Sequential anoxic/oxic conditions may favor complete microbial degradation of various organic contaminants (Zitomer and Speece, 1993; Chapelle, 2001; Umweltbundesamt, 2004) and a possible scenario is illustrated in Fig. 1.1.

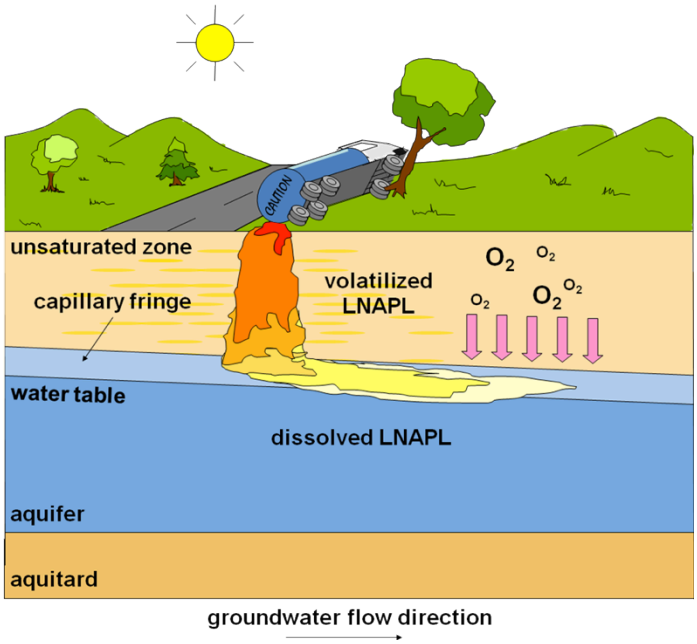

Fig. 1.1. The efficiency with which organic contaminants are completely degraded depends on the redox conditions present in an aquifer and on the succession of redox processes that the contaminants are exposed to along particular groundwater flow paths.

1.2 Identification of Open Questions

Although the capillary fringe may significantly affect the evolution of fluid flow and the solute transport from the vadose zone to the saturated zone below the water table, the capillary fringe is virtually ignored in a number of textbooks on groundwater hydrology (Silliman et al., 2002; Berkowitz et al., 2004). Most of the present knowledge about the behavior of the capillary fringe is based on experiments conducted under steady-state flow conditions, and much less literature is available on the dynamic behavior of capillary fringes at fluctuating groundwater levels. In fact, the dynamic interplay of flow and mass transfer mechanisms across and within the capillary fringe is

not well understood. In case of a fluctuating groundwater table, this transition zone is characterized by changes in water content, pore water velocity, and hydraulic conductivity according to saturation. These variations modify the water, solute, and gas transfer from the soil surface to the aquifer (Russo et al., 1989), but also transfer of volatile compounds from the aquifer to the soil gas. Besides, the redox conditions and, as a consequence, microbial activities or specific microbial dynamics may change (Anneser, 2008).

In context of the previous argumentation, the presented work aims to address the following questions regarding the mass transfer of oxygen in a fluctuating capillary fringe:

- Is oxygen transfer across the capillary fringe different from mass transport in the saturated zone under steady-state conditions? Answering this question gives the basis for understanding more complicated systems.
- What is the effect of different water table dynamics on oxygen transfer across the capillary fringe? We expect that gas partitioning, due to gas entrapment at rising water tables, plays an important role for the supply of oxygen to oxygen-depleted groundwater.
- How does a change in flow conditions or porous medium properties affect mass transfer within the transition region between the unsaturated and the saturated zone? In particular, we are interested in the amount of oxygen transferred from entrapped air to oxygen-depleted groundwater following an imbibition event.
- How does the presence of a coarse-material inclusion affect oxygen transfer in the capillary fringe region? The presence of physical heterogeneities near the water table should lead to significant amounts of entrapped gas (e.g., Dunn and Silliman, 2003) and, thus, increase oxygen supply to oxygen-depleted groundwater.

1.3 Objectives and Structure of the Thesis

To address the identified open questions, a detailed investigation is carried out with the aim of improving the understanding of oxygen transfer across the capillary fringe under transient conditions. Oxygen was chosen as the compound of interest since it plays an important role for microbial processes in groundwater, either by influencing the redox conditions present in the aquifer or by replenishing electron acceptors needed for microbial growth and respiration.

The objectives are:

- Quantification of diffusive and dispersive oxygen transfer across the unsaturated/-saturated interface.

- Investigation of oxygen transfer within the capillary fringe following an imbibition event as a function of the grain diameter, the horizontal flow velocity of the groundwater, and the magnitude and the speed of the water table fluctuation.
- Identification of the relevant mass transfer processes and quantification of the controlling parameters.

Within this dissertation, the following studies were carried out:

- Chapter 2 consists of a literature review to give the background to this study.
- In Chapter 3, a high-resolution non-invasive approach to quantify oxygen transfer across the capillary fringe and within the underlying groundwater is described. By evaluating measured steady-state vertical oxygen concentration profiles, the value of transverse hydrodynamic dispersion is determined to investigate the effectiveness of oxygen transfer under various experimental conditions.
- The hydraulic and mass transfer processes, relevant for the supply of oxygen to oxygen-depleted groundwater in case of a fluctuating water table, are identified in Chapter 4. We further discuss the importance of these processes in case of varying water table dynamics.
- With regard to the previous discussion, Chapter 5 focuses on the dependence of oxygen transfer within the capillary fringe on different flow conditions (horizontal groundwater flow velocity, magnitude and speed of the water table fluctuation) and porous medium properties (grain diameter). In doing so, an experimental sensitivity analysis is performed by conducting a number of imbibition experiments and changing one parameter of interest at a time.
- In Chapter 6, the impact of physical heterogeneities on flow and oxygen transfer in the capillary fringe is discussed. At steady state, we expect an increase in transverse vertical dispersion compared to the respective homogeneous case (e.g., Rolle et al., 2009). This may also imply an indirect effect of the heterogeneity on mixing-limited chemical reactions (Dentz et al., 2011). In case of a fluctuating water table, air entry barriers form, which may lead to significant amounts of entrapped gas, thus, resulting in increased values of overall oxygen flux (Dunn and Silliman, 2003).
- A synopsis of the work, the drawn conclusions, and some closing remarks are given in Chapter 7.

References

Anneser, B., 2008. Spatial and temporal dynamics of biogeochemical gradients in a tar oil-contaminated porous aquifer – biodegradation processes revealed by high-resolution measurements. Doctoral Thesis, Institute for Geoscience, University of Tübingen.

Barth, J.A.C., Kappler, A., Piepenbrink, M., Werth, C.J., Regenspurg, S., Semprini, L., Slater, G.F., Schüth, C. and Grathwohl, P., 2005. New challenges in biogeochemical gradient research. EOS, 86: 44 1 November 2005.

Bauer, R.D., Maloszewski, P., Zhang, Y., Meckenstock, R.U. and Griebler, C., 2008. Mixing-controlled biodegradation in a toluene plume – Results from two-dimensional laboratory experiments. Journal of Contaminant Hydrology, 96: 150-168.

Berkowitz, B., Silliman, S.E. and Dunn, A.M., 2004. Impact of the capillary fringe on local flow, chemical migration, and microbiology. Vadose Zone Journal, 3: 534-548.

Caron, F., Manni, G. and Workman, W.J.G., 1998. A large-scale laboratory experiment to determine the mass transfer of CO_2 from a sandy soil to moving groundwater. Journal of Geochemical Exploration, 64: 111-125.

Chapelle, F.H., 2001. Ground-water microbiology and geochemistry, 2nd ed., New York: John Wiley & Sons.

Cirpka, O.A., Olsson, Å., Ju, Q., Rahman, M.A. and Grathwohl, P., 2006. Determination of transverse dispersion coefficients from reactive plume lengths. Ground Water, 44: 212-221.

Dentz, M., Le Borgne, T., Englert, A. and Bijeljic, B., 2011. Mixing, spreading and reaction in heterogeneous media: A brief review. Journal of Contaminant Hydrology, 120-121: 1-17, doi: 10.1016/j.jconhyd.2010.05.002.

Dunn, A.M. and Silliman, S.E., 2003. Air and water entrapment in the vicinity of the water table. Ground Water, 41(6): 729-734.

Hinz, C., 1998. Analysis of unsaturated/saturated water flow near a fluctuating water table. Journal of Contaminant Hydrology, 33: 59-80.

Holocher, J., Peeters, F., Aeschbach-Hertig, W., Kinzelbach, W. and Kipfer, R., 2003. Kinetic model of gas bubble dissolution in groundwater and its implications for the dissolved gas composition. Environmental Science and Technology, 37: 1337-1343.

Jost, D., Winter, J. and Gallert, C., 2010. Distribution of motile and non-motile bacteria within the capillary fringe of silica sand. Water Research, 44: 1279-1287.

Jost, D., Winter, J. and Gallert, C., 2011. Water and oxygen dependence of *Pseudomonas putida* growing in silica sand capillary fringes. Vadose Zone Journal, 10: 1-9, doi: 10.2136/vzj2010.0092.

Klenk, I.D. and Grathwohl, P., 2002. Transverse vertical dispersion in groundwater and the capillary fringe. Journal of Contaminant Hydrology, 58: 111-128.

Lappala, E.G. and Thompson, G.M., 1983. Detection of groundwater contamination by shallow soil gas sampling in the vadose zone. *In* Proc. NWWA/EPA Conference in Characterisation and Monitoring of the Vadose (Unsaturated) Zone, Las Vegas, Nevada, pp. 659-679.

Liedl, R., Valocchi, A.J., Dietrich, P. and Grathwohl, P., 2005. Finiteness of steady-state plumes. Water Resources Research, 41, W12501, doi: 10.1029/2005WR004000.

Liu, S., 2008. Mass transfer of oxygen across the capillary fringe. Doctoral Thesis, Institute for Geoscience, University of Tübingen, 58 p.

Maier, U. and Grathwohl, P., 2005. Natural attenuation in the unsaturated zone and shallow groundwater: Coupled modeling of vapor phase diffusion, biogeochemical processes and transport across the capillary fringe. *In* Nützmann, G., Viotti, P. and Aagard, P. (Eds.) Reactive transport in soil and groundwater. Springer, pp. 141-155.

Maier, U. and Grathwohl, P., 2006. Numerical experiments and field results on the size of steady state plumes. Journal of Contaminant Hydrology, 85: 33-52.

Maier, U., Rügner, H. and Grathwohl, P., 2007. Gradients controlling natural attenuation of ammonium. Applied Geochemistry, 22: 2606-2617.

Maraqa, M.A., Wallace, R.B. and Voice, T.C., 1997. Effects of degree of water saturation on dispersivity and immobile water in sandy soil columns. Journal of Contaminant Hydrology, 25: 199-218.

Mayer, A., Sandman, T. and Breidenbach, M., 2008. Effect of flow regime on physical nonequilibrium transport in unsaturated porous media. Vadose Zone Journal, 7(3): 981-991.

McCarthy, K.A. and Johnson, R.L., 1993. Transport of volatile organic compounds across the capillary fringe. Water Resources Research, 29: 1675-1683.

Nützmann, G., Maciejewski, S. and Joswig, K., 2002. Estimation of water saturation dependence of dispersion in unsaturated porous media: experiments and modeling analysis. Advances in Water Resources, 25(5): 565-576.

Olsson, Å., 2005. Investigation and modelling of dispersion-reaction processes in natural attenuation groundwater. Doctoral Thesis, Institute for Geoscience, University of Tübingen. Tübinger Geowissenschaftliche Arbeiten (TGA) C91, 68 p.

Orlob, G.T. and Radhakrishna, G.N., 1958. The effect of entrapped gases on the hydraulic characteristics of porous media. Transactions, American Geophysical Union, 39: 648-659.

Rahman, M.A., Jose, S.C., Nowak, W. and Cirpka, O.A., 2005. Experiments on vertical transverse mixing in a large-scale heterogeneous model aquifer. Journal of Contaminant Hydrology, 80: 130-148.

Rolle, M., Eberhardt, C., Chiogna, G., Cirpka, O.A. and Grathwohl, P., 2009. Enhancement of dilution and transverse mixing in porous media: Experiments and model-based interpretation. Journal of Contaminant Hydrology, 110: 130-142.

Russo, D., Jury, W.A. and Butters, G.L., 1989. Numerical analysis of solute transport during transient irrigation, 2. The effect of immobile water. Water Resources Research, 25(10): 2119-2127.

Schürmann, A., Schroth, M.H., Saurer, M., Bernasconi, S.M. and Zeyer, J., 2003. Nitrate-consuming processes in a petroleum-contaminated aquifer quantified using push-pull tests combined with 15N isotope and acetylene-inhibition methods. Journal of Contaminant Hydrology, 66: 59-77.

Silliman, S.E., Berkowitz, B., Simunek, J. and van Genuchten, M.Th., 2002. Fluid flow and solute migration within the capillary fringe. Ground Water, 40(1): 76-84.

Thornton, S.F., Quigley, S., Spence, M.J., Banwart, S.A., Bottrell, S. and Lerner, D.N., 2001. Processes controlling the distribution and natural attenuation of dissolved phenolic compounds in a deep sandstone aquifer. Journal of Contaminant Hydrology, 53: 233-267.

Umweltbundesamt, 2004. Langzeituntersuchungen zu den Möglichkeiten und Grenzen der Nutzung natürlicher Selbstreinigungsprozesse für ausgewählte Schadstoffe am Beispiel kontaminierter militärischer Liegenschaften - Literaturstudie (Teilschritt 1), Forschungsbericht FKZ 298 76 712/02, UBA-Texte 49/04, Berlin, 106 S., 31 p. Anh., ISSN 0722-186X. http://www.umweltbundesamt.de/altlast/web1/start.htm

Vanderborght, J. and Vereecken, H., 2007. Review of dispersivities for transport modeling in soils. Vadose Zone Journal, 6(1): 29-52.

Werner, D. and Höhener, P., 2002. The influence of water table fluctuations on the volatilization of contaminants from groundwater. p. 213–218. *In* Thornton, S.F. and Oswald, S.E. (Eds.) Proc. Groundwater Quality 2001: Natural and Enhanced Restoration of Groundwater Pollution, Sheffield, UK. June 2001. IAHS publ. 275.

Williams, M.D. and Oostrom, M., 2000. Oxygenation of anoxic water in a fluctuating water table system: an experiment and numerical study. Journal of Hydrology, 230: 70-85.

Zitomer, D.H. and Speece, R.E., 1993. Sequential environments for enhanced biotransformation of aqueous contaminants. Environmental Science and Technology, 27(2): 226-244.

2. Background to this Work

The overall objective of this work is to investigate oxygen transfer in a fluctuating capillary fringe. Within this transition region, we aim at understanding the dynamic interplay of the occurring flow and mass transfer mechanisms. We are particularly interested in quantifying mass transfer for varying hydraulic conditions and porous medium properties. In the following paragraphs, we give a definition of the capillary fringe as well as the extended Darcy's law for unsaturated flow. Moreover, we present the basic mass transfer processes that have to be considered in this interface region.

2.1 The Capillary Fringe

The capillary fringe is the transition region between the unsaturated zone and the unconfined aquifer. It extends from the water table up to the limit of the capillary rise of water. In fact, water molecules at the water table are drawn upward due to surface tension of the air-water interface and the molecular attraction of the liquid and solid phases (Fetter, 2001). As a consequence, water pressure is less than atmospheric pressure within this zone. For illustration purposes, the capillary rise in a tube is given by the Laplace or Jurin's (Jurin, 1717) formula:

$$h_{cr} = \frac{2\sigma \cos \lambda_{cr}}{\rho_{aq} g r_{tube}} \tag{2.1}$$

in which h_{cr} [L] is the height of the capillary rise, σ [M T^{-2}] represents the surface tension of the fluid, and λ_{cr} [rad] is the angle of the meniscus with the capillary tube. ρ_{aq} [M L^{-3}] denotes the fluid density and g [L T^{-2}] is the gravitational acceleration. Finally, r_{tube} [L] represents the radius of the capillary tube.

Under natural conditions, the thickness of the capillary fringe depends on the physical properties of the fluids (Rockhold et al., 2002; Henry and Smith, 2002, 2003; Freitas et al., 2011) and the solid surface as well as on the homogeneity of the porous medium, mainly on the pore size distribution (Papafotiou, 2008; Bear and Cheng, 2010). Smaller pore openings create greater tension, which results in a higher capillary fringe in small-grained porous media than in coarse material (Fetter, 2001). Since the pores within a porous medium matrix are typically composed of numerous pore sizes, there is a gradual decrease in water content with height above the water table. Moreover, the upper limit of the capillary fringe has an irregular shape. For practical purposes, we often take some average smooth surface (where water saturation is, e.g., ~75 %) as the upper limit of the capillary fringe, such that, below it, the porous medium is assumed practically saturated (Bear and Cheng, 2010). In the present work, we define the upper limit of the capillary fringe as the vertical

position, where water saturation is about 80 % to 90 %, thus, inhibiting gaseous oxygen to diffuse freely in the pore space (Liu, 2008).

Analytical expressions for the general capillary pressure-saturation functional relationship have been proposed by various authors (e.g., Brutsaert, 1967; Campbell, 1974; Vauclin et al., 1979; Wang et al., 2008; Li, 2010; for an overview see Sheta, 1999; Bear and Cheng, 2010). Two parameterizations, with numerous modifications, are popular: the van Genuchten (van Genuchten, 1980) and the Brooks-Corey (Brooks and Corey, 1964, 1966) model. All of these analytical expressions employ shape parameters (e.g., Bloemen, 1977; Carsel and Parrish, 1988; Schaap and Leij, 1998) to fit measured and calculated capillary pressure-saturation data.

2.1.1 Transient Effects: Hysteresis and Storativity

Hysteresis describes the dependence of the capillary pressure curve on the direction and history of drainage and wetting of a sample (Stephens, 1995; Bear and Cheng, 2010). The entrapment of air represents one cause for hysteresis in the water content/pressure head relationship (Bear, 1972; Kaluarachchi and Parker, 1987; Parker and Lenhard, 1987; Lenhard and Parker, 1987; Bear and Cheng, 2010). Pore-geometry related hysteresis occurs as the processes of imbibition and drainage cause different pores to imbibe or drain first (ink-bottle effect, Fig. 2.1a: menisci having the same curvature occur at different elevations), but also affect the contact angle between the solid surface and the air/water interface (raindrop effect, Fig. 2.1b: contact angle at advancing front differs from that at receding one). Other factors contributing to hysteresis may be consolidation, swelling, and shrinkage of the solid matrix as it is dried and wetted (Bear and Cheng, 2010).

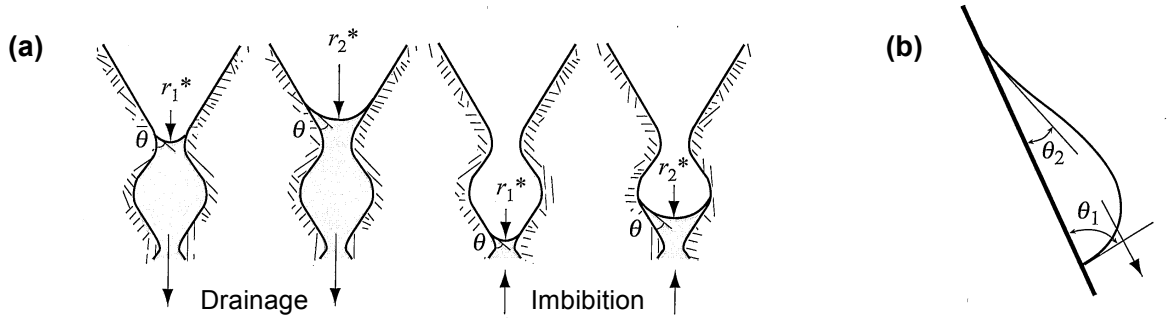

Fig. 2.1. Hysteresis due to (a) ink-bottle effect and (b) raindrop effect (from Bear and Cheng, 2010. Reprinted by permission of Springer Science + Business Media, Dordrecht).

Figure 2.2 shows the effect of entrapped air on the capillary pressure-saturation relationship. The main drainage and imbibition curves define the hysteresis envelope, which encompasses an infinite number of possible scanning curves (shown as dashed lines on the figure). We note that the residual gas saturation also depends on the drainage-imbibition history. Thus, the amount of

entrapped air is higher, when imbibition begins from a dryer state than when the sample had been previously drained.

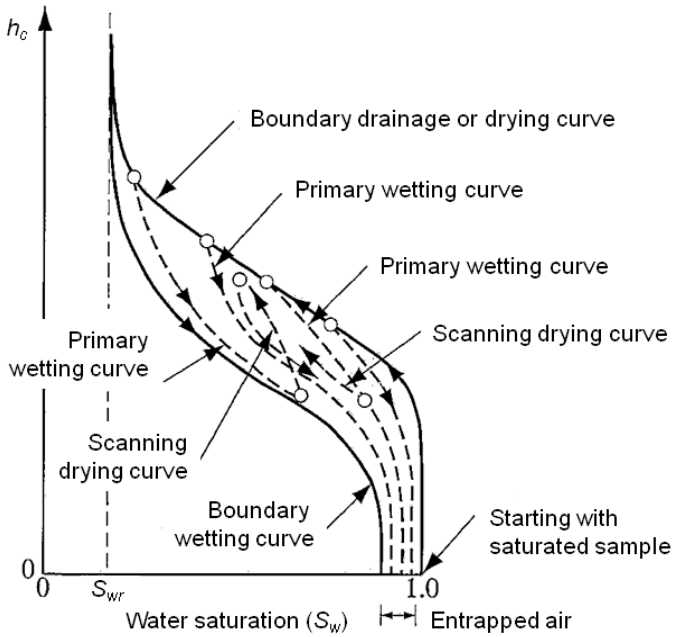

Fig. 2.2. Hysteresis and entrapped air in a capillary pressure curve (from Bear and Cheng, 2010. Reprinted by permission of Springer Science + Business Media, Dordrecht).

In addition to hysteresis in the water content/pressure head relationship, the storativity of the porous medium may also have to be considered in case of a fluctuating water table. The storativity for an unconfined aquifer is usually taken to be equal to the specific yield (e.g., Fetter, 2001; Bear and Cheng, 2010), which is defined as the ratio of the volume of water that drains from a saturated rock or soil, due to gravity, to the total volume of the porous formation (Meinzer, 1923; Fetter, 2001). Specific yield is a time-dependent quantity, because it takes time to establish a new moisture distribution following a rapid decrease in water table elevation (Nachabe, 2002; Bear and Cheng, 2010). Moreover, specific yield is influenced by the grain size and shows less time-dependence and variability for coarse sediments than for fine sediments since the latter drain less quickly.

2.1.2 Water Saturation Distribution in Heterogeneous Porous Media

Considering a homogeneous porous medium profile, water saturation, S_w [-], decreases with increasing capillary pressure head, h_c [L] (Fig. 2.3a). The relationship between the capillary pressure head and the water saturation is described by the capillary pressure head curve, $h_c = h_c(S_w)$.

When a porous medium is layered, i.e., coarse and fine materials are overlying each other, an interesting phenomenon occurs at the interface between the two porous materials. The assumption of local equilibrium prohibits any pressure jump across such an interface, in both the aqueous and the gaseous phases (Zilch, 2002; Papafotiou, 2008; Bear and Cheng, 2010). Since the capillary pressure has to be continuous at the interface and is additionally related to two different values of water saturation on each side, this results, in general, to saturation discontinuities at the interface (Fig. 2.3b). To be more precise, at the same capillary pressure head, the fine porous material may stay at high water saturation, whereas the moisture content of the coarse porous medium is essentially at the residual value.

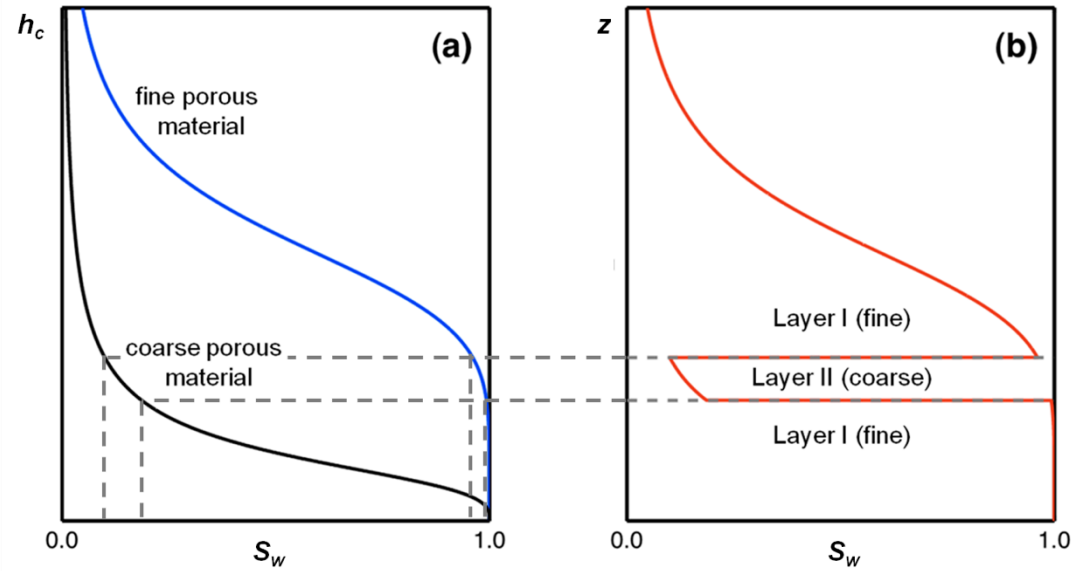

Fig. 2.3. Water saturation discontinuities at interfaces in a layered porous medium: (a) capillary pressure head curves for two porous media (coarse and fine); (b) water saturation distribution at equilibrium in a three-layered system.

2.2 Extended Darcy's Law for Unsaturated Flow

When several fluids are present in the void space of a porous medium, the fluids interfere with each other in their flow behavior. In fact, one fluid phase reduces the flow path of the other phase. The effect of other fluids in obstructing the flow of a fluid *i* is captured by the relative permeability, which can be considered as a scaling factor ranging between 0 and 1 (e.g., Allen, 1985; Bear and Cheng, 2010). Bear and Bachmat (1986, 1990) showed that the permeability of a considered fluid phase is a function of the saturation of that fluid. The extended Darcy's law can be used as an approximation for the flow of a fluid phase in a multiphase system (Buckingham, 1907; Richards, 1931; Childs, 1969):

$$v_a = \frac{-k_{r,i}(S_i)k^{sat}}{\mu_i \phi S_i}(\nabla p_i - \rho_i g \nabla z) \tag{2.2}$$

in which v_a [L T^{-1}] is the horizontal groundwater flow velocity, $k_{r,i}$ [-] represents the relative permeability of the fluid *i,* and k^{sat} [L^2] is the permeability at full saturation. Moreover, μ [M L^{-1} T^{-1}], S [-], p [M L^{-1} T^{-2}], and ρ [M L^{-3}] denote the dynamic viscosity, saturation, pressure, and density of the fluid, respectively. Φ [-] is the porosity of the porous medium, and z [L] represents the elevation. Equation 2.2 can be simplified by replacing k^{sat} with $k^{sat} = K\mu(\rho g)^{-1}$:

$$v_a = \frac{-k_{r,i}(S_i)}{\phi S_i} K \nabla h_i = \frac{k_{r,i}(S_i)}{\phi S_i} q_i^{sat} \tag{2.3}$$

where K [L T^{-1}] is the saturated hydraulic conductivity, h [L] represents the hydraulic head, and q^{sat} [L T^{-1}] denotes the Darcy velocity in the fluid-saturated zone.

Equations 2.2 and 2.3 are nonlinear, since the value of relative permeability depends on the phase effective saturation (and hence on fluid pressure; Fig. 2.4 for a two-fluid system). When S_i is at residual saturation, a continuous phase is not present and the relative permeability has to be zero. Similarly, for S_i = 1 it is valid that $k_{r,i}$ = 1. Between these extreme values, the relative permeability increases monotonically with phase saturation. As a consequence, in homogenous porous media the horizontal groundwater flow velocity continuously decreases with increasing height above the water table (Liu, 2008).

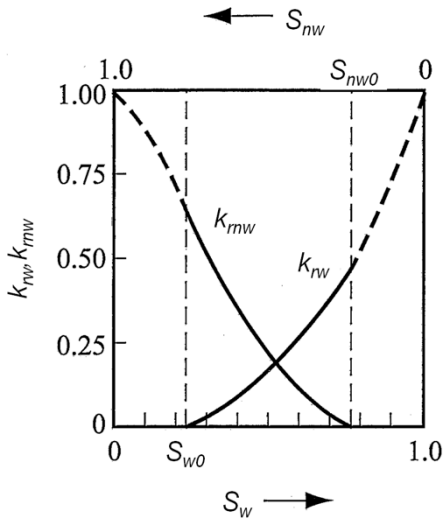

Fig. 2.4. Typical relative permeability curves without hysteresis (from Bear and Cheng, 2010. Reprinted by permission of Springer Science + Business Media, Dordrecht).

The relative permeability-saturation relationship has to be determined experimentally for each particular porous medium or can be derived using analytical expressions (e.g., Burdine, 1953; Irmay, 1954; Mualem 1976; Brooks and Corey, 1964, 1966; van Genuchten, 1980). These analytical expressions for the relative permeability-saturation relationship were usually obtained by analyzing simplified models of porous media, such as a bundle of capillary tubes or pore network models (Papafotiou, 2008; Bear and Cheng, 2010).

The two functional relationships $k_{r,w} = k_{r,w}(S_w)$ and $h_c = h_c(S_w)$, which are needed in order to solve unsaturated flow problems, are not unique, cannot be easily measured, and are subject to hysteresis. Hysteresis in $k_{r,w}(S_w)$ is generally ignored, since the capillary pressure head-saturation relationship usually exhibits far greater hysteretic effects (Bear and Cheng, 2010). Moreover, the parameter values required to describe hysteresis in the relative permeability-saturation relationship are highly uncertain.

2.3 Relevant Mass Transfer Processes in the Capillary Fringe

Mass transfer processes across and within the transition region between the unsaturated and the saturated zone are important for the supply of volatile compounds from the atmosphere to groundwater. At steady state, transverse vertical dispersion was found to be essential for mass transfer of volatile compounds across the capillary fringe (Klenk and Grathwohl, 2002; Liu, 2008). Moreover, molecular diffusion and advection play a role. Whereas molecular diffusion dominates in the unsaturated zone (e.g., Grathwohl, 1998; Bear and Cheng, 2010), transverse vertical dispersion and advective transport are the principal mechanisms for mass transfer in groundwater. In the intermediate zone, the transition between these processes (i.e., molecular diffusion and dispersion/advection) occurs (Maier et al., 2007; Liu, 2008). Additional mass transfer processes to be considered may be gas partitioning, sorption, and degradation.
In case of increasing water tables (i.e., imbibition), a significant amount of volatile compounds can be supplied to the aqueous phase by partitioning from entrapped gas (e.g., Donaldson et al., 1998; Klump et al., 2008). The latter process occurs until equilibrium between the two fluid phases is achieved (Cirpka and Kitanidis, 2001). Furthermore, entrapped gas influences the transfer of volatile compounds (e.g., soil gases, contaminants) through the aquifer, due to its effects on the hydraulic properties of the porous medium (e.g., Orlob and Radhakrishna, 1958; Bear and Cheng, 2010), the tortuosity (e.g., Klenk and Grathwohl, 2002), and the retardation of partitioning compounds (Fry et al., 1995).

2.3.1 Hydrodynamic Dispersion

The spreading of a solute in a porous medium domain, beyond the region it would be expected to occupy if it were subject to advective flow alone, is called hydrodynamic dispersion (Bear, 1972). It is an unsteady, irreversible process in which the mass of a tracer continuously ‘mixes’ with the non-labeled portion of the moving fluid. Hydrodynamic dispersion results from both molecular diffusion and mechanical dispersion; it is, thus, observed not only in the direction of the (averaged) uniform flow, but also normal to it. The separation between molecular diffusion and mechanical

dispersion is rather artificial, as they are inseparable (exception: diffusion in the absence of flow) (Bear, 1972; Fetter, 2001; Bear and Cheng, 2010).

In general, three factors are responsible for mechanical dispersion in longitudinal direction (e.g., Bear 1972; Fetter, 2001): (i) varying pore sizes, (ii) tortuosity, and (iii) the velocity distribution in a single pore. Lateral dispersion is caused by the fact that, as a fluid containing a tracer flows through a porous medium, the flow paths can split and branch out to the sides (Fig. 2.5). However, very little spreading is produced in the direction perpendicular to the average flow due to velocity variations alone. The mechanism of molecular diffusion also has to be taken into account. Molecular diffusion is caused by the random motion of the molecules (Brownian motion), which results in the spreading of solute particles from regions of higher concentrations to those of lower ones (Fetter, 2001). Thus, lateral molecular diffusion occurs across streamlines and tends to equalize the concentration across pores. It is this phenomenon, combined with the randomness of the streamlines that explains the observed ever-growing extent of transverse dispersion (Bear and Cheng, 2010).

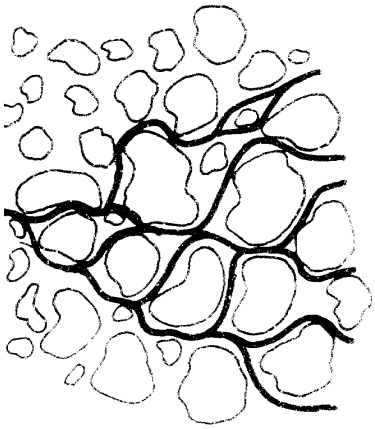

Fig. 2.5. Transverse hydrodynamic dispersion caused by the splitting of the individual streamlines (from Fetter, 2001. Reprinted by permission of Pearson Education, Inc., Upper Saddle River, NJ).

In multiphase flow, a dispersion coefficient is associated with each fluid phase. Thus, longitudinal and transverse hydrodynamic dispersion depend on the phase configuration within the void space since each of these components is a function of flow velocity and the phase saturation.

2.3.1.1 Fick's laws

It is generally assumed that dispersion of a solute travelling through a porous medium follows an extension of Fick's laws. These quantitative laws of diffusion were proposed in 1855 by Adolf Fick, when he was only 26 years old (Fick, 1855a, 1855b; Philibert, 2005; Cussler, 2009). Thinking about Graham's results (Graham, 1850) on diffusion of salts in water, Fick perceived that diffusion could be described according to the same mathematical formalism as Fourier's law for heat conduction (Fourier, 1822) or Ohm's law for electricity. Fick postulated that the mass flux, F [M L^{-2} T^{-1}], of a certain compound across a given cross-sectional area is proportional to the concentration gradient across that interface. Thus, Fick's first law states:

$$F = -D\frac{\partial C(x)}{\partial x} \tag{2.4}$$

in which D [L^2 T^{-1}] is the diffusion coefficient, that describes the rate at which the molecules spread (Grathwohl, 1998), and C [M L^{-3}] denotes the concentration of the diffusing compound depending on distance x [L].

Fick's first law does not consider the fact that the gradient and a compound's local concentration may vary over time, t [T]. Conservation of mass leads to Fick's second law stating that the change in concentration over time is equal to the change in local diffusion flux:

$$\frac{\partial C(x,t)}{\partial t} = -\frac{\partial F}{\partial x} = \frac{\partial\left(D\frac{\partial C(x,t)}{\partial x}\right)}{\partial x} \tag{2.5}$$

If the diffusion coefficient is independent of position, then Fick's second law may be further simplified into the following equation:

$$\frac{\partial C(x,t)}{\partial t} = D\frac{\partial^2 C(x,t)}{\partial x^2} \tag{2.6}$$

Effective and Apparent Diffusion Coefficients:

In porous media, diffusion of a compound is hindered by the reduced cross-sectional area available for diffusion as well as by the size and the tortuous nature of the pores (e.g., Grathwohl, 1998; Chiogna et al., 2010).

At steady state, the diffusive flux in a porous medium can be described by Fick's first law. Whereas C in Eqn. 2.4 refers to the concentration in the gaseous or the aqueous phase, the diffusion coefficient for the free fluid phase, D, has to be replaced by the effective diffusion coefficient. The latter is denoted as $D_{e,g}$ [L^2 T^{-1}] or D_e [L^2 T^{-1}], in order to describe mass transfer in the gaseous or in the aqueous phase, respectively. $D_{e,g}$ and D_e are typically derived by empirical correlations (Millington, 1959; Currie, 1960; Sallam et al., 1984; Maraqa et al., 1997; Moldrup et al., 2000); for a summary, also refer to Grathwohl, 1998). As an example, the empirical correlation according to Millington and Quirk (1960) is given for the effective diffusion coefficient in the unsaturated zone:

$$D_{e,g} = D_g\frac{\phi_g^{10/3}}{\phi^2} \tag{2.7}$$

in which D_g [L^2 T^{-1}] is the diffusion coefficient in the free gaseous phase. Φ_g [-] and Φ [-] are the gas-filled and the total porosity of the porous medium, respectively.

Under water-saturated conditions, a typical approximation for D_e is (e.g., Grathwohl, 1998):

$$D_e = D_{aq}\phi^m \tag{2.8}$$

in which D_{aq} [L^2 T^{-1}] is the diffusion coefficient in the free aqueous phase and m [-] represents an empirical exponent with a value of about 2 in natural porous media (Grathwohl, 1997).

For the transient case (i.e., when concentrations vary with time), Fick's second law (Eqns. 2.5 and 2.6) is valid. To account for retardation processes, such as sorption into or onto the solids and/or partitioning between the gas and aqueous phases, an apparent diffusion coefficient is introduced. In the unsaturated zone, the capacity factor, α [-] (e.g., Silka and Jordan, 1993; Grathwohl, 1998; Klenk 2000; Werner and Höhener, 2003), has to be used for the calculation of the apparent diffusion coefficient in the gaseous phase, $D_{a,g}$ [L^2 T^{-1}]:

$$D_{a,g} = \frac{D_{e,g}}{\alpha} = \frac{D_{e,g}}{\phi_g + \frac{\phi_{aq}}{K_H} + \frac{K_d \rho}{K_H}} \tag{2.9}$$

in which Φ_{aq} [-] denotes the water-filled pore volume and K_H [-] is the compound-specific Henry's Law coefficient. Moreover, K_d [L^3 M^{-1}] represents the distribution coefficient between the aqueous and the solid phases and ρ [M L^{-3}] is the dry bulk density.

Transient diffusion of a solute, e.g., subject to sorption in porous media, can be described using the following equation for the apparent diffusion coefficient, D_a [L^2 T^{-1}] in the aqueous phase:

$$D_a = \frac{D_e}{\alpha} = \frac{D_e}{\phi + K_d \rho} \tag{2.10}$$

Please note that the capacity factor α is now differently defined, when compared with Eqn. 2.9.

In case no sorption occurs, D_a equals the pore diffusion coefficient, D_p [L^2 T^{-1}] (Rahman et al., 2004). Thus, for D_p a typical approximation under water-saturated conditions is (Grathwohl, 1998; Boving and Grathwohl, 2001; Olsson and Grathwohl, 2007; Chiogna et al., 2010):

$$D_p = D_{aq}\phi \tag{2.11}$$

Regarding mass transfer across the capillary fringe, volatile compounds with high Henry's law coefficient are transferred quickly through regions with higher water saturation. In these regions, the partial pressure of the diffusing compound does not considerably differ from the compound's partial pressure at higher elevations (comprising lower values of water saturation). However, mass transfer is limited on the water-side, since gas diffusion coefficients are typically much higher than aqueous diffusion coefficients (by approximately four orders of magnitude; Reid et al., 1987). Transfer of volatile compounds with low Henry's law coefficient is additionally determined by the mass transfer in air/water-filled pores.

2.3.1.2 Parameterizations of Transverse Vertical Hydrodynamic Dispersion:

Diffusion is the primary mass transfer mechanism for gaseous compounds, since under natural conditions only minor pressure gradients exist in the subsurface environment (e.g., Jury et al., 1991; Grathwohl, 1998; Scott, 2000). In the liquid phase, both diffusive and advective flow processes operate and hydrodynamic dispersion coefficients are used to describe dispersive mass transfer of solutes in porous media. These coefficients are defined as the additive contribution of D_p and a mechanical dispersion coefficient, D_{mech} [L^2 T^{-1}]. The transverse vertical hydrodynamic dispersion coefficient, D_t [L^2 T^{-1}], can, thus, be written as:

$$D_t = D_p + D_{mech} \tag{2.12}$$

De Josselin de Jong (1958) and Saffman (1959) defined the mechanical dispersion in transverse direction as a quantity linearly proportional to the velocity and to the grain size. The authors introduced an empirical correction factor with a value of 3/16. Nowadays, the linear parametric model proposed by Scheidegger (1961) is commonly used (e.g., Fetter, 2001):

$$D_t = D_p + \alpha_t v_a \tag{2.13}$$

in which the transverse dispersivity, α_t [L], is assumed to be a property of the porous medium alone. If we accept this description (Eqn. 2.13), we assume molecular diffusion and mechanical dispersion can be treated as two separate phenomena, that is, D_{mech} is identical for all compounds. This separation between the two processes is, however, rather artificial (Bear, 1972; Fetter, 2001; Bear and Cheng, 2010).

Inspired by the statistical model of Bear and Bachmat (1967), Chiogna et al. (2010) derived an empirical formulation of D_t that retains an explicit dependence of the mechanical dispersion term on the aqueous diffusion coefficient of the transported tracer.

$$D_t \approx D_p + v_a \frac{d}{\sqrt{Pe + 123}} \tag{2.14}$$

This formulation shows a non-linear relationship with the average seepage velocity (Chiogna et al., 2010) and was further generalized by Rolle et al. (2012). The dimensionless grain Péclet number, *Pe*, is defined as:

$$Pe = \frac{v_a d_c}{D_{aq}} \tag{2.15}$$

in which d_c [L] is the characteristic length of a pore channel, represented by the average grain diameter, d [L].

2.3.2 Vertical Mass Transfer

In this study, we investigate mass transfer of oxygen across the capillary fringe under dynamic flow conditions. Therefore, we focus our attention on this interface region between the vadose zone and the underlying groundwater.

2.3.2.1 Total Effective Dispersion

In a subsurface system, mass transfer of a compound is limited, where a steep concentration gradient occurs (Jähne and Haußecker, 1998; Maier et al., 2007). For comparably shallow unsaturated zones without strong microbial activity, gas diffusion is so quick that the partial pressure of oxygen can be well approximated by the partial pressure in the free atmosphere. That is, studying oxygen profiles in the unsaturated zone is of interest only for thick vadose zones or soils with tremendous reactive oxygen consumption. This is different for the underlying aquifer, where diffusion coefficients are by orders of magnitude smaller (Reid et al., 1987). The weak vertical mixing in the aqueous phase may result in an abrupt change in concentration between the water table and the upper limit of the capillary fringe. As an example, this was observed by McCarthy and Johnson (1993) who studied the transfer of TCE from shallow groundwater to the unsaturated zone.

Effective diffusion/dispersion coefficients, acting in vertical direction, can be used to interpret steady-state concentration profiles (McCarthy and Johnson, 1993; Werner et al., 2004; Maier et al., 2007; Liu, 2008) since longitudinal dispersion is of minor importance for mixing compared to transverse dispersion. The total effective dispersion coefficient for the system considered is:

$$D_{tot} = \frac{\phi_g^{10/3}}{\phi^2} D_g + \theta_{aq} D_{mech} = \theta_g S_g^{7/3} \phi^{1/3} D_g + \theta_{aq} D_{mech} \tag{2.16}$$

in which θ_g [-] and θ_{aq} [-] are the volumetric gas and water content. S_g [-] denotes the saturation of the gaseous phase. To describe the effective diffusion coefficient in the gas phase, the correction of Millington and Quirk (1960; Eqn. 2.7) was implemented into Eqn. 2.16.

As already mentioned, gas diffusion represents the principal mass transfer mechanism for natural gases as well as volatile pollutants at low and moderate moisture contents and in the absence of pressure gradients (e.g., Grathwohl, 1998; Werner et al., 2004; Bear and Cheng, 2010). This can also be observed in Fig. 2.6. The effective gas diffusion coefficient (Eqn. 2.7) decreases with increasing water content in the transition region between the unsaturated and the saturated zones (Grathwohl, 1992; Scanlon et al., 2002), whereas hydrodynamic dispersion gets more and more dominant. In Fig. 2.6 mass transfer is limited on the water-side, i.e., by the transport of the volatile compound from the air-water interface across the aqueous boundary layer or vice versa.

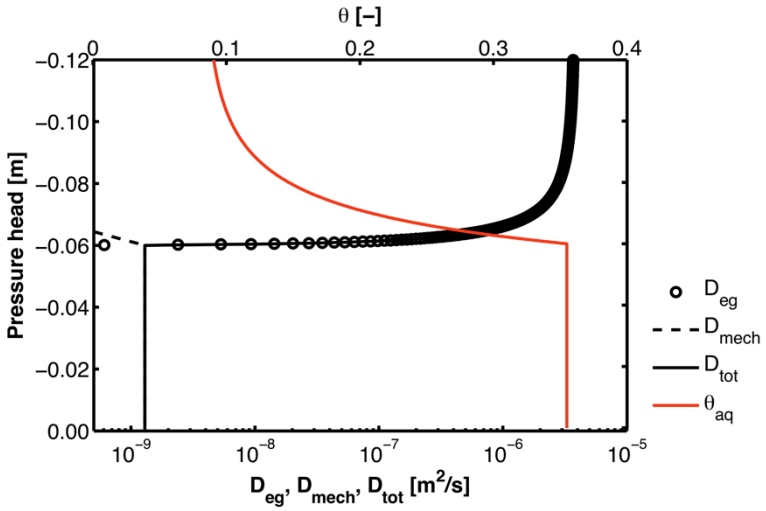

Fig. 2.6. Vertical profiles of effective gas diffusion (D_{eg}), mechanical dispersion (D_{mech}), and total effective dispersion (D_{tot}) across the capillary fringe (all of them acting in the vertical direction). As reference also the water content profile (θ_{aq}) is given.

2.3.2.2 Conceptual Theories of Mass Transfer

Different conceptual theories were developed to describe mass transfer from a gas phase to a liquid phase proceeding via an interfacial area. The following theories are frequently applied:

- Stagnant film theory (Nernst, 1904):

  Mass transfer is postulated to proceed via stationary diffusion in a stagnant film of thickness l [L]. Such a hypothetical film gives the simplest model of the interfacial region and the flux, F_1 [M T^{-1} L^{-2}], relative to the interface, is calculated by:

$$F_1 = \frac{D}{l}\left(C_{1i} - C_1\right) \tag{2.17}$$

  in which C_{1i} [M L^{-3}] and C_1 [M L^{-3}] are the interfacial and bulk concentrations in the liquid phase. In the present case, the unknown film thickness, l, varies with the fluid velocity.

- Penetration theory (Higbie, 1935):

  This theory is based on mass transfer into a semi-infinite fluid, where the residence time of a fluid element at the interface is used as the characteristic parameter. It is assumed that in the direction perpendicular to flow, diffusion is much more important than advection, whereas in the direction of flow, diffusion is much less important than advection. The average flux across the interface, F_1 [M T^{-1} L^{-2}], is:

$$F_1 = 2\sqrt{D\frac{v_{\max}}{L}\frac{1}{\pi}}\left(C_{1i} - C_1\right) \tag{2.18}$$

  in which v_{max} [L T^{-1}] denotes the interfacial velocity of the liquid and L [L] is the length of the exposed film. C_{1i} [M L^{-3}] represents the interfacial solute concentration in the liquid in equilibrium with the well-stirred gas and C_1 [M L^{-3}] is the bulk solute concentration.

- Surface-renewal theory (Danckwerts, 1951):

  The surface-renewal theory provides a better physical picture than the penetration theory, since a probability of replacement is introduced. This idea of replacement or 'surface-renewal' makes the penetration theory part of a more believable process. The average flux across the interface, F_1 [M T^{-1} L^{-2}], is:

$$F_1 = \sqrt{\frac{D}{\tau}}\left(C_{1i} - C_1\right) \tag{2.19}$$

  in which τ [T] is the surface-renewal rate.

The different theories discussed above are schematically shown in Fig. 2.7. For further details please refer to, e.g., Gulliver (2007) or Cussler (2009).

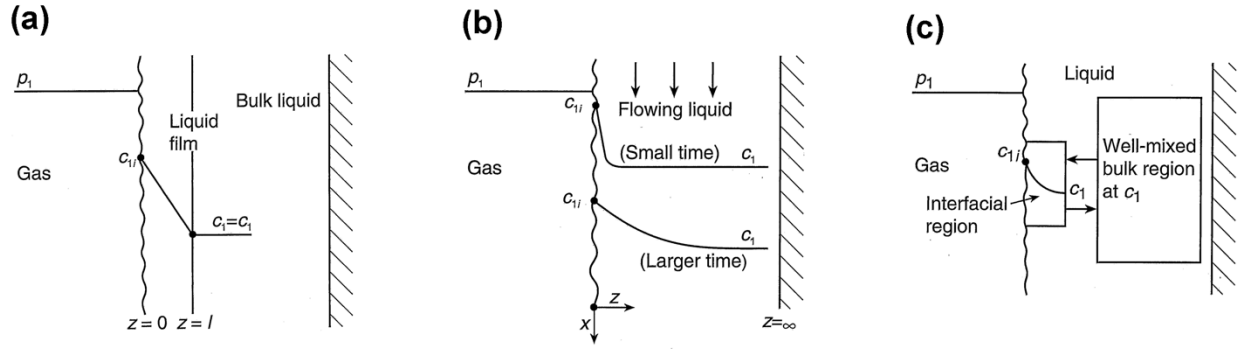

Fig. 2.7. Conceptual theories to describe mass transfer: (a) Stagnant film theory; (b) Penetration theory; (c) Surface-renewal theory (from Cussler, 2009. Reprinted by permission of Cambridge University Press, Cambridge).

2.3.2.3 Mathematical Description of the Partitioning of Volatile Compounds

Groundwater level fluctuations can directly impact dissolution rates (e.g., Williams and Oostrom, 2000) and/or contaminant volatilization rates from groundwater due to water table 'pumping' (e.g., Parker et al., 1994; Werner and Höhener, 2002; Parker, 2003). For example the entrapment of gas clusters leads to partitioning of volatile compounds between the liquid and the gaseous phases, thus, affecting the overall mass transfer compared to steady-state conditions.

Transfer of volatile compounds, between the aqueous and the gaseous phases, results from the difference in chemical potential of these compounds between the two phases (e.g., Anderson and Crerar, 1993; Nordstrom and Munoz, 1994). In most problems, multiple dissolved gases are transferred simultaneously (Donaldson et al., 1998). According to Cirpka and Kitanidis (2001), the total amount of volatile compounds determines the gas saturation, which tends to increase with the mass per pore volume of a specific volatile compound, while the total concentrations of the other compounds remain the same. Thus, the trapped gas volume may grow or shrink depending on whether gases are produced or consumed (Amos and Mayer, 2006).

Several models have been developed to describe partitioning of volatile compounds between the aqueous and entrapped gaseous phases (e.g., Heaton and Vogel, 1981; Stute et al., 1995; Aeschbach-Hertig et al., 2000; Mercury et al., 2004). Two different approaches have been proposed to couple gas partitioning between the two phases with solute transport in water: the kinetic bubble dissolution model (Holocher et al., 2003) and the local equilibrium model (Cirpka and Kitanidis, 2001). Klump et al. (2008) argued that gas-transfer kinetics are important when the contact time between the water and gas phases is relatively short. In contrast, the assumption of local equilibrium between the two phases is appropriate for low flow velocities and large distances (see also Geistlinger et al., 2005).

In the following, we assume that local equilibrium is appropriate for the experimental conditions applied in this study. The water and the entrapped gas phase are considered in local physico-chemical equilibrium and mass transfer between the liquid and the gaseous phase is solely controlled by the different equilibrium coefficients, i.e., by the compound-specific Henry's law constants. In fact, thermodynamic equilibrium exists between two fluid phases, when the chemical potential, μ [L^2 T^{-2}], for each given compound *i*, present in the multiphase system, is the same in both phases (e.g., Atkins and de Paula, 2006; Cussler, 2009), i.e.,

$$\mu_i^g = \mu_i^{aq} \tag{2.20}$$

The chemical potential of a compound in the gaseous or aqueous phase can be expressed as a function of the compound's fugacity (or partial pressure) or activity (or aqueous concentration) in the respective phase. In doing so, the chemical potential of a component *i* in a mixture of ideal gases is related to its partial pressure, p_i [M L^{-1} T^{-2}], by

$$\mu_i^g = \mu_i^{0,g} + \Re T \ln \frac{p_i}{p^0} \tag{2.21}$$

in which $\mu_i^{0,g}$ is the standard potential of the compound measured at a specific reference state. $\Re$ [L^2 t^{-1} T^{-2}] denotes the ideal gas constant and *T* [t] is the absolute temperature. In the current case, p^0 [M L^{-1} T^{-2}] represents the total pressure, which is equal to the sum of partial pressures.

Correspondingly, the chemical potential of the compound *i* in an ideally dilute solution is

$$\mu_i^{aq} = \mu_i^{0,aq} + \Re T \ln X_i \tag{2.22}$$

in which $\mu_i^{0,aq}$ is the chemical potential of the pure solute at infinite solution and X_i [-] represents the mole fraction of compound *i* in the aqueous phase.

Thus, for ideally diluted solutions and at equilibrium, the concentration, C_i^{aq} [M L^{-3}], of the dissolved gas *i* is related to its partial pressure and atmospheric concentration, C_i^{g} [M L^{-3}], by Henry's law:

$$K_{H,i} = \frac{C_i^{\,g}}{C_i^{\,aq}} = \frac{p_i}{\Re T C_i^{aq}} \tag{2.23}$$

Helfferich (1981) defined the total concentration, $C_i^{\,tot}$ [M L^{-3}], of each compound *i* as the mass in all phases per pore volume:

$$C_i^{\,tot} = \left(1 - S_g\right) C_i^{\,aq} + S_g C_i^{\,g} = \left[1 + \left(K_{H,i} - 1\right) S_g\right] C_i^{\,aq} \tag{2.24}$$

Thus, rearranging Eqn. 2.24 and implementing into Eqn. 2.23, the partial pressure can be expressed as:

$$p_i = \frac{C_i^{\,tot} \Re T K_{H,i}}{1 + \left(K_{H,i} - 1\right) S_g} \tag{2.25}$$

The transport of various volatile compounds in the presence of an immobile gas phase is coupled via the total gas pressure, *p* [M L^{-1} T^{-2}], i.e., the sum of atmospheric pressure, capillary pressure, and hydrostatic pressure (Cirpka and Kitanidis, 2001). Equilibrium is achieved, when the sum of partial pressures within the gaseous phase approximates this external pressure. In case of absence of a gaseous phase, the sum of partial pressures, computed through Henry's law, is smaller than *p*:

$$\sum_{i=1}^{N} p_i = \begin{cases} = p & \text{if } S_g > 0 \\ < p & \text{if } S_g = 0 \end{cases} \tag{2.26}$$

in which *N* is the number of volatile compounds.

Due to the hydrostatic pressure of the water, the potential equilibrium concentration in the aqueous phase increases with increasing water depth. In fact, it is evident that the depth of the entrapped gas volume in the water body determines the hydrostatic pressure, which is the dominating parameter responsible for the total amount of dissolved air (Holocher et al., 2002).

References

Aeschbach-Hertig, W., Peeters, F., Beyerle, U. and Kipfer, R., 2000. Palaeotemperature reconstruction from noble gases in ground water taking into account equilibration with entrapped air. Nature, 405: 1040-1044.

Allen, M.B., 1985. Numerical modelling of multiphase flow in porous media. Advances in Water Resources, 8: 162-187.

Amos, R.T. and Mayer, K.U., 2006. Investigating the role of gas bubble formation and entrapment in contaminated aquifers: Reactive transport modelling. Journal of Contaminant Hydrology, 87: 123-154.

Anderson, G.M. and Crerar, D.A., 1993. Thermodynamics in geochemistry – The equilibrium model. Oxford University Press, New York.

Atkins, P.W. and de Paula, J., 2006. Physikalische Chemie, 4th ed., Wiley-VCH.

Bear, J., 1972. Dynamics of fluids in porous media. New York: American Elsevier.

Bear, J. and Bachmat, Y., 1967. A generalized theory on hydrodynamic dispersion in porous media. *In* IAHS Symposium on Artificial Recharge and Management of Aquifers, Haifa, Israel, 72: 7-16.

Bear, J. and Bachmat, Y., 1986. Macroscopic modeling of transport phenomena in porous media, 2. Applications to mass, momentum, and energy transport. Transport in Porous Media, 1: 241-269.

Bear, J. and Bachmat, Y., 1990. Introduction to modeling phenomena of transport in porous media. Kluwer, Dordrecht, 553 p.

Bear, J. and Cheng, A.H.-D., 2010. Modeling groundwater flow and contaminant transport, 23rd Vol. Springer, New York.

Bloemen, G.W., 1977. Calculation of capillare conductivity and capillare rise from grain size distribution. ICW Wageningen nota no. 952, 962, 990, 1013.

Boving, T. and Grathwohl, P., 2001. Matrix diffusion coefficients in sandstones and limestones: Relationship to permeability and porosity. Journal of Contaminant Hydrology, 53(1-2): 85-100.

Brooks, R.H. and Corey, A.T., 1964. Hydraulic properties of porous media. Hydrology paper, Colorado State University, Ft. Collins

Brooks, R.H. and Corey, A.T., 1966. Properties of porous media affecting fluid flow. Journal of the Irrigation and Drainage Division, ASCE, 92(IR2): 61-87.

Brutsaert, W., 1967. Some methods of calculating unsaturated permeability. Transactions of the American Society of Agricultural Engineers, 10: 400-404.

Buckingham, E., 1907. Studies on the movement of soil moisture. Bulletin no. 38, Bureau of Soils, USDA, Washington, DC.

Burdine, N.T., 1953. Relative permeability calculations from pore-size distribution data. Research Report, Petroleum Transactions, AIME.

Campbell, G., 1974. A simple model for determining unsaturated hydraulic conductivity from moisture retention data. Soil Science, 117: 311-314.

Carsel, R.F. and Parrish, R.S., 1988. Developing joint permeability distributions of soil water retention characteristics. Water Resources Research, 24(5): 755-769.

Childs, E.C., 1969. An introduction to the physical basis of soil water phenomena. Wiley, New York.

Chiogna, G., Eberhardt, C., Grathwohl, P., Cirpka, O.A. and Rolle, M., 2010. Evidence of compound dependent hydrodynamic and (hydro)mechanical transverse dispersion with multi-tracer laboratory experiments. Environmental Science and Technology, 44(2): 688-693, doi: 10.1021/es9023964.

Cirpka, O.A. and Kitanidis, P., 2001. Transport of volatile compounds in porous media in the presence of a trapped gas phase. Journal of Contaminant Hydrology, 49: 263-285.

Currie, J.A., 1960. Gaseous diffusion in porous media – Part I: A non-steady state method, Part II: Dry granular materials. British Journal of Applied Physics, 12: 314-324.

Cussler, E.L., 2009. Diffusion: Mass transfer in fluid systems, 3rd ed., Cambridge University Press.

Danckwerts, P.V., 1951. Significance of liquid-film coefficients in gas absorption. Industrial and Engineering Chemistry, 43(6): 1460-1467.

de Josselin de Jong, G., 1958. Longitudinal and transverse diffusion in granular deposits. Transactions, American Geophysical Union, 39(1): 67-74.

Donaldson, J.H., Istok, J.D. and O'Reilly, K.T., 1998. Dissolved gas transport in the presence of a trapped gas phase: Experimental evaluation of a two-dimensional kinetic model. Ground Water, 36(1): 133-142.

Fetter, C.W., 2001. Applied Hydrogeology, 4th ed., Upper Saddle River, Prentice Hall, New Jersey.

Fick, A., 1855a. Ueber Diffusion. Annalen der Physik und Chemie, 170(1): 59-86, doi: 10.1002/andp.18551700105.

Fick, A., 1855b. On liquid diffusion. Philosophical Magazine, 294(X): 30-39.

Fourier, J.B.J., 1822. Théorie analytique de la chaleur. Firmin-Didot père et fils, Paris.

Freitas, J.G., Doulatyari, B., Molson, J.W., Barker, J.F., 2011. Oxygenated gasoline release in the unsaturated zone, Part 2: Downgradient transport of ethanol and hydrocarbons. Journal of Contaminant Hydrology, 125: 70-85.

Fry, V.A., Istok, J.D., Semprini, L., O'Reilly, K.T. and Buscheck, T.E., 1995. Retardation of dissolved oxygen due to a trapped gas phase in porous media. Ground Water, 33(3): 391-398.

Geistlinger, H., Beckmann, A. and Lazik, D., 2005. Mass transfer between a multicomponent trapped gas phase and a mobile water phase: Experiment and theory. Water Resources Research, 41, W11408, doi: 10.1029/2004WR003885.

Graham, T., 1850. The Bakerian Lecture: On the Diffusion of Liquids. Philosophical Transactions of the Royal Society of London, 140: 1-46.

Grathwohl, P., 1992. Die molekulare Diffusion als limitierender Faktor bei der Sanierung von Boden- und Grundwasserkontaminationen. UWSG – Zeitschrift für Umweltchemie und Ökotoxikologie, 4(4): 231-236.

Grathwohl, P., 1997. Gefährdung des Grundwassers durch Freisetzung organischer Schadstoffe: Methoden zur Berechnung der in-situ Schadstoffkonzentration. Zeitschrift der Fachsektion Hydrogeologie, 4: 157-166.

Grathwohl, P., 1998. Diffusion in natural porous media: Contaminant transport, sorption/desorption and dissolution Kinetics. Springer, ISBN 0-792-38102-5.

Gulliver, J.S., 2007. Introduction to chemical transport in the environment. Cambridge University Press, ISBN 0-521-85850-X.

Heaton, T.H.E. and Vogel, J.C., 1981. "Excess air" in groundwater. Journal of Hydrology, 50: 201-216.

Helfferich, F.G., 1981. Theory of multicomponent, multiphase displacement in porous media. Society of Petroleum Engineers Journal, 21(1): 51-62.

Henry, E.J. and Smith, J.E., 2002. The effect of surface-active solutes on water flow and contaminant transport in variably saturated porous media with capillary effects. Journal of Contaminant Hydrology, 56: 247-270.

Henry, E.J. and Smith, J.E., 2003. Surfactant-induced flow phenomena in the vadose zone: A review of data and numerical modeling. Vadose Zone Journal, 2: 154-167.

Higbie, R., 1935. The rate of absorption of a purge gas into a still liquid during short periods of exposure. Transactions of the American Institute of Chemical Engineers, 31: 365-389.

Holocher, J., Peeters, F., Aeschbach-Hertig, W., Hofer, M., Brennwald, M., Kinzelbach, W. and Kipfer, R., 2002. Experimental investigations on the formation of excess air in quasi-saturated porous media. Geochimica et Cosmochimica Acta, 66(23): 4103-4117.

Holocher J., Peeters, F., Aeschbach-Hertig, W., Kinzelbach, W. and Kipfer, R., 2003. Kinetic model of gas bubble dissolution in groundwater and its implications for the dissolved gas composition. Environmental Science and Technology, 37(7): 1337-1343.

Irmay, S., 1954. Solutions of the non-linear diffusion equation with a gravity term in hydrology. IAHS Symposium: Water in the Unsaturated Zone, Wageningen.

Jähne, B. and Haußecker, H., 1998. Air-water gas exchange. Annual Review of Fluid Mechanics, 30: 443-468.

Jurin, J., 1717. An account of some experiments shown before the Royal Society: With an enquiry into the cause of the ascent and suspension of water in capillary tubes. Philosophical Transactions, 30: 739-747.

Jury, W.A., Gardner, W.R. and Gardner, W.H., 1991. Soil Physics. 5th ed., John Wiley & Sons, ISBN: 0-471-83108-5.

Kaluarachchi, J.J. and Parker, J.C., 1987. Effects of hysteresis with air entrapment on water flow in the unsaturated zone. Water Resources Research, 23: 1967-1976.

Klenk, I.D., 2000. Transport of volatile organic compounds (VOC's) from soil-gas to groundwater. Doctoral thesis, Institute for Geoscience, University of Tübingen.

Klenk, I.D. and Grathwohl, P., 2002. Transverse vertical dispersion in groundwater and the capillary fringe. Journal of Contaminant Hydrology, 58: 111-128.

Klump, S., Cirpka, O.A., Surbeck, H. and Kipfer, R., 2008. Experimental and numerical studies on excess-air formation in quasi-saturated porous media. Water Resources Research, 44, W05402, doi: 10.1029/2007WR006280.

Lenhard, R.J. and Parker, J.C., 1987. A model for hysteretic constitutive relations governing multiphase flow, 2. Permeability-saturation relations. Water Ressources Research, 23: 2197-2206.

Li, K., 2010. More general capillary pressure and relative permeability models from fractal geometry. Journal of Contaminant Hydrology, 111(1-4): 13-24.

Liu, S., 2008. Mass transfer of oxygen across the capillary fringe. Doctoral Thesis, Institute for Geoscience, University of Tübingen, 58 p.

Maier, U., Rügner, H. and Grathwohl, P., 2007. Gradients controlling natural attenuation of ammonium. Applied Geochemistry, 22: 2606-2617.

Maraqa, M.A., Wallace, R.B. and Voice, T.C., 1997. Effects of degree of water saturation on dispersivity and immobile water in sandy soil columns. Journal of Contaminant Hydrology, 25: 199-218.

McCarthy, K.A. and Johnson, R.L., 1993. Transport of volatile organic compounds across the capillary fringe. Water Resources Research, 29(6): 1675-1683.

Meinzer, O.E., 1923. Outline of groundwater hydrology, with definitions. U.S. Geological Survey Water Supply Paper, 494.

Mercury, L., Pinti, D.L. and Zeyen, H., 2004. The effect of the negative pressure of capillary water on atmospheric noble gas solubility in ground water and palaeotemperature reconstruction. Earth Planetary Science Letters, 223: 147-161.

Millington, R.J., 1959. Gas diffusion in porous media. Science, 130: 100-102.

Millington, R.J. and Quirk, J.P., 1960. Transport in porous media. 7th International Congress of soil science, Madison, Wisconsin, USA, pp. 97-106.

Moldrup, P., Oleson, T., Schjønning, P., Yamaguchi, T. and Rolston, D.E., 2000. Predicting the gas diffusion coefficient in repacked soil: water-induced linear reduction model. Soil Science Society of America Journal, 64: 1588-1594.

Mualem, Y., 1976. A new model for predicting the hydraulic conductivity of unsaturated porous media. Water Resources Research, 12(3): 513-522.

Nachabe, M.H., 2002. Analytical expressions for transient specific yield and shallow water table drainage. Water Resources Research, 38(10), doi: 10.1029/2001WR001071.

Nernst, W., 1904. Theorie der Reaktionsgeschwindigkeit in heterogenen Systemen. Zeitschrift für Physikalische Chemie, 47(1): 52-55.

Nordstrom, D.K. and Munoz, J.L., 1994. Geochemical Thermodynamics, 2nd ed., Blackwell Scientific Publications, Cambridge.

Olsson, Å. and Grathwohl, P., 2007. Transverse dispersion of non-reactive tracers in porous media: A new nonlinear relationship to predict dispersion coefficients. Journal of Contaminant Hydrology, 92(3-4): 149-161.

Orlob, G.T. and Radhakrishna, G.N., 1958. The effect of entrapped gases on the hydraulic characteristics of porous media. Transactions, American Geophysical Union, 39: 648-659.

Papafotiou, A., 2008. Numerical investigations of the role of hysteresis in heterogeneous two-phase flow systems. Doctoral Thesis, University of Stuttgart, Institute of Hydraulic Engineering.

Parker, J.C., 2003. Physical processes affecting natural depletion of volatile chemicals in soil and groundwater. Vadose Zone Journal, 2: 222-230.

Parker, J.C. and Lenhard, R.J., 1987. A model for hysteretic constitutive relations governing multiphase flow, 1. Saturation-pressure relations, Water Resources Research, 23: 2187-2196.

Parker, J.C., Zhu, J.L., Johnson, T.G., Kremesec, V.J. and Hockman, E.L., 1994. Modeling the free product migration and recovery at hydrocarbon spill sites. Ground Water, 32: 119-128.

Philibert, J., 2005. One and a half century of diffusion: Fick, Einstein, before and beyond. Diffusion Fundamentals, 2: 1.1-1.10.

Rahman, M.M., Liedl, R. and Grathwohl, P., 2004. Sorption kinetics during macropore transport of organic contaminants in soils: laboratory experiments and analytical modeling. Water Resources Research, 40, W01503.

Reid, R.C., Prausnitz, J.M. and Poling, B.E., 1987. The properties of gases and liquids, 4th ed., McGraw-Hill, Inc.

Richards, L.A., 1931. Capillary conduction of liquids through porous mediums. Physics, 1: 318-333.

Rockhold, M.L., Yarwood, R.R., Niemet, M.R., Bottomley, P.J. and Selker, J.S., 2002. Consideration of modeling bacterial-induced changes in hydraulic properties of variably saturated porous media. Advances in Water Resources, 25: 477-495.

Rolle, M., Hochstetler, D., Chiogna, G., Kitanidis, P.K. and Grathwohl, P., 2012. Experimental investigation and pore-scale modeling interpretation of compound-specific transverse dispersion in porous media. Transport in Porous Media, 93(3): 347-362, doi: 10.1007/s11242-012-9953-8.

Saffman, P.G., 1959. A theory of dispersion on porous media. Journal of Fluid Mechanics, 6(3): 321-349.

Sallam, A., Jury, W.A. and Letey, J., 1984. Measurements of gas diffusion coefficient under relatively low air-filled porosity. Soil Science Society of America Journal, 48: 3-6.

Scanlon, B.R., Nicot, J.P. and Massmann, J.W., 2002. Soil gas movement in unsaturated systems. *In* Warwick, A.W. (ed.) Soil Physics Companion, CRC Press, Boca Raton, ISBN: 0-849-30837-2.

Schaap, M.G. and Leij, F.J., 1998. Database-related accuracy and uncertainty of pedotransfer functions. Soil Science, 163(10): 765-779.

Scheidegger, A.E., 1961. General theory of dispersion in porous media. Journal of Geophysical Research, 66(4): 3273-3278.

Scott, D.H., 2000. Soil physics: Agriculture and environmental applications. Wiley-Blackwell, ISBN: 0-813-82087-1.

Sheta, H., 1999. Simulation von Mehrphasenvorgängen in porösen Medien unter Einbeziehung von Hysterese-Effekten. Doctoral Thesis, University of Stuttgart, Institute of Hydraulic Engineering.

Silka, L.R. and Jordan, D.L., 1993. Vapor analysis/extraction. *In* Daniel, D.E. (ed.) Geotechnical Practice for Waste Disposal. Chapman & Hall, London, ISBN: 0-412-35170-6.

Stephens, D.B., 1995. Vadose Zone Hydrology, 1st ed., Boca Raton, Florida: CRC Press.

Stute, M., Forster, M., Frischkorn, H., Serejo, A., Clark, J.F., Schlosser, P., Broecker, W.S. and Bonani, G., 1995. Cooling of tropical Brazil (5 °C) during the Last Glacial Maximum, Science, 269: 379-383.

van Genuchten, M.T., 1980. A closed-form equation for predicting the hydraulic conductivity of unsaturated soils. Soil Science Society of America Journal, 44: 892-898.

Vauclin, M., Haverkamp, R. and Vachaud, G., 1979. Résolution numérique d'une équation de diffusion non-linéare. Presses Université de Grenoble, Grenoble.

Wang, Y., Grove, S.M. and Anderson, M.G., 2008. A physical-chemical model for the static water retention characteristic of unsaturated porous media. Advances in Water Resources, 31: 723-735.

Werner, D., Grathwohl, P. and Höhener, P., 2004. Review of field methods for the determination of the tortuosity and effective gas-phase diffusivity in the vadose zone. Vadose Zone Journal, 3: 1240-1248.

Werner, D. and Höhener, P., 2002. The influence of water table fluctuations on the volatilization of contaminants from groundwater. p. 213–218. *In* Thornton, S.F. and Oswald, S.E. (eds.) Proc. Groundwater Quality 2001: Natural and Enhanced Restoration of Groundwater Pollution, Sheffield, UK. June 2001. IAHS publ. 275.

Werner, D. and Höhener, P., 2003. In situ method to measure effective and sorption-affected gas-phase diffusion coefficients in soils. Environmental Science and Technology, 37(11): 2501-2510.

Williams, M.D. and Oostrom, M., 2000. Oxygenation of anoxic water in a fluctuating water table system: an experiment and numerical study. Journal of Hydrology, 230: 70-85.

Zilch, K., Diederichs, C.J. and Katzenbach, R., 2002. Handbuch für Bauingenieure: Technik, Organisation und Wirtschaftlichkeit – Fachwissen in einer Hand. Springer, Berlin, ISBN: 3-540-65760-6.

3. A High-Resolution Non-Invasive Approach to Quantify Oxygen Transport across the Capillary Fringe and within the Underlying Groundwater

Christina M. Haberer*, Massimo Rolle, Sanheng Liu, Olaf A. Cirpka, Peter Grathwohl
Journal of Contaminant Hydrology (2011), Vol. 122(1-4), pp. 26-39, doi: 10.1016/j.jconhyd.2010.10.006.

Abstract

Oxygen transport across the capillary fringe is relevant for many biogeochemical processes. We present a non-invasive technique, based on optode technology, to measure high-resolution concentration profiles of oxygen across the unsaturated/saturated interface. By conducting a series of quasi two-dimensional flow-through laboratory experiments, we show that vertical hydrodynamic dispersion in the water-saturated part of the capillary fringe is the process limiting the mass transfer of oxygen. A number of experimental conditions were tested in order to investigate the influence of grain size and horizontal flow velocity on transverse vertical dispersion in the capillary fringe. In the same setup, analogous experiments were simultaneously carried out in the fully water-saturated zone, therefore allowing a direct comparison with oxygen transfer across the capillary fringe. The outcomes of the experiments under various conditions show that oxygen transport in the two zones of interest (i.e., the unsaturated/saturated interface and the saturated zone) is characterized by very similar transverse dispersion coefficients. An influence of the capillary fringe morphology on oxygen transport has not been observed. These results may be explained by the narrow grain size distribution used in the experiments, leading to a steep decline in water saturation at the unsaturated/saturated interface and to the absence of trapped gas in this transition zone. We also modeled flow (applying the van Genuchten and the Brooks-Corey relationships) and two-dimensional transport across the capillary fringe, obtaining simulated profiles of equivalent aqueous oxygen concentration that were in good agreement with the observations.

Keywords: *capillary fringe; oxygen transport; hydrodynamic dispersion; 2-D experiments; fiber-optical sensor technique.*

3.1 Introduction

During the past decades, considerable effort has been undertaken to deepen the understanding of the capillary fringe and how it may influence mass transfer between the vadose and the saturated zones. A consistent definition of the capillary fringe is difficult to find in the literature (Berkowitz et al., 2004). Generally, it is considered the transition zone between the unsaturated and the saturated zones, the lower boundary being the groundwater table, at which the water and the atmospheric pressures are identical. The upper boundary is less clearly defined: a rigorous definition limits the capillary fringe to the water-saturated zone directly above the water table, where the water pressure is smaller than the atmospheric pressure due to capillary forces, whereas an extended definition of the capillary fringe includes the tension-saturated zone and the contiguous variably saturated parts above. Referring to the latter description, the capillary fringe reveals gradually decreasing water contents toward higher elevations, eventually reaching field capacity (Caron et al., 1998).

The relationship between water content and matric potential at the interface between the vadose and the saturated zone can be described by several empirical models. Two parameterizations, with numerous modifications, are most commonly used: the Brooks-Corey (1964, 1966) and the van Genuchten (1980) models. Both models are based on the assumption that the volumetric water content θ_{aq} [-] ranges between a minimum, so-called residual water content θ_r [-] and a maximum value θ_s [-], denoted saturated water content, which is identical to the storage-effective porosity. The residual water content is considered to be confined to small pores, which do not necessarily form a continuous network. The effective water saturation S_e [-], ranging between zero and one, normalizes the actual water content θ_{aq} to the scale between θ_r and θ_s:

$$S_e = \frac{\theta_{aq} - \theta_r}{\theta_s - \theta_r} \tag{3.1}$$

The van Genuchten model assumes a gradual change of water content from the water table up to the unsaturated zone until residual saturation is reached, i.e.,

$$\begin{aligned} S_e &= \left(1 + |\alpha h|^n\right)^{-m} && \text{if } h \le 0 \\ S_e &= 1 && \text{if } h > 0 \end{aligned} \tag{3.2}$$

where α [L^{-1}] is the capillary pressure parameter, which can be estimated as the reciprocal value of the capillary fringe height. h [L] is the matric head (difference between air and water pressure heads; a negative quantity above the water table), and n [-] and $m \approx 1\text{-}n^{-1}$ [-] are shape parameters, usually obtained by fitting.

In contrast to the van Genuchten model, the Brooks-Corey model assumes that the soil pores remain fully water-saturated up to some distance above the water table as long as the matric

potential is higher than a critical potential, i.e., the air-entry pressure of the largest pore. Such a fully saturated zone exists in very fine and homogeneous soils (Ronen et al., 1997). The water-retention curve is then described by

$$S_e = \left(\frac{h_b}{h}\right)^{\lambda} \quad \text{if } h \le h_b$$
$$S_e = 1 \quad \text{if } h > h_b \tag{3.3}$$

in which h_b [L] represents the air-entry pressure head or bubbling pressure head. This is approximately the minimum suction in the drainage cycle at which a continuous non-wetting phase (air) exists in a porous medium (Bear and Cheng, 2010). λ [-] is called the pore-size distribution index.

Pedotransfer functions (PTFs) can be used to predict soil hydraulic parameters, e.g., α and n in the van Genuchten model, from easy-to-determine soil variables, such as texture and bulk density (e.g., Carsel and Parrish, 1988; Schaap and Leij, 1998). Bloemen (1977) probably was the first to derive the relationships between the parameters of the Brooks-Corey model and particle-size distribution.

The capillary fringe thickness depends on the pore-size distribution and, thus, on soil type, vertical infiltration rates, fluctuations of the groundwater table (Berkowitz et al., 2004), and the presence of surface-active solutes (Henry and Smith, 2002). Significant lateral flow in the capillary fringe is restricted to the zone of high water content, i.e., below a critical height above the groundwater table (Ronen et al., 1997; Berkowitz et al., 2004).

Vertical mass transfer across the capillary fringe can cause groundwater contamination by volatile compounds (Baehr, 1987; McCarthy and Johnson, 1993), but it may also represent an important mechanism of oxygen supply. The latter process plays a pivotal role for subsurface microbial activity, providing the electron acceptor necessary for aerobic metabolism and influencing the redox potential within the aquifer. Mass transfer in porous media differs from diffusion through free fluids as the presence of solids reduces the cross sectional area and increases the mean path length for compounds transported in soils. In the unsaturated zone, the effective diffusion coefficient additionally takes the volumetric water and gas content into account. With increasing water saturation from the unsaturated zone toward the groundwater, the effective gaseous diffusion coefficient decreases (Affek et al., 1998; Maier et al., 2007). Simultaneously, the horizontal flow velocity increases and hydrodynamic dispersion in the aqueous phase becomes important.

Many experimental and computational studies have been conducted to evaluate longitudinal hydrodynamic dispersion as a function of water saturation and its effect on transport of dissolved compounds (e.g., Elrick and French, 1966; Salter and Mohanty, 1982; De Smedt et al., 1986; Seyfried and Rao, 1987; Sahimi and Imdakm, 1988; Lake, 1989; Sahimi, 1993; Maraqa et al.,

1997; Matsubayashi et al., 1997; Padilla et al., 1999; Nützmann et al., 2002; Toride et al., 2003; Mayer et al., 2008). In case of decreasing water content, higher dispersion coefficients were found, which were attributed to significant increases in the diversity of solute travel times or in the tortuosity of flow at the pore scale. In contrast to that finding, Orlob and Radhakrishna (1958) concluded, from their experimental work using chloride as tracer, that a 10 % increase in gas saturation reduced longitudinal hydrodynamic dispersion by about 50 %. Vanderborght and Vereecken (2007) also pointed out that several studies found lower dispersion coefficients in unsaturated than in saturated systems. Roth and Hammel (1996) demonstrated that the variability of the flow field in heterogeneous soils strongly depends on water content, resulting in minimal longitudinal hydrodynamic dispersion coefficients at intermediate saturations, and elevated dispersion coefficients under very dry conditions.

With regard to the mass transfer of volatile compounds across the capillary fringe, earlier works (e.g., Klenk and Grathwohl, 2002; Liu, 2008) showed that transverse vertical dispersion is essential in experiments conducted at the bench-scale. Klenk and Grathwohl (2002) suggested that flow in the capillary fringe also enhances transverse dispersion due to the presence of entrapped gas bubbles, which lead to more tortuous flow paths. In addition, the gas bubbles act as 'mixing chambers' because of fast diffusion within the gas phase.

The contrasting findings about the role of hydrodynamic dispersion in variably saturated soils and the lack of studies dealing with the mass transfer of volatile compounds across the capillary fringe indicate the need of further investigations directly comparing transverse dispersion at the interface and in the fully water-saturated zone. This is the main objective of the present study. Additionally, we present a non-invasive approach to determine profiles of oxygen concentration across the capillary fringe and in the fully water-saturated zone at the pore-scale resolution. The method is based on an optode technology, in which luminescence within a polymer foil is quenched in the presence of oxygen. We demonstrate the applicability of the proposed method under various conservative and reactive conditions. Analytical solutions of the governing transport equation under different boundary conditions are used to quantitatively interpret the experimental results. Numerical simulations of flow and transport further confirm the results for an illustrative case of oxygen mass transfer across the capillary fringe.

3.2 Experimental Setup

We performed quasi two-dimensional flow-through experiments to study oxygen transport. Recently, such experimental settings have been used to investigate solute transport by high-resolution imaging techniques (e.g., Zinn et al., 2004; Oates and Harvey, 2006; Olsson and Grathwohl, 2007; Catania et al., 2008; Jaeger et al., 2009; Werth et al., 2010), to perform multi-

tracer experiments with different dissolved compounds (Chiogna et al., 2010), and to study coupled mixing and reactive processes including both abiotic (e.g., Cirpka et al., 2006; Rolle et al., 2009) and biodegradation reactions (e.g., Huang et al., 2003; Bauer et al., 2009a and 2009b; Rolle et al., 2010).

In this study, a quasi two-dimensional porous medium setup was specifically designed for the investigation of oxygen transport across the capillary fringe and within the fully water-saturated zone. Figure 3.1 shows a photograph of the flow-through system used.

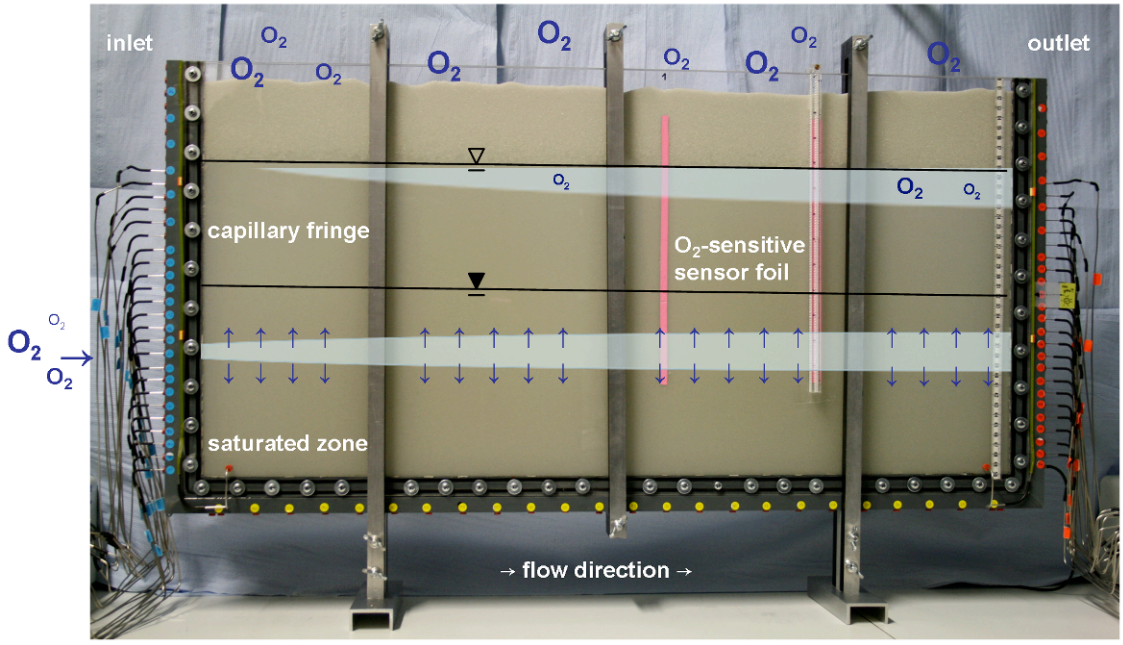

Fig. 3.1. Experimental setup; inner dimensions of the flow-through chamber: 80 cm × 40 cm × 0.5 cm.

The inner dimensions of the chamber were 80 cm × 40 cm × 0.5 cm (length × height × width). Furthermore, the transparent panes at the front and back of the flow-through system were made of acrylic glass with a thickness of 6 mm. Vertical external supports ensured an accurate placing of the glass panes and, therefore, a constant cross-sectional area. Glass beads (Sartorius GmbH, Göttingen, Germany) with grain size diameters of 0.4 - 0.6 mm and 1.0 - 1.5 mm were used as porous medium. During the filling procedure, the water table was slowly raised and constantly maintained above the top of the porous medium in order to avoid entrapment of air bubbles. After the flow-through chamber had been completely packed, the water table was lowered to its final stage such that the top of the capillary fringe was kept below the surface of the porous medium and an unsaturated zone was created in the upper region of the packing (Fig. 3.1).

In order to determine the height of the water table, two piezometers were connected to the porous medium via two holes drilled in the front pane. We also used two 24-channel peristaltic pumps (IPC 24, ISMATEC, Glattbrugg, Switzerland), connected to the inlet and outlet ports of the chamber, to create steady-state horizontal flow. The pumps were operated at constant flow rates

and had been calibrated for each experimental run. The tubing material used for the pumps consisted of Fluran HCA (ISMATEC; inner diameter: 0.64 mm), which is characterized by low gas permeability, thus, minimizing oxygen uptake when oxygen-depleted water is flowing through the tubes. Hollow needles with an inner diameter of 0.9 mm were used to connect the tubing with the flow-through chamber. In order to prevent clogging by the porous medium, the needles were shielded by small stainless steel sieves (0.125 mm mesh size). The inlet and outlet ports of the flow-through chamber were vertically spaced by 12.5 mm.

The experiments were conducted by injecting oxygen-depleted water into the flow-through chamber, which was covered by a lid to prevent considerable evaporation but remained open to the atmosphere. This allowed the mass transfer of oxygen from ambient air across the capillary fringe into the saturated zone. The oxygen-depleted solution was prepared by stripping the necessary volume of Milli-Q water with nitrogen until the measured oxygen concentration was below 0.1 mg L^{-1}. To minimize oxygen contamination, the feed solution was immediately stored in a gastight Tedlar bag (Alltech, Germany), which had been flushed with nitrogen. The oxygen concentration of this reservoir solution was monitored over time by measuring oxygen in a small flow-through cell interconnected in the feeding line.

In order to study oxygen transport in the fully water-saturated zone, we created a plume of high oxygen concentrations by connecting a central inlet port to an air-equilibrated solution of Milli-Q water (see Fig. 3.1). For reference, the oxygen concentration of this solution was also monitored over time using a small flow-through cell.

Rather than placing the oxygen-sensitive material onto the tip of a sensor, we measured oxygen concentrations, both at the interface and in the saturated zone, using two vertical stripes of oxygen-sensitive polymer optode foil (26 cm × 0.5 cm; SP-PtSt3-NAU from PreSens GmbH, Regensburg, Germany). The optode foil had been glued onto the inner side of the front pane of the flow-through chamber and the stripes were placed at distances of 45 cm and 60 cm from the inlet, respectively. Each stripe allowed measuring high-resolution vertical profiles of oxygen concentrations, with more than 100 measurement locations spaced by 2.5 mm. The measurements were performed using an optical fiber (PreSens GmbH, Regensburg, Germany), carrying the excitation and the luminescence light. In doing so, the fiber was located outside the flow-through chamber and was moved stepwise in vertical direction through the different measuring points.

The porosity of the porous medium was determined after each experimental run. For this, a solution of sodium fluorescein (15 mg L^{-1}) was continuously injected into the saturated zone through the same central port that was previously used to create the oxygen-rich plume. An average value of porosity was determined from the mean breakthrough time of the tracer at the outlet and the flow rate.

Reactive experiments were conducted to demonstrate the applicability of the proposed method in the presence of an oxygen-consuming reaction. Here the experimental setup was similar as described before (grain size used: 1.0 to 1.5 mm), except for the dimensions of the flow-through chamber (80 cm × 10 cm × 1 cm, L × H × W; see Liu, 2008). Instead of pure deoxygenated Milli-Q water, a sodium sulfite (Na_2SO_3) solution (8.1×10^{-4} mol L^{-1}) was pumped into the system. The reaction (i.e., the oxidation of sulfite in the presence of dissolved oxygen) was studied in the absence and in the presence of a catalyst. In the latter case Co^{2+} was added in concentrations of 9.1×10^{-5} mol L^{-1} to the prepared sodium sulfite solution. Although the ready oxidation of sulfite is fundamental for the considered instantaneous reactive process, it is disadvantageous with regard to sampling and measurement. In fact, as soon as a water parcel reaches the outlet of the flow-through chamber, the formation of sulfate has to be inhibited to quantify the reactant (i.e., sulfite) and the product (i.e., sulfate) separately. In order to stabilize the sulfite samples during sampling and the subsequent measurement, a formaldehyde/sodium hydroxide solution was used (according to the DIN EN ISO 10304-3:1997). The addition of sodium hydroxide ensures that sulfite is present in its deprotonated form. Formaldehyde adds then to sulfite, so that its reaction to sulfate is considerably retarded, therefore allowing the measurements of the two ionic species. These two ions were measured for mass balance purposes (results not shown), using an ion chromatograph (Dionex).

3.2.1 Non-Invasive Oxygen Measurement

Measurements of oxygen concentrations were performed after establishing steady-state flow conditions, i.e., after the exchange of at least two pore volumes of water. The technique for measuring oxygen is based on the dynamic luminescence quenching of a luminophore by molecular oxygen. Hereby, the luminescent dye molecules are embedded in the oxygen sensitive polymer glued onto the inner side of the front pane. Via an optical fiber the luminophore is excited with sinusoidally modulated light from the outside of the flow-through chamber. In the presence of molecular oxygen the luminescence properties change as energy is transferred from the excited luminophore molecules to oxygen (Klimant et al., 1995). Oxygen passes from its ground state to its excited state and the luminescent dye does not emit light, which decreases the measurable luminescence signal (Huber and Krause, 2006). Thus, the collision between the luminophore in its excited state and the quencher, i.e., oxygen, results in radiationless deactivation.

The luminescence intensity as well as the luminescence decay time are related to the relative oxygen content [O_2] through the Stern-Volmer equation (Stern and Volmer, 1919):

$$\frac{I_0}{I} = \frac{\tau_0}{\tau} = 1 + K_{SV}\left[O_2\right] \tag{3.4}$$

where I, τ and I_0, τ_0 represent the luminescence intensity [-] and the decay time [T] in presence and absence of oxygen, respectively. K_{SV} is the dimensionless Stern-Volmer constant, which quantifies the quenching efficiency and, thus, also the sensitivity of the sensor.

The instrument used in this study measures the luminescence decay time of the immobilized luminophore as the oxygen-dependent parameter (Huber and Krause, 2006). Due to the luminescence decay time of the indicator, there is a shift in phase angle between the emitted light and the excitation signal, which can be expressed as

$$\tan \Theta = 2\pi f_{\mathrm{mod}} \tau \tag{3.5}$$

where Θ [rad] is the phase angle and f_{mod} [T^{-1}] is the modulation frequency of the light source.

Evaluating the luminescence decay time has various advantages compared to conventional intensity measurements. In fact, the luminescence decay time does neither depend on the concentration of the indicator in the sensitive layer nor on the potentially fluctuating intensity of the light source. Moreover, this method allows measuring oxygen concentrations in both the gaseous and the aqueous phases (e.g., Balcke et al., 2004; Huber and Krause, 2006). The technique does not consume any oxygen during the measurement and has a low detection limit for dissolved oxygen in water (0.015 mg L^{-1}) as well as oxygen partial pressures in the gas phase (0.31 hPa; Huber and Krause, 2006).

In the present study, the applicability of the method is extended to the transition zone between the unsaturated and the saturated zones to obtain profiles of equivalent aqueous oxygen concentration resulting from mass transfer from the atmosphere into the oxygen-depleted groundwater. We obtain consistent continuous oxygen profiles regardless of the phases involved as the optode-based measurement technique measures partial pressures rather than concentrations.

To be more precise, because the capillary fringe is characterized by varying water saturation, we need to measure oxygen concentrations in the liquid and gaseous phases simultaneously. Oxygen transfer between the two phases occurs by diffusion. The direction and rate of the oxygen mass flux are controlled by the gradient in chemical potential (Donaldson et al., 1997). In fact, under the experimental conditions of this study, the inter-phase mass transfer can be considered instantaneous compared to the characteristic time of physical transport of dissolved oxygen in the aqueous phase (e.g. Fry et al., 1995; Cirpka and Kitanidis, 2001; Klump et al., 2008). Under local equilibrium conditions the partitioning of oxygen between the two phases is described by Henry's law. While Henry's law states that oxygen concentrations (mass per volume) in the two phases differ even under equilibrium conditions, the partial pressures are identical assuming 100 % humidity in the vadose zone. In porous media this assumption is justified as a result of the complex ramification of the pore system and thus, the comparatively much bigger phase boundaries between water and air compared to their volumes. Under these conditions, the amount of oxygen molecules entering the aqueous system equals the amount leaving it. The measurement value is

then translated into volumetric aqueous concentration, regardless whether the value was measured in the unsaturated or in the saturated zone, or at the interface. This procedure results in a continuous profile of equivalent aqueous oxygen concentration across the capillary fringe. In the following, all values of oxygen concentration are given referring to the liquid phase.

3.3 Modeling Conservative and Reactive Transport

The advection-dispersion equation for conservative, non-volatile solutes in variably saturated porous media reads as

$$\nabla \cdot \left(\theta_{aq} \mathbf{D} \nabla C\right) - \mathbf{q} \cdot \nabla C = \frac{\partial \left(\theta_{aq} C\right)}{\partial t} \tag{3.6}$$

in which **D** [L^2 T^{-1}] represents the dispersion tensor, C [M L^{-3}] is the volumetric concentration of the compound of interest in water, **q** [L T^{-1}] is the specific-discharge vector, and t [T] is the time. Various analytical solutions of Eqn. 3.6 have been derived for simplified cases.

For a compound partitioning between the aqueous and gaseous phases, storage and transport in both phases must be considered. In case of local gas-water equilibrium, the oxygen partial pressure, p_{O2} [Pa], is the same in both phases. In our application, we may safely assume that transport in the gaseous phase is by diffusion only as significant pressure fluctuations and gradients in the unsaturated zone, inducing advective gas flow, can be neglected (see also e.g., Parker, 2003; Atteia and Höhener, 2010). Then, the partial pressure p_{O2} undergoes the following transport equation:

$$\nabla \cdot \left(\mathbf{D}_{tot} \nabla p_{O_2}\right) - \mathbf{q} \cdot \nabla p_{O_2} = \phi \frac{\partial p_{O_2}}{\partial t} \tag{3.7}$$

in which $\mathbf{D}_{tot}$ [L^2 T^{-1}] is a total effective dispersion tensor summarizing the diffusive-dispersive fluxes in both phases, and Φ [-] is the porosity. Expressions for $\mathbf{D}_{tot}$ will be discussed below.

In the following, we determine aqueous dispersion coefficients by fitting analytical solutions of the governing steady-state equation for mass transport in the saturated zone to the measured oxygen concentration profiles in the saturated zone and across the capillary fringe. In the latter case, we also consider a reactive system, described by an instantaneous bimolecular reaction.

3.3.1 Saturated Zone: Conservative Transport under Steady-State Conditions

When a plume of high oxygen concentration (i.e., air-equilibrated) is established in the fully water-saturated, oxygen-depleted zone, the inlet condition can be described as a line source perpendicular to flow. In uniform horizontal flow, the following analytical solution for the steady-

state two-dimensional concentration distribution applies (adapted after Domenico and Palciauskas, 1982):

$$C_{norm}(x,z) = \frac{C - C_{bg}}{C_0 - C_{bg}} = \frac{1}{2}\left\{ erf\left[\frac{(z + Z/2)}{2\sqrt{D_t \frac{x}{v_a}}}\right] - erf\left[\frac{(z - Z/2)}{2\sqrt{D_t \frac{x}{v_a}}}\right]\right\} \quad (3.8)$$

in which C_{norm} [-] is the normalized oxygen concentration, $v_a = q/\theta_s$ [L T^{-1}] is the horizontal seepage velocity, and D_t [L^2 T^{-1}] is the transverse hydrodynamic dispersion coefficient. While C is the measured oxygen concentration at the horizontal and vertical coordinates x [L] and z [L], C_{bg} [M L^{-3}] is the measured background concentration of oxygen. C_0 [M L^{-3}] refers to the oxygen concentration of the air-equilibrated water at the source. In the experimental setup, the source-width Z [L] equals the distance between two consecutive inlet ports.

3.3.2 Capillary Fringe: Conservative Transport under Steady-State Conditions

Similarly to the dissolution of NAPL pools (Johnson and Pankow, 1992; Eberhardt and Grathwohl, 2002), the mass transfer of volatile compounds across the capillary fringe can be treated as diffusion into a semi-infinite medium if the water-saturated thickness is considered much larger than the diffusion length $\sqrt{D_t x / v_a}$. Under steady-state conditions, the capillary fringe can be assumed to represent an upward extension of the water-saturated zone (Liu et al., 2010). At the air-water interface, local equilibrium is reached between the oxygen in the gaseous and aqueous phase according to Henry's law. Since the gaseous-phase transport of oxygen is fast, the aqueous concentration at the top of the capillary fringe remains constant.
Mass transfer across the capillary fringe can then be described by the following analytical equation:

$$C_{norm}(x,z) = \frac{C - C_{bg}}{C_0 - C_{bg}} = erfc\left(\frac{z}{2\sqrt{D_t \frac{x}{v_a}}}\right) \quad (3.9)^*$$

in which C_0 [M L^{-3}] now denotes the oxygen concentration at the air/water interface; and z [L] is the vertical coordinate, with the origin at the top of the fully water-saturated capillary fringe, pointing downward.

*) This solution is derived in detail from the governing transport equation, see Appendix A1.1.

3.3.3 Capillary Fringe: Reactive Transport under Steady-State Conditions

We also measured oxygen profiles across the capillary fringe in a reactive case. An instantaneous bimolecular redox reaction involving two reactive species (i.e., an electron acceptor *A* and an electron donor *B*) may be written as

$$Y_a A + Y_b B \rightarrow C \tag{3.10}$$

in which Y_a and Y_b are the stoichiometric coefficients characterizing the reaction. *C* denotes the reaction product.

An example for an almost instantaneous bimolecular redox reaction is the reaction between oxygen and sulfite, which was used in the reactive experiments. The resulting normalized oxygen concentration profile across the capillary fringe can be described as

$$C_{norm}(x,z) = \frac{C_A}{C_{A0}} = \left(1 + \frac{Y_a}{Y_b}\frac{C_{B0}}{C_{A0}}\right) erfc\left(\frac{z}{2\sqrt{D_t \frac{x}{v_a}}}\right) - \frac{Y_a}{Y_b}\frac{C_{B0}}{C_{A0}} \tag{3.11}$$

in which C_A [M L^{-3}] denotes the measured aqueous concentration of the electron acceptor, in this case oxygen, at the point of interest, C_{A0} [M L^{-3}] is the aqueous concentration of the electron acceptor at the air/water interface, and C_{B0} [M L^{-3}] is the concentration of the electron donor at the inlet.

For the different conservative and reactive experimental setups described above, the transverse hydrodynamic dispersion coefficients were determined by fitting the appropriate analytical solution (i.e., Eqns. 3.8, 3.9, and 3.11) to the measured oxygen concentration profiles. In doing so, an additional fitting parameter was introduced to vertically align the measured and fitted profiles. The value of D_t was obtained by minimizing the sum of the squared differences between the measured and simulated oxygen concentrations.

3.4 Evaluation of the Experimental Results

We measured high-resolution oxygen concentration profiles, both in the saturated zone and in the capillary fringe, under identical hydraulic conditions. Figure 3.2 shows the distribution of oxygen concentration in a conservative experimental run at a distance of x = 45 cm from the inlet of the flow-through chamber. Two typical oxygen profiles, characteristic of both types of oxygen sources, are displayed in the plot. The lower profile is determined by the oxygen plume in the saturated zone and presents a quasi Gaussian shape, which is characteristic of advective-dispersive transport in a homogeneous porous medium. The upper profile was measured for oxygen transport across the capillary fringe. The groundwater table, where the total pressure equals the

atmospheric pressure, corresponds to the pressure head of 0.00 m. Its approximate location was determined using the hydraulic head measurements near the inlet and outlet of the flow-through chamber. At a pressure head of about -0.02 m, the upper boundary of the capillary fringe is indicated by the sharp decrease in oxygen concentrations. No oxygen gradient was detectable in the unsaturated zone (pressure head < -0.02 m) as gas diffusion coefficients are much higher than aqueous diffusion coefficients (by approximately four orders of magnitude; Reid et al., 1987). The results shown in Fig. 3.2 were determined in an experiment with a grain size of 1.0 - 1.5 mm, a porosity of 40.5 % and a seepage velocity of 8.91 m d^{-1}. With the selected coarse grain size, relatively low capillary fringe heights (~ 22 mm) were observed. For experimental runs with finer material, higher capillary fringe heights (e.g. ~ 117 mm for 0.4 - 0.6 mm grain size) resulted from the increased capillary rise in the smaller pores.

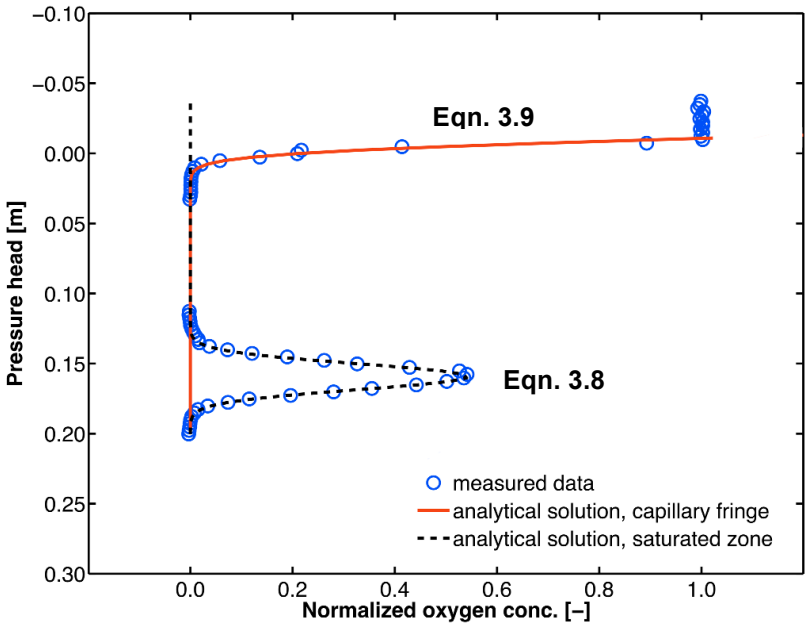

Fig. 3.2. Vertical oxygen concentration profiles at x = 0.45 m during an experimental run with the coarse grain size (1.0 - 1.5 mm) and a seepage velocity of 8.91 m d^{-1}. The pressure head of 0.00 m indicates the location of the water table.

By fitting the analytical solution (Eqn. 3.8) to the normalized concentration profile in the saturated zone, an aqueous D_t-value of 8.10×10^{-9} m^2 s^{-1} was determined. Similarly, applying the same procedure and the appropriate analytical solution (Eqn. 3.9) for oxygen mass transfer across the capillary fringe, a transverse dispersion coefficient of 8.57×10^{-9} m^2 s^{-1} was obtained. The uncertainty of the estimated values of D_t is in the range of ± 10 %, implying practically identical transverse dispersion coefficients in groundwater and in the capillary fringe.

3.4.1 Transverse Dispersion Coefficients in the Capillary Fringe

Transverse hydrodynamic dispersion of oxygen across the capillary fringe was studied in detail by several experimental runs. We investigated the influence of grain size and horizontal flow velocity. In the following sections, we discuss these results and compare conservative with reactive systems.

3.4.1.1 Impact of Grain Size and Seepage Velocity

Figure 3.3 gives an overview of normalized oxygen concentration profiles (measured and simulated) and respective D_t-values obtained using different grain sizes and seepage velocities. These results were derived for the conservative case (i.e., without reactions involving oxygen) at steady state. Figures 3.3a and 3.3b refer to a grain size of 0.4 - 0.6 mm; the lower plots (Figs. 3.3c and 3.3d) show the results obtained for a coarser grain size (1.0 - 1.5 mm).

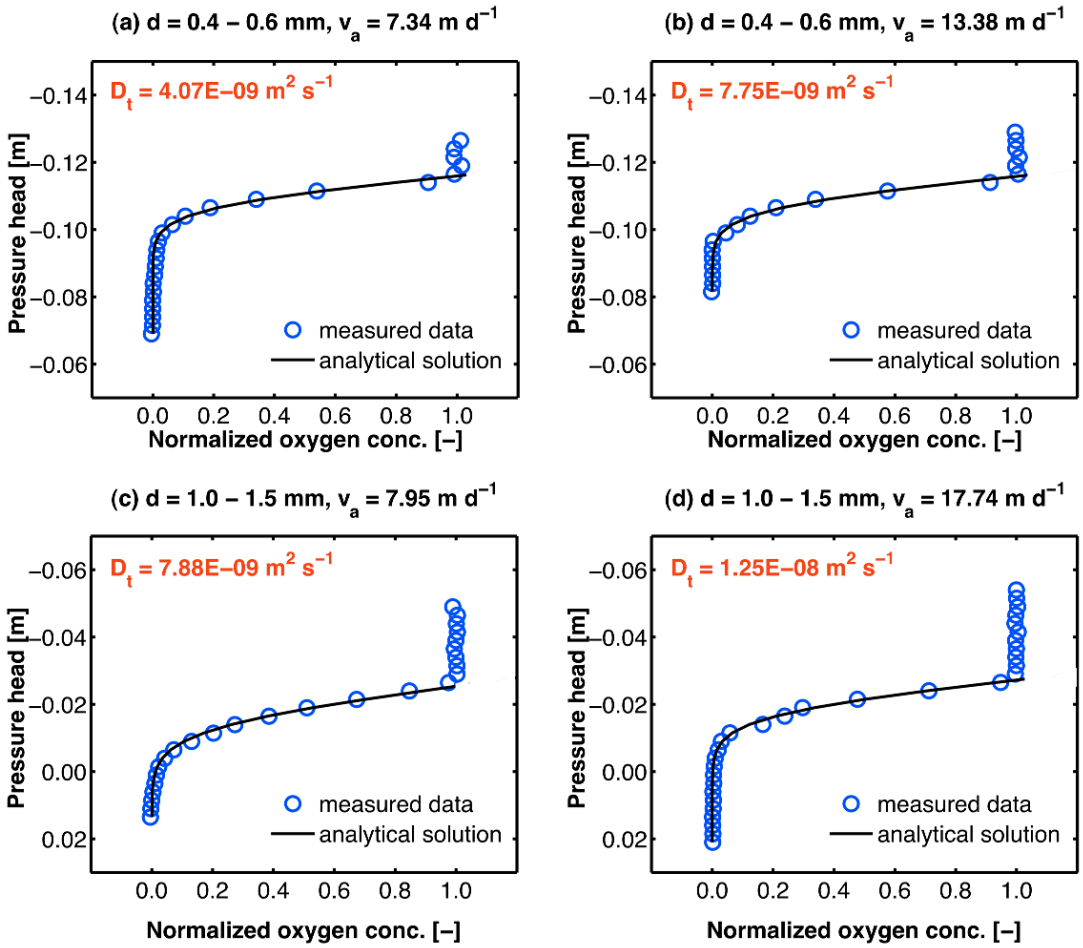

Fig. 3.3. Dependence of vertical oxygen concentration profiles across the capillary fringe on different grain size diameters (d) and seepage velocities (v_a) at x = 0.60 m. The pressure head of 0.00 m indicates the height of the water table.

The experimental results shown in Figs. 3.3a and 3.3c differ exclusively by the grain size. It can be noticed that the penetration depth for the grain size of 1.0 - 1.5 mm is bigger than for the grain size of 0.4 - 0.6 mm; also the value of D_t is by a factor of about two larger (see also Table 3.1). An increase of transverse dispersion coefficients with increasing grain size diameter was also observed in numerous earlier studies focusing on transport in the saturated zone (e.g., de Josselin de Jong, 1958; Grane and Gardner, 1961; Olsson and Grathwohl, 2007).

Rearranging Eqn. 3.9 leads to the following expression:

$$z = 2erfc^{-1}\left(C_{norm}\right)\sqrt{D_t \frac{x}{v_a}} \tag{3.12}$$

where erfc^{-1} is the inverse complementary error function and z is a depth at which a particular value of C_{norm} is found. For C_{norm} = 0.5, the value of erfc^{-1} (C_{norm}) equals 0.477. We consider the corresponding value of z as penetration depth (or boundary layer thickness). Equation 3.12 implies that z is proportional to the square root of the transverse dispersion coefficient. Thus,

$$z_{C_{norm}=0.5} \cong \sqrt{D_t \frac{x}{v_a}} \tag{3.13}$$

For the same values of C_{norm}, x, and v_a, the relative values of penetration depth and D_t for different grain sizes can be directly compared to each other (Eqn. 3.13). Table 3.1 shows that the results for the case described are in very good agreement.

Table 3.1. Comparison between relative values of penetration depth and hydrodynamic transverse dispersion coefficient (D_t) according to Eqn. 3.12.

Figure	Grain size diameter d [mm]	Horizontal flow velocity v_a [m d^{-1}]	Penetration depth z for C_{norm} = 0.5 [m]	D_t [m^2 s^{-1}]	$\frac{z_{0.4-0.6\,mm}}{z_{1.0-1.5\,mm}}$ [-]	$\sqrt{\frac{D_{t,0.4-0.6\,mm}}{D_{t,1.0-1.5\,mm}}}$ [-]
3.3a	0.4 - 0.6	7.34	5.1×10^{-3}	4.07×10^{-9}	0.75	0.72
3.3c	1.0 - 1.5	7.95	6.8×10^{-3}	7.88×10^{-9}		
3.3b	0.4 - 0.6	13.38	5.2×10^{-3}	7.75×10^{-9}	0.91	0.79
3.3d	1.0 - 1.5	17.74	5.8×10^{-3}	1.25×10^{-8}		

The relative value of penetration depth may also scale with the square root of velocity if the latter varies between two experiments (for identical values of x, see Eqns. 3.12 and 3.13). Thus, comparing the results shown in Figs. 3.3b and 3.3d leads to a deviation between the relative values of z and D_t (Table 3.1), as the difference in seepage velocities also has to be considered when calculating the penetration depth.

Considering different horizontal flow velocities with respect to a given grain size (i.e., comparing Figs. 3.3a and 3.3b, or Figs. 3.3c and 3.3d, respectively), it can be noticed that an increase in the seepage velocity leads to an increase in transverse hydrodynamic dispersion coefficients.

3.4.1.2 Comparison between Reactive and Conservative Experiments

In the reactive experiments, we studied the redox reaction of oxygen with sulfite. This reaction can be considerably accelerated in the presence of catalysts such as Fe^{2+}, Cu^{2+}, or Co^{2+}. Linek and Vacek (1981) found that Co^{2+} catalyzes the reaction, when added in concentrations of 10^{-7} to 10^{-4} mol L^{-1}. The reaction can be written as

$$O_2 + 2SO_3^{2-} \xrightarrow{catalyst} 2SO_4^{2-} \quad (3.14)$$

Equation 3.11 has been derived under the assumption of an 'instantaneous' reaction. It can be considered applicable to the reaction used in the experiments, if the mass transfer of oxygen to the reaction site is significantly slower than the reaction itself (Danckwerts, 1970). To test this hypothesis, we compared equivalent aqueous oxygen concentration profiles of two distinct cases: one test with and the other without addition of the catalyst to the sodium sulfite solution. Because the oxygen concentration profile, obtained when no Co^{2+} was added (as $CoCl_2$) to the sodium sulfite solution, does not differ from the case where the catalyst was added in a concentration of 2×10^{-4} mol L^{-1} (see Liu, 2008), we conclude that the time scale for oxygen transport to the reaction site is sufficiently larger than the time scale for the reaction itself, and it is permitted to interpret the experimental results with a model based on an instantaneous bimolecular reaction.

Figure 3.4 shows measured and simulated oxygen concentration profiles for the reactive and conservative cases. For both experiments, a good agreement between the measured concentrations and the fitted analytical profiles (i.e., Eqn. 3.9 and Eqn. 3.11) can be observed. In comparison to the conservative case, the presence of an electron donor causes a sharper concentration gradient because oxygen is consumed. A seepage velocity of 7.33 m d^{-1} was applied in both experiments and oxygen concentration profiles were measured at x = 0.60 m from the inlet. The fitted D_t-value for the reactive case is 6.44×10^{-9} m^2 s^{-1}, similar to the case where no reaction occurred (5.61×10^{-9} m^2 s^{-1}).

In Fig. 3.4, both oxygen profiles show minor limitations by mass transfer above the upper boundary of the capillary fringe. In the conservative case this was observed in some experiments and may be due to slightly higher values of water saturation in this zone. In comparison, a more pronounced oxygen gradient in the unsaturated zone is present for the reactive case. Assuming a similar distribution of water saturation in the conservative and reactive experiments, the more pronounced oxygen gradient in the unsaturated zone is mainly due to the additional consumption of oxygen by the reaction in the underlying capillary fringe, which also causes the significantly lower penetration depth in this zone. As the transverse dispersion coefficients for both cases (i.e., the reactive and the non-reactive) are not significantly different, the mass flux of oxygen across the capillary fringe has to be higher in the reactive than in the conservative case. Thus, the more pronounced oxygen concentration gradient in the unsaturated zone indicates an increased mass flux due to the oxygen-consuming reaction.

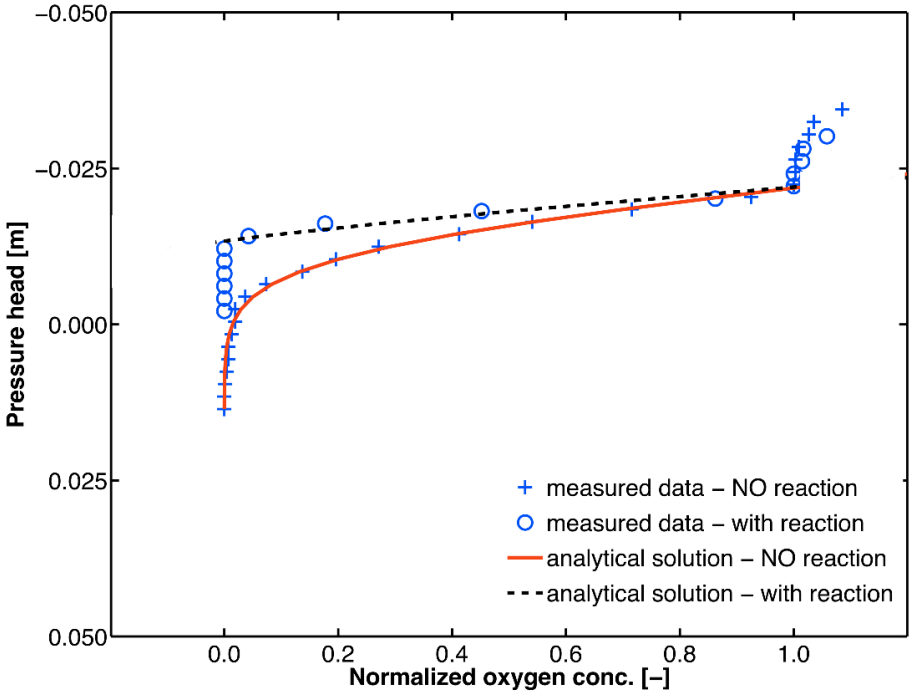

Fig. 3.4. Measured (at x = 0.60 m) and simulated normalized oxygen concentration profiles for conservative (Eqn. 3.9) and reactive (Eqn. 3.11) experiments with a seepage velocity of 7.33 m d^{-1}.

3.4.2 Comparison of D_t-values between the Capillary Fringe and the Saturated Zone

As mentioned above, measuring the oxygen concentration profiles in both regions of interest in the same experimental setup gives the advantage of identical conditions with regard to data evaluation. The experiments were done in duplicate, and in each experimental run the resulting oxygen concentration profiles were measured four to five times. The background concentration of the oxygen-depleted water was also regularly checked and showed average values in a range of 0.82 - 1.34 mg L^{-1}.

Table 3.2 summarizes the flow and transport parameters of all the conservative experiments conducted. The values of D_t represent average values of the measurements taken during the respective experiment and facilitate the direct comparison between the vertical transverse dispersion coefficients in the saturated zone and across the capillary fringe. Additionally, the standard deviation of the respective D_t-measurements is given.

Table 3.2. Parameters and results of the conservative experiments at steady state.

Grain size diameter d [mm]	Horizontal flow velocity v_a [m d^{-1}]	Porosity Φ [%]	D_t determined ± standard deviation ×10^{-9} [m^2 s^{-1}]
Mass transfer across the capillary fringe			
0.4 - 0.6	7.10	39.7	4.39 ± 0.68
	7.04	39.7	4.92 ± 0.61
	13.02	39.7	7.86 ± 0.22
	13.53	39.7	8.18 ± 0.90
1.0 - 1.5	8.81	40.5	7.59 ± 0.70
	7.92	41.3	8.10 ± 0.54
	16.16	40.5	11.3 ± 1.01
	17.20	41.3	12.2 ± 0.57
Mass transfer in the saturated zone			
0.4 - 0.6	7.10	39.7	4.69 ± 0.42
	7.04	39.7	5.34 ± 0.35
	13.02	39.7	7.55 ± 0.19
	13.53	39.7	7.73 ± 0.38
1.0 - 1.5	8.81	40.5	8.17 ± 0.40
	7.92	41.3	7.38 ± 0.15
	16.16	40.5	11.8 ± 0.51
	17.20	41.3	11.1 ± 0.56

In Fig. 3.5, the complete experimental dataset is graphically represented in a normalized plot (i.e., D_t/D_{aq} as a function of the dimensionless Péclet number, *Pe*). D_{aq} [L^2 T^{-1}] denotes the aqueous diffusion coefficient of oxygen, which is 1.97×10^{-9} m^2 s^{-1} at 22 °C (for further reference, see Cussler, 1984; Atkins, 1990; Worch, 1993). The grain Péclet number, *Pe*, is defined as

$$Pe = \frac{v_a d_c}{D_{aq}} \tag{3.15}$$

in which d_c [L] is the characteristic length of a pore channel, represented by the average grain size diameter, d [L].

The plot also displays the non-linear relationship between the transverse dispersion coefficient and the seepage velocity, which was found in an earlier study conducted by Chiogna et al. (2010), i.e.,

$$D_t \approx D_p + v_a \frac{d}{\sqrt{Pe + 123}} \tag{3.16}$$

where D_p [L^2 T^{-1}] is the pore diffusion coefficient. Its value can be approximated under water-saturated conditions by

$$D_p = \phi D_{aq} \tag{3.17}$$

The model described in Eqn. 3.16 is a modification of an expression derived by Bear and Bachmat (1967) and has been tested by Chiogna et al. (2010) in laboratory settings similar to those used in the present study. Figure 3.5 shows a comparison between our findings, obtained for transport

across the capillary fringe and within the saturated zone, and the expression derived by Chiogna et al. (2010) for fully water-saturated conditions. As already discussed in Section 3.4.1.1, the transverse vertical hydrodynamic dispersion coefficient (D_t) across the capillary fringe increases with increasing horizontal flow velocity and with increasing grain size.

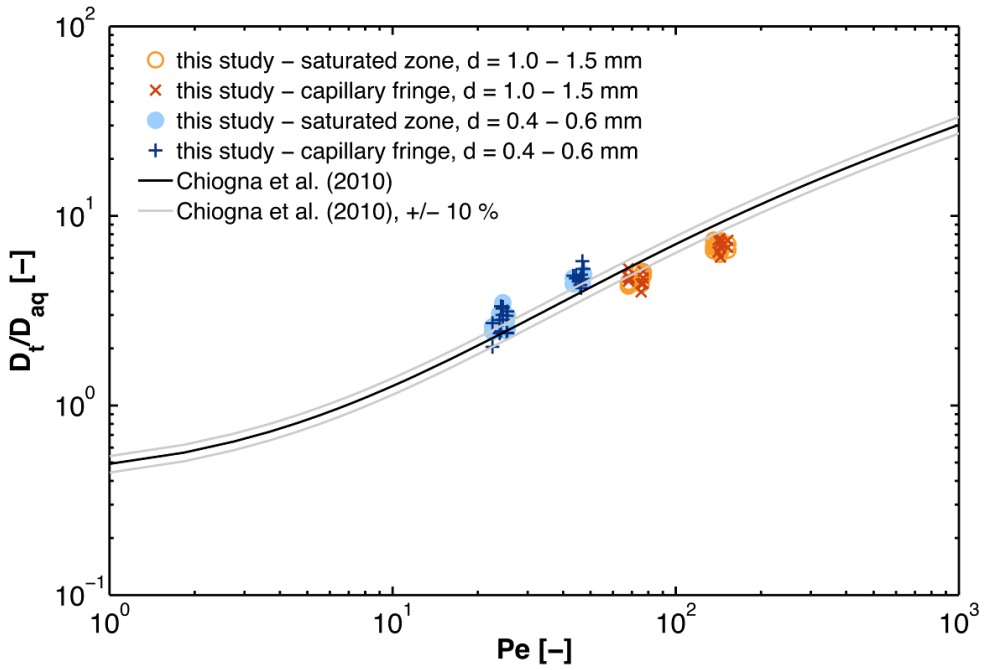

Fig. 3.5. Normalized representation of D_t-values determined for mass transfer of oxygen in the saturated zone and across the capillary fringe during conservative experiments under steady-state conditions. The relationship from Chiogna et al. (2010, Eqn. 3.16) was derived from a dataset of oxygen, fluorescein and bromide measurements exclusively taken in the saturated zone using a grain size of 0.50 - 0.75 mm.

The data collected in this study (Table 3.2 and Fig. 3.5) suggest that the D_t-values derived from oxygen concentration profiles measured in the saturated zone and across the capillary fringe are essentially the same provided the horizontal flow velocity and the grain size are identical. This finding demonstrates that mass transfer at the interface and in the saturated zone are both limited by diffusion in the aqueous phase. Our experimental results also agree with common intuition about inter-phase mass transfer: Transport of oxygen across the capillary fringe should be fast in the gaseous phase, because of the high gaseous-phase diffusion coefficient, and be limited on the water-side, where diffusion is very slow. Therefore, it is a valid assumption to treat the capillary fringe as an upward extension of the water-saturated zone (Liu et al., 2010) as it was done in the derivation of Eqns. 3.9 and 3.11.

This assumption is also substantiated by a visual inspection of the capillary fringe morphology as depicted in Fig. 3.6. The picture was taken placing a homogeneous light source behind the flow-through chamber such that the intensity of the transmitted light is an indicator of water saturation, with light colors indicating high water saturation (Rezanezhad et al., 2006). In sediments or artificial

porous media of uniform grain size and mineralogy, e.g., uniformly sized sand or glass beads, the water content in the capillary fringe can be an abrupt step function of height above the water table (where pressure head is zero). In such an idealized case, the water content profile would also be independent of sampling location within the studied field (Ronen et al., 1997).

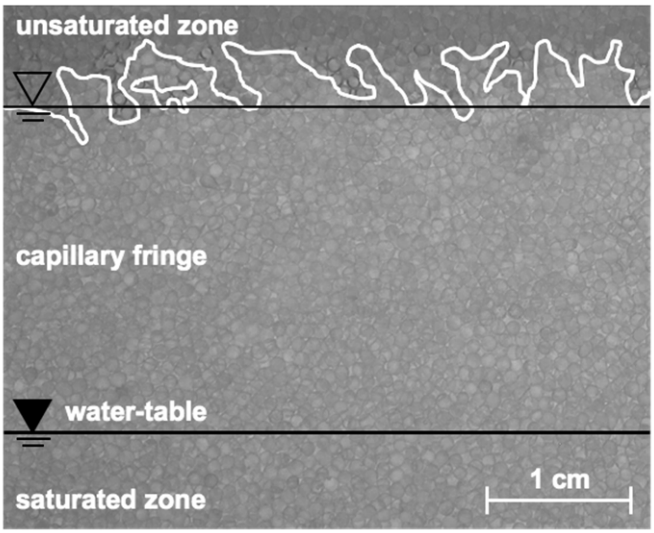

Fig. 3.6. Capillary fringe morphology under steady-state conditions, here shown for a grain size of 1.0 - 1.5 mm.

In Fig. 3.6, the upper edge of the capillary fringe seems to deviate from this idealized case of an abrupt step function. However, the transition zone is very narrow and water content drops from presumably fully water-saturated to unsaturated conditions over a small vertical distance. Gas diffusion is the dominant factor for transport in the gaseous phase. Thus, the mass transport of oxygen in the capillary fringe becomes only limited when water saturation is already very high. These reasons considerably limit the effective vertical extent of the transition zone, in which entrapped gas is present and where the mass transport of oxygen is relevant. Hence, referring to the experimental setup of this study, the upper boundary of the capillary fringe can be considered a horizontal line, and the pore space within the capillary fringe is fully water-saturated. No entrapped gas can be observed in the region below the top of the capillary fringe (Fig. 3.6). Thus, for the water-retention curve, we assume that the relationship between water content and matric potential can be adequately described by the Brooks-Corey model or by an appropriate van Genuchten parameterization.

The absence of trapped gas in the capillary fringe region minimizes the error in estimating the transverse vertical dispersion coefficient by assuming a constant horizontal flow velocity with depth (Atteia and Höhener, 2010). In cases where the structure of the porous medium allows a more efficient entrapment of air, the effective hydraulic conductivity is reduced. Therefore, the horizontal flow velocity in the capillary fringe can be significantly lower than in the saturated zone and thus, smaller values of transverse dispersion are expected. This decreasing effect, however, may be counterbalanced by the enhanced tortuosity due to entrapped air. In the present work (see Fig.

3.5), the observed small differences between the dispersion coefficients in the saturated zone and the capillary fringe can be attributed to measurement inaccuracies rather than changes in groundwater flow velocity with depth.

3.4.3 Interplay between Water Content, Total Effective Dispersion, and O_2-Concentration

In the following, we use a modeling approach to interpret experimental data and to further illustrate how the mass transport of oxygen across the capillary fringe becomes limited as a result of an increase in water saturation. As an example, we investigate the interplay between the water content, the total effective dispersion coefficient, and the profile of equivalent aqueous oxygen concentration for an experiment conducted using a grain size of 0.4 - 0.6 mm. A horizontal groundwater flow velocity of 1.94 m d^{-1} had been established before steady-state oxygen concentration profiles were measured. The van Genuchten and the Brooks Corey models (Eqns. 3.2 and 3.3) are considered here to derive the water saturation profile.

We estimated the van Genuchten parameters with the computer program ROSETTA (Schaap et al., 2001). It assembles five different hierarchical PTFs, which allow us to determine the van Genuchten water-retention parameters using limited (textural classes only) to more extended (texture, bulk density, and one or two water retention points) input data (Schaap et al., 2001). The simplest model (H1) is a class PTF, consisting of a lookup table that provides parameter averages for each USDA textural class. In Table 3.3, the values for sand with a grain size diameter between 0.05 and 2.00 mm (according to the respective range of the USDA soil textural classification system) are given. For large values of capillary pressure head, h_c [L], the resulting van Genuchten parameters, α and n, are related to the corresponding Brooks-Corey parameters, h_b and λ, by (e.g., Webb, 2006)

$$h_b \approx \alpha^{-1} \qquad \text{for } (\alpha h_c)^n >> 1 \tag{3.18}$$

and

$$\lambda \approx n - 1 \qquad \text{for } (\alpha h_c)^n >> 1 \tag{3.19}$$

Note that in Eqns. 3.18 and 3.19 the matric head h (Eqn. 3.2) is replaced by the positive quantity h_c. The estimated van Genuchten and Brooks-Corey parameters for this study are also listed in Table 3.3. θ_r is chosen in accordance to the suggested range of the ROSETTA computer program. The value of θ_s equals the porosity determined at the end of the experiment. A first approximation of h_b, and thus α, is also experimentally given by the height of the capillary fringe. n and λ are fitted to the observed water saturation profile shown in Fig. 3.7b. The significant deviation from the parameter range of n and λ given by the ROSETTA model might be explained by the relatively

homogeneous packing of glass beads used. The assumed water content profiles are shown in Fig. 3.7c.

Table 3.3. Overview of ROSETTA class average hydraulic parameters for sand (grain size diameter of 0.05 - 2.00 mm, according to the USDA soil textural classification system) and estimated van Genuchten and Brooks-Corey parameters used in this study.

van Genuchten-Model (1980)	Residual volumetric water content θ_r ± standard deviation [-]	Saturated volumetric water content θ_s ± standard deviation [-]	$\log_{10}(\alpha)$ ± standard deviation [cm^{-1}]	$\log_{10}(n)$ ± standard deviation [-]
ROSETTA (H1)	0.053 ± 0.029	0.375 ± 0.055	-1.453 ± 0.25	0.502 ± 0.18
this study: diam.: 0.4 - 0.6 mm	0.082	0.355	-1.100	1.554
Brooks-Corey-Model (1964)	Residual volumetric water content θ_r ± standard deviation [-]	Saturated volumetric water content θ_s ± standard deviation [-]	Air-entry pressure head h_b [cm]	Pore size distribution index λ [-]
ROSETTA (H1)[1)]	0.053 ± 0.029	0.375 ± 0.055	33.24 ± 17.24	2.454 ± 1.355
this study: diam.: 0.4 - 0.6 mm	0.082	0.355	11.40	12.808

1) the van Genuchten parameters given by the ROSETTA model are transferred into the corresponding Brooks-Corey parameters using Eqns. 3.18 and 3.19.

From the profile of water content $\theta(h_c)$ and the seepage velocity, v_a, in the water-saturated domain, we estimate the profiles of the unsaturated horizontal seepage velocity and the dispersion coefficients. Starting point, is the estimation of the relative permeabilities, $k_{r,i}$ [-], for water in the unsaturated zone by the following commonly used expressions:

$$k_{r,vG} = S_e^{0.5}\left(1-\left(1-S_e^{m^{-1}}\right)^m\right)^2 \qquad \text{for the van Genuchten model}$$
$$k_{r,BC} = S_e^{\frac{2+3\cdot\lambda}{\lambda}} \qquad \text{for the Brooks-Corey model} \tag{3.20}$$

in which index *i* relates to the chosen soil water-retention model.

From this the respective depth-dependent profiles of horizontal groundwater flow velocity, $v_{a,i}$ [L T^{-1}], are computed by

$$v_{a,i}(h_c) = \frac{k_{r,i}(h_c)}{\theta_{\text{aq}}}\phi v_a \tag{3.21}$$

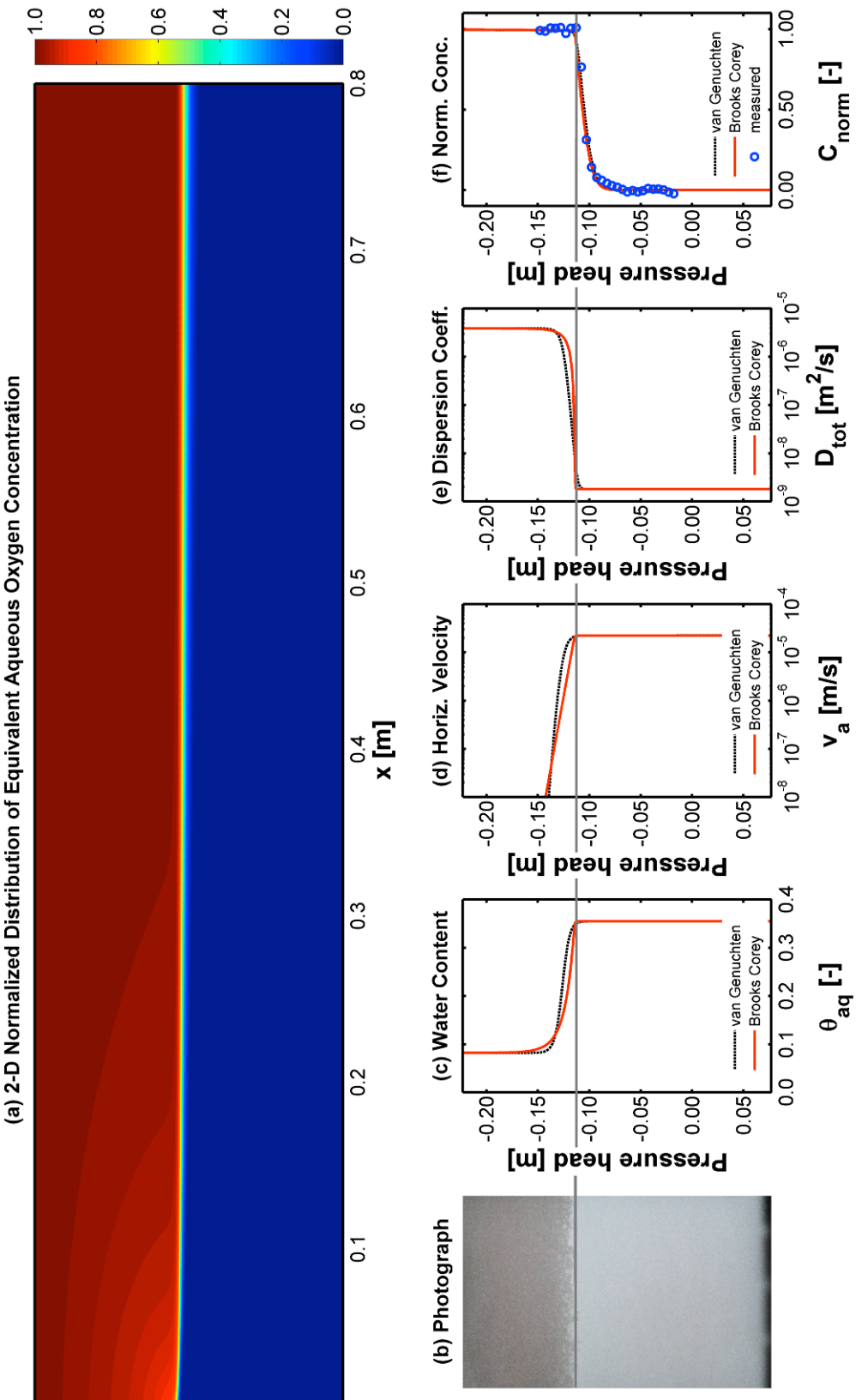

Fig. 3.7. (a) Simulated normalized distribution of equivalent aqueous oxygen concentration. (b) Detailed view of the interface zone in the experimental setup. (c)-(f) Interplay between (c) water content, (d) horizontal flow velocity, (e) total effective dispersion (D_{tot}), and (f) normalized equivalent aqueous oxygen concentration. The horizontal line marks the beginning of the steep decline in oxygen concentration.

Using the selected soil hydraulic parameters (Table 3.3) and neglecting diffusion of oxygen in the aqueous phase, we can estimate the total effective dispersion coefficients for the system considered by

$$\mathbf{D}_{tot} = \theta_g S_g^{7/3} \phi^{1/3} \mathbf{D}_g + \theta_{aq} \mathbf{D}_{mech} \tag{3.22}$$

in which θ_g [-] is the volumetric gas content and S_g [-] denotes the saturation of the gaseous phase. $\mathbf{D}_g$ [L^2 T^{-1}] is the free air diffusion coefficient, expressed as diagonal tensor and $\mathbf{D}_{mech}$ [L^2 T^{-1}] represents the mechanical dispersion tensor. To describe the effective diffusion coefficient in the gaseous phase, the correction of Millington (1959) was implemented into Eqn. 3.22. The resulting profiles of the vertical component of $\mathbf{D}_{tot}$ are plotted in Fig. 3.7e.

We computed the steady-state two-dimensional distribution of equivalent aqueous oxygen concentration C by simulating the steady-state version of Eqn. 3.7 with the Finite Element Method using bilinear elements and the streamline-upwind Petrov-Galerkin (SUPG) for stabilization (Brooks and Hughes, 1982). We assume that the velocity profile varies only in the vertical direction and remains constant in the horizontal one. The normalized oxygen concentration in the inflow at the left-hand side boundary is assumed zero, whereas the normalized equivalent aqueous oxygen concentration at the top of the domain is fixed to unity. Additionally, the oxygen flux at the bottom boundary is zero and the flux at the right-hand side boundary is restricted to the advective component. The length of the simulated domain is 80 cm, but the normalized profiles of equivalent aqueous oxygen concentration shown in Fig. 3.7f together with the measured data are at x = 0.6 m. This procedure also facilitates to plot the approximated normalized oxygen concentration distribution across the flow-through chamber as shown in Fig. 3.7a.

With increasing depth, the water saturation increases, whereas the effective gaseous diffusion coefficient, and thus the total effective dispersion coefficient, decreases. At the same time, the horizontal flow velocity increases and transverse vertical dispersion becomes important in mass transfer of oxygen (Eqn. 3.22). As soon as the water saturation is high enough to inhibit gaseous oxygen to diffuse freely in the pore space, D_{tot} is significantly decreased and the oxygen concentration gradient starts to develop rapidly. This is depicted in Fig. 3.7 by the horizontal line marking the beginning of the steep decline in equivalent aqueous oxygen concentrations.

3.5 Summary and Conclusions

This study focused on the mass transport of oxygen across the interface between the unsaturated and the saturated zones and within groundwater. The experiments were carried out in homogeneous porous media with relatively uniform grain sizes. We applied a non-invasive technique to measure profiles of equivalent aqueous oxygen concentration at high spatial (vertical)

resolution at distinct cross-sections. The oxygen concentrations were measured directly inside the porous medium without disturbing the flow field. For these characteristics, the proposed experimental approach presents a clear advantage compared to conventional sampling techniques at the outlet ports of bench-scale flow-through systems. Moreover, the technique is easy to apply and several measurements can be performed in considerably shorter time periods compared to traditional chemical analysis of tracer concentrations of samples withdrawn at the outlet ports.

We performed a series of experiments to investigate the effectiveness of mass transfer processes and, in particular, to determine the values of transverse hydrodynamic dispersion coefficients under various experimental conditions. The results, obtained from the evaluation of many high-resolution vertical profiles of equivalent aqueous oxygen concentration suggest that no significant difference exists between transverse hydrodynamic dispersion across the capillary fringe and within the saturated zone. The finding of the same D_t-values for the two cases, under the same experimental conditions, clearly indicates the limitation exerted by transport in the aqueous phase to the overall mass transfer of oxygen. We have compared the results of this study to the non-linear relationship between the transverse dispersion coefficient and the seepage velocity of Chiogna et al. (2010) for the mass transport of oxygen in the saturated zone. The two datasets show similar dependence of the transverse dispersion coefficients on porous medium's grain size and seepage velocity. The results were further confirmed by numerical modeling of flow and transport, which emphasized that in fact, the steep gradient in the vertical profile of equivalent aqueous oxygen concentration starts to develop when water saturation is very high.

It is widely hypothesized that the active horizontal and vertical flow and transport processes within the capillary fringe make this zone highly active in terms of physico-chemical and microbiological processes (Barber et al., 1990; Kerfoot, 1994; Berkowitz et al., 2004; Maier and Grathwohl, 2005; Barth et al., 2005). We have investigated oxygen because it is the most important electron acceptor in the capillary fringe and shallow groundwater transferred by vertical dispersion. The outcomes of this study show that steep gradients may exist in the capillary fringe region, which however also apply to the saturated zone. This implies that the capillary fringe is not different from other regions in aquifers, if strong microbial activity is attributed to regions where steep physico-chemical gradients exist. Other processes such as the presence of physical heterogeneities may enhance dispersion of oxygen in the transition zone between the saturated and the unsaturated zone, especially if the groundwater table fluctuates. Such conditions could lead to significant capillary barrier effects and entrapment of air, which potentially increases oxygen transfer, dispersion and therefore mixing of reaction partners. The proposed method can be extended to study such processes in more complex flow-through systems. These investigations will help to deepen our quantitative understanding of flow and transport processes in the capillary fringe.

Acknowledgement

This study was funded by the DFG (German Research Foundation) through the Research Group FOR 831 'Dynamic Capillary Fringes: A Multidisciplinary Approach' (grant GR971/22-1).

References

Affek, H.P., Ronen, D. and Yakir, D., 1998. Production of CO_2 in the capillary fringe of a deep phreatic aquifer. Water Resources Research, 34: 989-996.

Atkins, P.W., 1990. Physical Chemistry. Oxford: Oxford University Press.

Atteia, O. and Höhener, P., 2010. Semianalytical model predicting transfer of volatile pollutants from groundwater to the soil surface. Environmental Science and Technology, 44(16): 6228-6232, doi: 10.1021/es903477f.

Baehr, A.L., 1987. Selective transport of hydrocarbons in the unsaturated zone due to aqueous and vapor-phase partitioning. Water Resources Research, 23(10): 1926-1938.

Balcke, G.U., Turunen, L.P., Geyer, R., Wenderoth, D.F. and Schlosser, D., 2004. Chlorobenzene biodegradation under consecutive aerobic-anaerobic conditions. FEMS Microbiology Ecology, 49(1): 109-120.

Barber, C., Davis, G.B., Briegel, D. and Ward, J.K., 1990. Factors controlling the concentration of methane and other volatiles in groundwater and soil gas around a waste site. Journal of Contaminant Hydrology, 5(2): 155-170.

Barth, J.A.C., Kappler, A., Piepenbrink, M., Werth, C.J., Regenspurg, S., Semprini, L., Slater, G.F., Schüth, C. and Grathwohl, P., 2005. New challenges in biogeochemical gradient research. EOS, 86: 44 1 November 2005.

Bauer, R.D., Rolle, M., Bauer, S., Eberhardt, C., Grathwohl, P., Kolditz, O. and Meckenstock, R.U., 2009a. Enhanced biodegradation by hydraulic heterogeneities in petroleum hydrocarbon plumes. Journal of Contaminant Hydrology, 105: 56-68.

Bauer, R.D., Rolle, M. Kürzinger, P., Grathwohl, P., Meckenstock R.U. and Griebler, C., 2009b. Two-dimensional flow-through microcosms: Versatile test systems to study biodegradation processes in porous aquifers. Journal of Hydrology, 369(3-4): 284-295.

Bear, J. and Bachmat, Y., 1967. A generalized theory on hydrodynamic dispersion in porous media. I.A.H.S Symp. Artificial Recharge and management of aquifers, Haifa, Israel IASH, P.N., 72: 7-16.

Bear, J. and Cheng, A.H.-D., 2010. Modeling groundwater flow and contaminant transport, 23rd Volume. Springer, New York.

Berkowitz, B., Silliman, S.E. and Dunn, A.M., 2004. Impact of the capillary fringe on local flow, chemical migration, and microbiology. Vadose Zone Journal, 3(2): 534-548.

Bloemen, G.W., 1977. Calculation of capillare conductivity and capillare rise from grain size distribution. ICW Wageningen nota no. 952, 962,990, 1013.

Brooks, R.H. and Corey, A.T., 1964. Hydraulic properties of porous media. Hydrology paper, Colorado State University, Ft. Collins

Brooks, R.H. and Corey, A.T., 1966. Properties of porous media affecting fluid flow. Journal of the Irrigation and Drainage Division, ASCE, Vol. 92, No. IR2, pp. 61-87.

Brooks, A.N. and Hughes, T.J.R., 1982. Streamline upwind/Petrov-Galerkin formulations for convection dominated flows with particular emphasis on the incompressible Navier-Stokes equations. Computer Methods in Applied Mechanics and Engineering, 32(1-3): 199-259.

Caron, F., Manni, G., Workman, W.J.G., 1998. A large-scale laboratory experiment to determine the mass transfer of CO_2 from a sandy soil to moving groundwater. Journal of Geochemical Exploration, 64(1-3): 111-125.

Carsel, R.F. and Parrish, R.S., 1988. Developing joint permeability distributions of soil water retention characteristics. Water Resources Research, 24(5): 755-769.

Catania, F., Massabò, M., Valle, M., Bracco, G. and Paladino O., 2008. Assessment of quantitative imaging of contaminant distributions in porous media. Experiments in Fluids, 44: 167-177, doi 10.1007/s00348-007-0388-x.

Chiogna, G., Eberhardt, C., Grathwohl, P., Cirpka, O.A. and Rolle, M., 2010. Evidence of compound dependent hydrodynamic and (hydro)mechanical transverse dispersion with multi-tracer laboratory experiments. Environmental Science and Technology, 44(2): 688-693, doi: 10.1021/es9023964.

Cirpka, O.A. and Kitanidis, P.K., 2001. Transport of volatile compounds in porous media in the presence of a trapped gas phase. Journal of Contaminant Hydrology, 49: 263-285.

Cirpka, O.A., Olsson, Å., Ju, Q., Rahman, M.A. and Grathwohl, P., 2006. Determination of transverse dispersion coefficients from reactive plume lengths. Ground Water, 44: 212-221.

Cussler, E.L., 1984. Diffusion: Mass transfer in fluid systems. New York: Cambridge University Press.

Danckwerts, P.V., 1970. Gas-Liquid reactions. New York: McGraw-Hill Book Company.

de Josselin de Jong G., 1958. Longitudinal and transverse diffusion in granular deposits. Transactions, American Geophysical Union, 39: 67-74.

De Smedt, F., Wauters, F. and Sevilla, J., 1986. Study of tracer movement through unsaturated sand. Journal of Hydrology, 85: 169-181.

Domenico, P.A. and Palciauskas, V.V., 1982. Alternative boundaries in solid waste management. Ground Water, 20: 303-311.

Donaldson, J.H., Istok, J.D., Humphrey, M.D., O'Reilly, K.T., Hawelka, C.A. and Mohr, D.H., 1997. Development and testing of a kinetic model for oxygen transport in porous media in the presence of trapped gas. Ground Water, 35(2): 270-279.

Eberhardt, C. and Grathwohl, P., 2002. Time scales of pollutants dissolution from complex organic mixtures: blobs and pools. Journal of Contaminant Hydrology, 59: 45-66.

Elrick, D.E. and French, L.K., 1966. Miscible displacement patterns in disturbed and undisturbed soil cores. Soil Science Society of America Proceedings, 30: 153-155.

Fry, V.A., Istok, J.D., Semprini, L., O'Reilly, K.T. and Buscheck, T.E., 1995. Retardation of dissolved oxygen due to a trapped gas phase in porous media. Ground Water, 33(3): 391-398.

Grane, F.E. and Gardner, G.H.F., 1961. Measurements of transverse dispersion in granular media. Journal of Chemistry and Engineering Data, 6: 283-287.

Henry, E.J., Smith J.E., 2002. The effect of surface-active solutes on water flow and contaminant transport in variably saturated porous media with capillary fringe effects. Journal of Contaminant Hydrology, 56: 247-270.

Huang, W.E., Oswald, S.E., Lerner, D.N., Smith, C.C. and Zheng, C.M., 2003. Dissolved oxygen imaging in a porous medium to investigate biodegradation in a plume with limited electron acceptor supply. Environmental Science and Technology, 37(9): 1905-1911.

Huber, C. and Krause, C., 2006. Instruction manual Fibox 3. PreSens GmbH, Regensburg, Germany, 85 p.

Jaeger, S., Ehni, M., Eberhardt, C., Rolle, M., Grathwohl, P., Gauglitz, G., 2009. CCD camera analysis for mapping solute concentrations in saturated porous media. Analytical and bioanalytical chemistry, 395(6): 1867-1876.

Johnson, R.L. and Pankow, J.F., 1992. Dissolution of dense chlorinated solvents into groundwater, 2: Source functions of pools of solvent. Environmental Science and Technology, 26: 896-901.

Kerfoot, H.B., 1994. In situ determination of the rate of unassisted degradation of saturated-zone hydrocarbon contamination. Journal of the Air and Waste Management Association, 44: 877-880.

Klenk, I.D. and Grathwohl, P., 2002. Transverse vertical dispersion in groundwater and the capillary fringe. Journal of Contaminant Hydrology, 58(1-2): 111-128.

Klimant, I., Meyer, V. and Kuhl, M., 1995. Fiberoptic oxygen microsensors: A new tool in aquatic biology. Limnology and Oceanography, 40(6): 1159-1165.

Klump, S., Cirpka, O.A., Surbeck, H. and Kipfer, R., 2008. Experimental and numerical studies on excess-air formation in quasi-saturated porous media. Water Resources Research, 44(5).

Lake, L.W., 1989. Enhanced oil recovery. New Jersey: Prentice Hall.

Linek, V. and Vacek, V., 1981. Chemical engineering use of catalyzed sulfite oxidation kinetics for the determination of mass transfer characteristics of gas-liquid contactors. Chemical Engineering Science, 36: 1747-1768.

Liu, S., 2008. Mass transfer of oxygen across the capillary fringe. Doctoral Thesis, Institute for Geoscience, University of Tübingen.

Liu, S., Liedl, R. and Grathwohl, P., 2010. Simple analytical solutions for oxygen transfer into anaerobic groundwater. Water Resources Research, 46, W10542, doi: 10.1029/2009WR008434.

Maier, U. and Grathwohl, P., 2005. Natural attenuation in the unsaturated zone and shallow groundwater: Coupled modeling of vapor phase diffusion, biogeochemical processes and transport across the capillary fringe. *In* Nützmann, G., Viotti, P. and Aagard, P. (eds.) Reactive transport in soil and groundwater. Springer, pp. 141-155.

Maier, U., Rügner, H. and Grathwohl, P., 2007. Gradients controlling natural attenuation of ammonium. Applied Geochemistry, 22: 2606-2617.

Maraqa, M.A., Wallace, R.B. and Voice, T.C., 1997. Effects of degree of water saturation on dispersivity and immobile water in sandy soil columns. Journal of Contaminant Hydrology, 25: 199-218.

Matsubayashi, U., Devkota, L.P. and Takagi, F., 1997. Characteristics of the dispersion coefficient in miscible displacement through a glass beads medium. Journal of Hydrology, 192: 51-64.

Mayer, A., Sandman, T. and Breidenbach, M., 2008. Effect of flow regime on physical nonequilibrium transport in unsaturated porous media. Vadose Zone Journal, 7(3): 981-991.

McCarthy, K.A. and Johnson, R.L., 1993. Transport of volatile organic compounds across the capillary fringe. Water Resources Research, 29: 1675-1683.

Millington, R.J., 1959. Gas diffusion in porous media. Science, 130: 100-102.

Nützmann, G., Maciejewski, S. and Joswig, K., 2002. Estimation of water saturation dependence of dispersion in unsaturated porous media: experiments and modelling analysis. Advances in Water Resources, 25(5): 565-576.

Oates, P.M. and Harvey, C.F., 2006. A colorimetric reaction to quantify fluid mixing. Experiments in Fluids, 41(5): 673-683.

Olsson, Å. and Grathwohl, P., 2007. Transverse dispersion of non-reactive tracers in porous media: a new non-linear relationship to predict dispersion coefficients. Journal of Contaminant Hydrology, 92: 149-161.

Orlob, G.T. and Radhakrishna, G.N., 1958. The effect of entrapped gases on the hydraulic characteristics of porous media. Transactions, American Geophysical Union, 39: 648-659.

Padilla, I.Y., Yeh, T.C.J. and Conklin, M.H., 1999. The effect of water content on solute transport in unsaturated porous media. Water Resources Research, 35(11): 3303-3313.

Parker, J.C., 2003. Physical processes affecting natural depletion of volatile chemicals in soil and groundwater. Vadose Zone Journal, 2: 222-230.

Reid, R.C., Prausnitz, J.M. and Poling, B.E., 1987. The properties of gases and liquids, Fourth Edition, McGraw-Hill, Inc.

Rezanezhad, F., Vogel, H.J. and Roth, K., 2006. Experimental study of fingered flow through initially dry sand. Hydrology and Earth System Sciences Discussions, 3: 2595-2620.

Rolle, M., Eberhardt, C., Chiogna, G., Cirpka, O.A. and Grathwohl P., 2009. Enhancement of dilution and transverse mixing in porous media: Experiments and model-based interpretation. Journal of Contaminant Hydrology, 110: 130-142.

Rolle, M., Chiogna, G., Bauer, R., Griebler, C. and Grathwohl, P., 2010. Isotopic fractionation by transverse dispersion: flow-through microcosms and reactive transport modeling study. Environmental Science and Technology, 44, 6167-6173.

Ronen, D., Scher, H. and Blunt, M., 1997. On the structure and flow processes in the capillary fringe of phreatic aquifers. Transport in Porous Media, 28(2): 159-180.

Roth, K. and Hammel, K., 1996. Transport of conservative chemical through an unsaturated two-dimensional Miller-similar medium with steady-state flow. Water Resources Research, 32(6): 1653-1663.

Sahimi, M. and Imdakm, A.O., 1988. The effect of morphological disorder on hydrodynamic dispersion in flow through porous media. Journal of Physics A: Mathematical and General, 21: 3833-3870.

Sahimi, M., 1993. Flow phenomena in rocks: From continuum models to fractals, percolation, cellular automata, and simulated annealing. Reviews of Modern Physics, 65: 1393-1534.

Salter, S.J. and Mohanty, K.K., 1982. Multiphase flow in porous media 1: Macroscopic observations and modeling. Society of Petroleum Engineers AIME, 57: 1-23.

Schaap, M.G. and Leij, F.J., 1998. Database-related accuracy and uncertainty of pedotransfer functions. Soil Science, 163(10): 765-779.

Schaap, M.G., Leij, F.J. and van Genuchten, M.T., 2001. ROSETTA: a computer program for estimating soil hydraulic parameters with hierarchical pedotransfer functions. Journal of Hydrology, 251: 163-176.

Seyfried, M.S. and Rao, P.S.C., 1987. Solute transport in undisturbed columns of an aggregated tropical soil: Preferential flow effects. Soil Science Society of America Journal, 51: 1434-1444.

Stern, O. and Volmer, M., 1919. Über die Abklingzeit der Fluoreszenz. Physikalische Zeitschrift, 20: 183-188.

Toride, N., Inoue, M. and Leij, F.J., 2003. Hydrodynamic dispersion in an unsaturated dune sand. Soil Science Society of America Journal, 67: 703-712.

Vanderborght, J. and Vereecken, H., 2007. Review of dispersivities for transport modeling in soils. Vadose Zone Journal, 6(1): 29-52.

van Genuchten, M.T., 1980. A closed-form equation for predicting the hydraulic conductivity of unsaturated soils. Soil Science Society of America Journal, 44: 892-898.

Webb, S.W., 2006. Two-phase gas transport. *In* Ho, C.K. and Webb, S.W. (eds.) Gas Transport in Porous Media. Springer Verlag, pp. 55-70.

Werth, C.J., Zhang, C., Brusseau, M.L., Oostrom, M. and Baumann, T., 2010. A review of non-invasive imaging methods and applications in contaminant hydrogeology research. Journal of Contaminant Hydrology, 113: 1-24.

Worch, E., 1993. Eine neue Gleichung zur Berechnung von Diffusionskoeffizienten gelöster Stoffe. Vom Wasser, 81: 289-297.

Zinn, B., Meigs, L.C., Harvey, C.F., Haggerty, R., Peplinski, W.J. and Von Schwerin, C.F., 2004. Experimental visualization of solute transport and mass transfer processes in two-dimensional conductivity fields with connected regions of high conductivity. Environmental Science and Technology, 38(14): 3916-3926.

4. Oxygen Transfer in a Fluctuating Capillary Fringe

Christina M. Haberer*, Massimo Rolle, Olaf A. Cirpka, Peter Grathwohl
Vadose Zone Journal (2012), 11(3), doi: 10.2136/vzj.2011.0056.

Abstract

Dynamic fluctuations in water table elevation cause the entrapment of air, which affects the hydraulic properties of the porous medium in the capillary fringe as well as the biogeochemical status of the underlying, potentially oxygen-depleted groundwater. In this study, we conducted quasi two-dimensional flow-through experiments at the laboratory bench-scale to investigate in detail the mass transfer of oxygen in a fluctuating capillary fringe. We evaluated the effects of different boundary conditions such as single drainage and imbibition events as well as periodic fast and slow water table fluctuations. High-resolution vertical profiles of oxygen concentration, measured at two distances in the horizontal groundwater flow direction, and mass fluxes, determined in the effluent of the flow-through chamber, were used to quantify oxygen transfer under the different boundary conditions applied. The results show that the partitioning between the aqueous and the gaseous phases plays a significant role in the supply of oxygen to groundwater at medium time scales. In case of fast water table fluctuations, the specific yield has to be considered. The experiments with a periodically changing boundary condition demonstrate that highly dynamic fluctuations of the water table enhance the mass transfer of oxygen from the atmosphere into the groundwater when compared with steady-state conditions. Moreover, the characteristics of the water table fluctuations determine a specific dynamic response of the system: we observed an approximately double amount of oxygen transferred to the groundwater when applying slow fluctuations compared with the case of cyclic, abrupt changes in the water table elevation.

Keywords: *fluctuating water table; 2-D flow-through experiments; oxygen transfer; capillary fringe.*

4.1 Introduction

Dissolved oxygen is of primary importance for groundwater quality. It is the thermodynamically most favorable electron acceptor for a number of (bio)chemical redox reactions (Stumm and Morgan, 1996). In aquifers contaminated by organic compounds, aerobic microorganisms use dissolved oxygen to oxidize the pollutants. The oxygen concentration in subsurface environments

is determined by the rates of oxygen transfer from the atmosphere and the rates of consumption due to respiratory processes (Chapelle, 2001). The flux of oxygen across the unsaturated/saturated interface is severely limited, however, by the low solubility of oxygen in water. As a consequence, oxygen demanding processes and the restricted exchange with the atmosphere may lead to rapid depletion of dissolved oxygen (Balcke et al., 2007).

In unconfined aquifers, entrapped air can provide a significant amount of oxygen to anoxic water (Fry et al., 1995; Holocher et al., 2002, 2003; Amos and Mayer, 2006). The supply of oxygen near the water table may create favorable conditions for aerobic microorganisms and, therefore, enhance the degradation of groundwater contaminants in this region (e.g., Rainwater et al., 1993; Hinz, 1998; Amos and Mayer, 2006; Jost et al., 2011). In the presence of endogeneous microbial communities mediating the contaminants' degradation and capable of readily adjusting to the changes in environmental conditions, enhanced mass transfer, mixing and chromatographic effects induced by transient conditions can favor the natural attenuation of groundwater plumes. To quantify the oxygen supply and its impact on aquifers' redox conditions and biogeochemical processes, it is of primary importance to understand the hydraulic and mass transfer dynamics. In field-scale contamination scenarios, this knowledge might help to tackle the effects of a fluctuating water table on the spatial and temporal distribution of the pollutants, their degradation rates, as well as other important redox processes.

Air entrapment occurs regularly in aquifers because of changing elevations of the water table and the capillary fringe caused, e.g., by seasonal variations in recharge, uptake by vegetation, and groundwater withdrawal (Zhang et al., 1998). Seasonal water table fluctuations are often observed in shallow groundwater systems. Moreover, variations in the water table elevation during shorter periods of time may arise due to fluctuations in the stage of nearby water bodies (Williams and Oostrom, 2000), e.g., rivers and reservoirs. Changes in water table elevation can also occur across longer periods of time, when average recharge rates exceed the average withdrawal and natural groundwater discharge or vice versa (Lucas and Robinson, 1995).

A number of experimental and numerical studies have addressed the dynamics of a fluctuating water table and capillary fringe as well as its impact on the hydraulic properties of porous media (e.g., Parker and Lenhard, 1987; Lehmann et al., 1998; Hinz, 1998; Fry et al., 1997; Nielsen and Perrochet, 2000; Werner and Lockington, 2003; Schneider-Zapp, 2009). Less literature is available focusing on solute transport under these conditions (e.g., Legout et al., 2009), and only a few additional works have been conducted to investigate mass transfer of volatile compounds in the capillary fringe in the presence of dynamic boundary conditions (e.g., Williams and Oostrom, 2000; Werner and Höhener, 2002; Geistlinger et al., 2010). Caron et al. (1994) studied the influence of the capillary fringe on mass transfer of CO_2 from the unsaturated to the saturated zone to evaluate the migration of $^{14}CO_2$ gas from radioactive waste disposal sites. Dobson et al. (2007) conducted

laboratory experiments, where air entrapment during water table rise favored the dissolution of a multi-component LNAPL and biodegradation activity.

In this study, we investigated oxygen transfer in the presence of a fluctuating capillary fringe. We focused on the physical processes occurring in flow-through systems in which a horizontal groundwater flow is established and vertical movements of the water table are additionally induced. Hitherto, only a few experimental studies (e.g., McCarthy and Johnson, 1993; Caron et al., 1998; Klenk and Grathwohl, 2002; Dobson et al., 2007; Haberer et al., 2011) have considered mass transfer of volatile compounds across the capillary fringe with horizontal groundwater flow. We performed quasi two-dimensional flow-through laboratory experiments under transient conditions, where we measured oxygen fluxes at the outlet of the flow-through system as a function of time. The effect of different boundary conditions was investigated including both single drainage or imbibition events and periodic water table fluctuations. Vertical profiles of equivalent aqueous oxygen concentration were measured at distinct positions along the horizontal flow direction and at high spatial resolution using a non-invasive optode technique.

The objectives of our investigation were: (i) to gain an improved understanding of the processes determining oxygen transfer in porous media under transient flow conditions such as drainage and imbibition; (ii) to quantify the enhancement of oxygen transfer due to periodic water table fluctuations; and (iii) to compare the specific response of flow-through systems to different boundary conditions (i.e., fast vs. slow water table fluctuations).

4.2 Theoretical Background

4.2.1 Capillary Fringe and Hydraulics of a Fluctuating Groundwater Table

In the capillary fringe, a transition occurs from primarily vertical flow in the vadose zone to predominantly horizontal flow in the saturated zone. Within this interface zone, water contents gradually decrease toward higher elevations, and at the upper limit, only the smallest connected pores contain water (Bear and Cheng, 2010). Significant lateral flow in the capillary fringe is restricted to the zone of high water content, that is, below a critical height above the phreatic surface (Ronen et al., 1997; Berkowitz et al., 2004).

Vertical movements of the groundwater table cause the entrapment of air. This process not only affects the mass transfer of volatile compounds, which is discussed below, but also has significant consequences on the effective hydraulic properties of porous media and, therefore, on the flow regime. Fry et al. (1997) found that the value of the relative hydraulic conductivity of porous media with an entrapped gas volume of 14 to 55 % ranged from 0.62 to 0.05.

During transient conditions, the storativity of the porous medium, which for an unconfined aquifer is usually taken to be equal to the specific yield (e.g., Bear and Verruijt, 1987; Fetter, 2001), has to be considered. Specific yield is defined as the ratio of the volume of water that drains from a saturated rock or soil due to gravity to the total volume of the porous formation (Meinzer, 1923; Fetter, 2001). It is a time-dependent quantity because it takes time to establish a new moisture distribution following a rapid decrease in water table elevation (Nachabe, 2002; Bear and Cheng, 2010). Because water flows faster at high values of water saturation than low values, this results also in self-broadening water-content profiles (Hinz, 1998; Schneider-Zapp, 2009). In contrast, when the height of the water table decreases slowly, the corresponding changes in moisture distribution have sufficient time to continuously adjust, and the lag between the lowering of the water table and the total volume of water drained practically vanishes. The thickness of the capillary fringe is therefore related to the time period during which the water table fluctuates over one cycle (Berkowitz et al., 2004). Moreover, specific yield is influenced by the grain size. Values of the specific yield for unconfined aquifers generally range between 0.05 and 0.3, although lower or higher values are possible, especially in cases of finer grained and less uniform material (lower values) and uniform coarse sand or gravel (higher values) (see Krešić, 2007).
In the zone of varying extensions of the capillary fringe and, in particular, in the presence of transient, fluctuating flow conditions, the water content, pore water velocity, and hydraulic conductivity change. The variations of these effective hydraulic properties not only modify the water flow regime, but also have an important impact on solute and gas transport from the unsaturated porous medium to the aquifer (Russo et al., 1989) and on the transport of volatile compounds from the aquifer to the gas phase.

4.2.2 Oxygen Transfer

Two main physical processes determine the mass transfer of volatile compounds across a fluctuating capillary fringe: (i) partitioning between the gaseous (i.e., entrapped air) and the aqueous phases and (ii) transverse hydrodynamic dispersion in the groundwater.
Partitioning of volatile compounds occurs in the presence of entrapped air. In groundwater systems, air may be entrapped during water infiltration or because of an increase in the groundwater table. Fry et al. (1997) summarize several literature results and suggest that the volume of gas entrapped in porous media due to water table fluctuations is typically in the range of 10 to 20 % of the pore space.
In the presence of entrapped air, volatile compounds are transferred between the aqueous and gaseous phases as a result of the difference in chemical potential of these compounds between the two phases (e.g., Anderson and Crerar, 1993; Nordstrom and Munoz, 1994). The transport of

these volatile compounds is coupled via the total gas pressure p [M L^{-1} T^{-2}], i.e., the sum of atmospheric pressure, capillary pressure, and hydrostatic pressure (e.g., Cirpka and Kitanidis, 2001). Local equilibrium is reached when the chemical potential, μ [L^2 T^{-2}], for a given compound present in the multiphase system is the same in both phases (e.g., Washington, 1996; Atkins and de Paula, 2006; Engel and Reid, 2010) and when the sum of partial pressures within the gaseous phase approximates the external pressure p. In the absence of a gaseous phase, the sum of partial pressures computed through Henry's law is smaller than p.

Depending on the total amount of volatile compounds present in the system, the trapped gas volume may change due to transport, or it may grow or shrink depending on whether gases are produced or consumed (Cirpka and Kitanidis, 2001; Amos and Mayer, 2006). The volume of the entrapped gas phase and the properties of volatile compounds significantly affect the transport of these species in the subsurface: because volatile compounds move back and forth between two adjacent phases, chromatographic separation of the compounds occurs in accordance with their physicochemical properties. Donaldson et al. (1998) reported substantial retardation and tailing of partitioning tracers (i.e., dissolved oxygen and helium) relative to a non-partitioning compound (i.e., bromide).

Hydrodynamic dispersion also represents an important process for oxygen transfer across the capillary fringe. In previous experiments performed under steady-state conditions (Haberer et al., 2011), we demonstrated that transverse vertical dispersion coefficients measured in the saturated zone and across the capillary fringe are essentially the same and can be well described using the nonlinear parameterization of Chiogna et al. (2010). An influence of the capillary fringe morphology on oxygen transfer was not observed. This may be explained by the narrow grain size distribution used in the experiments, which resulted in a steep decline in water saturation at the unsaturated/saturated interface and the absence of entrapped gas in this transition zone (Haberer et al., 2011). Under these conditions, the oxygen flux across an interface can be determined using Fick's first law for a porous medium. Entrapment of air, caused by a fluctuating water table may affect the oxygen transfer, however, due to the partitioning between the gaseous and aqueous phases and for its impact on the hydraulics of the system (e.g., more tortuous flow paths due to the presence of gas clusters).

4.3 Materials and Methods

4.3.1 Experimental Setup

Laboratory bench-scale experiments were performed to investigate oxygen transfer in a fluctuating capillary fringe under various boundary conditions (single drainage and imbibition events as well as

slow and fast periodic water table fluctuations). We worked with a quasi two-dimensional experimental setup (Fig. 4.1) similar to the ones we recently used to study conservative and (bio)reactive transport in the saturated zone (Rolle et al., 2009; Bauer et al., 2009) and transfer of oxygen across the capillary fringe under steady-state conditions (Haberer et al., 2011). The flow-through chamber has inner dimensions of 80 cm × 40 cm × 0.5 cm ($L \times H \times W$). Horizontal water flow in the system (from left to right) was established by connecting two peristaltic pumps (Pumps 1 and 2 in Fig. 4.1a; ISMATEC IPC 24, Glattbrugg, Switzerland) to the inlet and outlet ports at each side of the chamber. These ports (12 on each side) were vertically spaced 12.5 mm apart. To create a steady-state horizontal flow field before starting the transient phase in each experiment, both pumps were operated at the same pumping rate. In addition, a third high-precision peristaltic pump (Pump 3 in Fig. 4.1a; ISMATEC IPC-N 24, Glattbrugg, Switzerland) was connected to the ports at the base of the flow-through chamber. This pump was used to induce the water table fluctuations according to a predetermined pumping scheme. The 24 ports at the base of the chamber were spaced 33.3 mm apart.

All injection and extraction ports were made of Alltech rubber septa (Deerfield, USA) pierced by hollow needles. These needles were directly connected to Fluran HCA pump tubing (ISMATEC) with an inner diameter of 0.64 mm. This material is characterized by low gas permeability, thus minimizing oxygen uptake when oxygen-depleted water is flowing through the tubes. To prevent porous material from entering the hollow needles and the pump tubings, all injection and extraction ports in the system were screened with small stainless steel mesh screens (0.125 mm mesh size). For the total duration of the experiments, the flow-through system was kept in a temperature-controlled room at 22 °C.

As porous medium, we used glass beads (Sartorius GmbH, Göttingen, Germany) with a grain diameter of 0.4 to 0.6 mm. The glass beads were packed into the flow-through chamber using a wet-packing procedure, i.e., the water table was slowly raised and constantly maintained a small distance above the top of the porous medium to avoid entrapment of air but also to minimize the separation of grain sizes due to different settling rates. After the flow-through chamber had been completely packed, the water table was lowered to its final stage so that the top of the capillary fringe was kept below the surface of the porous medium and an unsaturated zone was created in the upper region of the packing (Fig. 4.1a). Due to the narrow grain size distribution used in the experiments, we observed a steep decline in water saturation at the unsaturated/saturated interface. As a consequence, the vertical position of the capillary fringe's upper limit could be accurately identified visually. In the following, we define the upper limit of the capillary fringe as the vertical position where the water content is about 80 % to 90 %, thus inhibiting gaseous oxygen from diffusing freely in the pore space (Liu, 2008; Haberer et al., 2011).

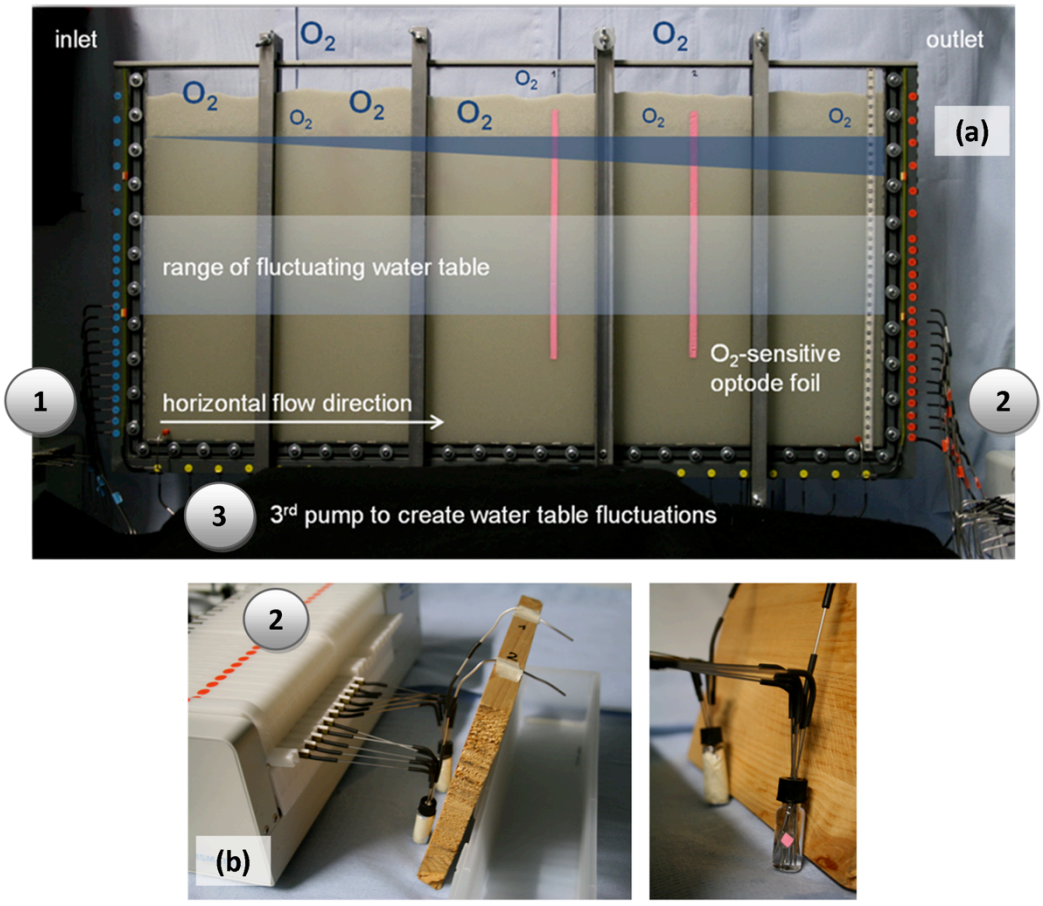

Fig. 4.1. (a) Experimental setup (inner dimensions of the flow-through chamber were 80 cm × 40 cm × 0.5 cm, length × height × width): steady-state horizontal flow was established using Pumps 1 and 2 before inducing a change in water table height using Pump 3. (b) Oxygen flux measurement in the effluent.

During the experiments, the location of the phreatic surface was measured using two piezometers connected to the porous medium via two holes drilled in the front of the chamber. These piezometers were installed near the inlet and the outlet of the flow-through chamber and allowed assessment of the height of the capillary fringe (~117 mm) for the porous material used. For additional flow and mass transfer parameters, see Table 4.1.

Mass transfer in the capillary fringe was investigated in several experiments, where we injected oxygen-depleted Milli-Q water into the flow-through chamber. We prepared the oxygen-depleted solution by stripping the necessary amount of water with nitrogen and then storing it in a gas-tight Tedlar bag (Alltech, Germany). This Tedlar bag had been flushed with nitrogen before filling with the prepared solution, thus minimizing the oxygen contamination of the water. During the experiment, the flow-through chamber remained open to the atmosphere but was covered by a lid to prevent considerable evaporation of water. We applied a noninvasive optode technique (FIBOX 3, PreSens GmbH, Regensburg, Germany) to measure vertical profiles of equivalent aqueous oxygen concentrations using two strips of oxygen-sensitive foil (26 cm × 0.5 cm, SP-PtSt3-NAU from PreSens GmbH) glued onto the inner side of the front pane of the flow-through chamber. The

strips were placed at 45 cm and 60 cm distance from the inlet. We detected the measurement signal with an optical fiber located outside of the flow-through chamber and moveable in its vertical position. Measurements were taken in the fully water-saturated zone, across the region with entrapped air, and in the zone of aeration. The measurement signals, which correspond to values of oxygen partial pressure, were then converted into the respective values of volumetric aqueous concentration. This procedure allowed us to obtain high-resolution vertical profiles (>100 measurement points with 2.5-mm spacing) of equivalent aqueous oxygen concentration across the capillary fringe. Further details on the measurement technique were described by Haberer et al. (2011). The comparison between the noninvasive optode technique used here and a standard method of oxygen measurement (i.e., an electrode with a galvanic sensor: CellOx 325 with Oxi 330 Set, WTW GmbH, Germany) showed an excellent agreement (RMSE: 0.1 mg L^{-1}) between simultaneously measured values of oxygen concentration using the two methods (results not shown).

The impact of transient conditions on mass transfer across the capillary fringe was quantified by additional mass flux measurements at the system's outlet. Two 1.7-mL glass vials with a spot of oxygen sensor foil were connected to the outlet tubing and used as flow-through cells for the measurement of oxygen (Fig. 4.1b). The discharge at the outlet was collected in the two vials and simultaneous measurements of oxygen concentrations and flow rates were used to determine the oxygen fluxes. The effluent, sampled in the respective vial, corresponds to the upper or lower volume of the flow-through chamber through which water flow occurred. Therefore, mass fluxes determined for each vial also give an estimate of the region of the porous medium impacted by the water table fluctuations.

Table 4.1. Summary of flow and mass transfer parameters.

Parameter	**Value**
Inner dimensions of the flow-through chamber, $L \times H \times W$ [m]	0.80 × 0.40 × 0.005
Average grain size diameter [mm]	0.50
Average porosity [%]	41.1
Height of the capillary fringe at steady state [mm]	~117
Aqueous diffusion coefficient for oxygen [m^2 s^{-1}] (at 22 °C)	1.97×10^{-9}

4.3.2 Mathematical Description of Steady-State Dispersive Mass Flux

At steady state, transverse hydrodynamic dispersion was found to be essential for the mass transfer of volatile compounds across the capillary fringe (e.g., Klenk and Grathwohl, 2001; Liu, 2008; Haberer et al., 2011). Considering an abrupt change in the vertical distribution of the water content at the upper limit of the capillary fringe, the oxygen profile in the topmost saturated zone is

described by the following analytical solution of the governing two-dimensional transport equation (e.g., Cussler, 2009; Liu et al., 2010):

$$C_{norm}(x,z) = \frac{C - C_{bg}}{C_0 - C_{bg}} = erfc\left(\frac{z}{2\sqrt{D_t \frac{x}{v_a}}}\right) \tag{4.1}$$

where C_{norm} [-] is the normalized concentration of the compound of interest, here oxygen. The measured value of equivalent aqueous oxygen concentration, C [M L^{-3}], at the horizontal and vertical coordinates x [L] and z [L] is standardized using the background concentration in the aqueous phase, C_{bg} [M L^{-3}], and the concentration at the air/water interface, C_0 [M L^{-3}]. The origin of z is set at the top of the fully water-saturated zone, pointing downward; v_a [L T^{-1}] denotes the horizontal seepage velocity.

The transverse vertical dispersion coefficient, D_t [L^2 T^{-1}], can be parameterized using the following expression by Chiogna et al. (2010), which retains a nonlinear relationship with the average seepage velocity:

$$D_t = D_p + v_a \frac{d}{\sqrt{Pe + 123}} \tag{4.2}$$

where d [L] represents the grain size diameter, and D_p [L^2 T^{-1}] is the pore diffusion coefficient. The latter can be approximated under water-saturated conditions by:

$$D_p = \phi D_{aq} \tag{4.3}$$

where ϕ [-] is the porosity and D_{aq} [L^2 T^{-1}] denotes the aqueous diffusion coefficient of oxygen, which is 1.97×10^{-9} m^2 s^{-1} at 22 °C (Worch, 1993; Cussler, 2009).

In Eqn. 4.2, Pe denotes the dimensionless grain Péclet number defined as:

$$Pe = \frac{v_a d}{D_{aq}} \tag{4.4}$$

To quantify the oxygen flux across the interface (i.e., at z = 0), the derivative of Eqn. 4.1 has to be combined with Fick's first law for a porous medium (see also Cussler, 2009):

$$F\big|_{z=0} = -\phi D_t \frac{\partial C}{\partial z}\bigg|_{z=0} = \left(C_0 - C_{bg}\right)\phi\sqrt{D_t \frac{v_a}{x}\frac{1}{\pi}} \tag{4.5}$$

which is the mass flux, F [M L^{-2} T^{-1}], per unit interfacial area, i.e., the mass flux density, at a specific value of x. The porosity appears in Eqn. 4.5 because the dispersive mass transfer can occur only through the pore space. Integrating the mass flux density over the interfacial area leads to:

$$\dot{m} = \int_0^L \int_0^W F\big|_{z=0}\, dy\, dx = \left(C_0 - C_{bg}\right) 2\phi W \sqrt{D_t L v_a \frac{1}{\pi}} \tag{4.6}^*$$

*) The derivation of this equation is explained in detail in Appendix A1.2.

where $\dot{m}$ [M T^{-1}] is the total mass flux across the interface between the saturated and the unsaturated zone, while *L* [L] and *W* [L] define the length and the width of the interfacial area.
A theoretical value of the total oxygen flux in the effluent of the flow-through chamber can be derived when adding the measured mass flux at the inlet (resulting from the measured background concentration in the system) to the total dispersive flux, $\dot{m}$, across the capillary fringe. The theoretical result may differ from the experimentally determined value of oxygen flux in the effluent of the flow-through chamber, thus indicating a change in interfacial mass flux. We attribute the difference between the theoretical and the experimental values to partitioning between two fluid phases and the impact of entrapped gas on the system's hydraulics. Under these conditions (i.e., D_t and $v_a \neq$ const.), Eqn. 4.6 cannot be directly applied; however, it represents a valuable framework to calculate the oxygen fluxes for the (quasi) steady-state conditions before and after lowering or raising the water table in the drainage and imbibition experiments, respectively. The comparison of the calculated values (Eqn. 4.6) with the measured oxygen fluxes under (quasi) steady-state conditions allowed us to quantify the impact of entrapped gas on oxygen transfer.
Moreover, it is possible to consider the amount of oxygen transferred from the atmosphere to the oxygen-depleted groundwater as a time-dependent quantity (i.e., as a function of the number of exchanged pore volumes). To do so, the total mass flux across the interface is multiplied by the respective time interval elapsed between two consecutive measurements. The results are summed up to yield the cumulative oxygen mass supplied across the unsaturated/saturated interface within a certain period of time. This allowed us to estimate the specific contribution of transient conditions on oxygen transfer, as shown below.

4.4 Results and Discussion

To study the physical processes influencing oxygen transfer in a fluctuating capillary fringe, we performed different flow-through experiments. First, we focused on the impact of imbibition and drainage as single events occurring over a short period of time (15 min). Afterward, we investigated the behavior of periodic fluctuations during a time span of 42 hours. We considered two distinct forcing functions inducing a quasi-rectangular and a triangular pressure head signal. These conditions are representative of an abrupt and a gradual fluctuation, respectively, of the water table of an unconfined aquifer. Table 4.2 provides an overview of the experiments conducted, including the seepage velocity, the difference in the locations of the capillary fringe's upper limit, ΔH_{CF} [L], the characteristic time of the induced water table fluctuation, Δt [T], and the measured parameters.

Table 4.2. Overview of the experiments conducted. Measured parameters included the capillary fringe and water table height, vertical oxygen concentration profiles, oxygen fluxes in the effluent, and groundwater flow rates.

	v_a [m d^{-1}]	ΔH_{CF} [cm]	Δt [min]
Single drainage	4.06 - 5.63	10.0	15
Single imbibition	4.40 - 6.04	8.5	15
Periodic fast	4.09 - 6.63	11.0 - 12.0	15
Periodic slow	4.21 - 7.11	9.2 - 12.5	420

For better comparability of the results presented below, we use the nondimensional pore volume, *PV*, instead of time *t* [T]:

$$PV = \frac{qt}{\phi L} \tag{4.7}$$

in which *q* [L T^{-1}] is the specific discharge across the fully water-saturated and quasi-saturated cross-sectional area of the porous medium. According to this definition, the reference height of the cross-sectional area varies with the fluctuating groundwater table.

4.4.1 Single Events: Drainage and Imbibition Experiments

Different physical processes occur during lowering or raising of the water table. Longitudinal and transverse vertical dispersion (e.g., Goode and Konikow, 1990; Walter et al., 2003), pore-scale effects resulting in hysteresis, storativity of the porous medium, and partitioning of a volatile compound between the aqueous and gaseous phases may have distinct impacts on mass transfer in the capillary fringe. We performed two experiments in which a single drainage or imbibition event was induced. Depending on the vertical location of the phreatic surface, the underlying groundwater flow velocity was in the range of 4.1 to 6.0 m d^{-1}. In both cases, the height of the water table was changed by about 10 cm within 15 min.

4.4.1.1 Drainage

Figure 4.2 shows the experimental results for the case of a falling water table. The vertical profiles of normalized oxygen concentration at *x* = 0.45-m distance from the inlet are displayed in Fig. 4.2a as a function of the number of pore volumes flushed through the system after inducing the drop in water table elevation. Figure 4.2b represents the corresponding locations of the phreatic surface and the upper limit of the capillary fringe.

As described above, the oxygen flux in the effluent was measured in two distinct flow-through cells. These measurements and the total mass flux at the outlet of the flow-through chamber are

reported in Fig. 4.2c. A dash-dotted trend line indicates that the total oxygen flux in the effluent reached a constant value (3.95×10^{-5} mg s^{-1}), when ≥1.5 PVs of water had been flushed through the system. Additionally, the average steady-state value of the incoming oxygen flux (influent, 3.21×10^{-5} mg s^{-1}) is displayed.

The cumulative oxygen mass, i.e., the amount of oxygen transferred from the atmosphere to the oxygen-depleted groundwater, is shown in Fig. 4.2d as a function of time. Assuming a 'sequence of steady states' and applying Eqn. 4.6, we also calculated the expected amount of oxygen transferred across the capillary fringe due to transverse vertical dispersion alone (and in the absence of entrapped gas). We compared this result with the amount of oxygen supplied across the unsaturated/saturated interface simply using the dispersive mass flux determined at the end of the experiment (difference between the steady-state oxygen flux in the effluent for ≥1.5 PV and the incoming mass flux: 0.74×10^{-5} mg s^{-1}).

The described procedure allowed us to estimate the change in transverse dispersive flux due to the drop in water table elevation. We argue that the value of D_t, following drainage and describing the mass transfer across the capillary fringe, is the same as the transverse vertical dispersion coefficient calculated assuming saturated conditions. This assumption is corroborated by the fact that the two lines (in Fig. 4.2d), representing the amount of oxygen supplied to the aqueous phase as result of the dispersive mass fluxes across the capillary fringe (i.e., calculated by Eqn. 4.6 and measured at the end of the experiment) coincide. This is explained by the fact that the morphology of the capillary fringe at the end of the experiment is similar to the initial steady state.

For the porous material used, the water saturation value changed rapidly within a small vertical distance across the unsaturated/saturated interface. Because oxygen transfer in this transition zone is controlled by aqueous-phase processes, e.g., diffusion and dispersion in the liquid phase, a steep gradient in equivalent aqueous oxygen concentrations starts to develop when the water content is sufficiently high (e.g., Maier et al., 2007; Haberer et al., 2011). Comparing Figs. 4.2a and 4.2b, the normalized values of oxygen concentration started to drop at the upper limit of the capillary fringe. This experimental evidence substantiates the assumption of earlier modeling studies (e.g., Barber et al., 1990; Walter et al., 2003; Liu et al., 2010), in which a constant oxygen concentration was assigned as a boundary condition at the upper limit of the capillary fringe in order to describe this interface mass transfer process.

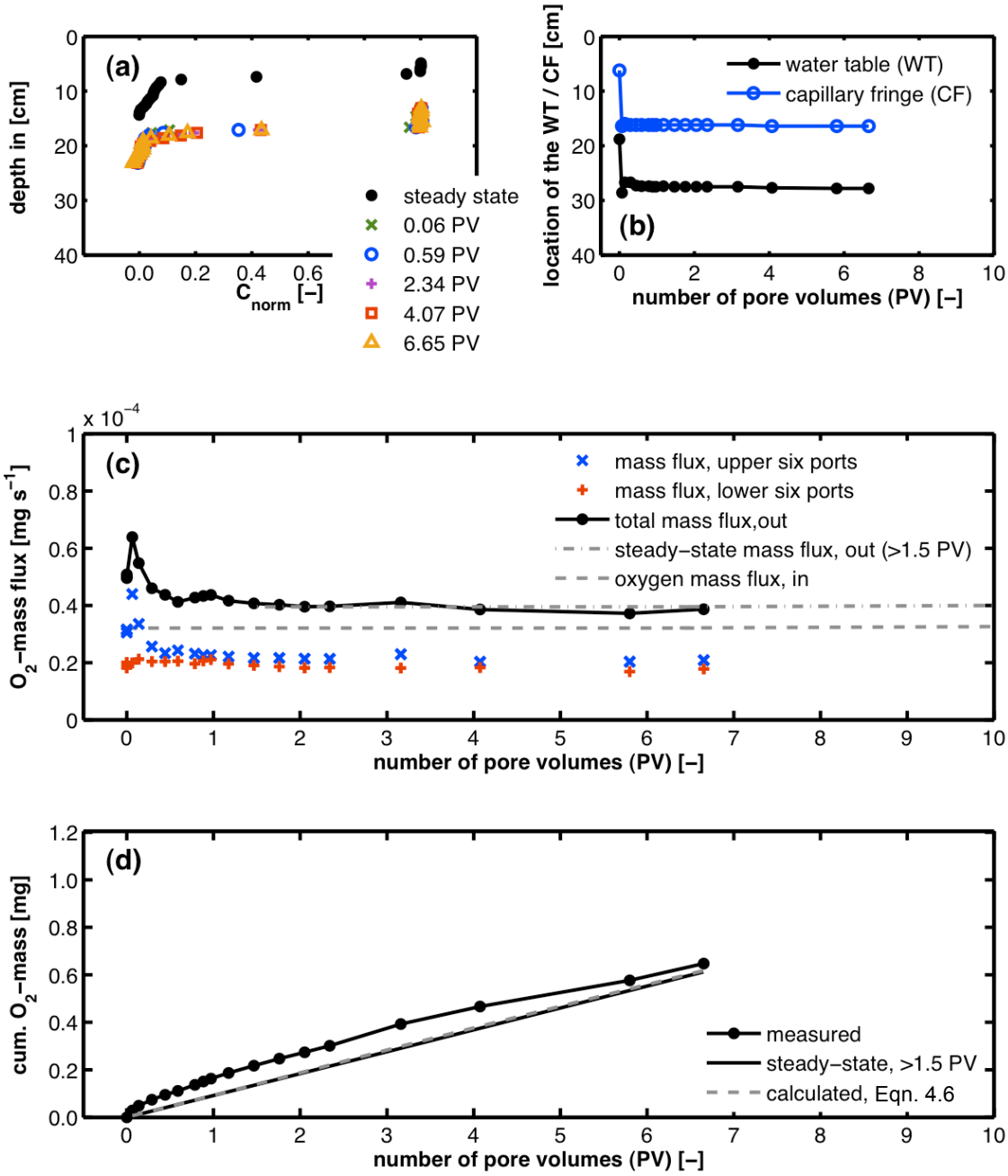

Fig. 4.2. Drainage: (a) vertical profiles of normalized oxygen concentration, C_{norm} [-], at x = 45 cm (the depth of 0 cm indicates the upper edge of the flow-through chamber); (b) vertical location of the water table and capillary fringe vs. the number of pore volumes (0 PV marks the beginning of the change in water table height starting from steady-state flow); (c) oxygen fluxes at the outlet of the chamber: dash-dotted line, steady-state mass flux, ≥1.5 PV (3.95×10^{-5} mg s^{-1}); dashed line, average mass flux in the influent (3.21×10^{-5} mg s^{-1}); (d) cumulative oxygen mass supplied to the system across the unsaturated/saturated interface.

As can be observed in Fig. 4.2a, the gradient of oxygen concentrations immediately follows the falling pressure head. This may lead to the conclusion that a considerable change in oxygen flux in the effluent of the flow-through chamber does not occur. The values of oxygen flux in the effluent increase during a short time period (the first 0.2 PVs), however, right after lowering the water table

(Fig. 4.2c). This observation can be explained by the time-dependent vertical flow component caused by the rapid drop in hydraulic head. In fact, the saturation-dependent and thus lower value of effective hydraulic conductivity in the upper part of the capillary fringe led to broader water content profiles during drainage. Consequently, water content values decreased more slowly in this upper region. The originally saturated porous medium gradually drained; the draining water picked up oxygen in the now unsaturated zone and advected it downward to the receding groundwater. That is, the draining water led to increased values of oxygen flux during a short period of time until the new steady-state moisture distribution profile was established. No further input of oxygen into the system due to transient flow conditions (i.e., drop of the water table) occurred, and the vertical distance between the two solid lines in Fig. 4.2d stays approximately constant with time. In our experiment, about 0.1 mg of oxygen was additionally supplied to the groundwater due to the drop in water table elevation (Fig. 4.2d, maximum vertical distance between the two solid lines). This corresponds to approximately 11.3 mL of O_2-saturated water (O_2-saturation concentration: 8.84 mg L^{-1} at 20 °C) and represents a lower limit for the volume of water drained in the experiment. A conservative estimate of the specific yield, S_y [-], can be calculated as (Fetter, 2001; Walter et al., 2003):

$$S_y = \frac{V_{aq}}{A\Delta H} \tag{4.8}$$

where V_{aq} [L^3] is the volume of water drained, here assumed to be 11.3 mL, and A [L^2] represents the interfacial area between the unsaturated and the saturated zone.

Substituting all known parameters into Eqn. 4.8 results in a value of specific yield of about 3 %. This value is lower than the values generally reported (Krešić, 2007) for the specific yield of unconfined aquifers, which typically range between 0.05 and 0.3. We think that this difference can be attributed to the underestimation of the volume of water drained.

From Fig. 4.2c it is evident that the drop in water table elevation did not affect the oxygen flux in the lower portion of the flow-through chamber. In fact, the change in the total oxygen flux is solely due to variations in the mass flux of the upper six outlet ports.

In the absence of vertical groundwater flow, transverse vertical hydrodynamic dispersion is essential for the mass transfer of volatile compounds from the unsaturated zone into the groundwater and vice versa. Additional advective and dispersive fluxes (i.e., longitudinal dispersion in the *z* direction) occur when water moves vertically, thus increasing the mass transport in this direction (e.g., Walter et al., 2003). For the conditions of this drainage experiment, however, it was not possible to distinguish the additional small contribution due to longitudinal hydrodynamic dispersion acting in vertical direction as the height of the water table was lowered.

4.4.1.2 Imbibition

Significantly different results were observed for the imbibition experiment. During the upward movement of the water table, air was entrapped, and oxygen, present in the gaseous phase, was partitioned into the flowing oxygen-depleted water. The measured vertical concentration profiles are shown in Fig. 4.3a. It can be seen that these profiles are very different from the ones measured during drainage (Fig. 4.2a). In case of imbibition, dissolution fronts propagate through the newly formed transition zone and, at a certain *x* position, oxygen concentration profiles slowly evolve and disappear until a new quasi-equilibrium state was formed. Simultaneously, nitrogen partitions from the liquid into the gaseous phase, changing the gas saturation of the system toward lower values (e.g., Fry et al., 1995; Cirpka and Kitanidis, 2001; Balcke et al., 2007; Klump et al., 2008) but sustaining the gaseous phase. This process was observed for approximately four to six pore volumes and the corresponding oxygen fluxes in the effluent were significantly increased during this time (Figs. 4.3a and 4.3c). The increase in water table elevation affected the measured oxygen fluxes in both the upper and lower parts of the porous medium, as indicated by the measurements in the flow-through cells at the system's outlet.

Partitioning of oxygen between the gaseous and the aqueous phases diminishes when no further oxygen can be supplied from entrapped air. The amount of oxygen transferred from the entrapped gas into the oxygen-depleted groundwater is determined by the initially entrapped gas volume: the more air is entrapped, the higher the number of pore volumes needed for the dissolution process. Assuming that the gas saturation does not substantially change during the observed time period, the partitioning process can be conceptualized with a constant retardation factor (estimated to be ~4 to 6) affecting the transport of oxygen (e.g., Fry et al., 1995). As result of the oxygen transfer in the capillary fringe, the estimated range of the retardation factor yields a gas saturation value between 9 and 14 %. It may be noted that theory predicts dissolution of the entrapped gas when the sum of partial pressures in the injected water is at atmospheric pressure. The pressure in the entrapped gas is elevated due to the hydrostatic and capillary pressure contributions causing a gas-dissolution front, which is much more retarded than the oxygen-depletion front (Cirpka and Kitanidis, 2001; Klump et al., 2008). This effect was not observed, however, during the time frame of our experiment.

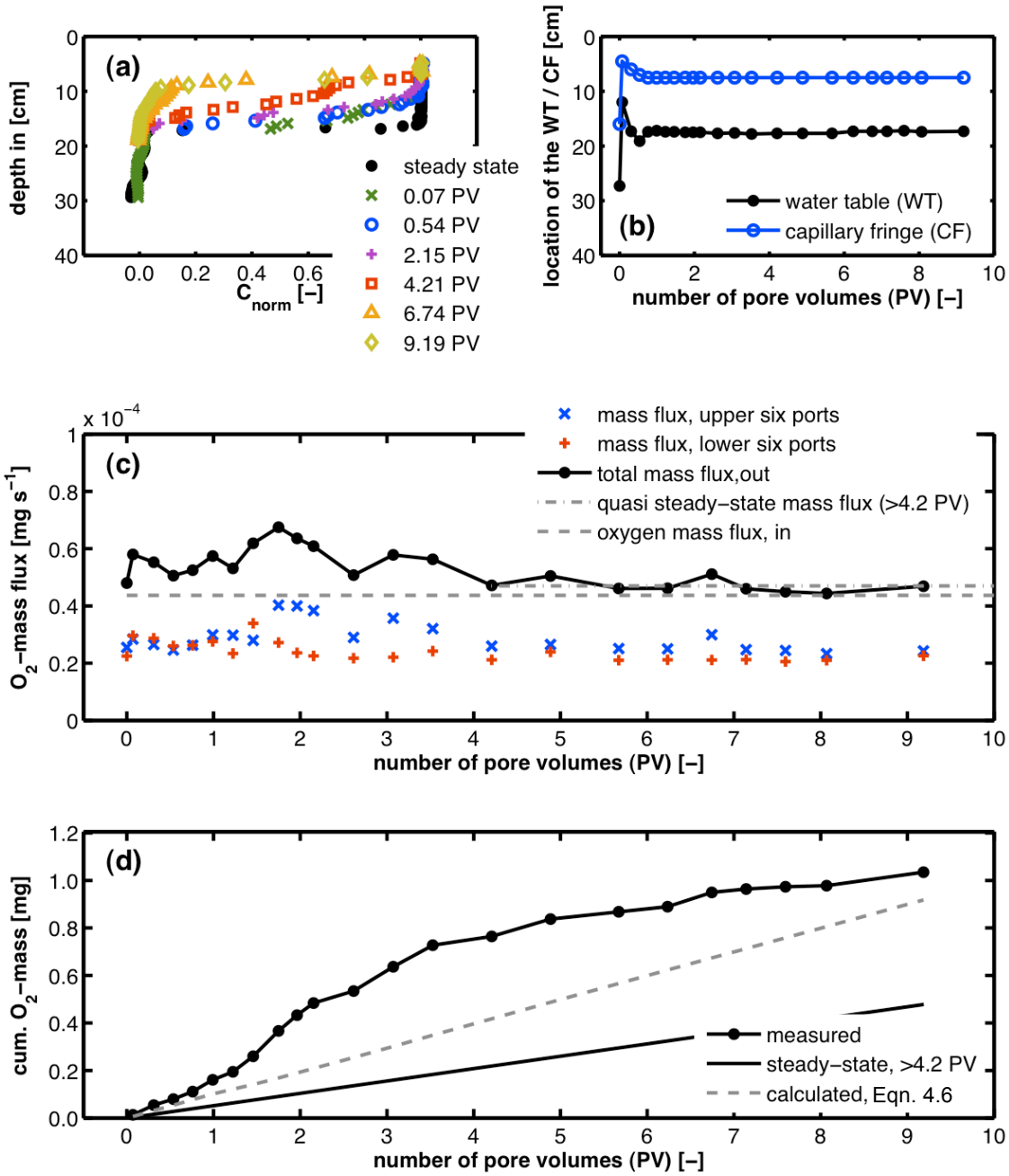

Fig. 4.3. Imbibition: (a) vertical profiles of normalized oxygen concentration, C_{norm} [-], at x = 45 cm (the depth of 0 cm indicates the upper edge of the flow-through chamber); (b) vertical location of the water table and capillary fringe vs. the number of pore volumes (0 PV marks the beginning of the change in water table height starting from steady-state flow); (c) oxygen fluxes at the outlet of the chamber: dash-dotted line, quasi steady-state mass flux, ≥4.2 PV (4.70×10^{-5} mg s^{-1}); dashed line, average mass flux in the influent (4.37×10^{-5} mg s^{-1}); (d) cumulative oxygen mass supplied to the system across the unsaturated/saturated interface.

As for the previous drainage experiment (Fig. 4.2d), we calculated the cumulative oxygen mass transferred from the unsaturated zone to the oxygen-depleted groundwater. The results at different points in time (expressed as number of PVs) are reported in Fig. 4.3d together with the amount of oxygen supplied due to transverse vertical dispersion alone (calculated according to Eqn. 4.6, i.e.,

in absence of entrapped gas) or using the interfacial mass flux measured at quasi steady state (0.56×10^{-5} mg s^{-1} for ≥4.2 PV).

The comparison between the drainage and imbibition experiments (Fig. 4.2d and Fig. 4.3d) indicates that significantly more (approximately six times) oxygen is dissolved into the groundwater during imbibition than during drainage. Moreover, the additional supply of oxygen is, in both cases, a transient phenomenon that extends across a significantly longer time in the case of imbibition (~4.2 PV compared with the 0.2 PV during drainage). It is important to note that different physical processes cause the observed increases in oxygen transfer: the draining water enriched in oxygen content for a falling water table and the entrapment of air and subsequent partitioning between the aqueous and gaseous phases during imbibition.

4.4.1.3 Evaluation of Oxygen Fluxes

Figure 4.3d illustrates that the amount of oxygen transferred across the capillary fringe as a result of the interfacial mass flux determined at the end of the imbibition experiment deviated from the oxygen mass calculated according to Eqn. 4.6. In contrast, the two lines coincide when looking at the respective result of the drainage experiment (Fig. 4.2d). This indicates that the presence of an entrapped gaseous phase impacts mass transfer at the unsaturated/saturated interface. To quantify this effect, we considered the (quasi) steady-state conditions before and after lowering or raising the water table in the drainage and imbibition experiments. Applying Eqn. 4.6, we can directly calculate the dispersive oxygen flux, $\dot{m}$, across the capillary fringe (in the absence of entrapped gas) as well as the corresponding theoretical value of the total oxygen flux in the effluent. An overview of the mass fluxes calculated according to Eqn. 4.6 as well as that measured in the experiment ((quasi) steady-state conditions before and after the movement of the water table) is given in Table 4.3.

For the drainage experiment, the measured and calculated values of the oxygen flux across the interface are very similar for both steady-state conditions considered, indicating that the analytical solution for the concentration (Eqn. 4.1) and the corresponding total mass flux (Eqn. 4.6) correctly describe the observed mass-transfer behavior. This conclusion is supported by the morphology of the capillary fringe, which in the case of drainage did not show a trapped gaseous phase (as an example, see Fig. 4.4a and Fig. 4.4b). Similar considerations apply for the steady-state case before increasing the height of the water table in the imbibition experiment: also in this case, the measured and calculated oxygen fluxes are very close. However, this does not hold true for the quasi steady state following imbibition. In fact, in the presence of entrapped gas (Fig. 4.4c), the oxygen flux across the unsaturated/saturated interface is lower by a factor of 1.7 than the theoretical value (i.e., assuming a fully water-saturated capillary fringe). We attribute this to the decrease in relative permeability and, thus, horizontal groundwater flow velocity as a result of the

entrapped gaseous phase within the interface region. Because the horizontal flow velocity is smaller, this also results in a lower transverse hydrodynamic dispersion value.

Table 4.3. Measured vs. calculated oxygen fluxes during drainage and imbibition.

	Drainage		**Imbibition**	
	Measured	Calculated	Measured	Calculated
Steady state when the water table is at its initial position (without entrapped gas)				
vertical flow-through area [cm^2]	16.9	16.9	12.0	12.0
v_a [$m\ d^{-1}$]	4.06	4.06	6.04	6.04
mass flux, inlet [$mg\ s^{-1}$]	4.38×10^{-5}	4.38×10^{-5}	4.05×10^{-5}	4.05×10^{-5}
mass flux, outlet [$mg\ s^{-1}$]	4.97×10^{-5}	4.94×10^{-5}	4.80×10^{-5}	4.83×10^{-5}
Δin/out [$mg\ s^{-1}$] [1)]	5.88×10^{-6}	5.55×10^{-6}	7.47×10^{-6}	7.76×10^{-6}
(Quasi) steady state after the change in water table height (entrapped gas present after imbibition; not considered in calculated values)				
vertical flow-through area [cm^2]	11.9	11.9	16.3	16.3
v_a [$m\ d^{-1}$]	5.58	5.58	4.35	4.35
mass flux, inlet [$mg\ s^{-1}$]	3.21×10^{-5}	3.21×10^{-5}	4.37×10^{-5}	4.37×10^{-5}
mass flux, outlet [$mg\ s^{-1}$]	3.95×10^{-5}	4.00×10^{-5}	4.70×10^{-5}	4.93×10^{-5}
Δin/out [$mg\ s^{-1}$] [1)]	7.40×10^{-6}	7.87×10^{-6}	3.30×10^{-6}	5.60×10^{-6}

[1)] oxygen flux across the unsaturated/saturated interface

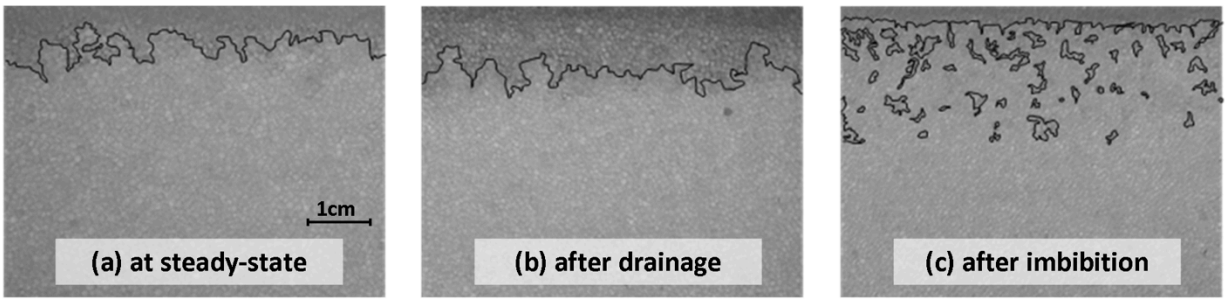

Fig. 4.4. Capillary fringe morphology (a) at steady state, (b) after drainage, and (c) after imbibition. The black lines indicate the interface between the aqueous and the gaseous phases.

4.4.2 Periodic Water Table Fluctuations

The results discussed above show the importance of air entrapment and subsequent partitioning between the gaseous and the aqueous phases as well as of specific yield in the supply of oxygen to groundwater during single imbibition and drainage events. We now extend the investigation to repeated water table fluctuations, considering both fast and slow movements of the phreatic surface.

4.4.2.1 Fast Water Table Fluctuations

When applying a pulse-like forcing, we observed quasi-rectangular water table fluctuations. Under these conditions, we investigated the impact of a rapid raising and lowering of the pressure head on oxygen transfer across the capillary fringe. We selected the same characteristic time of the induced water table fluctuations (15 min) and the same horizontal seepage velocity (4.09 to 6.63 m d^{-1}) as for the single events studied above (Table 4.2). The main difference is that in these sequential fluctuations, the sudden drop in the water table occurred (after 7 h) when gas partitioning in the unsaturated/saturated interface region was still ongoing.

After the establishment of steady-state conditions (i.e., exchange of 2 PVs), three cycles of vertical movement of the water table were completed during a time period of 42 hours. Figure 4.5a shows the preset pumping scheme at the base of the flow-through chamber, representing the boundary conditions inducing the vertical oscillations of the water table. A positive or negative value indicates that water is flowing into or out of the system, whereas a value of 0 refers to the case where the pump was not operating. The corresponding vertical locations of the water table and the upper limit of the capillary fringe are displayed in Fig. 4.5b as a function of the number of pore volumes flushed through the system. Apart from an initial peak in the location of the water table observed at the piezometers, the system's hydraulic response to the applied external forcing is a quasi-rectangular wave function. In terms of mass transfer, the oxygen fluxes measured in the effluent of the flow-through chamber are shown in Fig. 4.5c. The cumulative oxygen mass supplied to the aqueous phase as a consequence of the transient fluctuations is shown in Fig. 4.5d. Additionally, the calculated amount of oxygen transferred across the unsaturated/saturated interface due to transverse hydrodynamic dispersion alone and in the absence of entrapped gas is shown.

During imbibition, air was entrapped in the transition region between the unsaturated and the fully water-saturated zones. Subsequently, oxygen dissolved into the flowing oxygen-depleted groundwater, resulting in high oxygen fluxes in the effluent (Fig. 4.5c). Also, the cumulative oxygen mass slowly increased after each imbibition event (Fig. 4.5d). Toward the end of each stabilizing period following imbibition, the dissolution process just started to slow down (evident from the lower rate at which the cumulative oxygen mass increased) as drainage already sets in. The rapid decrease in water table height interrupted the gas partitioning between the aqueous and gaseous phases because the source of oxygen, i.e., the entrapped gas, was removed due to the falling water table. As in the single-event drainage experiment, a peak in oxygen flux can be observed. The observed maximum mass flux in the effluent was higher (1.2×10^{-4} mg s^{-1}, Fig. 4.5c) than the previous one (0.7×10^{-4} mg s^{-1}, Fig. 4.2c). Similarly, also the oxygen mass additionally supplied to the system during the respective periodic half cycle (0.2 mg, Fig. 4.5d) was larger than in the case of the single-event drainage experiment (0.1 mg). This increase in the supply of oxygen mass across the unsaturated/saturated interface resulted not only from the effect of specific yield, as

already discussed above. A second effect comes into play as the rapid vertical downward flow during drainage forces the oxygen mass deep into the water-saturated zone. We assume that this latter effect accounts for the observed difference in oxygen mass additionally supplied to the aqueous phase when compared with the single-event drainage experiment.

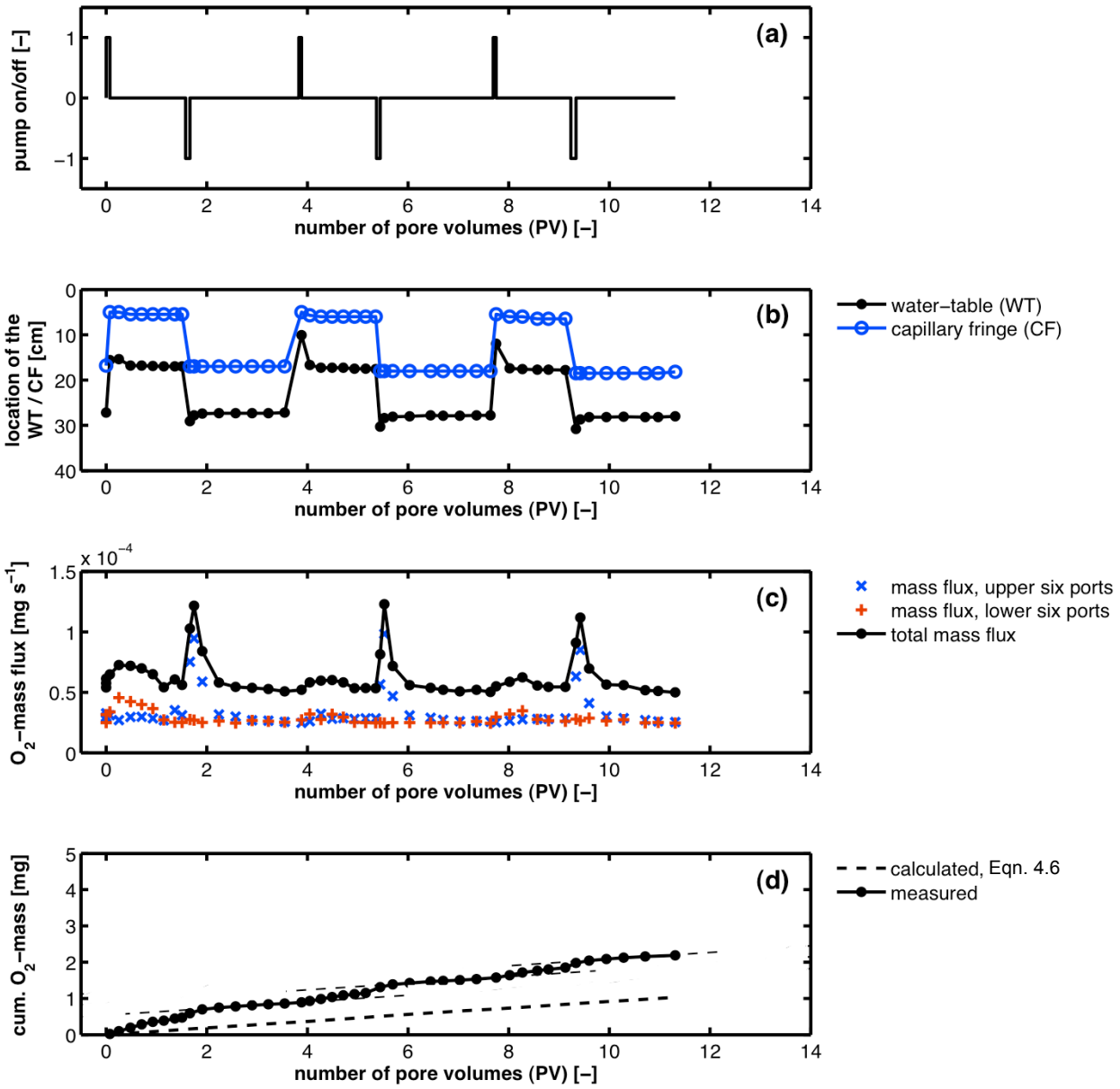

Fig. 4.5. Fast water table fluctuations: (a) pumping scheme of Pump 3 (0 PV marks the beginning of the change in water table height starting from steady-state flow); (b) vertical location of the water table and capillary fringe with respect to the upper edge of the chamber; (c) oxygen fluxes in the effluent of the flow-through system; (d) cumulative oxygen mass supplied across the interface due to the vertical movement of the water table. The additional thinner dashed lines indicate the time periods when the measured oxygen flux across the interface was similar to the calculated flux (i.e., same slope).

As an example, Fig. 4.6 shows the vertical profiles of equivalent aqueous oxygen concentration, measured during the third drainage phase, starting from the state just before the water table was

lowered (9.12 PVs). For reference, the diagram also shows the location of the upper limit of the capillary fringe before and after the drainage event.

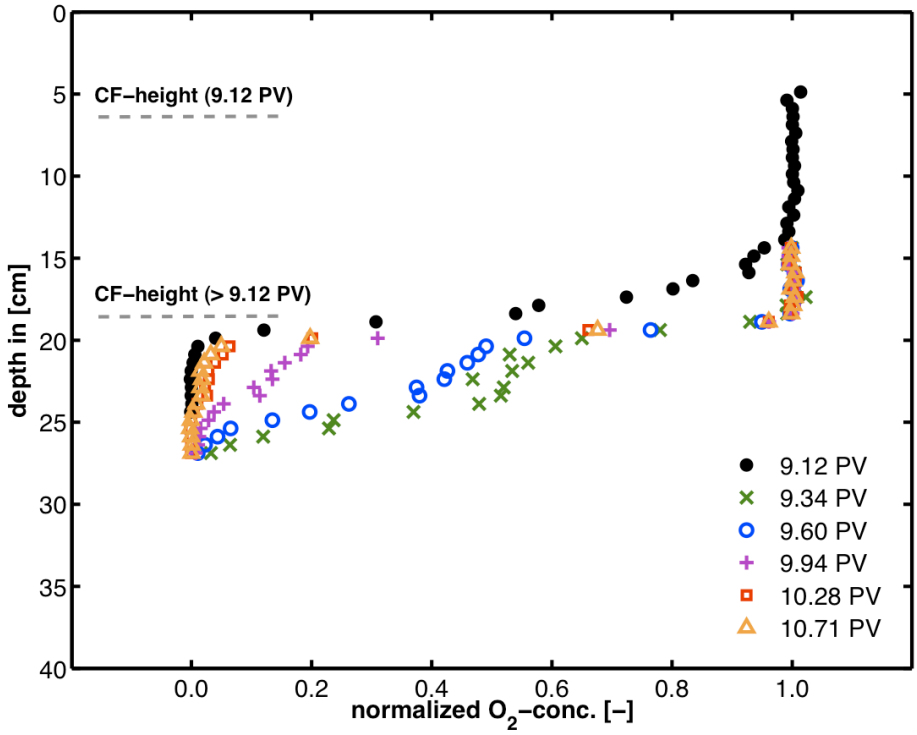

Fig. 4.6. Fast water table fluctuations: profiles of normalized equivalent aqueous oxygen concentration (at x = 0.60 m) during the third drainage period with respect to the capillary fringe (CF). The number of pore volumes (PVs) corresponds to those given in Fig. 4.5.

At the end of the last half-period, during which the water table had been raised, oxygen still dissolved from the entrapped gaseous phase into the bypassing oxygen-depleted water. This caused the oxygen concentration profile (9.12 PVs) to be in an intermediate position between two (quasi) steady states and represents the situation at the beginning of the drainage phase.

Under transient conditions (i.e., raising or lowering of the water table), the resulting flow field is characterized by both a horizontal and a vertical flow component. In fact, the flow direction and its magnitude depend on the underlying horizontal groundwater flow velocity as well as the preset water table fluctuation amplitude and speed. Drainage thus leads to additional advective flux and longitudinal dispersion in the vertical direction, causing the oxygen profile to move downward. Due to the rapid decrease in water table height, the relative thickness (i.e., the ratio between the penetration depth of oxygen and the total water depth) of the oxygen-containing layer increased in the present case. Thus, higher oxygen fluxes in the effluent were observed (Fig. 4.5c). This effect is expected to be more pronounced for fast water table fluctuations but probably also depends on the magnitude of change in water table height and the thickness of the unconfined aquifer.

Subsequently to the lowering of the water table, the values of the cumulative oxygen mass increased by the same rate (as indicated by the parallel dashed lines additionally shown in Fig. 4.5d). The slope of the measured curve equals the one representing the calculated amount of oxygen supplied across the unsaturated/saturated interface as a result of transverse vertical dispersion alone (Eqn. 4.6). This can be observed for each half period and is due to the fact that after drainage no entrapped gas was present within the capillary fringe. Moreover, steady-state conditions applied shortly after the lowering of the water table because seepage water with high oxygen concentrations was flushed out of the system after one pore volume. This effect can also be noticed in the oxygen concentration profiles, which reached a new quasi equilibrium state after this time (Fig. 4.6, compare 9.34 with 10.28 and 10.71 PVs). During the time period in which the values of cumulative oxygen mass (measured and calculated using Eqn. 4.6) increased by the same rate, the oxygen flux across the capillary fringe was only provided by the dispersive mechanism and no additional supply of oxygen was observed.

4.4.2.2 Slow Water Table Fluctuations

We also examined the case of slow water table fluctuations induced with the pumping scheme shown in Fig. 4.7a. The hydraulic response of the system was a triangular fluctuation in the locations of the water table and capillary fringe (Fig. 4.7b). The time allowed to raise or lower the water table by 10 cm was 7 h, which is considerably longer than in the previous case (15 min). In Fig. 4.7b, the vertical locations of the water table and the capillary fringe vs. the number of pore volumes are displayed.

During the rise of the water table, the amount of entrapped gas gradually increased, thus causing an increase in the oxygen flux in the effluent (Fig. 4.7c). Partitioning between the aqueous and gaseous phases was still ongoing as the water table started to drain again. In the case of slow water table fluctuations, however, the entrapped gas was not released at once, as in the previous case (pulse-like forcing), but gradually. As a consequence, we still observed higher oxygen flux values during the subsequent drainage phase. When the entrapped gas was completely released due to drainage, and thus no additional oxygen could dissolve into the aqueous phase, mass fluxes were again similar to the initial value. This behavior is reflected in the trend of the cumulative oxygen mass, with longer periods of effective additional transfer of oxygen to the aqueous phase followed by periods characterized by a flatter trend in which the entrapped gas was completely released. The slopes of both the measured and calculated curves in Fig. 4.7d do not align toward the end of each respective half period during which the drop in water table elevation occurred. This highlights the fact that oxygen still would have to be flushed out from the system to reach steady-state conditions again.

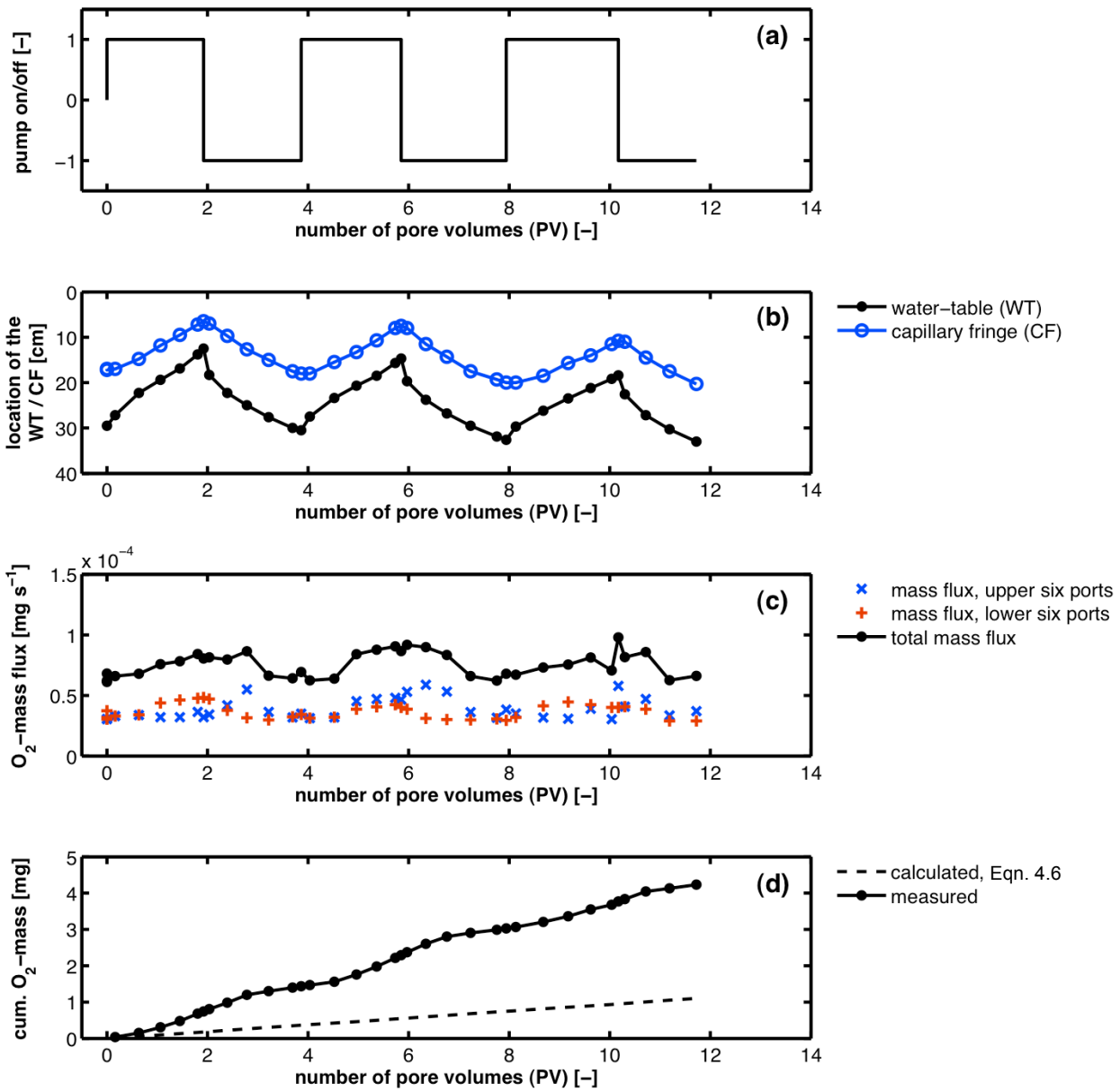

Fig. 4.7. Slow water table fluctuations: (a) pumping scheme of Pump 3 (0 PV marks the beginning of the change in water table height starting from steady-state flow); (b) vertical location of the water table and capillary fringe with respect to the upper edge of the chamber; (c) oxygen fluxes in the effluent of the flow-through system; (d) cumulative oxygen mass supplied across the interface due to the vertical movement of the water table.

The pronounced peak in oxygen flux right after inducing the lowering of the water table could not be observed in the present experiment (Fig. 4.7c) because the relative thickness of the oxygen-containing layer did not vary extensively throughout the experiment and the effect of specific yield can be neglected. Figure 4.8 shows the vertical profiles of normalized oxygen concentration measured during the third drainage period. The concentration profiles illustrate the effect of the gradual decline in water table elevation during this period of time based on the transition of the measured oxygen profiles between the beginning and the end of the drainage period.

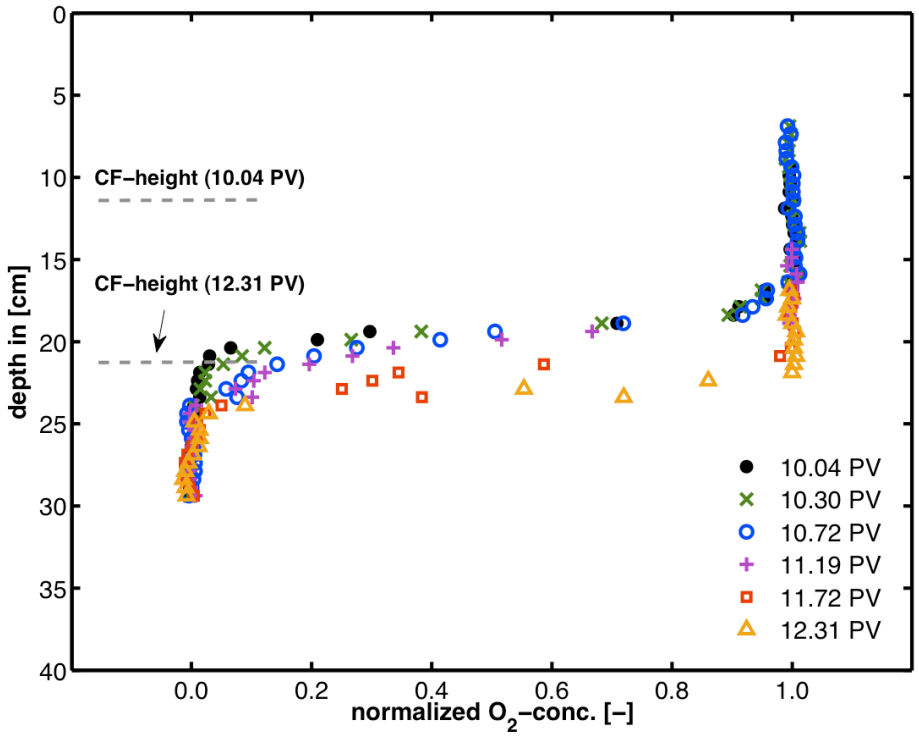

Fig. 4.8. Slow water table fluctuations: profiles of normalized equivalent aqueous oxygen concentration (at x = 0.60 m) during the third drainage period with respect to the capillary fringe (CF). The number of pore volumes (PVs) corresponds to those given in Fig. 4.7.

4.4.2.3 Comparison between Different Boundary Conditions

As discussed above, different processes are relevant for the mass transfer of oxygen in the capillary fringe depending on the boundary conditions applied. Figure 4.9 shows the cumulative oxygen masses supplied across the interface that were measured during the long-term experiments. It becomes evident that for the experimental conditions investigated in this study, the rectangular forcing resulting in a slow fluctuation of the water table caused a higher oxygen transfer (4.2 mg at the end of the third periodic cycle) than the pulse-like forcing (2.2 mg at the end of the third periodic cycle).

We also calculated the amount of oxygen that would have been supplied to the aqueous phase exclusively by dispersive mass transfer across the interface, assuming a ‘sequence of steady states’ (Eqn. 4.6). In such calculations, an influence on the cumulative oxygen mass due to the effects of specific yield, gas partitioning, or a possible change in the dispersive mass flux across the capillary fringe (caused by the presence of entrapped air) is not considered. Despite the difference in the variation of the horizontal flow velocity in the two experiments, the calculated values of the cumulative oxygen mass supplied to the system are very similar (continuous lines in Fig. 4.9). In contrast, for fast water table fluctuations, the measured and calculated values are rather different (by a factor of 2) because of the transient effects (e.g., specific yield) not taken into account by Eqn. 4.6. Even more pronounced is the difference between the measured and

calculated values for the case of slow water table fluctuations. In fact, the cumulative oxygen mass experimentally observed at the end of the experiment is almost three times larger than the calculated strictly dispersive one, thus pointing out the important role of air entrapment and gas/liquid partitioning for the oxygen supply to oxygen-depleted groundwater. The calculated cumulative oxygen mass considerably underestimated the actual oxygen transfer for both cases of fast and slow movements of the water table.

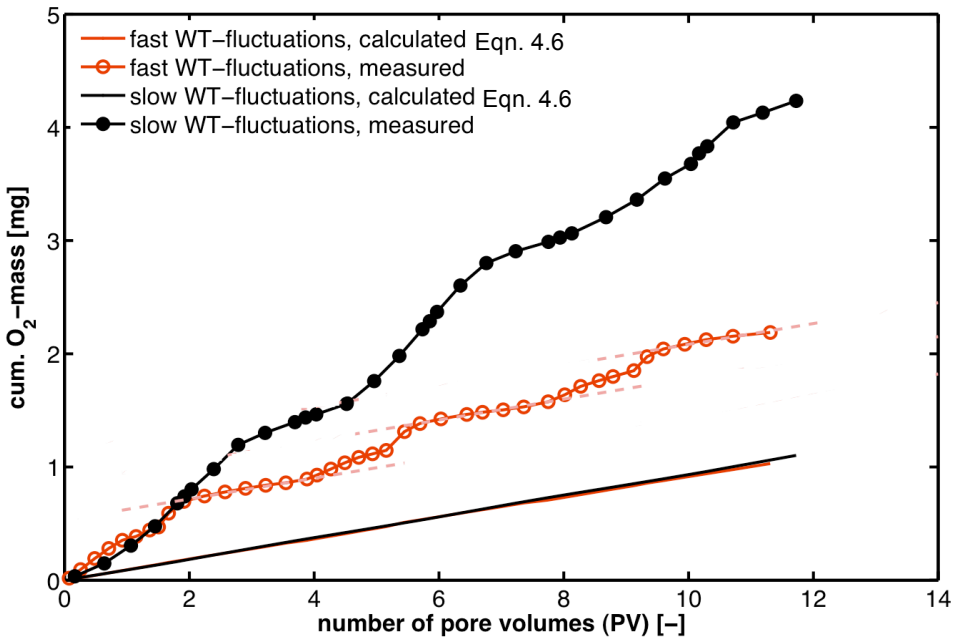

Fig. 4.9. Measured (symbols) and calculated (Eqn. 4.6, solid lines) cumulative oxygen masses for the long-term experiments with fast and slow water table (WT) fluctuations. The dashed lines indicate the time periods when the measured oxygen flux across the interface was similar (i.e., same slope) to the calculated flux.

It is important to point out that we did not observe a buildup of oxygen mass in the aqueous phase under any experimental condition tested. The results of our flow-through experiments indicate that the total amount of oxygen mass present in the system always returned to a certain 'background level' after the effect of gas partitioning between the aqueous and gaseous phases had ceased (Figs. 4.5c and 4.7c). This finding is due to the horizontal flow, which flushes out the additional oxygen transferred into the aqueous phase, and contrasts with previously published works. For instance, Caron et al. (1994) and Williams and Oostrom (2000) studied mass transfer across the capillary fringe in static laboratory systems (i.e., without the application of horizontal groundwater flow). In both studies, the researchers observed a steady increase in the mass of the volatile compounds considered due to the water table fluctuations applied.

4.5 Conclusions

In this study, we experimentally investigated the oxygen transfer in a fluctuating capillary fringe in both single drainage or imbibition events and in presence of a periodically changing water table. We could identify transient processes such as the dynamics of specific yield and the partitioning from air entrapment during drainage and imbibition, respectively, as effective mechanisms of oxygen transfer to oxygen-depleted groundwater. For the different experimental conditions, we quantified the additional contribution of these transient processes to the oxygen flux across the capillary fringe measured and calculated under (quasi) steady-state conditions.

As shown in the long-term experiments, hydraulic processes such as the dynamics of the water table fluctuations and the presence of a significant underlying horizontal groundwater flow velocity play an important role in the total oxygen mass present in the system. We conclude that, in the presence of significant horizontal groundwater flow, the mass of a volatile compound is continuously flushed out and the net increase of the mass of this species in the underlying water is considerably smaller than under static conditions. In our opinion, flow-through conditions are more relevant to represent and understand the complex interplay of different physical processes occurring in subsurface natural systems.

Moreover, we found that the dynamics of the water table fluctuations considerably affects the oxygen distribution in the capillary fringe and thus the measured oxygen fluxes in the effluent. We suggest that even more oxygen may be supplied to the aqueous phase in the case of a dynamic system, where the time period after rapidly lowering the water table is significantly shorter (<1 PV) than the time after increasing the height of the water table.

On the basis of our experimental outcomes, we hypothesize that mass transfer of volatile compounds from and to unconfined aquifers strongly depends on the characteristic time and frequency of the water table fluctuations, the induced change in pressure head, as well as the rate of groundwater flow. The amplitude and the speed with which the water table rises determine the amount of entrapped gas. Especially the ratio between the time needed to flush the additional amount of oxygen out of the system and the time available until the next increase in water table height occurs determines the buildup of oxygen mass in the system. Under natural conditions, seasonal fluctuations of the water table of an unconfined aquifer, comprising a comparably fast groundwater flow velocity, are likely to induce additional oxygen transfer only close to the interface because the oxygen supplied to the groundwater is efficiently flushed out. On the contrary, in a more static system, i.e., at slow groundwater flow, water table fluctuations can lead to a significant buildup of oxygen mass in the upper region of an unconfined aquifer.

Acknowledgement

This study was funded by the DFG (German Research Foundation) through the Research Group FOR 831 'Dynamic Capillary Fringes – A Multidisciplinary Approach' (grant GR971/22-1).

References

Amos, R.T. and Mayer, K.U., 2006. Investigating the role of gas bubble formation and entrapment in contaminated aquifers: Reactive transport modelling. Journal of Contaminant Hydrology, 87: 123-154.

Anderson, G.M. and Crerar. D.A., 1993. Thermodynamics in geochemistry – The equilibrium model. Oxford University Press, New York.

Atkins, P.W. and de Paula, J., 2006. Physikalische Chemie, 4th ed., Wiley-VCH.

Balcke, G.U., Meenken, S., Hoefer, C. and Oswald, S.E., 2007. Kinetic gas-water transfer and gas accumulation in porous media during pulsed oxygen sparging. Environmental Science and Technology, 41: 4428-4434.

Barber, C., Davis, G.B. and Farrington, P., 1990. Sources and sinks for dissolved oxygen in groundwater in an unconfined sand aquifer, Western Australia. *In* Barto-Kyriakidis, A. and Farrell, L. (eds.) Geochemistry of Gaseous Elements and Compounds. Theophrastus Publications, Athens, pp. 353-368.

Bauer, R.D., Rolle, M., Bauer, S., Eberhardt, C., Grathwohl, P., Kolditz, O. and Meckenstock, R.U, 2009. Enhanced biodegradation by hydraulic heterogeneities in petroleum hydrocarbon plumes. Journal of Contaminant Hydrology, 105: 56-68.

Bear, J. and Cheng, A.H.-D., 2010. Modeling groundwater flow and contaminant transport, 23rd Vol. Springer, New York.

Bear, J. and Verruijt, A., 1987. Modeling groundwater flow and pollution: with computer programs for sample cases. D. Reidel Publ. Co., Dordrecht, the Netherlands.

Berkowitz, B., Silliman, S.E. and Dunn, A.M., 2004. Impact of the capillary fringe on local flow, chemical migration, and microbiology. Vadose Zone Journal, 3: 534-548.

Caron, F., Wilkinson, S.R., Torok, J. Haas, M.K. and Selander, W.N., 1994. CO_2 transport through the capillary fringe in sand. Waste Management, 14(5): 421-433.

Caron, F., Manni, G., Workman, W.J.G., 1998. A large-scale laboratory experiment to determine the mass transfer of CO_2 from a sandy soil to moving groundwater. Journal of Geochemical Exploration, 64(1-3): 111-125.

Chapelle, F.H., 2001. Ground-water microbiology and geochemistry, 2nd ed., John Wiley & Sons, New York.

Chiogna, G., Eberhardt, C., Grathwohl, P., Cirpka, O.A. and Rolle, M., 2010. Evidence of compound dependent hydrodynamic and (hydro)mechanical transverse dispersion with multi-tracer laboratory experiments. Environmental Science and Technology, 44(2): 688-693, doi: 10.1021/es9023964.

Cirpka, O.A. and Kitanidis, P.K., 2001. Transport of volatile compounds in porous media in the presence of a trapped gas phase. Journal of Contaminant Hydrology, 49: 263-285.

Cussler, E.L., 2009. Diffusion: Mass transfer in fluid systems, 3rd ed., Cambridge University Press.

Dobson, R., Schroth, M.H. and Zeyer, J., 2007. Effect of water-table fluctuation on dissolution and biodegradation of a multi-component, light nonaqueous-phase liquid. Journal of Contaminant Hydrology, 94: 235-248.

Donaldson, J.H., Istok, J.D. and O'Reilly, K.T., 1998. Dissolved gas transport in the presence of a trapped gas phase: Experimental evaluation of a two-dimensional kinetic model. Ground Water, 36(1): 133-142.

Engel, T. and Reid, P., 2010. Physical Chemistry, 2nd ed. Upper Saddle River, Prentice Hall, New Jersey.

Fetter, C.W., 2001. Applied Hydrogeology, 4th ed., Upper Saddle River, Prentice Hall, New Jersey.

Fry, V.A., Istok, J.D. Semprini, L., O'Reilly, K.T. and Buschek, T.E., 1995. Retardation of dissolved oxygen due to a trapped gas phase in porous media. Ground Water, 33: 391-398.

Fry, V.A., Selker, J.S. and Gorelick, S.M., 1997. Experimental investigations for trapping oxygen gas in saturated porous media for in situ bioremediation. Water Resources Research, 33(12): 2687-2696.

Geistlinger, H., Jia, R., Eisermann, D. and Stange, C.F., 2010. Spatial and temporal variability of dissolved nitrous oxide in near-surface groundwater and bubble-mediated mass transfer to the unsaturated zone. Journal of Plant Nutrition and Soil Science, 173: 601-609.

Goode, D.J. and Konikow. L.F., 1990. Apparent dispersion in transient groundwater flow. Water Resources Research, 26(10): 2339-2351.

Haberer, C.M., Rolle, M., Liu, S., Cirpka, O.A. and Grathwohl, P., 2011. A high-resolution non-invasive approach to quantify oxygen transport across the capillary fringe and within the underlying groundwater. Journal of Contaminant Hydrology, 122(1-4): 26-39, doi: 10.1016/j.jconhyd.2010.10.006.

Hinz, C., 1998. Analysis of unsaturated/saturated water flow near a fluctuating water table. Journal of Contaminant Hydrology, 33(1-2): 59-80.

Holocher, J., Peeters, F., Aeschbach-Hertig, W., Hofer, M., Brennwald, M., Kinzelbach, W. and Kipfer, R., 2002. Experimental investigations on the formation of excess air in quasi-saturated porous media. Geochimica et Cosmochimica Acta, 66(23): 4103-4117.

Holocher J., Peeters, F., Aeschbach-Hertig, W., Kinzelbach, W. and Kipfer, R., 2003. Kinetic model of gas bubble dissolution in groundwater and its implications for the dissolved gas composition. Environmental Science and Technology, 37(7): 1337-1343.

Jost, D., Winter, J. and Gallert, C., 2011. Water and oxygen dependence of *Pseudomonas putida* growing in silica sand capillary fringes. Vadose Zone Journal, 10: 532-540, doi: 10.2136/vzj2010.0092.

Klenk, I.D. and Grathwohl, P., 2002. Transverse vertical dispersion in groundwater and the capillary fringe. Journal of Contaminant Hydrology, 58: 111-128.

Klump, S., Cirpka, O.A., Surbeck, H., Kipfer, R., 2008. Experimental and numerical studies on excess-air formation in quasi-saturated porous media. Water Resources Research, 44(5): W05402, doi: 10.1029/2007WR006280.

Krešić, N., 2007. Hydrogeology and groundwater modeling, 2nd ed. CRC Press, Boca Raton.

Legout, C., Molenat, J. and Hamon, Y., 2009. Experimental and modeling investigation of unsaturated solute transport with water-table fluctuations. Vadose Zone Journal, 8(1): 21-31, doi: 10.2136/vzj2007.0182.

Lehmann, P., Stauffer, F., Hinz, C., Dury, O. and Fluhler, H., 1998. Effect of hysteresis on water flow in a sand column with a fluctuating capillary fringe. Journal of Contaminant Hydrology, 33(1-2): 81-100.

Liu, S. 2008. Mass transfer of oxygen across the capillary fringe. Doctoral thesis. Institute for Geoscience, University of Tübingen, 58 p.

Liu, S., Liedl, R. and Grathwohl, P., 2010. Simple analytical solutions for oxygen transfer into anaerobic groundwater. Water Resources Research, 46: W10542, doi: 10.1029/2009WR008434.

Lucas, H.C. and Robinson, V.K., 1995. Modeling of rising groundwater levels in the chalk aquifer of the London basin. Quarterly Journal in Engineering Geology, 28 (Suppl. 1): S51-S61.

Maier, U., Rügner, H. and Grathwohl, P., 2007. Gradients controlling natural attenuation of ammonium. Applied Geochemistry, 22: 2606-2617.

McCarthy, K.A. and Johnson, R.L., 1993. Transport of Volatile Organic Compounds across the Capillary Fringe. Water Resources Research, 29(6): 1675-1683.

Meinzer, O.E., 1923. Outline of groundwater hydrology, with definitions. U.S. Geological Survey Water Supply Paper, 494.

Nachabe, M.H., 2002. Analytical expressions for transient specific yield and shallow water table drainage. Water Resources Research, 38(10), doi: 10.1029/2001WR001071.

Nielsen, P. and Perrochet, P., 2000. Water table dynamics under capillary fringes: experiments and modelling. Advances in Water Resources, 23(5): 503-515 [erratum: 23: 907-908].

Nordstrom, D.K. and Munoz, J.L., 1994. Geochemical Thermodynamics, 2nd ed., Blackwell Scientific Publications, Cambridge.

Parker, J.C. and Lenhard, R.J., 1987. A model for hysteretic constitutive relations governing multiphase flow, 1. Saturation-pressure relations, Water Resources Research, 23: 2187-2196.

Rainwater, K., Mayfield, M.P., Heintz, C. and Claborn, B.J., 1993. Enhanced in situ biodegradation of diesel fuel by cyclic vertical water table movement: preliminary studies. Water Environmental Research, 65: 717-725.

Rolle, M., Eberhardt, C., Chiogna, G., Cirpka, O.A. and Grathwohl, P., 2009. Enhancement of dilution and transverse mixing in porous media: Experiments and model-based interpretation. Journal of Contaminant Hydrology, 110: 130-142.

Ronen, D., Scher, H. and Blunt, M., 1997. On the structure and flow processes in the capillary fringe of phreatic aquifers. Transport in Porous Media, 28: 159-180.

Russo, D., Jury, W.A. and Butters, G.L., 1989. Numerical analysis of solute transport during transient irrigation, 2. The effect of immobile water. Water Resources Research, 25(10): 2119-2127.

Schneider-Zapp, K., 2009. Dynamics of water movement near boundaries of the vadose zone. Doctoral Thesis, University of Heidelberg, Heidelberg, 158 pp.

Stumm, W. and Morgan, J., 1996. Aquatic chemistry, chemical equilibria and rates in natural waters, 3rd ed. John Wiley and Sons Inc., New York.

Walter, G.R., Geddis, A.M., Murray, R. and Bentley, H.W., 2003. Vapor phase transport as a groundwater contamination process at arid landfill sites. Presented at the 18th International Conference on Solid Waste Technology and Management, Philadelphia, USA.

Washington, J.W., 1996. Gas partitioning of dissolved volatile organic compounds in the vadose zone: Principles, temperature effects and literature review. Ground Water, 34(4): 709-718.

Werner, A.D. and Lockington, D.A., 2003. Influence of hysteresis on tidal capillary fringe dynamics in a well-sorted sand. Advances in Water Resources, 26(11): 1199-1204.

Werner, D. and Höhener, P., 2002. The influence of water table fluctuations on the volatilization of contaminants from groundwater. p. 213–218. *In* Thornton, S.F. and Oswald, S.E. (ed.) Proc. Groundwater Quality 2001: Natural and Enhanced Restoration of Groundwater Pollution, Sheffield, UK. June 2001. IAHS publ. 275.

Williams, M.D. and Oostrom, M., 2000. Oxygenation of anoxic water in a fluctuating water table system: An experimental and numerical study. Journal of Hydrology, 230: 70-85.

Worch, E., 1993. Eine neue Gleichung zur Berechnung von Diffusionskoeffizienten gelöster Stoffe. Vom Wasser, 81: 289-297.

Zhang, M.H., Geng, S. and Ustin, S.L., 1998. Quantifying the agricultural landscape and assessing spatio-temporal patterns of precipitation and groundwater use. Landscape Ecology, 13(1): 37-53.

5. Experimental Sensitivity Analysis of Oxygen Transfer in the Capillary Fringe

Christina M. Haberer*, Olaf A. Cirpka, Massimo Rolle, Peter Grathwohl
Ground Water (2013), doi: 10.1111/gwat.12028.

Abstract

Oxygen transfer in the capillary fringe is of primary importance for a wide variety of biogeochemical processes occurring in shallow groundwater systems. In case of a fluctuating groundwater table two distinct mechanisms of oxygen transfer within the capillary zone can be identified: vertical predominantly diffusive mass flux of oxygen, and mass transfer between entrapped gas and groundwater. In this study, we perform a systematic experimental sensitivity analysis in order to assess the influence of different parameters on oxygen transfer from entrapped air within the capillary fringe to underlying anoxic groundwater. We carry out quasi two-dimensional flow-through experiments focusing on the transient phase following imbibition to investigate the influence of the horizontal flow velocity, the average grain diameter of the porous medium, as well as the magnitude and the speed of the water table rise. We present a numerical flow and transport model that quantitatively represents the main mechanisms governing oxygen transfer. Assuming local equilibrium between the aqueous and the gaseous phase, the partitioning process from entrapped air can be satisfactorily simulated. The different experiments are monitored by measuring vertical oxygen concentration profiles at high spatial resolution with a non-invasive optode technique as well as by determining oxygen fluxes at the outlet of the flow-through chamber. The results show that all parameters investigated have a significant effect and determine different amounts of oxygen transferred to the oxygen-depleted groundwater. Particularly relevant are the magnitude of the water table rise and the grain size of the porous medium.

Keywords: *2-D flow-through experiments; capillary fringe; water table fluctuation; oxygen transfer; experimental sensitivity analysis.*

5.1 Introduction

Fluctuations of the groundwater table can occur over a wide range of different spatial and temporal scales (e.g., Freeze and Cherry, 1979). In addition to natural factors like infiltration of rainwater and evaporation, changes in groundwater levels may arise from human activities such as

extensive groundwater pumping or artificial aquifer recharge. When the water table and the capillary fringe rise, air entrapment regularly occurs in the interface region between the unsaturated and the saturated zone. The volume of entrapped gas typically ranges between 10 % and 20 % of the pore space (Fry et al., 1997) and reduces the hydraulic conductivity in the quasi-saturated zone. Since most naturally occurring gases dissolve in water, the presence of an entrapped gaseous phase has a significant effect on groundwater geochemistry (e.g., Sinke et al., 1998; Zilberbrand, 2003; Amos and Mayer, 2006; Klump et al., 2008).

Several studies have pointed out how important water table fluctuations are for transport of different volatile compounds from groundwater to the unsaturated zone (e.g., Lappala and Thompson, 1983; Werner and Höhener, 2002), the implications for risk assessment (e.g., soil gas monitoring), and the impact on remediation effectiveness at contaminated sites (McCarthy and Johnson, 1993; Werner et al., 2004; Oswald et al., 2008). Other contributions focused on the influence of water table fluctuations on mass transfer (e.g., of oxygen) from the unsaturated zone to the underlying groundwater (Barber et al., 1990; Williams and Oostrom, 2000; Balcke et al., 2007; Geistlinger et al., 2010; Haberer et al., 2012). A term that often occurs in this context is “excess air” (Heaton and Vogel, 1981), indicating the supersaturation of atmospheric gases in groundwater resulting from the dissolution of entrapped gas at pressures higher than the atmospheric pressure.

The concurrent presence of oxygen and water in the capillary fringe provides a beneficial environment for endogenous aerobic strains (Yadav and Hassanizadeh, 2011; Rasa et al., 2011; Jost et al., 2011). Therefore, biogeochemical processes that are limited by oxygen availability may be enhanced within this transition zone by increased rates of oxygen transfer (Holocher et al., 2003; Dobson et al., 2007; Farnsworth et al., 2012).

In a recent study (Haberer et al., 2012), we investigated oxygen transfer in a fluctuating capillary fringe. In that work, we identified the entrapment of air and the subsequent partitioning of oxygen between the aqueous and gaseous phases as key mechanisms resulting in the enhancement of oxygen supply to oxygen-depleted groundwater. We also highlighted the important role of flow-through conditions, showing that the horizontal groundwater velocity can prevent a significant buildup of oxygen mass in an unconfined aquifer.

The objective of this work is to investigate oxygen dissolution from entrapped gas during the transient phase following a single imbibition event (here: a rise of the groundwater table). With rising water levels, the extent of air entrapment is affected by flow conditions and porous media properties. We perform an experimental sensitivity analysis on oxygen transfer to anoxic groundwater in a quasi two-dimensional flow-through laboratory setup: a reference scenario is identified and different experiments are subsequently run systematically changing one parameter at a time. Therefore, we can evaluate the specific influence of (i) the average grain size, (ii) the

time over which the water table rises, (iii) the groundwater flow velocity, and (iv) the magnitude of the water table increase on oxygen transfer.

5.2 Theoretical Background

In this study, we define the capillary fringe as the region extending from the water table up to the limit of the capillary rise of water. The capillary fringe's thickness and the vertical distribution of water content depend on the properties and on the homogeneity of the porous medium. Moreover, gas clusters (i.e., local zones of entrapped air) may also be present below the water table (Berkowitz et al., 2004).

Essentially, three processes describe the interaction of groundwater with entrapped gas (Amos and Mayer, 2006): the entrapment and the release of air during raising and lowering of the water table, the formation of a gaseous phase and its growth and shrinkage resulting from changes in dissolved gas pressure, as well as the permeability changes due to variations in gas saturation.

Transport of a volatile compound within quasi-saturated porous media is affected by the presence of an entrapped gaseous phase (Fry et al., 1995; Donaldson et al., 1997; Cirpka and Kitanidis, 2001; Geistlinger et al., 2005; Klump et al., 2008; Geistlinger et al., 2010; Rudolph et al., 2012): volatile compounds are transferred between the aqueous and gaseous phases as a result of the difference in their chemical potentials between the two phases. Equilibrium is achieved, when the chemical potential for each given compound, present in the multiphase system, is identical in all phases (e.g., Atkins and de Paula, 2006). Under this condition the concentration, C_i^{aq} [M L^{-3}], of the dissolved gas i is related to its partial pressure, p_i [M L^{-1} T^{-2}], and atmospheric concentration, C_i^g [M L^{-3}], in the ideal gas phase by the compound-specific Henry's law coefficient, $K_{H,i}$ [-]:

$$C_i^{aq} = \frac{p_i}{\Re T K_{H,i}} = \frac{C_i^g}{K_{H,i}} \tag{5.1}$$

in which $\Re$ [L^2 t^{-1} T^{-2}] denotes the ideal gas constant and T [t] is the absolute temperature in K.

In most problems multiple dissolved gases are transferred simultaneously between the aqueous and the gaseous phases (Donaldson et al., 1998). If net transfer of all volatile compounds is directed from the gaseous to the aqueous phase, while equilibrium between the two has to be maintained, the volume of the entrapped gas has to shrink in order to balance the decrease in $\sum p_i$ in the gaseous phase. Locally, at the gas/water interface, a balance of forces is reached when the sum of partial pressures within the gas phase approximates the total gas pressure, p [M L^{-1} T^{-2}], equal to the sum of atmospheric pressure, capillary pressure, and hydrostatic pressure (Cirpka and Kitanidis, 2001). No gaseous phase is present at equilibrium when the sum of partial pressures computed through Henry's law is smaller than p.

For typical groundwater flow velocities, the timescale of gas transfer is small in comparison to the advective-dispersive timescale. In fact, the timescale for gas transfer between groundwater and entrapped gas is usually smaller than an hour. Therefore, in such flow-through systems, local equilibrium between the aqueous and entrapped gaseous phases can be assumed to hold (Cirpka and Kitanidis, 2001; Geistlinger et al., 2005; Klump et al., 2008). The total amount of oxygen, transferred from the entrapped gas into the oxygen-depleted water flowing by, is determined by the initially entrapped gas volume: the more air is entrapped, the higher the number of pore volumes needed for the dissolution process. Assuming the gas saturation (defined as the volume of gas per pore volume) does not change, a constant retardation factor, *R* [-], can be defined for a compound *i* according to the linear theory of partitioning tracers:

$$R_i = \frac{t_i}{t_c} = 1 + \frac{K_{H,i} S_g}{1 - S_g} \tag{5.2}$$

where t_i [T] and t_c [T] denote the mean arrival time of a partitioning and a non-partitioning tracer, while S_g [-] represents the value of gas saturation within the quasi-saturated region of the unconfined aquifer.

However, in most of the reported studies (Fry et al., 1995 and 1997; Donaldson et al., 1997 and 1998), the volatile tracer test itself triggered changes in gas saturation, thus, complicating the analysis of the results. This is explained by the fact that, if the concentration of one compound varies, the gas saturation and, therefore, also the retardation factors of all compounds undergoing partitioning may change (Cirpka and Kitanidis, 2001; Geistlinger et al., 2005). The system can be described using the total concentration, C_i^{tot} [M L^{-3}], denoted as the mass of compound *i* in all phases per pore volume (Helfferich, 1981):

$$C_i^{tot} = \left(1 - S_g\right) C_i^{aq} + S_g C_i^{g} = \left[1 + \left(K_{H,i} - 1\right) S_g\right] C_i^{aq} \tag{5.3}$$

The right-hand side in Eqn. 5.3 is valid under the assumption of local equilibrium at the gas-water interface. After combining Eqns. 5.1 and 5.3 and rearranging, the partial pressure for each compound *i* can be expressed as:

$$p_i = \frac{C_i^{tot} \Re T K_{H,i}}{1 + \left(K_{H,i} - 1\right) S_g} \tag{5.4}$$

Thermodynamic equilibrium is reached by adjusting the value of S_g such that Henry's Law is satisfied for all compounds and a balance of forces between the sum of partial pressures and the total gas pressure at the gas/water interface is achieved.

5.3 Experimental Setup

In this study, we investigate oxygen transfer in the capillary fringe in the presence of anoxic water moving in the horizontal direction. We assume that the water table rises in response to upward flow of groundwater. Under field-conditions this situation is relevant for a number of hydrogeological settings such as close to water bodies with changing water levels, water management in cities, or in the case where recharge occurs in a remote area, causing the water table to rise in another region, where no overlying strata is present (semi-confined aquifer).

The experiments were performed using the same experimental setup as described by Haberer et al. (2012), which consists of a quasi two-dimensional flow-through chamber with inner dimensions of 80 cm (length, *L*) × 40 cm (height, *H*) × 0.5 cm (width, *W*) (see Fig. 5.1a). To prevent considerable evaporation of water during the experiment, the chamber was covered by a lid but remained open to the atmosphere. We conducted the experimental runs in a temperature-controlled room at 22 °C.

Glass beads with two different ranges in grain diameter were used as porous media. The grain diameter of the 'fine' material (Sartorius GmbH, Göttingen, Germany) ranged between 0.4 and 0.6 mm, resulting in an average porosity of 40.2 % and a capillary fringe height of ~117 mm. The 'coarse' material (Fisher Scientific GmbH, Schwerte, Germany) diameter was in the range of 1.0 to 1.5 mm with an average porosity of 40.4 % and a capillary fringe height of ~22 mm.

Two peristaltic pumps (IPC 24, ISMATEC, Glattbrugg, Switzerland), connected to the ports at the inlet and the outlet of the flow-through chamber, were used to establish a predominantly horizontal flow field. Steady-state conditions for flow and transport were reached after flushing the system with at least two pore volumes of oxygen-depleted water (prepared by stripping it with nitrogen gas and stored in a gas-tight Tedlar® sampling bag). Subsequently, we changed the water table height with a third pump (IPC-N 24, ISMATEC, Glattbrugg, Switzerland) connected to the ports at the base of the flow-through chamber. After raising the water table, the water level was kept constant by adjusting the lowermost, free outlet port to the desired water table position. The position of the water table was identified with two piezometers located near the inlet and the outlet of the flow-through chamber (Fig. 5.1a). Furthermore, we visually determined the upper limit of the capillary fringe. This was easily done in both porous materials used since the water saturation changed rapidly over a small vertical distance in this transition zone (~0.7 cm; Haberer et al., 2011).

A tracer experiment* was performed within a porous medium packing consisting of the fine material (0.4 to 0.6 mm glass beads). The tracer test allowed visualizing and understanding the (quasi) steady-state flow field before (Fig. 5.1b) and after the fluctuation of the water table. A red dye (New Coccine, CAS: 2611-82-7, 75 mg L^{-1}) was continuously injected via all inlet ports located

*) Photographs taken during the tracer experiment are included as a movie in the Appendix A.2.

along the lower 15 cm of the flow-through chamber (i.e., by using Pump 1 in Fig. 5.1). The propagation of the tracer front was followed by mapping isochrones (lines of equal mean travel time, that is, tracer front positions at given time points) at 30 min time intervals on the front pane of the chamber. The isochrones provide important information on the velocity distribution in the domain, which was useful in setting up the numerical simulations.

Vertical profiles of equivalent aqueous oxygen concentration were measured at two distances from the inlet (i.e., at x_1 = 45 cm and x_2 = 60 cm, which are the latter two polymer stripes in Fig. 5.1b) and at high spatial resolution (2.5 mm spacing). The method applied is based on a non-invasive optode technology (Fibox3, PreSens GmbH, Regensburg, Germany), in which the luminescence within a polymer foil is quenched in the presence of oxygen (e.g., Haberer et al., 2011; Rudolph et al., 2012). Furthermore, we used two flow-through cells (1.7 mL volume each, Fig. 5.1a) at the outlet to determine the total oxygen flux in the effluent of the flow-through chamber. The mass flux measurements in the effluent allowed quantifying the amount of oxygen supplied to the aqueous phase across the unsaturated/saturated interface.

In the case of an imbibition event, the overall mass transfer process can be divided into the following steps (Fig. 5.2):

1. Steady state (before imbibition): the water table is held constant and no entrapped gas is present within the capillary fringe. Mass flux across the fully water-saturated capillary fringe can be described by hydrodynamic transverse vertical dispersion (Klenk and Grathwohl, 2002; Haberer et al., 2011).

2. The time period (Δt) during which the water table is raised by ΔH_{WT}: within the transition zone air is entrapped. As a consequence, volatile compounds partition between the aqueous and entrapped gaseous phase in order to reach equilibrium. Just looking at the main air constituents (i.e., oxygen and nitrogen), oxygen is transferred into the mobile aqueous phase, whereas nitrogen partitions into the gaseous phase. The gas saturation adapts in accordance to the local equilibrium assumption (Eqns. 5.3 and 5.4).

3. The time period during which oxygen is still supplied from entrapped gas to the oxygen-depleted aqueous phase; the position of the water table is held constant. A retarded oxygen dissolution front travels through the system.

4. Quasi steady state following imbibition: after exchange of R_{O2} pore volumes, oxygen partial pressure within the entrapped gaseous phase is in equilibrium with the oxygen content of the incoming water (background concentration), modified only by the dispersive flux across the unsaturated/saturated interface. Nitrogen (more strongly retarded than oxygen, see Eqn. 5.2) and other volatile compounds (e.g., helium, neon) are still transferred between the two fluid phases in order to achieve equilibrium in the system.

5. Steady state (after imbibition): entrapped gas tends to dissolve toward a new steady state where mass transfer across the fully water-saturated capillary fringe again is a function of transverse vertical dispersion alone.

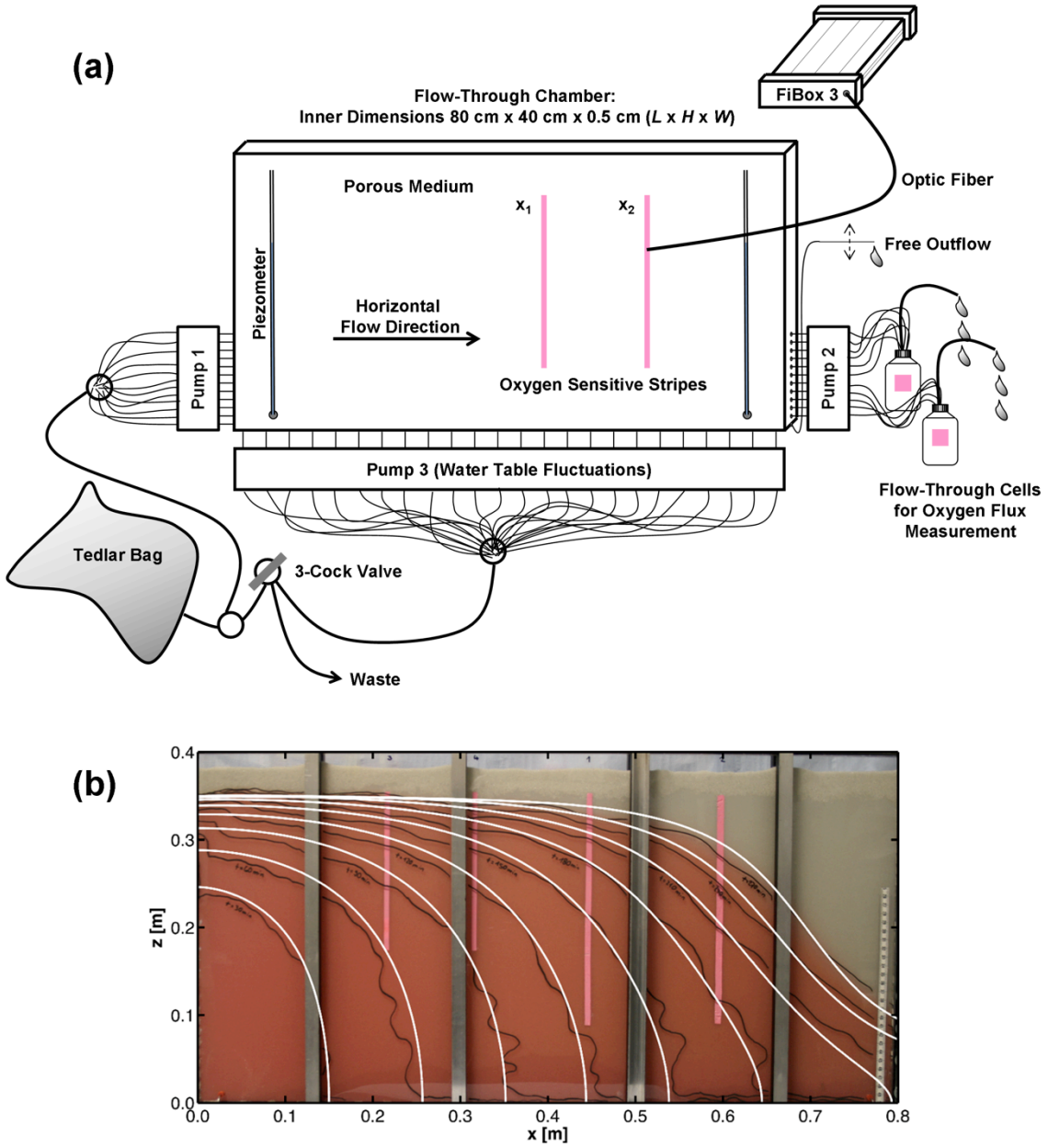

Fig. 5.1. Experimental setup and tracer test: (a) Experimental setup: Pump 1 and Pump 2 are used to establish the horizontal flow field, whereas the water table fluctuations are induced with Pump 3; (b) photograph of the flow-through chamber with experimentally determined isochrones (black lines) mapped during the tracer test when steady state for flow was reached and before the water table fluctuation was induced (i.e., no entrapped gas present within the upper region of the water-filled porous medium). Superimposed are the numerically simulated isochrones (white lines). The groundwater flow-direction is from left to right and the vertical pink lines are the polymer stripes used for the non-invasive oxygen measurement.

The focus of this study is the transient phase of oxygen dissolution following imbibition, that is, steps 3 to 4 in Fig. 5.2, in different experiments. Imbibition was initiated by activating the pump at the bottom of the flow-through chamber (Pump 3 in Fig. 5.1a), which provided a vertical flow component and caused the water table to rise.

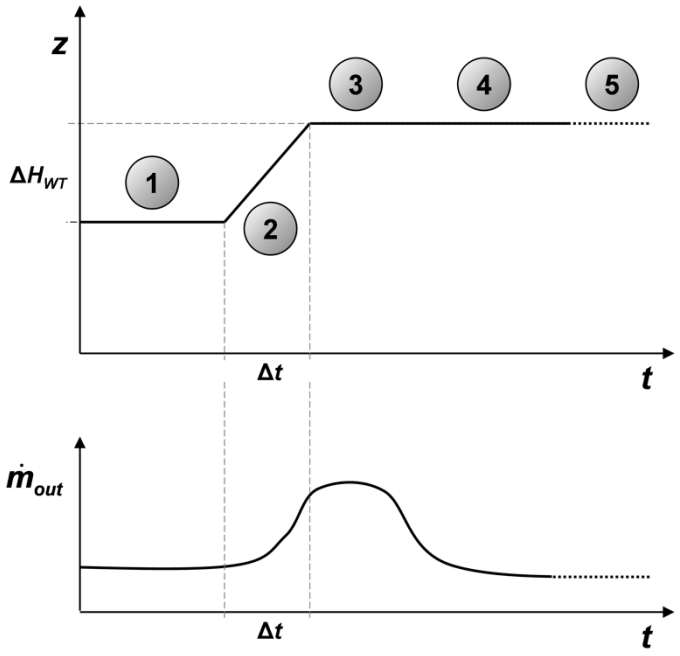

Fig. 5.2. Overall mass transfer process for an imbibition event: (1) steady state before imbibition; (2) water table is raised; (3) oxygen supply from entrapped gas to the aqueous phase; (4) quasi steady state following imbibition; (5) steady state after imbibition: all entrapped gas has dissolved. Δt is the time it takes to raise the water table by ΔH_{WT} and $\dot{m}_{out}$ is the mass flux determined in the effluent of the flow-through chamber.

5.4 Modeling Approach and Data Analysis

5.4.1 Flow and Transport Model

We simulated the flow field observed in the experimental setup and the most relevant mass transfer processes affecting oxygen transport with a two-dimensional numerical model, following the approach of Cirpka et al. (1999). First, we constrained the flow parameters by comparing the simulated isochrones to the experimental ones obtained from the tracer test (Fig. 5.1b). Subsequently, we focused on the imbibition phase of a selected reference scenario ('Experiment 1') and applied the flow and transport model to quantitatively interpret our experimental observations.

Steady-state flow was computed by solving the continuity equation:

$$\nabla \cdot \left(k_r K \nabla h \right) = 0 \tag{5.5}$$

subject to constant flux boundary conditions at the inlet and outlet, no flow boundary conditions at the bottom and the top of the domain, and a fixed-head boundary condition at the bottom node of the outlet boundary. k_r [-] is the relative permeability, K [L T^{-1}] is the saturated hydraulic conductivity, here assumed isotropic, and h [L] represents the hydraulic head.

The Brooks-Corey (1964) model was used to parameterize the vertical profile of effective water saturation, S_e [-], which is defined as the normalized volumetric water content:

$$S_e = \frac{\theta_{aq} - \theta_r}{\theta_s - \theta_r} \tag{5.6}$$

It is assumed that the volumetric water content, θ_{aq} [-], ranges between a minimum, so-called residual water content, θ_r [-], and a maximum value, θ_s [-], denoted saturated water content; the latter being identical to the storage-effective porosity. S_e, therefore, ranges between zero and one and the water saturation profile is described by:

$$\begin{aligned} S_e &= \left(\frac{h_b}{h_c}\right)^{\lambda} && \text{if } h_c \geq h_b \\ S_e &= 1 && \text{if } h_c < h_b \end{aligned} \tag{5.7}$$

in which h_b [L] is the air-entry pressure head, or bubbling pressure head, and h_c = max(z-h,0) [L] denotes the capillary pressure head, a positive quantity above the water table. Furthermore, λ [-] represents the pore-size distribution index.

We applied the following commonly used expression to estimate the relative permeability for water in the unsaturated zone (Burdine, 1953):

$$k_r(h_c) = S_e(h_c)^{\frac{2+3\lambda}{\lambda}} \tag{5.8}$$

Hydraulic conductivity is reduced in the quasi-saturated zone of an unconfined aquifer (e.g., Ryan et al., 2000; Amos and Mayer, 2006), which leads to a change of groundwater flow. The seepage velocity, v_a [L T^{-1}], needed for solute transport was computed as:

$$v_a(h_c) = \frac{k_r(h_c)}{\theta_{aq}} q^{sat} \tag{5.9}$$

in which q^{sat} [L T^{-1}] is the specific discharge in the fully water-saturated zone.

Potentials and stream-function values were calculated by bilinear Finite Elements, applying Picard iteration to address the nonlinearity of relative permeability. Travel time, τ [T], needed to make use of experimental isochrones of the tracer test (Fig. 5.1b), was computed with temporal-moment generating equations (e.g., Harvey and Gorelick, 1995):

$$-\nabla \cdot \left(\theta_{aq} \mathbf{D} \nabla \tau\right) + \mathbf{q} \cdot \nabla \tau = \theta_{aq} \tag{5.10}$$

in which $\mathbf{D}$ [L^2 T^{-1}] is the dispersion tensor and $\mathbf{q}$ [L T^{-1}] represents the specific-discharge vector. As boundary conditions, we fixed the travel time to zero at the inlet, and applied zero-diffusive-flux conditions at all other boundaries.

The moment-generating equation as well as the transport equation discussed below were simulated by the linear finite element method applying the streamline-upwind Petrov-Galerkin approach (Brooks and Hughes, 1982) for stabilization. A good agreement between simulated and experimental isochrones was achieved with the Brooks-Corey parameters λ = 2.0 and h_b = 0.086 m (here just determined for glass beads with d = 0.4 to 0.6 mm; an additional tracer test for the coarse porous material was not performed and, thus, the respective Brooks-Corey parameters were not determined).

In case of lowering of the water table, the water saturation profile moves downward and does not considerably change its shape, except for a short-term impact caused by the effect of specific yield (Haberer et al., 2012). A rather significant change in the shape of the water saturation profile is found, however, for the upward movement of the water table, where entrapment of air occurs in the upper volume of the water-filled porous medium. Since in a natural porous medium, the capillary forces usually dominate over the buoyancy forces (e.g., Fry et al., 1997), the entrapped gas clusters are spatially fixed. In the simulations, we also assumed the gas clusters to be homogeneously distributed. We simulated the concentration distributions for oxygen and nitrogen (since both compounds are highly relevant for gas partitioning; see e.g., Cirpka and Kitanidis, 2001; Klump et al., 2008) solving the advection-dispersion equation:

$$\frac{\partial\left(\theta_{aq}C_i^{tot}\right)}{\partial t}+\mathbf{q}\cdot\nabla C_i^{aq}-\nabla\cdot\left(\theta_{aq}\mathbf{D}\nabla C_i^{aq}\right)=0 \qquad (5.11)$$

where t [T] is time.

In each time step, the total concentrations were updated by solving Eqn. 5.11, keeping the gas saturation constant. Subsequently, the aqueous-phase concentrations and the gas saturation were updated by re-equilibration. The inflow solution was reduced in oxygen, whereas the aqueous oxygen concentration at the top of the domain was fixed to the concentration in equilibrium with the atmosphere. The oxygen flux at the bottom boundary was set to zero and the flux at the outlet boundary was restricted to the advective component. Gas partitioning and pressure induced changes in gas saturation were modeled based on the local equilibrium approach described above (Eqns. 5.1 through 5.4) and elsewhere (e.g., Cirpka and Kitanidis, 2001; Amos and Mayer, 2006; Klump et al., 2008). It would have been conceptually incorrect to apply simpler models that were derived for closed systems (e.g., Heaton and Vogel, 1981; Stute et al., 1995; Aeschbach-Hertig et al., 2000) to analyze the oxygen distribution in our flow-through system (Klump et al., 2008). In fact, in the present case dissolution fronts evolved with chromatographic separation of more and less soluble volatile compounds (Cirpka and Kitanidis, 2001).

Transverse dispersion is essential for mass transfer of volatile compounds across the capillary fringe (e.g., Klenk and Grathwohl, 2002; Liu et al., 2010). Based on the results of previous steady-

state experiments (Haberer et al., 2011), we used the empirical expression proposed by Chiogna et al. (2010) to parameterize the transverse vertical hydrodynamic dispersion coefficient, D_t [L^2 T^{-1}]:

$$D_t \approx D_p + v_a \frac{d}{\sqrt{\frac{v_a d}{D_{aq}} + 123}} \tag{5.12}$$

in which $D_p \approx \phi D_{aq}$ [L^2 T^{-1}] is the pore diffusion coefficient, D_{aq} [L^2 T^{-1}] represents the aqueous molecular diffusion coefficient, ϕ [-] denotes the porosity, and d [L] is the grain diameter. This expression retains an explicit dependence of the mechanical dispersion term on the aqueous diffusion coefficient of the transported tracer and shows a non-linear relationship with the average seepage velocity due to the compound-specific incomplete mixing in the pore channels (Rolle et al., 2012). Our former results (Haberer et al., 2011) showed that mass transfer across the fully-water saturated capillary fringe can be successfully described using this parameterization.

As aforementioned, the model was applied to reproduce the experimental results (i.e., measured vertical oxygen concentration profiles; nitrogen was not detected during the experiment) obtained for a reference case ('Experiment 1'). The measured flow rate in the horizontal direction was 2 mL min^{-1}. Within the scope of the experimental sensitivity analysis, we also performed further imbibition experiments for which, however, the numerical model was not fitted to the data.

All concentrations of dissolved gases were expressed as normalized equivalent aqueous concentrations, C_{norm} [-], defined as:

$$C_{norm}(x,z) = \frac{C - C_{bg}}{C_0 - C_{bg}} \tag{5.13}$$

In doing so, we standardized the simulated and measured values of equivalent aqueous oxygen concentration, C [M L^{-3}], at any point within the domain using the background concentration in the aqueous phase, C_{bg} [M L^{-3}], and the concentration at the air-water interface, C_0 [M L^{-3}].

The normalized root mean squared error (*NRMSE*) was used as measure of the goodness of the fit:

$$NRMSE = \frac{\sqrt{\frac{1}{N}\sum_{j=1}^{N}\left(S_j - O_j\right)^2}}{O_{\max} - O_{\min}} \tag{5.14}$$

where *NRMSE* is expressed in dimensionless form and N [-] represents the total number of observations. S_j and O_j are the simulated and observed values with units in [M L^{-3}].

5.4.2 Excess Mass of Oxygen Supplied from Entrapped Gas

The quantification of oxygen fluxes transferred through the capillary fringe to the underlying groundwater was of key importance to assess the influence of the specific parameters tested in this study. Our specific interest was to determine the excess mass of oxygen, EM_{O2} [M], transferred from the entrapped gas to oxygen-depleted groundwater during the different imbibition experiments. We define the excess mass of oxygen as the amount of oxygen that additionally dissolves into the aqueous phase solely due to the partitioning from entrapped gas during the transient phase following imbibition. It is a time-dependent quantity since oxygen dissolution from entrapped air takes place until quasi steady state (step 4 in Fig. 5.2) is reached. Therefore, we calculated the net input as a time-dependent quantity, that is, as a function of displaced pore volumes, where the number of pore volumes, PV [-], is defined as:

$$PV = \frac{Q_{in}}{\phi\left(h_{CF}W\right)L}t \tag{5.15}$$

in which Q_{in} [L^3 T^{-1}] is the average flow rate used in the horizontal direction and h_{CF} [L] represents the height of the capillary fringe's upper limit.

In the experiments, we determined the total oxygen flux in the effluent of the flow-through chamber, $\dot{m}_{out}$[M T^{-1}], at regular time intervals after raising the water table. When quasi steady state is reached, $\dot{m}_{out}$ stays constant and gives the value of $\dot{m}_{out}^{qss}$ [M T^{-1}]. The latter was subtracted from each value of the total oxygen flux, $\dot{m}_{out}$, measured during the transient phase of the experiments, where $\dot{m}_{out} > \dot{m}_{out}^{qss}$. The differences were then integrated over time to yield the excess mass of oxygen supplied from entrapped gas:

$$EM_{O2} = \int_0^{t_{end}}\left(\dot{m}_{out}(t) - \dot{m}_{out}^{qss}\right)dt \tag{5.16}$$

Thus, the oxygen mass supplied during the corresponding quasi steady-state condition (step 4 in Fig. 5.2) is not considered in the EM_{O2}. When the value of the EM_{O2} stays approximately constant over time, no additional oxygen input into the system due to gas partitioning occurs. This method provides a good framework to estimate net oxygen fluxes and to directly compare the outcomes of the different experiments performed in this work.

5.5 Results and Discussion

The main focus of our study was to investigate the impact of different flow conditions and porous medium properties on oxygen transfer during single imbibition events. An overview of the experiments conducted is given in Table 5.1, which also reports the parameters changed (bold

characters) in the different experimental runs: the grain diameter, d [L], the induced change in water table elevation, ΔH_{WT} [L], the time taken to increase the water table, Δt [T], and the flow-rate used for injection of oxygen-depleted water at the inlet (Pump 1 in Fig. 5.1a), Q_{in}.

Table 5.1. Overview of the imbibition experiments conducted (the grey-shaded area highlights the parameters of the reference experiment, i.e., 'Experiment 1').

	Experiment				
	1	2	3	4	5
d [mm]	0.4 - 0.6	**1.0 - 1.5**	0.4 - 0.6	0.4 - 0.6	0.4 - 0.6
ΔH_{WT} [cm]	8.6	9.4	9.0	10.6	**4.0**
Δt [min]	15	15	**120**	15	7.5
Q_{in} [mL min^{-1}]	2.00	1.93	1.96	**3.90**	1.90

In the following sections, we first describe the experimental and numerical results for the reference case, i.e., 'Experiment 1'; subsequently, we present and discuss the results of the experimental sensitivity analysis by comparing the outcomes of the other experiments listed in Table 5.1.

5.5.1 Numerical Simulation of 'Experiment 1'

The reference case 'Experiment 1' was used to test the flow and transport model. Figure 5.3a shows the computed two-dimensional flow field for the case of quasi steady state following imbibition. The streamlines have a distinct vertical component close to the inlet and the outlet of the flow-through chamber because the aqueous solution was injected/extracted along the lower 15 cm at the inlet and the outlet of the domain while the upper limit of the capillary fringe was at a much higher elevation (z = 31.1 cm). We found that the resulting curvilinear flow field considerably affected the fitted value(s) regarding the initial gas saturation and relative permeability (Eqn. 5.6).
Figure 5.3b depicts the simulated isochrones as well as the computed distribution of water saturations. Since oxygen is entrapped within the transition zone between the unsaturated and the fully water-saturated zone, the streamlines and the equipotential lines as well as the isochrones are deflected at the interface between the quasi-saturated and the fully water-saturated domain. This is in accordance to our observations made in the tracer experiment (results not shown). Moreover, flow within the quasi-saturated zone is much slower than in the fully water-saturated region below, as indicated by the computed flow net (Fig. 5.3a).

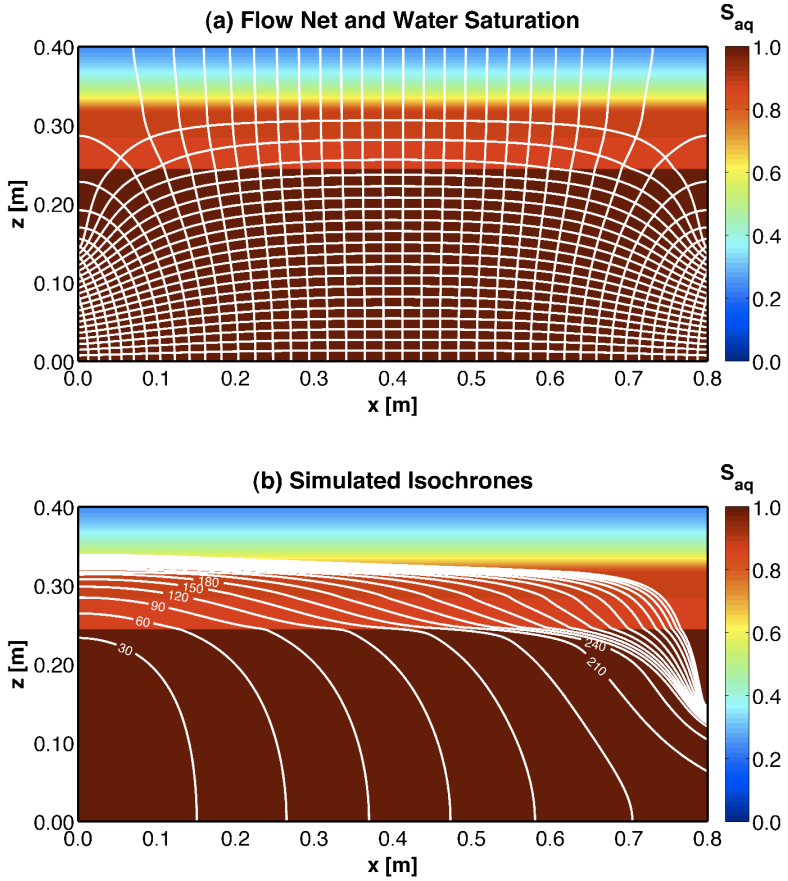

Fig. 5.3. Simulation results for 'Experiment 1'. The general groundwater flow-direction is from left to right. (a) Flow net and S_{aq} at quasi steady state after increase of the water table; (b) simulated isochrones (at a time interval of 30 min) and S_{aq}.

Figure 5.4 presents the normalized profiles of equivalent aqueous oxygen concentration at x_1 = 0.45 m as a function of time. A zone of higher gas saturation (S_g = 13.0 %) in the region between z = 24.5 and 28.5 cm was needed to achieve an improved fit between the measured and the simulated results (see also Fig. 5.3). At elevations higher than z = 28.5 cm, the initial gas saturation was estimated as 11.8 %; below z = 24.5 cm no entrapped gas was present.

The vertical black lines in Fig. 5.4 depict the difference between the measured and the simulated oxygen concentrations at a specific point in time and space. As indicated by the value of *NRMSE* of 7.78 % (total number of measurements, N = 421), our model captures the observed experimental behavior fairly well. Furthermore, the results point out that, in this case, the partitioning process could indeed be satisfactorily modeled assuming local equilibrium between the mobile aqueous and the entrapped gaseous phases. S_g changed just slightly over the course of the simulation (results not shown). The effect of gas partitioning between the aqueous and the gaseous phases diminished after about 20 h, since quasi steady state between the two fluid phases was achieved and no further oxygen could be supplied from the entrapped gaseous phase (i.e., oxygen partial pressure within the entrapped gas was in equilibrium with the oxygen content

of the injected solution, modified by transverse vertical dispersion). A minor kinetic effect is observed when oxygen dissolution fades at the end of the experiment leading to a slightly different temporal behavior of the simulated break-through curves (at a specific location *z*) compared to the measured ones.

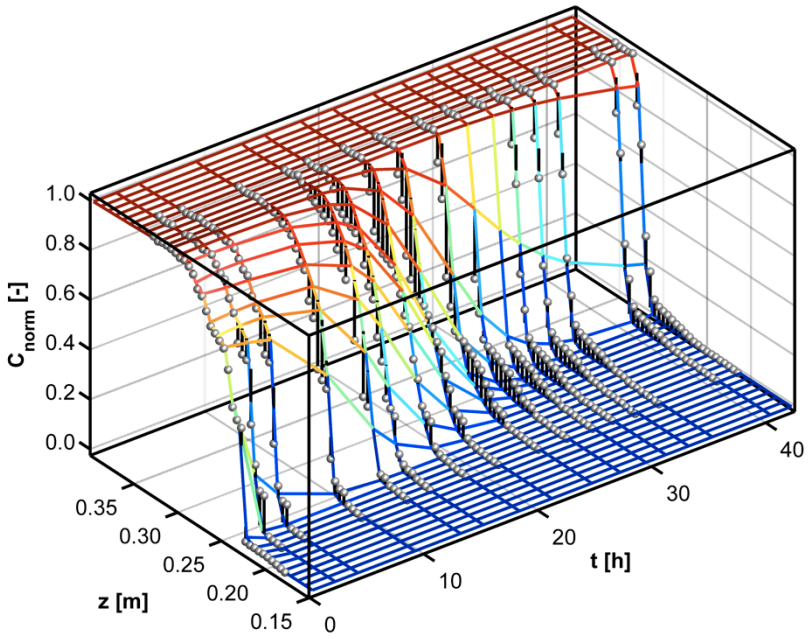

Fig. 5.4. Measured (spheres) and simulated (chromatic lines; concentration values are indicated by color, ranging between 0, blue, and 1, red) normalized profiles of equivalent aqueous oxygen concentration determined at x_1 = 0.45 m as a function of time ('Experiment 1'). t = 0 h indicates the beginning of the water table increase, which is completed after 0.25 h. The base of the flow-through domain is at z = 0 m.

Knowing that S_g changed just slightly over the course of the experiment, we used Eqn. 5.2 and the estimated values of gas saturation to calculate the mean retardation factor in the quasi-saturated zone. The result of R_{O2} = 5.6 compares well to the break-through curves shown in Fig. 5.4; in this case the time needed to flush one pore volume of water through the chamber is 4.36 h (calculated based on Eqn. 5.15; this time period represents the lower limit of time needed for a non-partitioning tracer to propagate through the system due to the curvilinear flow field).

5.5.2 Experimental Sensitivity Analysis of Oxygen Transfer

In this section, we describe and compare the outcomes of the different imbibition experiments listed in Table 5.1. The vertical distribution of equivalent aqueous oxygen concentration across the capillary fringe was measured at two distinct locations. Taking measurements at high spatial resolution and at different times allowed us to follow the dynamics of oxygen transfer. Moreover, we used the total oxygen fluxes determined at the outlet of the flow-through chamber for a quantitative comparison of the experiments. The results are shown in Fig. 5.5.

'Experiment 1': Reference Case

This experimental run was already described in detail above. The mass flux measured in the effluent of the flow-through chamber as well as the excess mass of oxygen supplied due to the increase in water table height are shown in Figs. 5.5e and 5.5f, respectively. Since no further oxygen could be supplied from the entrapped gaseous phase, the effect of gas partitioning diminished after the exchange of about five pore volumes. About 0.6 mg of oxygen was supplied to the oxygen-depleted groundwater from air entrapped by the rising water table. The oxygen supply adds up to the transverse dispersive flux across the unsaturated/saturated interface.

'Experiment 2': Larger Grain Size

The effect of using a larger grain size (d = 1.0 to 1.5 mm compared with d = 0.4 to 0.6 mm in 'Experiment 1') was investigated in 'Experiment 2'. Although in former experiments using glass beads it was shown that the residual nonwetting phase saturation does not depend on the grain size (Chatzis et al., 1983; Fry et al., 1997), we observed a distinct zone of higher gas saturation forming just above the upper limit of the former capillary fringe as result of the imbibition process. This zone of higher S_g is illustrated in the photograph shown in Fig. 5.6, where the continuous lines represent the interface between the aqueous and the gaseous phase. Recently, this behavior was observed in a similar experimental setup (Schneider-Zapp, 2009) and explained on the basis of the different time periods available for equilibration of the saturation front and for adjustment of the menisci. In fact, when the interface moves fast there is no time available for the menisci to adjust and, thus, more gas is entrapped; this contrasts the case where the water table is held constant. Our experimental results suggest that the observed effect of trapping larger amounts of air at the upper limit of the former capillary fringe in case of imbibition is more pronounced for the coarse porous material compared with the fine glass beads.

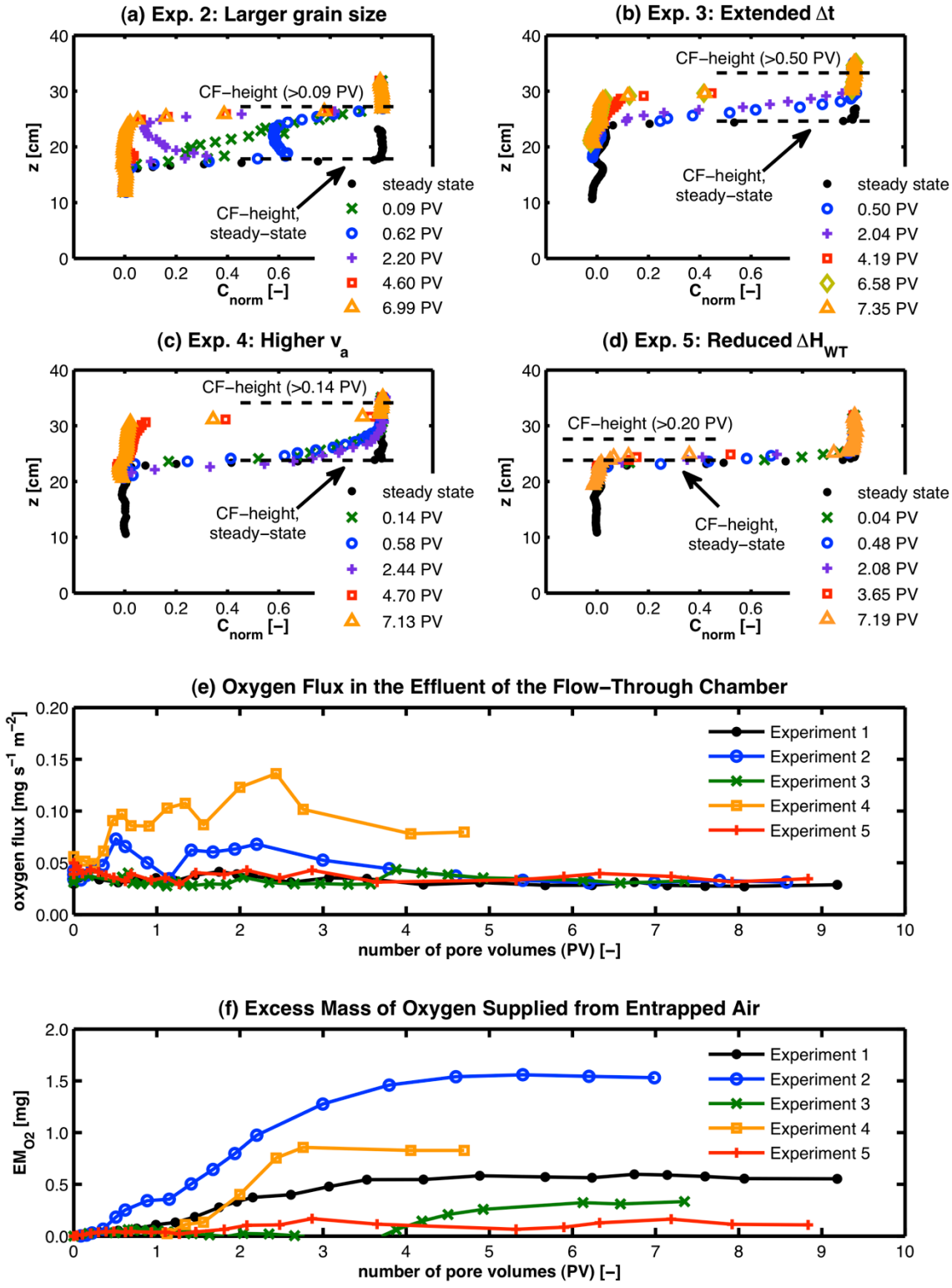

Fig. 5.5. (a)-(d) Vertical profiles of oxygen concentration at x_1 = 0.45 m. The vertical position of the upper limit of the capillary fringe is indicated by the dashed lines for the (quasi) steady-state case before (symbol: '●') and after increase of the water table (symbol: '△'). (a) 'Experiment 2': Larger grain size; (b) 'Experiment 3': Extended Δt, that is slower rise of the water table; (c) 'Experiment 4': Higher flow velocity; (d) 'Experiment 5': Reduced magnitude of the water table rise, ΔH_{WT}; (e) Oxygen flux in the effluent of the flow-through chamber, normalized by the flow-through area; (f) EM_{O2} (Eqn. 5.16) as function of the number of pore volumes.

The large amount of entrapped air, and thus oxygen present in the lower region of the newly formed transition zone, considerably affected the vertical distribution of oxygen (Fig. 5.5a). From the temporal behavior of the vertical oxygen concentration profiles the dissolution of oxygen into the flowing groundwater can be clearly noticed. This enhancement effect is also shown by the mass flux in the effluent of the flow-through chamber (Fig. 5.5e) and the curve representing the excess mass of oxygen supplied to the aqueous phase: the latter is considerably higher for the current case (1.5 mg; Fig. 5.5f) than for the reference case (0.6 mg; Fig. 5.5f: 'Experiment 1').

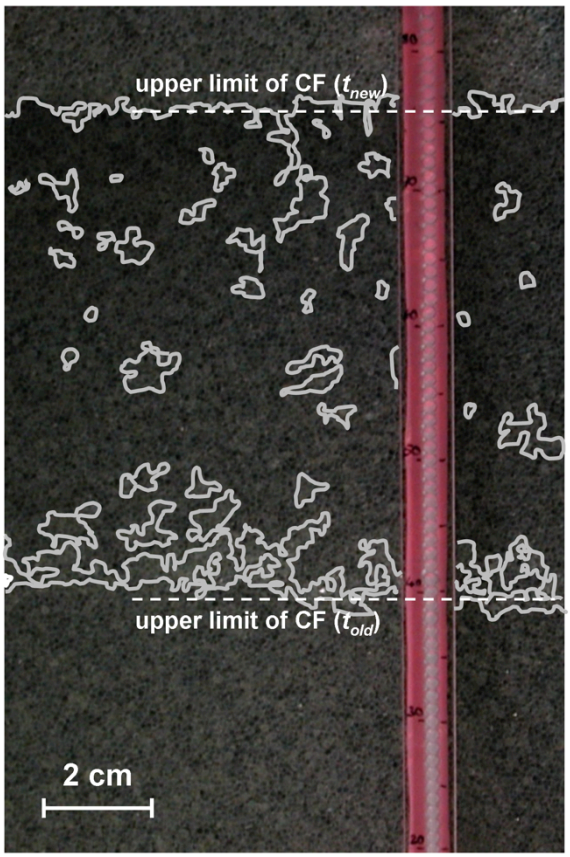

Fig. 5.6. Zone with larger volume of entrapped gas localized at the previous (i.e., before starting the imbibition phase) upper limit of the capillary fringe. In the figure, the previous (t_{old}) and current (t_{new}) upper limits are shown by the dashed horizontal lines; the continuous gray lines indicate the gas-water interfaces. The picture was taken close to the first oxygen-sensitive stripe (at x_1 = 0.45 m) during 'Experiment 2', performed using a larger grain size, d = 1.0 to 1.5 mm.

'Experiment 3': Slower Rise of the Groundwater Table, i.e., Extended Δt

We also considered the case in which the increase of the water table was similar to the reference setup (~9 cm), but where the change occured over a much longer period of time (120 min compared with 15 min in 'Experiment 1').

The vertical concentration profiles are shown in Fig. 5.5b, where a more gradual change in the distribution of oxygen over time can be observed. The slow increase in the water table elevation resulted in a lower amount of entrapped air; therefore, less oxygen dissolved in the aqueous phase (Fig. 5.5e and Fig. 5.5f). This observation is in agreement with the experimental results of Lehmann et al. (1998), who also observed higher water contents within the capillary fringe for the case of a slowly fluctuating water table. In our experiments the maximum increase in the value of the EM_{O2} was only 0.3 mg, corresponding to 56 % of the excess mass supplied in 'Experiment 1'.

'Experiment 4': Higher Flow Velocity, v_a

In this experiment we increased the horizontal flow rate by a factor of two with respect to the reference case ('Experiment 1'). Figure 5.5c shows the measured profiles of equivalent aqueous oxygen concentration at x_1 = 45 cm.

Due to the increased horizontal groundwater flow velocity, the oxygen flux of the background solution was approximately doubled compared with the previous cases (Fig. 5.5e). Moreover, the transverse dispersive flux across the capillary fringe increased (e.g., Klenk and Grathwohl, 2002; Haberer et al., 2011). These factors as well as the effect of entrapped gas (more tortuous flow paths and/or reduced hydraulic conductivity within the quasi-saturated porous medium that may affect the interfacial oxygen flux) were taken into account by measuring $\dot{m}_{out}^{qss}$ at the end of the experiment.

Because $\dot{m}_{out}^{qss}$ is subtracted from each measurement value $\dot{m}_{out}$ in Eqn. 5.16, the above mentioned factors are not considered in the value of the excess mass of oxygen, which is only 46 % higher than in the reference case (0.8 mg of oxygen dissolved in the oxygen-depleted groundwater compared with the 0.6 mg of 'Experiment 1'; see Fig. 5.5f).

'Experiment 5': Reduced Change in Water Table Elevation, ΔH_{WT}

In this experiment we increased the water table elevation only by 4 cm (i.e., almost half of the magnitude of the water table rise of 'Experiment 1'), keeping the speed of the upward movement, however, the same. Figure 5.5d shows the vertical oxygen concentration profiles measured at x_1 = 45 cm, where just small changes in the distribution of C_{norm} subsequent to the raise of the water table can be observed. Moreover, the oxygen flux in the effluent of the flow-through chamber did not considerably vary (Fig. 5.5e). When the value of EM_{O2} stabilized, only 0.1 mg of oxygen were additionally supplied to the aqueous phase (Fig. 5.5f). This is much less than observed in the reference case ('Experiment 1'). We hypothesize that the reduction in ΔH_{WT} led to a disproportionately smaller volume of entrapped air compared with the reference case since the upward movement of the water table is dampened (Hinz, 1998). Additionally, the increase in hydrostatic pressure acting on the entrapped gaseous phase is smaller than in the reference case. These factors determined the significantly smaller amount of oxygen dissolving into the aqueous phase.

Table 5.2 summarizes the results of the different experiments performed. We calculated the ratios by which the parameters of interest (i.e., the horizontal flow velocity, the grain size, and the magnitude and the speed of the water table rise) differ between the respective experiment and the reference case ('Experiment 1'). Additionally, we list the excess mass of oxygen supplied to the aqueous phase due to the increase in water table elevation and its relative value in comparison

with the reference case, denoted as Ratio(O_2). The numbers printed in boldface help identifying the key parameters changed in each experimental run and the observed differences in the excess mass of oxygen dissolved in the oxygen-depleted groundwater.

Table 5.2. Ratio of the parameter variation (relative to the reference case, 'Experiment 1') and its effect on the excess mass of oxygen.

Experiment	Parameter[1)]	Ratio(v_a^{qss})[2)] [-]	Ratio(d) [-]	Ratio(ΔH_{WT}) [-]	Ratio(Δt) [-]	EM_{O2} [mg]	Ratio(O_2) [-]
1	-	1.00	1.00	1.00	1.00	0.57	**1.00**
2	d (+)	1.17	**2.50**	1.09	1.00	1.54	**2.70**
3	Δt (+)	0.90	1.00	1.05	**8.00**	0.32	**0.56**
4	v_a (+)	**1.93**	1.00	1.23	1.00	0.83	**1.46**
5	ΔH_{WT} (-)	1.10	1.00	**0.47**	0.50	0.11	**0.19**

1) The (+) and (-) signs indicate whether the respective parameter was increased or decreased compared to the refenence case.

2) v_a^{qss} [L T^{-1}] is the groundwater flow velocity measured at quasi steady state.

In the given setup, most parameters considered correlate positively with the amount of oxygen dissolved from entrapped air. Only the time over which the water table is raised scales inversely with the excess mass of oxygen ('Experiment 3').

In 'Experiment 2' an approximately proportional increase in the ratio of the EM_{O2} is observed: the grain diameter was changed by a factor of 2.5 compared with the reference case and the Ratio(O_2) increased by a factor of 2.7. This result is influenced by the significant amount of entrapped air in the lower region of the newly formed transition zone. As shown by 'Experiment 3', the value of Ratio(O_2) appears to be relatively insensitive to the change in Δt. In fact, the eightfold increase in the characteristic time of the water table rise with respect to the reference case experiment resulted in less amount of entrapped air, and thus, only half Ratio(O_2). For 'Experiment 4' we note that the increase in the value of Ratio(O_2) may be the result of both the altered value of the horizontal seepage velocity (Ratio(v_a^{qss}) = 1.93) as well as the determined larger change in pressure head (Ratio(ΔH_{WT}) = 1.23). Finally, in 'Experiment 5' we applied the same speed to raise the water table as in the reference case but only half of the magnitude. We observed a considerably lower Ratio(O_2)-value (0.19) than would be expected from the respective change in pressure head (Ratio(ΔH_{WT}) = 0.47).

In summary, the highest relative effects on the excess oxygen mass transferred to the oxygen-depleted groundwater were observed when the grain diameter ('Experiment 2': larger grain size) and the magnitude of water table rise ('Experiment 5': reduced ΔH_{WT}) were changed.

5.6 Summary and Conclusions

In this study a systematic experimental sensitivity analysis has been performed to investigate the effect of different flow conditions and porous media properties on oxygen transfer within the capillary fringe. We focused on the transient phase following imbibition, where the partitioning of oxygen from entrapped gas to the water phase plays a significant role in enhancing the overall mass transfer. Our results clearly show that both the properties of the porous medium (i.e., grain size) and the flow field (i.e., groundwater flow velocity, magnitude and speed of the water table rise) influence the extent of air entrapment and, thus, the amount of oxygen transferred to the oxygen-depleted groundwater. In particular, we observed most significant differences when the grain size and the magnitude of the water table rise were varied.

We have also developed a numerical model describing the flow field in the experimental setup and the mass transfer processes based on the assumption of local equilibrium. Applying our model we were able to quantitatively capture the main characteristics of oxygen transfer observed in the reference experiment. While the flow field in the given experimental setup was exceptional due to the location of the inlet and outlet ports, the numerical model can easily be applied to standard situations in which groundwater flow is essentially horizontal. As shown earlier (Cirpka and Kitanidis, 2001; Geistlinger et al., 2005; Amos and Mayer, 2006; Klump et al., 2008), gas transfer between entrapped gas and groundwater follows comparably simple physical rules. The assumption of local equilibrium is valid at sufficiently small groundwater flow velocitites and sufficiently large travel distances. In typical field situations, velocities are likely to be smaller and distances of interest larger than in our experiments so that the local equilibrium assumption would even be more valid. For the prediction of gas-transfer induced by the increase of the water table, the quantity most difficult to predict is the initial saturation of entrapped gas formed, which is proportional to the total amount of oxygen introduced by the water table rise.

Since oxygen fluxes are vital for many biogeochemical processes in shallow aquifers, quantitative approaches to describe oxygen transfer dynamics are necessary to understand and manage such complex systems. We think that further research effort should be addressed to elucidate the mechanisms of mass transfer in the capillary fringe and in particular the interaction between the supplied oxygen fluxes and oxygen-limited reactive processes. Although dissolution of oxygen from entrapped gas may significantly contribute to the oxygen availability in a groundwater body, it is usually not considered (Holocher et al., 2002). Especially in predicting effects of natural attenuation, variations in water levels should be considered, since they affect microbial activities as well as the rates of biogeochemical reactions at the interface between groundwater and the unsaturated zone (Dobson et al., 2007; Cozarelli et al., 2011).

Acknowledgements

We thank the editor and three anonymous reviewers for their constructive remarks. This study was funded by the DFG (German Research Foundation) through the Research Group FOR 831 'Dynamic Capillary Fringes – A Multidisciplinary Approach' (grant GR971/22-1).

References

Aeschbach-Hertig, W., Peeters, F., Beyerle, U. and Kipfer, R., 2000. Paleotemperature reconstruction from noble gases in groun water taking into account equilibration with entrapped air. Nature, 405(6790): 1040-1044.

Amos, R.T. and Mayer, K.U., 2006. Investigating the role of gas bubble formation and entrapment in contaminated aquifers: Reactive transport modelling. Journal of Contaminant Hydrology, 87(1-2): 123-154.

Atkins, P.W. and de Paula, J., 2006. Physikalische Chemie. 4th ed. Wiley VCH, Weinheim, Germany.

Balcke, G.U., Meenken, S., Hoefer, C. and Oswald, S.E., 2007. Kinetic gas-water transfer and gas accumulation in porous media during pulsed oxygen sparging. Environmental Science and Technology, 41(12): 4428-4434.

Barber, C., Davis, G.B. and Farrington, P., 1990. Sources and sinks for dissolved oxygen in groundwater in an unconfined sand aquifer, Western Australia. *In* Geochemistry of Gaseous Elements and Compounds. Eds.: Barto-Kyriakidis, A., Farrel., L., Theophrastus Publications, Athens, pp. 353-368.

Berkowitz, B., Silliman, S.E. and Dunn, A.M., 2004. Impact of the capillary fringe on local flow, chemical migration, and microbiology. Vadose Zone Journal, 3(2): 534-548.

Brooks, R.H. and Corey, A.T., 1964. Hydraulic properties of porous media. Hydrology paper, Colorado State University, Ft. Collins

Brooks, A.N. and Hughes, T.J.R., 1982. Streamline upwind/Petrov-Galerkin formulations for convection dominated flows with particular emphasis on the incompressible Navier-Stokes equations. Computer Methods in Applied Mechanics and Engineering, 32(1-3): 199-259.

Burdine, N.T., 1953. Relative permeability calculations from pore-size distribution data. Journal of Petroleum Technology, 5(3): 71-78.

Chatzis, I., Lim, H.T. and Morrow, N.R., 1983. Magnitude and detailed structure of residual oil saturation. SPEJ Society of Petroleum Engineers Journal, 23(2): 311-326.

Chiogna, G., Eberhardt, C., Grathwohl, P., Cirpka, O.A. and Rolle, M., 2010. Evidence of compound dependent hydrodynamic and (hydro)mechanical transverse dispersion with multi-tracer laboratory experiments. Environmental Science and Technology, 44(2): 688-693. doi: 10.1021/es9023964.

Cirpka, O.A., Helmig, R. and Frind, E.O., 1999. Streamline-oriented grid-generation for transport modeling in two-dimensional domains including wells. Advances in Water Resources, 22(7): 697-710.

Cirpka, O.A. and Kitanidis, P.K., 2001. Transport of volatile compounds in porous media in the presence of a trapped gas phase. Journal of Contaminant Hydrology, 49(3-4): 263-285.

Cozarelli, I.M., Böhlke, J.K., Masoner, J., Breit, G.N., Lorah, M.M., Tuttle, M.L.W. and Jaeschke, J.B., 2011. Biogeochemical evolution of a landfill leachate plume, Norman, Oklahoma. Ground Water 49(5): 663-687.

Dobson, R., Schroth, M.H. and Zeyer, J., 2007. Effect of water-table fluctuation on dissolution and biodegradation of a multi-component, light nonaqueous-phase liquid. Journal of Contaminant Hydrology, 94(3-4): 235-248.

Donaldson, J.H., Istok, J.D., Humphrey, M.D., O'Reilly, K.T.O., Hawelka, C.A. and Mohr, D.H., 1997. Development and testing of a kinetic model for oxygen transport in porous media in the presence of trapped gas. Ground Water, 35(2): 270-279.

Donaldson, J.H., Istok, J.D. and O'Reilly, K.T., 1998. Dissolved gas transport in the presence of a trapped gas phase: Experimental evaluation of a two-dimensional kinetic model. Ground Water, 36(1): 133-142.

Farnsworth, C.E., Voegelin, A. and Hering, J.G., 2012. Manganese oxidation induced by water table fluctuations in a sand column. Environmental Science and Technology, 46(1): 277-284, doi: 10.1021/es2027828.

Freeze, R.A. and Cherry, J.A., 1979. Groundwater. Prentice-Hall, Englewood Cliffs, New Jersey.

Fry, V.A., Istok, J.D., Semprini, L., O'Reilly, K.T. and Buschek, T.E., 1995. Retardation of dissolved oxygen due to a trapped gas phase in porous media. Ground Water 33(3): 391-398.

Fry, V.A., Selker, J.S. and Gorelick, S.M., 1997. Experimental investigations for trapping oxygen gas in saturated porous media for in situ bioremediation. Water Resources Research, 33(12): 2687-2696.

Geistlinger, H., Beckmann, A. and Lazik, D., 2005. Mass transfer between a multicomponent trapped gas phase and a mobile water phase: Experiment and theory. Water Resources Research, 41, W11408, doi: 10.1029/2004WR003885.

Geistlinger, H., Jia, R., Eisermann, D. and Stange, C.F., 2010. Spatial and temporal variability of dissolved nitrous oxide in near-surface groundwater and bubble-mediated mass transfer to the unsaturated zone. Journal of Plant Nutrition and Soil Science, 173: 601-609, doi: 10.1002/jpln.200800278.

Haberer, C.M., Rolle, M., Liu, S., Cirpka, O.A. and Grathwohl, P., 2011. A high-resolution non-invasive approach to quantify oxygen transport across the capillary fringe and within the underlying groundwater. Journal of Contaminant Hydrology, 122(1-4): 26-39, doi: 10.1016/j.jconhyd.2010.10.006.

Haberer, C.M., Rolle, M., Cirpka, O.A. and Grathwohl, P., 2012. Oxygen transfer in a fluctuating capillary fringe. Vadose Zone Journal, 11(3), doi: 10.2136/vzj2011.0056.

Harvey, C.F., Gorelick, S.M., 1995. Temporal moment-generating equations: modeling transport and mass transfer in heterogeneous aquifers. Water Resources Research, 31(8): 1895-1911, doi: 10.1029/95WR01231.

Heaton, T.H.E. and Vogel, J.C., 1981. "Excess Air" in groundwater. Journal of Hydrology, 50: 201-216.

Helfferich, F.G., 1981. Theory of multicomponent, multiphase displacement in porous media. Society of Petroleum Engineers Journal, 21(1): 51-62.

Hinz, C., 1998. Analysis of unsaturated/saturated water flow near a fluctuating water table. Journal of Contaminant Hydrology, 33(1-2): 59-80.

Holocher, J., Peeters, F., Aeschbach-Hertig, W., Hofer, M., Brennwald, M., Kinzelbach, W. and Kipfer, R., 2002. Experimental investigations on the formation of excess air in quasi-saturated porous media. Geochimica et Cosmochimica Acta, 66(23): 4103-4117.

Holocher J., Peeters, F., Aeschbach-Hertig, W., Kinzelbach, W. and Kipfer, R., 2003. Kinetic model of gas bubble dissolution in groundwater and its implications for the dissolved gas composition. Environmental Science and Technology, 37(7): 1337-1343.

Jost, D., Winter, J. and Gallert, C., 2011. Water and oxygen dependence of *Pseudomonas putida* growing in silica sand capillary fringes. Vadose Zone Journal, 10(2): 532-540, doi: 10.2136/vzj2010.0092.

Klenk, I.D. and Grathwohl, P., 2002. Transverse vertical dispersion in groundwater and the capillary fringe. Journal of Contaminant Hydrology, 58(1-2): 111-128.

Klump, S., Cirpka, O.A., Surbeck, H. and Kipfer, R., 2008. Experimental and numerical studies on excess-air formation in quasi-saturated porous media. Water Resources Research, 44(5): W05402, doi: 10.1029/2007WR006280.

Lappala, E.G. and Thompson, G.M., 1983. Detection of groundwater contamination by shallow soil gas sampling in the vadose zone. *In* Proc. NWWA/EPA Conference in Characterisation and Monitoring of the Vadose (Unsaturated) Zone, Las Vegas, Nevada, pp. 659-679.

Lehmann, P., Stauffer, F., Hinz, C., Dury, O. and Flühler, H., 1998. Effect of hysteresis on water flow in a sand column with a fluctuating capillary fringe. Journal of Contaminant Hydrology, 33(1-2): 81-100.

Liu, S., Liedl, R. and Grathwohl, P., 2010. Simple analytical solutions for oxygen transfer into anaerobic groundwater. Water Resources Research, 46: W10542, doi: 10.1029/2009WR008434.

Rasa, E., Chapman, S.W., Bekins, B.A., Fogg, G.E., Scow, K.M. and Mackay, D.M., 2011. Role of back diffusion and biodegradation reactions in sustaining an MTBE/TBA plume in alluvial media. Journal of Contaminant Hydrology. 126(3-4): 235-247, doi: 10.1016/j.jconhyd.2011.08.006.

McCarthy, K. and Johnson, R.L., 1993. Transport of volatile organic compounds across the capillary fringe. Water Resources Research, 29(6): 1675-1683.

Oswald, S.E., Griepentrog, M., Schirmer, M. and Balcke, G.U., 2008. Interplay between oxygen demand reactions and kinetic gas-water transfer in porous media. Water Research, 42(14): 3579-3590.

Rolle, M., Hochstetler, D., Chiogna, G., Kitanidis, P.K. and P. Grathwohl, 2012. Experimental investigation and pore-scale modeling interpretation of compound-specific transverse dispersion in porous media. Transport in Porous Media, 93(3): 347-362, doi: 10.1007/s11242-012-9953-8.

Rudolph, N., Esser, H.G., Carminati, A., Moradi, A.B., Hilger, A., Kardjilov, N., Nagl, S. and Oswald, S.E., 2012. Dynamic oxygen mapping in the root zone by fluorescence dye imaging combined with neutron radiography. Journal of Soils and Sediments, 12: 63-74, doi: 10.1007/s11368-011-0407-7.

Ryan, M.C., MacQuarrie, K.T.B., Harman, J. and Mclellan, J., 2000. Field and modeling evidence for a 'stagnant flow' zone in the upper meter of sandy phreatic aquifers. Journal of Hydrology, 233: 223-240.

Schneider-Zapp, K., 2009. Dynamics of water movement near boundaries of the vadose zone. – Dissertation, Ruperto-Carola University of Heidelberg, Germany, 158 p.

Sinke, A.J.C., Dury, O. and Zobrist, J., 1998. Effects of a fluctuating water table: column study on redox dynamics and fate of some organic pollutants. Journal of Contaminant Hydrology, 33(1-2): 231-246.

Stute, M., Forster, M., Frischkorn, H., Serejo, A., Clark, J.F., Schlosser, P., Broecker, W.S. and Bonani, G., 1995. Cooling of tropical Brazil (5 °C) during the last glacial maximum. Science, 269 (5222): 379-383.

Werner, D. and Höhener, P., 2002. The influence of water table fluctuations on the volatilization of contaminants from groundwater. *In* Groundwater Quality: Natural and Enhanced Restoration of Groundwater Pollution (Proceedings of the Groundwater Quality 2001 Conference held at Sheffield, UK, June 2001). Thornton, S.F. and Oswald, S.E. (eds.) IAHS Publ. 275: 213-218.

Werner, D., Grathwohl, P. and Höhener, P., 2004. Review of field methods for the determination of the tortuosity and effective gas-phase diffusivity in the vadose zone. Vadose Zone Journal, 3(4): 1240-1248.

Williams, M.D. and Oostrom, M., 2000. Oxygenation of anoxic water in a fluctuating water table system: An experimental and numerical study. Journal of Hydrology, 230: 70-85.

Yadav, B.K. and Hassanizadeh, S.M., 2011. An overview of biodegradation of LNAPLs in coastal (semi)-arid environment. Water Air Soil Pollution, 220(1-4): 225-239.

Zilberbrand, M., 2003. Degassing water around air bubbles entrapped in the vadose zone as a mechanism of carbonate precipitation – a hypothesis. Journal of Sedimentary Research, 73(4): 491-497.

6. Impact of a Coarse-Material Inclusion on Oxygen Transfer in a Fluctuating Capillary Fringe

Christina M. Haberer

The following experimental results are presented as a draft. Further work will be done to complete this manuscript to publish our results within the framework of the DyCap-project ('Dynamic Capillary Fringes – A Multidisciplinary Approach', Research Group FOR 831, grant GR971/22-1, DFG)

Abstract

We performed a quasi two-dimensional flow-through laboratory experiment to investigate the effect of a coarse-material inclusion, present in the vicinity of the water table, on flow and oxygen transfer in the capillary fringe. During the experiment, a fluctuation of the water table was induced. Monitoring involved a combination of visual inspection, measurement of vertical oxygen concentration profiles, and determination of oxygen fluxes in the effluent of the flow-through chamber. We relate the results to observations presented in prior literature as well as to findings made in an earlier experiment comprising a homogeneous porous medium packing. At steady state, the oxygen flux across the unsaturated/saturated interface was considerably enhanced due to the presence of the coarse-material inclusion. During drainage, a zone of higher water saturation formed in the fine material overlying the coarse lens. The entrapped aqueous phase became enriched in oxygen, thus, contributing to the total amount of oxygen supplied to the system, when the water table was raised back to its initial level. Simultaneously, pronounced entrapment of air occurred in the coarse lens, causing volatile compounds to partition between the aqueous and the gaseous phases. The actual amount of oxygen mass, supplied to the aqueous phase solely due to dissolution from entrapped air, was found to be lower in the heterogeneous system compared with the homogeneous case. We argued that this is due to less entrapped air contributing to the temporary dissolution of oxygen in the heterogeneous case.

Keywords: *2-D experiments; capillary fringe; heterogeneous porous medium; water table fluctuation; gas partitioning.*

6.1 Introduction

Geologic formations in nature seldom exhibit uniform porous medium characteristics in different locations. In fact, there exists enormous heterogeneity in subsurface domains with respect to lithology, soil types, and others, which is manifested primarily in varying values of permeability and porosity. Physical heterogeneity does not only occur on the scale of large aquifers, but also for relatively small domains in the unsaturated zone. People dealing with groundwater issues are interested to identify the pathways travelled by water, the impact of these pathways on the movement of chemicals, and the viability of microbial populations in the subsurface.

Water preferentially bypasses low-permeable zones, whereas highly conductive lenses act as conduits for flow, attracting water from the surrounding aquifer. Flow converges toward the high-conductivity zone on the upgradient end and diverges away from it on the downgradient side. Porous medium heterogeneities and, thus, spatial fluctuations of the flow field result in irregular shapes of the plumes. At early times, these mechanisms may result in faster spreading than mixing of the solute; in the long term, the rate of mixing increases (Kitanidis, 1994). This is different from mass transfer in homogeneous porous media, where mixing and spreading can both be described by the same local dispersion coefficients. In fact, several authors (e.g., Kitanidis, 1994; Cirpka, 2002; Rolle et al., 2009; Dentz et al., 2011) pointed out the difference between the concept of spreading and mixing, where spreading is associated with the stretching and deformation of a contaminant plume, whereas mixing refers to the change of volume occupied by the solute. Rolle et al. (2009) showed that coarse-material inclusions surrounded by finer grains and under fully water-saturated conditions enhanced mixing, therefore, resulting in higher values of transverse vertical dispersion compared with the respective homogeneous case.

In the present study, we are especially interested in the physical processes occurring at the interface between the unsaturated and the saturated zone. These processes and the capillary fringe's function for diverse occurrences with respect to flow and transport are still not fully understood. Various authors (e.g., Barber et al., 1990; Kerfoot, 1994; Berkowitz et al., 2004; Maier and Grathwohl, 2005; Barth et al., 2005) hypothesize that the horizontal and vertical flow and transport processes within the capillary fringe make this zone highly active in terms of physico-chemical and microbiological processes. Silliman et al. (2002) and Berkowitz et al. (2004) observed that exchange of water within the capillary fringe with water from below the water table occurs in both directions. The flux between the two zones is thereby enhanced by the presence of physical heterogeneity. This led to the assumption that, at the local scale, the natural geochemical and microbiological conditions present at the interface between the unsaturated and the saturated zone, in fact, may be affected far more significantly than is usually assumed.

The objective of this study is to evaluate the influence of a physical heterogeneity, i.e., a coarse-material inclusion surrounded by finer porous material, on oxygen transfer in the capillary fringe.

We additionally investigate the effect of a fluctuating water table. Tracer experiments were performed to visualize the flow field in a quasi two-dimensional flow-through laboratory setup. Results from simultaneous measurements (Fibox 3, PreSens GmbH, Regensburg, Germany) of vertical oxygen concentration profiles across the capillary fringe and of oxygen fluxes in the effluent of the flow-through system are used to draw conclusions on oxygen transfer in the transition region between the unsaturated and the saturated zone. We investigated oxygen transfer since oxygen is the most important electron acceptor in the capillary fringe and shallow groundwater.

6.2 Basic Concepts

In the past, multiple definitions have been presented for the capillary fringe (e.g., Ronen et al., 1997; Fetter, 2001; Berkowitz et al., 2004; Bear and Cheng, 2010). In the strictest sense, the capillary fringe is defined as the interface region between the water table and the partially water-saturated vadose zone above, where water saturation approaches 100 %. Its name stems from the fact that water molecules at the water table are subject to upward attraction due to surface tension of the air-water interface and the molecular attraction of the liquid and solid phases, called capillarity (Fetter, 2001). Tensiometer readings will reveal that the head is negative in this zone (e.g., Bear and Cheng, 2010). In porous media, the pore openings comprise a range of different sizes, which causes capillary water not to rise to an even height above the water table, but rather forming an irregular fringe. Because of the greater tensions created by smaller openings in fine-grained porous media, the capillary fringe is higher in this case than in coarse materials.

6.2.1 Formation of Air Entry Barriers

In the capillary fringe region, air usually gets entrapped as a result of air entrainment during water infiltration or because of an increase in water table elevations. Dunn and Silliman (2003) studied the effect of air entry barriers caused by the presence of coarse sand lenses in the region of the capillary fringe during rise and fall of the water table. The term ‘air entry barrier’, hereby, refers to the phenomenon of coarse porous media remaining at high moisture content at significant distances above the water table due to low air permeability in the overlying fine material. In fact, Dunn and Silliman (2003) showed that in case of a declining water table, water was entrapped in the coarse sand zones above the water table at heights significantly greater than anticipated from consideration of capillary rise in the coarse sand. These same coarse zones rapidly drained when air penetrated into these zones through the surrounding fine sands. The authors extended the concept to entrapment of air below the phreatic surface as result of an increase in water table

elevation and the differences in capillary rise in the coarse vs. the fine sediments. Experimentally, it was observed that, before the air in the upper region of the coarse sand was released to the unsaturated zone, the fine-grained sand overlying the coarse sand was already water-saturated due to capillary rise in the fine sediments. Therefore, the air in the coarse sand became entrapped. The pressure in this entrapped air phase was thereby significantly greater than the pressure in the water phase in the surrounding fine sand. Dunn and Silliman (2003) suggested that partitioning and, thus, overall mass fluxes may be enhanced by pronounced air entrapment, due to the presence of heterogeneities.

In subsequent laboratory experiments, Dunn (2005) could also show that significant volumes of entrapped air and LNAPL lead to changes in the transport behaviour of microspheres. Due to the presence of a gaseous phase, the effective hydraulic properties and, consequently, the flow regime change. Already Orlob and Radhakrishna (1958) reported a decrease in permeability by 35 %, when the gas content of the porous medium investigated reached a value of ten percent. Fry et al. (1997) found that the value of relative hydraulic conductivity of porous media with trapped gas volume of 14 - 55 % even ranged between 0.62 - 0.05. In the worst case, entrapped air may even lead to hydraulic isolation of the zone, where the gas is present.

As oxygen supply from entrapped air may be essential for reoxygenation of oxygen-depleted groundwater (e.g., Haberer et al., 2012 and 2013), we are interested in studying heterogeneous systems in more detail with respect to mass transfer in the capillary fringe. We have to note that additional oxygen mass may also be supplied from (partially) air-saturated water entrapped in finer material overlying a coarse porous medium zone. The latter is based on the capillary barrier effect, i.e., the contrast in hydrologic properties between two adjacent phases keeps infiltrating water in the upper layer.

6.2.2 Quantifying Oxygen Transfer in the Capillary Fringe

The presence of a coarse-material inclusion in the direct vicinity of the water table may impact the mass transfer of volatile compounds in the capillary fringe. In heterogeneous porous media, the flow and transport processes, acting in vertical direction, as well as the effect of capillary and air entry barriers have to be considered. To evaluate oxygen transfer in the transition region between the unsaturated and the saturated zone, we define the following parameters: the total mass flux across the capillary fringe, the cumulative oxygen mass supplied across this interface, and the excess mass of oxygen supplied solely due to the increase of the water table.

Calculation of the Total Oxygen Flux:

We quantify the effects of entrapped gas (more tortuous flow paths, reduced permeability) and/ or a distorted flow field (due to heterogeneity) on the total (quasi) steady-state oxygen flux across the capillary fringe by comparing the experimentally determined mass flux across the capillary fringe with a theoretical, purely dispersive one.

At steady state and considering an abrupt change in the vertical distribution of water content at the upper limit of the capillary fringe, the total dispersive mass flux across this interface, $\dot{m}^{calc}$ [M T^{-1}], for a homogeneous porous medium and in the absence of entrapped gas, is described by (e.g., Cussler, 2009; Klenk and Grathwohl, 2002; Haberer et al., 2012):

$$\dot{m}^{calc} = \int_0^L \int_0^W F\big|_{z=0} dy dx = \left(C_0 - C_{bg}\right) 2\phi W \sqrt{D_t L v_a \frac{1}{\pi}} \tag{6.1}$$

in which the length, L [L], and the width, W [L], of the interfacial area are related to the coordinates in longitudinal, x [L], and transverse horizontal direction, y [L], of groundwater flow. The origin of the vertical coordinate, z [L], is located at the air/water interface across which the mass flux density, F [M L^{-2} T^{-1}], occurs at a specific value of x. C_0 [M L^{-3}] represents the atmospheric oxygen concentration at z = 0.00 m, while C_{bg} [M L^{-3}] is the background concentration in the aqueous phase. ϕ [-] denotes the porosity and v_a [L T^{-1}] is the horizontal seepage velocity.

In Eqn. 6.1 the transverse vertical dispersion coefficient, D_t [L^2 T^{-1}], is parameterized using the non-linear relationship by Chiogna et al. (2010). The applicability of this equation with respect to mass transfer across the capillary fringe was already shown in Haberer et al. (2011):

$$D_t \approx D_p + v_a \frac{d}{\sqrt{\frac{v_a d}{D_{aq}} + 123}} \tag{6.2}$$

where $D_p \approx \phi D_{aq}$ [L^2 T^{-1}] is the pore diffusion coefficient, D_{aq} [L^2 T^{-1}] denotes the aqueous molecular diffusion coefficient, and d [L] is the average grain diameter.

Adding the incoming mass flux, $\dot{m}_{in}$[M T^{-1}], to the total dispersive mass flux across the capillary fringe, the oxygen flux in the effluent of the flow-through chamber, $\dot{m}_{out}^{calc}$ [M T^{-1}], can be computed as:

$$\dot{m}_{out}^{calc} = \dot{m}^{calc} + \dot{m}_{in} \tag{6.3}$$

Please note that $\dot{m}_{out}^{calc}$ refers to the homogeneous case, where steady-state oxygen transfer across the capillary fringe occurs in the absence of entrapped gas.

Cumulative Oxygen Mass Supplied across the Unsaturated/Saturated Interface:

To estimate the specific contributions of the dispersive flux and transient conditions on oxygen transfer, we calculate the cumulative oxygen mass supplied across the unsaturated/saturated interface, $cum_{O2\text{-}mass}$ [M], as a time-dependent quantity. To do so, the total oxygen flux across the interface (calculated, $\dot{m}^{calc}$, or experimentally determined, $\dot{m}$) is integrated over the time, *t* [T]. As an example, Eqn. 6.4 gives the computational procedure for the experimental case:

$$cum_{O2-mass} = \int_0^{t_{end}} (\dot{m}) dt \tag{6.4}$$

Excess Mass of Oxygen Supplied During the Transient Phase Following Imbibition:

In Haberer et al. (2013), we investigated the impact of different flow conditions and porous medium properties on oxygen transfer in the capillary fringe following imbibition. We performed laboratory bench-scale experiments using homogeneous porous medium packings. The excess mass of oxygen, EM_{O2} [M], was defined as the amount of oxygen that additionally dissolves into the aqueous phase solely due to the partitioning from entrapped gas during the transient phase after the water table had been raised.

According to our earlier study, we compute the excess mass of oxygen by determining the effluent mass flux, $\dot{m}_{out}$, at regular time intervals in the experiment. When quasi steady state is reached, $\dot{m}_{out}$ stays constant and gives the value of $\dot{m}_{out}^{qss}$ [M T^{-1}]. The EM_{O2} is then given as:

$$EM_{O2} = \int_0^{t_{end}} \left(\dot{m}_{out}(t) - \dot{m}_{out}^{qss}\right) dt \tag{6.5}$$

The quasi steady-state dispersive flux across the unsaturated/saturated interface is, therefore, not considered in the value of the excess mass of oxygen. When the EM_{O2} stays approximately constant over time, no additional oxygen input into the system occurs. With regard to a homogeneous porous medium this indicates that partitioning between the two fluid phases has ceased. In heterogeneous porous media, the resupply of (partially) air-equilibrated water, entrapped in capillary barriers, during imbibition may additionally result in temporary increased oxygen fluxes to the groundwater. The latter, thus, also affects the value of the EM_{O2}.

6.3 Experimental Setup

We investigated the impact of a coarse-material inclusion on oxygen transfer in the capillary fringe by performing a quasi two-dimensional flow-through laboratory experiment. A photograph of the experimental setup, comprising a flow-through chamber with inner dimensions of 80 cm (length, *L*)

× 40 cm (height, *H*) × 0.5 cm (width, *W*) is shown in Fig. 6.1. The experiment was conducted in a temperature-controlled room at 22 °C to avoid possible temperature effects.

Commercially available glass beads with two different grain-size ranges, herein termed 'fine' and 'coarse', were used as porous media. The grain diameter of the fine glass beads ranged between 0.4 - 0.6 mm (Sartorius GmbH, Göttingen, Germany), with a saturated hydraulic conductivity of ~2.1×10^{-3} m s^{-1} and an air entry pressure of ~11.7 cm. The grain diameter of the coarse glass beads (Fisher Scientific GmbH, Schwerte, Germany) ranged between 1.0 - 1.5 mm, with a saturated hydraulic conductivity of ~1.3×10^{-2} m s^{-1} and an air entry pressure of ~2.2 cm.

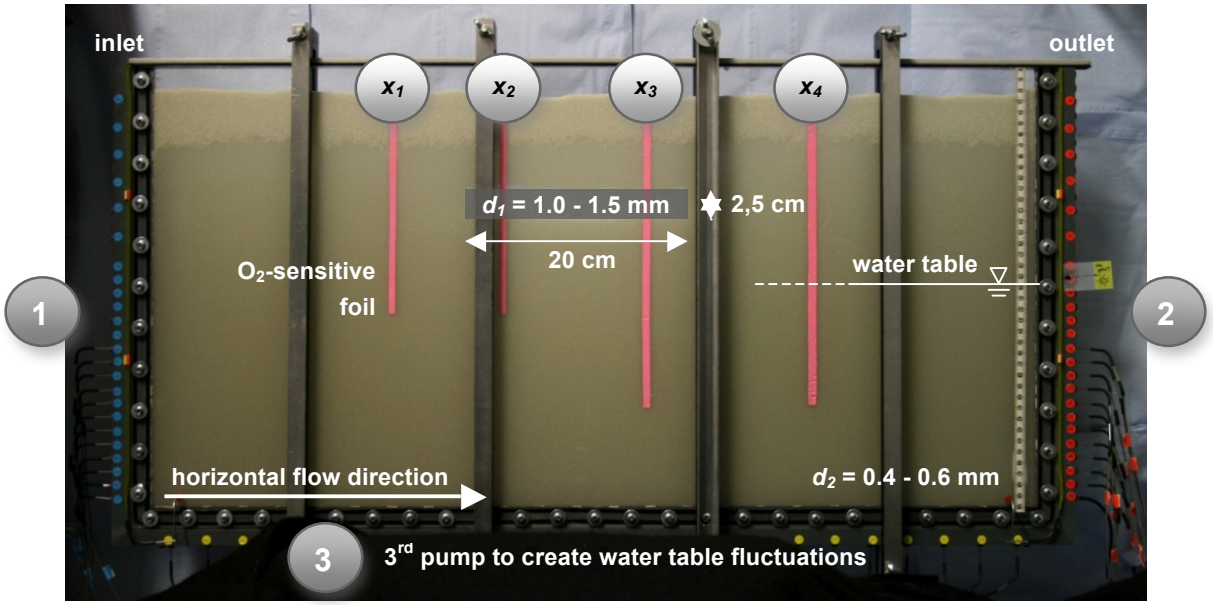

Fig. 6.1. Experimental setup (inner dimensions of the flow-through chamber were 80 cm × 40 cm × 0.5 cm, length × height × width): steady-state horizontal flow was established using Pumps 1 and 2 before inducing a change in water table height using Pump 3. Oxygen-sensitive stripes, used to measure vertical profiles of equivalent aqueous oxygen concentration across the capillary fringe, were placed at x_1 = 22 cm, x_2 = 32 cm, x_3 = 45 cm, and x_4 = 60 cm distance from the inlet.

To fill the flow-through chamber, we increased the water table step-wise, maintaining the water level always a small distance above the upper surface of the porous medium packing. This prevented entrapment of air and fractionation of the grains due to different settling rates. We embedded a coarse-material inclusion (rectangular parallelepiped of dimensions: 20 cm × 2.5 cm × 0.5 cm, L_1 × H_1 × W_1; central position: 27.5 cm above the base of the chamber) within the finer porous medium, as shown in Fig. 6.1. When the flow-through chamber was completely packed, the height of the water table was lowered to form an unsaturated zone in the upper part of the porous medium packing (see Fig. 6.1, light-colored area in the upper region of the porous medium packing).

Steady-state horizontal flow was established before inducing a change in water table elevation. In doing so, we connected two peristaltic pumps (IPC 24, ISMATEC, Glattbrugg, Switzerland) to the vertical sides of the flow-through chamber. At the inlet an aqueous solution was injected via twelve inlet ports. In contrast, only eleven ports were connected to the outlet pump. The twelfth and lowermost port was used as an overflow during the time periods, in which no fluctuation occurred, thus, keeping the water table at a constant level. The ports at the inlet and at the outlet of the flow-through chamber were vertically spaced by 12.5 mm.

During the run of the experiment, the water table was lowered and raised by 10 cm within 15 min, respectively. The change in hydraulic head was created using a third pump (IPC-N 24, ISMATEC, Glattbrugg, Switzerland) connected to the 24 ports at the base of the flow-through chamber. These ports were spaced by 33.3 mm. We followed the raising and lowering of the water table, using two piezometers, which were installed near the inlet and the outlet of the chamber. The height of the capillary fringe was determined visually.

Oxygen-depleted Milli-Q water (stripped with nitrogen) and an aqueous solution containing New Coccine (CAS: 2611-82-7, 75 mg L^{-1}) as a red dye were alternately injected into the chamber to visualize the flow field at different stages of the experiment. We studied oxygen transfer in the capillary fringe at steady state and over the time period following the rise of the water table, i.e., when transient conditions applied. Vertical profiles of equivalent aqueous oxygen concentration were measured at distinct positions (x_1 = 22 cm, x_2 = 32 cm, x_3 = 45 cm, and x_4 = 60 cm) along the horizontal flow direction, using a non-invasive optode technique. In doing so, vertical stripes of oxygen-sensitive polymer optode foil (26 cm × 0.5 cm and 18 cm × 0.5 cm; SP-PtSt3-NAU from PreSens GmbH, Regensburg, Germany) were glued onto the inner side of the front pane and the measurement signal was detected with an optical fibre from the outside. Details on the measurement technique applied can be found, e.g., in Haberer et al. (2011) or Rudolph et al. (2012). Furthermore, we determined mass fluxes in the effluent of the flow-through chamber by interconnecting two flow-through cells (1.7 mL each) in the tubing lines. Simultaneous measurements of flow rate and oxygen concentration were used to calculate the total oxygen flux. For reference, also the oxygen concentration of the oxygen-depleted reservoir solution (i.e., the Milli-Q water stored in the Tedlar bag) was monitored over time. A summary of the flow and transport parameters is listed in Table 6.1.

Table 6.1. Summary of porous medium properties, flow and transport parameters.

Parameter	Value
Inner dimensions of the flow-through chamber, $L \times H \times W$ [m]	0.80 × 0.40 × 0.005
Dimensions of the coarse-material inclusion, $L_1 \times H_1 \times W_1$ [m]	0.20 × 0.025 × 0.005
Average fine grain diameter [mm]	0.50
Average coarse grain diameter [mm]	1.25
Porosity fine material [-]	0.396
Porosity coarse material [-]	0.403
Saturated hydraulic conductivity of fine material [m s^{-1}]	2.1×10^{-3}
Saturated hydraulic conductivity of coarse material [m s^{-1}]	1.3×10^{-2}
Air entry pressure fine material [mm]	~117
Air entry pressure coarse material [mm]	~22
Average flow-rate used in horizontal direction, Q_{in} [mL min^{-1}]	1.84
Aqueous diffusion coefficient for oxygen [1)] [m^2 s^{-1}] (at 22 °C)	1.97×10^{-9}

[1)] for further reference, see Atkins (1990) and Cussler (2009)

6.4 Results and Discussion

The experiments discussed here were designed to investigate the effect of air entry barriers on the entrapment of air or water due to the rise or the lowering of the water table. Especially, we demonstrate the impact of a coarse-material inclusion, embedded in finer porous material, on oxygen transfer in the capillary fringe.

In the following, we first summarize our observations made in the experiment comprising a heterogeneous porous medium packing (‘Experiment 1’). We focus on the temporal changes in the flow field and the vertical distribution of oxygen concentration during the experiment. Afterward, oxygen concentration profiles and mass fluxes determined in the heterogeneous case are compared with an equivalent but homogeneous case. The experimental results with a homogeneous porous medium packing were already presented in Haberer et al. (2012, 2013). Table 6.2 gives an overview on the experiments that we discuss, including the measured parameters and the experimental sequence applied. The latter is additionally depicted in Fig. 6.2.

Table 6.2. Overview of the experiments discussed.

	Experiment 1 (this study)	**Experiment 2** [1)]
	heterogeneous packing	homogeneous packing
Diameter of glass beads	d_1 = 1.0 - 1.5 mm, d_2 = 0.4 - 0.6 mm	d = 0.4 - 0.6 mm
Visualization of the flow field	yes	no
Measured parameters	• porosity • vertical O_2-concentration profiles • O_2-flux, outlet	• porosity • vertical O_2-concentration profiles • O_2-flux, outlet
Experimental sequence [2)]	• **steady state (1)** → O_2-profiles → O_2-flux, outlet • tracer injection (2) • **drainage (3)** → O_2-depleted water • **steady state (4)** → O_2-profiles → O_2-flux, outlet • **imbibition (5)** → O_2-profiles → O_2-flux, outlet • **quasi steady state (6)** → O_2-profiles → O_2-flux, outlet • tracer injection	• **steady state** → O_2-profiles → O_2-flux, outlet • **imbibition** → O_2-profiles → O_2-flux, outlet • **quasi steady state** → O_2-profiles → O_2-flux, outlet

1) results already shown in Haberer et al. (2012, 2013)
2) the numbers given in brackets refer to the current state in Fig. 6.2

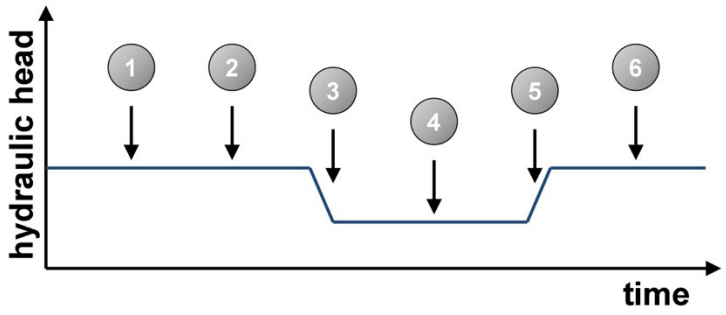

Fig. 6.2. Experimental sequence of 'Experiment 1' (with the heterogeneous porous medium packing). The numbers refer to those given in brackets in Table 6.2.

Throughout this study, measured values of equivalent aqueous oxygen concentration, C [M L^{-3}], are presented in their normalized form, C_{norm} [M L^{-3}], according to the following equation:

$$C_{norm} = \frac{C - C_{bg}}{C_0 - C_{bg}} \tag{6.6}$$

For better comparability of the results presented below, we also use the nondimensional pore volume, PV, instead of time:

$$PV = \frac{qt}{\phi L} \tag{6.7}$$

where q [L T^{-1}] is the specific discharge across the fully water-saturated and quasi-saturated cross-sectional area of the porous medium.

6.4.1 Visualization of the Flow Field and Vertical Oxygen Distribution

Photographs of the experiment ('Experiment 1', Table 6.2) are shown in Figs. 6.3a-d, where the horizontal flow direction is from left to right. We visualized the flow field before, during, and after the change in water table height by alternately injecting oxygen-depleted Milli-Q water and an aqueous solution containing New Coccine as a red dye.*

Initially, oxygen-depleted Milli-Q water was supplied until steady state for flow and transport was reached. Then, we changed the inlet reservoir to inject the red dye solution; the photograph in Fig. 6.3a was taken 3 h after starting the tracer injection. The tracer solution had almost completely replaced the clear aqueous phase, when drainage set in. Figure 6.3b shows the spatial distribution of the red dye solution during drainage, 12 min after inducing the lowering of the water table. This step was followed by establishing steady-state conditions for flow and transport again. To do so, oxygen-depleted tracer-free solution was injected into the flow-through chamber, while the vertical location of the water table remained constant. When steady state had been achieved, we started to increase the water table. Figure 6.3c presents the case 12 min after inducing the transient phase. Following the increase in water table height, oxygen fluxes were measured at the outlet until quasi steady-state conditions were reached. Then, the red dye solution was injected again. Figure 6.3d visualizes the flow field 3 h after the tracer was injected. The qualitative results of the experiment are discussed in the following paragraphs.

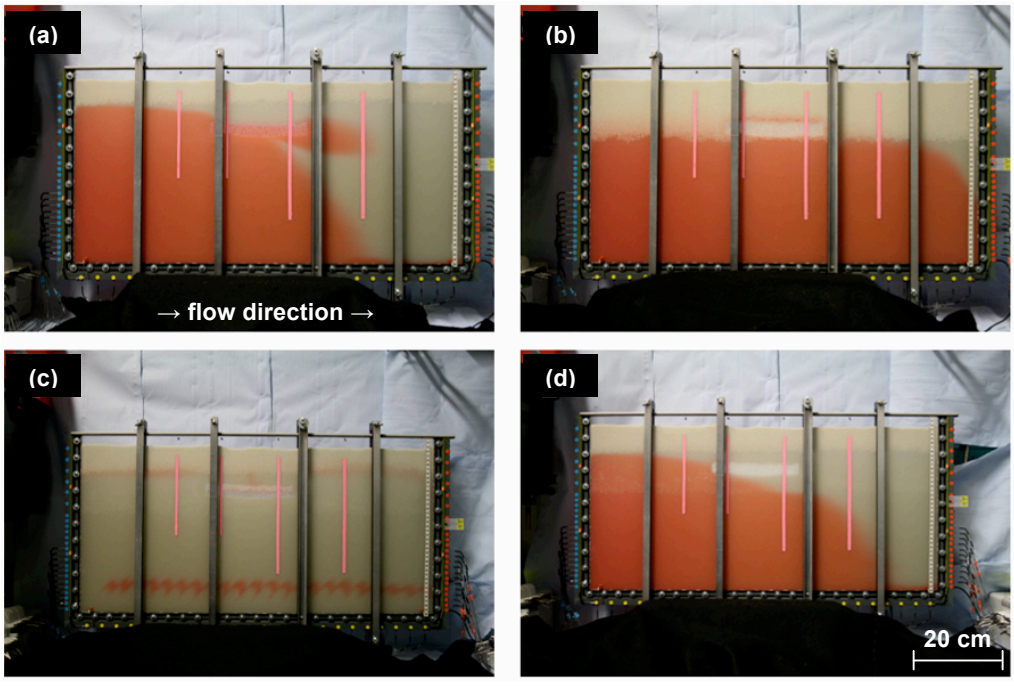

Fig. 6.3. Visualization of the flow field before, during, and after the change in water table height: (a) steady state for flow, 3 h after starting the tracer injection; (b) drainage, 12 min after inducing the lowering of the water table; (c) imbibition, 12 min after inducing the rise of the water table; (d) quasi steady state for flow after the water table fluctuation had occurred, 3 h after starting the tracer injection.

*) Snapshots taken during 'Experiment 1' are included as a movie in the Appendix A.2.

Steady State for Flow, Fully Water-Saturated Coarse-Material Inclusion (Fig. 6.3a):

Oxygen-depleted Milli-Q water was used to establish steady-state horizontal groundwater flow (v_a = 4.33 ± 0.05 m d^{-1}). After flushing through two pore volumes of water, steady state was reached and vertical profiles of equivalent aqueous oxygen concentration were measured at distinct distances from the inlet. The measured profiles are displayed in Fig. 6.4, superimposed on a photograph that was taken at a certain point in time after starting the tracer injection (New Coccine, 75 mg L^{-1}), but under the same experimental flow conditions as they applied, when the oxygen measurements were performed. In doing so, the flow field is visualized and the impact of the deformed flow field due to the presence of the coarse-material inclusion on the vertical distribution of oxygen concentration is presented.

Like in the works from Silliman et al. (2002) and Dunn and Silliman (2003), we observed that the coarse-material inclusion stayed fully water-saturated, although the water table was at a much lower position (~20.5 cm above the base of the porous medium packing, Fig. 6.4), so that capillary rise in the coarse material alone could not account for this effect. In fact, the low air-permeability in the overlying fine material caused the coarse-material inclusion to stay at high moisture content (Dunn, 2005).

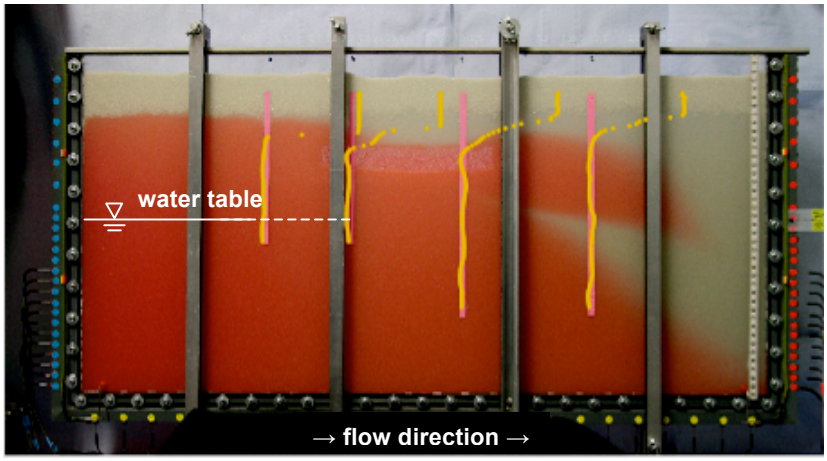

Fig. 6.4. Fully water-saturated coarse-material inclusion: Vertical oxygen profiles were measured at steady state and are shown as the yellow data points with the highest values of equivalent aqueous oxygen concentration in the unsaturated zone (close to equilibrium with the atmosphere). The red dye solution was injected afterward and an intermediate time-step is shown here, as a photograph in the background, to visualize the flow field.

The fully water-saturated coarse-material inclusion comprises a higher value of hydraulic conductivity and, thus, permeability than the surrounding fine material. Therefore, the coarse lens acts as a conduit for flow and streamlines converge toward this zone on the upgradient side, as shown in Figs. 6.3a and 6.4. Downgradient of the coarse-material inclusion, spreading of the tracer plume occurs. Consequently, this also impacts the oxygen distribution in the system. Near the coarse-material inclusion the higher oxygen concentrations, present in the upper part of the

capillary fringe, are drawn toward the higher permeable zone in accordance to the underlying flow field (Fig. 6.4).

Drainage (Fig. 6.3b):

When the red dye solution had almost completely flushed through the system, we started to lower the hydraulic head by 10 cm over a time period of 15 min. As soon as air penetrated through the fine material to the coarse lens, this latter zone started to drain. This behavior was also observed previously by Dunn and Silliman (2003).

In Fig. 6.3b, the fine porous medium overlying the coarse-material inclusion comprises higher water saturations than the surrounding porous material. A capillary barrier formed, which is caused by different values of water saturation in adjacent porous media, where the same suction power applies (Zilch et al., 2002; Papafotiou, 2008).

Imbibition (Fig. 6.3c):

When the water table reached its lower position, we started to inject the oxygen-depleted tracer-free solution until steady-state conditions were established again (v_a = 5.93 ± 0.04 m d^{-1}; height of the water table: ~10.1 cm above the base of the porous medium packing). We measured vertical profiles of oxygen concentration and the oxygen flux in the effluent of the flow-through chamber to confirm steady state. Afterward, the height of the water table was raised by 10 cm within 15 min. To follow up the changes in the vertical oxygen distribution as well as in the oxygen flux in the effluent of the flow-through chamber, we injected the oxygen-depleted solution into the system also during the subsequent time period.

From the previous process of lowering the phreatic surface, some tracer was still present in the tubing lines connected to the third pump (see Fig. 6.1); this pump was used to create the water table fluctuation. Due to reinjection of a small amount of red dye solution, the flow pattern is, thus, also visible in the lower region of the flow-through chamber (Fig. 6.3c). At the same time, pronounced gas entrapment occurred in the coarse material zone. This is shown as the light-coloured area in Figs. 6.3c-d. In the fine material entrapment of gas was not as pronounced, but the affected area, where air got entrapped, is still visible (compare Fig. 6.3a with Figs. 6.3c and 6.3d). In earlier studies (e.g., Fry et al., 1995; Williams and Oostrom 2000; Cirpka and Kitanidis, 2001; Haberer et al., 2012 and 2013), it was already shown that gas entrapment results in partitioning of volatile compounds between the aqueous and gaseous phases. In the present case, e.g., oxygen dissolved from the entrapped air into the mobile oxygen-depleted water.

Quasi Steady State for Flow, Dewatered Coarse-Material Inclusion (Fig. 6.3d):

Oxygen-depleted tracer-free Milli-Q water was pumped through the system till the effect of partitioning diminished and quasi steady-state conditions (i.e., stable values of oxygen flux in the effluent) were achieved. During this time period, the height of the water table decreased slightly causing the coarse zone to dewater again. Therefore, this indicates the presence of an air passage between the unsaturated zone and the coarse-material inclusion. Oxygen concentration profiles were measured at quasi steady state (v_a = 4.05 ± 0.04 m d^{-1}; height of the water table: ~20.7 cm above the base of the porous medium packing) and the results are superimposed on a photograph, showing the flow field in Fig. 6.5. Due to the vertical connection between the unsaturated zone and the coarse lens, oxygen concentrations in the coarse-material inclusion are close to those measured in the unsaturated zone (at positions x_2 = 32 cm and x_3 = 45 cm). Consequently, also a plume of higher oxygen concentrations developed downgradient (at x_4 = 60 cm).

After quasi steady state had been reached, we started to inject the red dye solution via the twelve inlet ports on the left-hand side of the domain in Figs. 6.3d and 6.5. As the coarse-material inclusion is dewatered, this zone comprises now a much lower relative permeability than the surrounding fine porous medium. Therefore, the water is forced to bypass the coarse lens. Moreover, due to the presence of entrapped gas, flow in the capillary fringe also seems to be slightly slower, when compared with the fully water-saturated case displayed in Figs. 6.3a and 6.4 (see also Haberer et al., 2013).

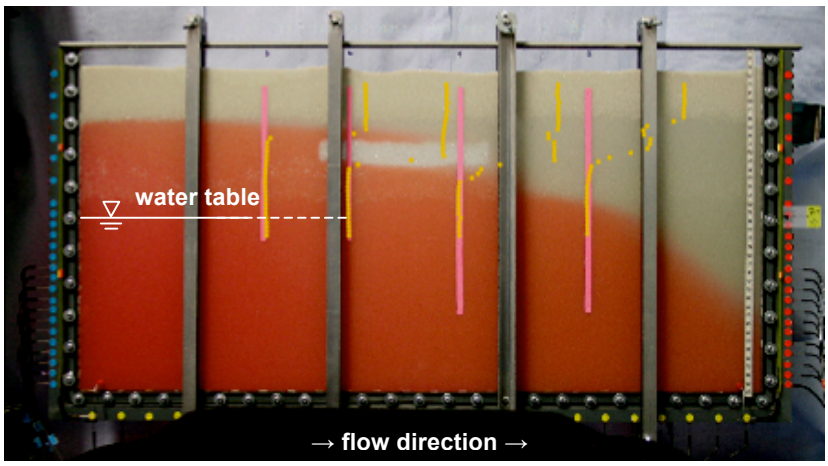

Fig. 6.5. Dewatered coarse-material inclusion: Vertical oxygen profiles were measured at quasi steady state, after having increased the water table, and are shown as the yellow data points with the highest values of equivalent aqueous oxygen concentration in the unsaturated zone (close to equilibrium with the atmosphere). The red dye solution was injected afterward and an intermediate time-step is shown here, as a photograph in the background, to visualize the flow field.

6.4.2 Vertical O_2-Distribution and Effluent Mass Fluxes in the Presence of a Coarse Lens

In the following, we first establish a link between the various oxygen profiles measured at (quasi) steady state in 'Experiment 1' (Table 6.2, heterogeneous porous medium packing). The objective is to show the importance of differing hydraulic conditions (i.e., a fully water-saturated vs. a dewatered coarse lens) on oxygen transfer in the capillary fringe. We especially focus on changes in the vertical distribution of oxygen concentration along the horizontal groundwater flow direction, since the concentration profiles are also impacted by complex deformation of the flow field. Moreover, (quasi) steady-state oxygen fluxes, determined in the effluent of the flow-through chamber, are discussed. Time-dependent dissolution of oxygen from entrapped gas into the oxygen-depleted aqueous phase, following the rise of the water table, is investigated next. We do this by relating the results of the experiment with the heterogeneous porous medium packing to the homogeneous case ('Experiment 2').

6.4.2.1 (Quasi) Steady-State Oxygen Transfer across the Capillary Fringe

For the time periods of the experiment ('Experiment 1') during which (quasi) steady state applied and the water table was at its upper position, the measured profiles of equivalent aqueous oxygen concentration have been qualitatively presented in Figs. 6.4 and 6.5. Figure 6.6 displays these vertical profiles again, dependent on their horizontal location and the respective hydraulic conditions that prevailed (i.e., fully water-saturated vs. dewatered coarse lens).

The measured oxygen concentration profiles upgradient of the coarse-material inclusion, at x_1 = 22 cm distance from the inlet (Fig. 6.6a), are very similar despite the different hydraulic conditions that prevailed. Values of normalized oxygen concentration start to decrease when water saturation is already very high (e.g., Liu, 2008; Haberer et al., 2011). An oxygen gradient was established as a result of the mass transfer limitation of oxygen on the water-side. Just the slight decrease observed in the thickness of the capillary fringe (-0.9 cm between the fully water-saturated case and the dewatered coarse lens) had an impact on the vertical position of the oxygen gradient.

In contrast, we observed a significant effect of the coarse-material inclusion on the vertical distribution of normalized oxygen concentrations at x_2 = 32 cm and x_3 = 45 cm. In Figs. 6.6b and 6.6c, the two dashed lines indicate the vertical location of the coarse lens. The measured profiles are distorted according to the underlying flow field resulting from the different grain sizes and the varying values of water content present at these positions.

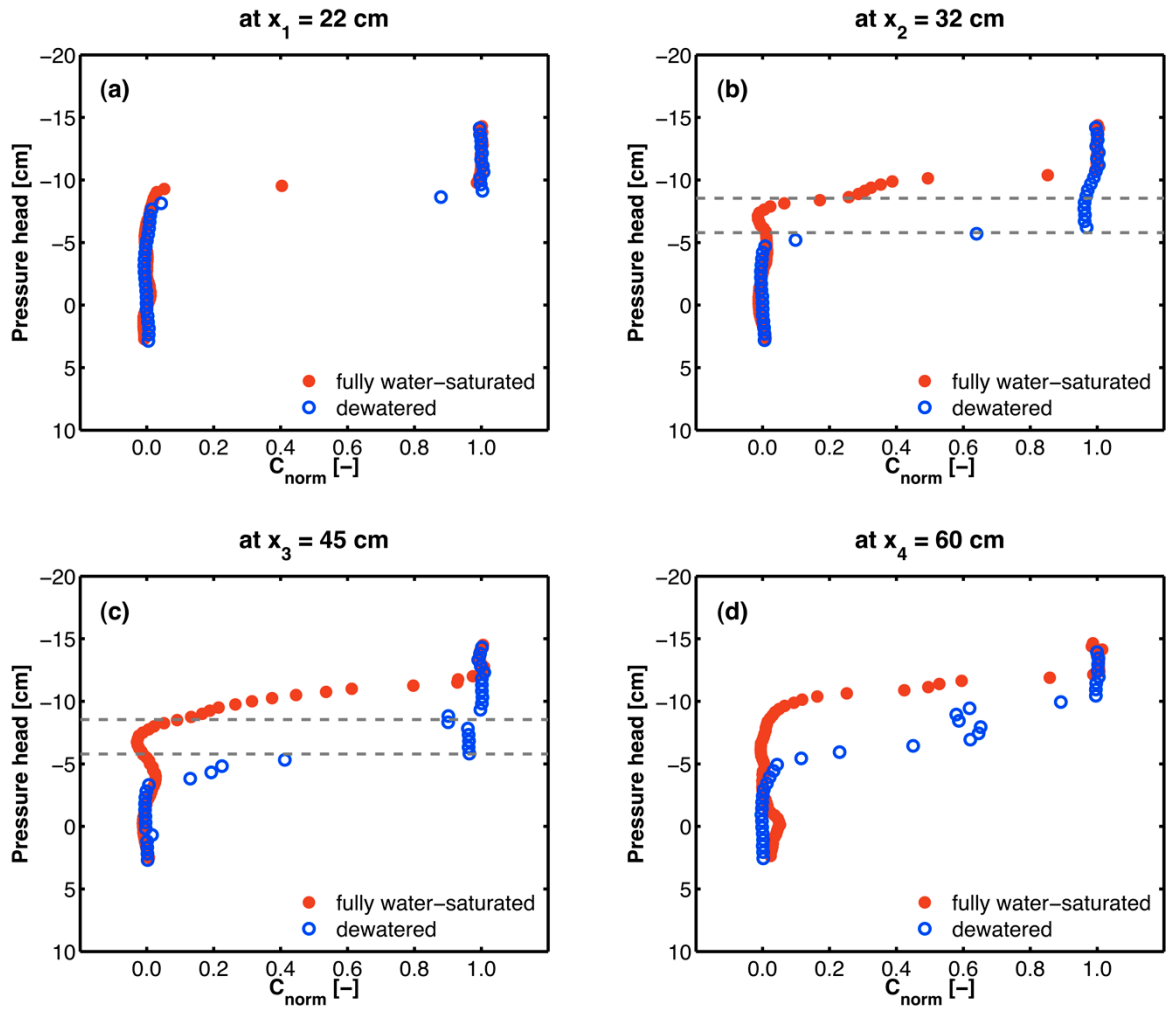

Fig. 6.6. (Quasi) steady-state profiles of normalized oxygen concentration at (a) x_1 = 22 cm, (b) x_2 = 32 cm, (c) x_3 = 45 cm, and (d) x_4 = 60 cm. The pressure head of 0.00 cm indicates the location of the water table, while the dashed lines show the vertical position of the coarse-material inclusion (see also Fig. 6.1).

First, we look at the oxygen concentration profiles that refer to the case, in which the coarse lens is fully water-saturated. At the interface between the fine and the coarse material the different grain sizes mix, causing the oxygen gradient to change its steepness in this transition zone. Eberhardt et al. (2001) observed that the transverse vertical dispersion coefficient decreases when the porous medium contains a fraction of smaller grains. This cannot be deduced from the present results (Figs. 6.6b and 6.6c) since these are also impacted by a change in flow direction and groundwater flow velocity. In fact, the fully water-saturated coarse-material inclusion has a higher permeability than the surrounding fine material. This results in higher flow velocities in the coarse lens, which not only affects the flow field, but also the oxygen concentration gradient in the inclusion. We recall that spreading and mixing must be separated for heterogeneous porous media (e.g., Kitanidis, 1994; Dentz et al., 2011). Therefore, we cannot directly interpret the vertical oxygen concentration profiles with respect to mass transfer of oxygen across the unsaturated/saturated interface. Due to the vertical flow component near the upper limit of the capillary fringe, we may assume that mass

transfer is increased. In order to quantify oxygen supply from the atmosphere, the results have to be evaluated numerically; otherwise, additional information about the total oxygen flux in the effluent is needed. The latter is discussed below.

When the coarse lens is dewatered and quasi steady-state conditions are established, the oxygen concentration profiles indicate the exact vertical position of the coarse-material inclusion (Figs. 6.6b and 6.6c). Oxygen is now transferred much deeper into the porous medium than in the previous case (i.e., when the coarse lens was fully water-saturated). The occurrence of an air passage between the unsaturated zone and the coarse lens favors this result, and we assume that the passage is at or close to the measured profile at x_2 = 32 cm. Such air passages exist in nature in the root zone, as earthworm burrows, or may be formed due to redeposition of soil. We hypothesize that the values of oxygen concentration measured in the entrapped air pocket would be much lower if this air passage did not exist. Then oxygen would not be resupplied from the atmosphere into this lower region, thus, causing the entrapped air phase to get depleted in this important electron acceptor over time. Finally, the oxygen partial pressure in the gaseous phase would reach equilibrium with the oxygen concentration prevailing in the mobile aqueous phase.

Figure 6.6d shows the oxygen concentration profiles measured 12.5 cm downgradient of the coarse-material inclusion (at x_4 = 60 cm). Deformation of the flow field, caused by the presence of the coarse lens, still affects the vertical oxygen distribution at this *x*-position. However, the effect is not as pronounced as it was at positions x_2 and x_3 (Figs. 6.6b and 6.6c). In the case of the dewatered coarse lens, we also observed an oxygen plume on the downgradient side of the lens due to dissolution of gaseous oxygen into the aqueous phase.

The foregoing considerations imply that the (quasi) steady-state oxygen flux in the effluent of the flow-through chamber may be higher due to the presence of a coarse-material inclusion. This is further investigated in the following paragraphs by comparing the mass fluxes determined in the experiments with a homogeneous and a heterogeneous porous medium packing, respectively.

Comparing (Quasi) Steady-State Oxygen Fluxes:

Oxygen fluxes at the inlet and in the effluent of the flow-through chamber were determined at different points in time during the experiments. In this section, we compare the mass fluxes gained when flow and transport were at (quasi) steady state. Table 6.3 gives an overview of the experimental values. The results from theoretical considerations according to Chapter 6.2.2 and Haberer et al. (2012) are also presented.

Oxygen flux across the unsaturated/saturated interface is relevant (in the following: Δin/out, see Table 6.3) to the current discussion. When the water table is at its lower position, entrapped air is absent and the coarse-material inclusion does not affect the flow field in the experiment comprising a heterogeneous porous medium packing (‘Experiment 1’; the upper boundary of the capillary

fringe is below the lower *z*-position of the coarse-material inclusion). Therefore, the experimentally determined values of oxygen flux across the capillary fringe compare well to the theoretically expected mass fluxes. Moreover, since the controlling parameters – e.g., the horizontal seepage velocity, the flow-through area, and the background concentration in the aqueous phase – differ just slightly between the two experiments, the interfacial mass fluxes (7.01×10^{-6} mg s^{-1} ± 7 %) are very similar.

In the homogeneous case ('Experiment 2', Table 6.3), interfacial mass flux decreases (Eqns. 6.1 and 6.2) when the height of the water table increases since the horizontal groundwater flow velocity slows down accordingly. Compared to the theoretical values, we note a higher decrease in oxygen flux across the unsaturated/saturated interface in the real experiment (-55.8 % compared with -27.8 % in the theoretical case, assuming no entrapped gas is present). This may be explained by the fact, that the presence of entrapped gas additionally affects the effective hydraulic permeability in the capillary fringe region, thereby resulting in a lower value of interfacial oxygen flux.

Table 6.3. Experimentally determined and theoretical values (see Eqns. 6.1 - 6.3) of oxygen flux.

	Experiment 1 (this study)	**Experiment 1 (theory)**	**Experiment 2** [1)]	**Experiment 2** [1)] **(theory)**
	heterogeneous packing	homogeneous packing	homogeneous packing	homogeneous packing
1. Steady state before lowering the water table (without entrapped gas)				
vertical flow-through area [cm^2]	16.5	16.5	-	-
v_a [m d^{-1}]	4.33	4.33	-	-
mass flux, inlet [mg s^{-1}]	5.35×10^{-5}	5.35×10^{-5}	-	-
mass flux, outlet [mg s^{-1}]	7.68×10^{-5}	5.87×10^{-5}	-	-
Δin/out [mg s^{-1}] [2)]	2.33×10^{-5}	5.26×10^{-6}	-	-
$P_{\Delta in/out}$ [%] [3)]	+343%	±0 %	-	-
2. Steady state when the water table is at its lower position (without entrapped gas)				
vertical flow-through area [cm^2]	11.5	11.5	12.0	12.0
v_a [m d^{-1}]	5.93	5.93	6.04	6.04
mass flux, inlet [mg s^{-1}]	5.49×10^{-5}	5.49×10^{-5}	4.05×10^{-5}	4.05×10^{-5}
mass flux, outlet [mg s^{-1}]	6.14×10^{-5}	6.16×10^{-5}	4.80×10^{-5}	4.83×10^{-5}
Δin/out [mg s^{-1}] [2)]	6.55×10^{-6}	6.80×10^{-6}	7.47×10^{-6}	7.76×10^{-6}
$P_{\Delta in/out}$ [%] [3)]	+4 %	±0 %	-4 %	±0 %
3. (Quasi) steady state after the increase in water table height (with entrapped gas, except theory)				
vertical flow-through area [cm^2]	16.2	16.2	16.3	16.3
v_a [m d^{-1}]	4.05	4.05	4.35	4.35
mass flux, inlet [mg s^{-1}]	3.82×10^{-5}	3.82×10^{-5}	4.37×10^{-5}	4.37×10^{-5}
mass flux, outlet [mg s^{-1}]	6.13×10^{-5}	4.35×10^{-5}	4.70×10^{-5}	4.93×10^{-5}
Δin/out [mg s^{-1}] [2)]	2.30×10^{-5}	5.35×10^{-6}	3.30×10^{-6}	5.60×10^{-6}
$P_{\Delta in/out}$ [%] [3)]	+330 %	±0 %	-41 %	±0 %

[1)] data from Haberer et al. (2012)
[2)] Oxygen flux across the unsaturated/saturated interface
[3)] Increase/decrease in oxygen flux across the unsaturated/saturated interface, theoretical value taken as 100 %

When the water table is at its upper position, the presence of the coarse-material inclusion considerably affects mass flux across the unsaturated/saturated interface (‘Experiment 1’, Table 6.3). We note fourfold higher interfacial oxygen fluxes in the experiment compared to a theoretical case; in the latter, we assume a homogeneous porous medium packing and the absence of entrapped air. This is due to the deformation of the flow field as well as the continuous partitioning of oxygen between the aqueous and gaseous phases. Approximately the same amount of oxygen is supplied to the oxygen-depleted water before and after the fluctuation of the water table. The latter is, however, dependent on the specific experimental condition that applied in the current case, i.e., the resupply of oxygen via an air passage between the unsaturated zone and the coarse-material inclusion. We hypothesize that the interfacial oxygen flux at quasi steady state, following imbibition, would be lower if this air passage did not exist.

6.4.2.2 Time-Dependent Oxygen Dissolution Following the Rise of the Water Table

Due to imbibition and the concomitant entrapment of air, oxygen partitions between the entrapped gas and the oxygen-depleted mobile aqueous phase. As a result oxygen dissolution fronts travel through the system. Figure 6.7 presents the measured oxygen concentration profiles (at x_3 and x_4) as a function of time for both the homogeneous and the heterogeneous case. The presence of a coarse-material inclusion in the direct vicinity of the water table significantly affects the vertical distribution of oxygen as shown by comparing Figs. 6.7a and 6.7c for the homogeneous case with Figs. 6.7b and 6.7d for the experiment comprising the heterogeneous porous medium packing. In the two experiments, the water table ($H_{WT,hom}$ = 20.5 cm, $H_{WT,het}$ = 20.7 cm) and the upper edge of the capillary fringe ($H_{CF,hom}$ = 32.5 cm, $H_{CF,het}$ = 32.4 cm) are located at the same vertical positions, respectively. However, higher values of oxygen concentration were found at much lower vertical positions in the heterogeneous than in the homogeneous case.

In both kinds of porous medium packing, we found that it takes longer to reach quasi steady state at x_4 = 60 cm than at x_3 = 45 cm. At x_4 = 60 cm, the oxygen dissolution front is also more smeared out. Furthermore, it appears that a smaller number of pore volumes have to be flushed through the heterogeneous system to reach quasi steady state compared to the homogeneous case. We note that this is not the actual case, when looking at the cumulative oxygen mass and the value of the EM_{O2}; this is discussed in greater detail below.

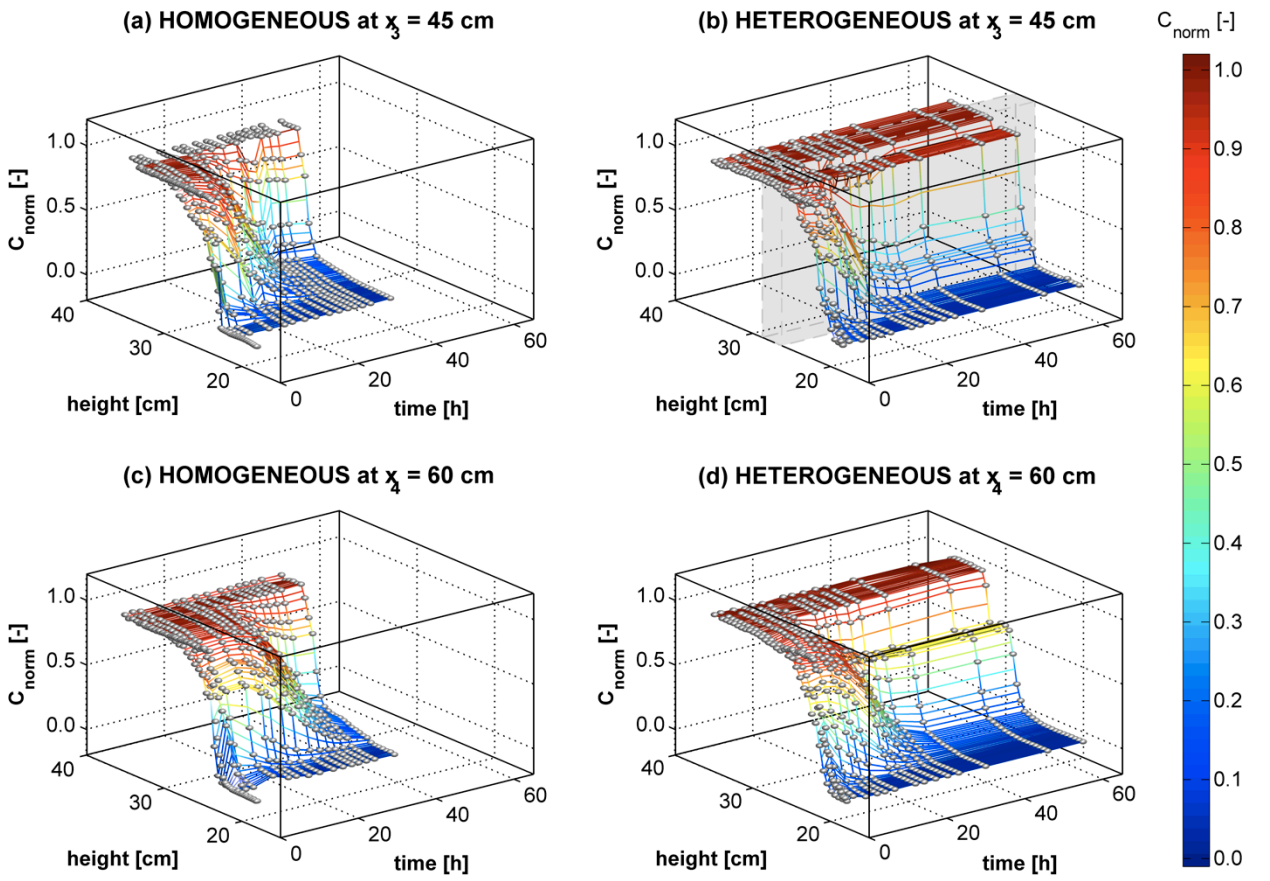

Fig. 6.7. Time-dependent profiles of normalized oxygen concentration after imbibition: (a) homogeneous porous medium packing, x_3 = 45 cm, (b) heterogeneous porous medium packing, x_3 = 45 cm; the grey-shaded cuboid indicates the vertical position (h_{incl} = 26.3 - 28.8 cm) of the coarse-material inclusion, (c) homogeneous porous medium packing, x_4 = 60 cm, and (d) heterogeneous porous medium packing, x_4 = 60 cm. The spheres in each graph indicate the measurements.

Measured Oxygen Fluxes in the Effluent of the Flow-Through Chamber:

During drainage a zone of higher water saturation formed in the fine material overlying the coarse lens (see Fig. 6.3b). The water trapped in this zone became air-equilibrated over time. When we started to imbibe the porous medium, the subsequent rise of the phreatic surface re-established horizontal flow in the upper zone of the porous medium packing. Thus, the entrapped water parcels were again carried on as part of the underlying flow field, possibly resulting in an additional supply of oxygen to the oxygen-depleted groundwater. For this account, we intend to determine oxygen fluxes in the effluent of the flow-through chamber immediately after imbibition. Figure 6.8 displays the cumulative oxygen mass supplied to the aqueous phase as well as the EM_{O2} vs. the number of pore volumes after inducing the rise of the water table for both experiments comprising the homogeneous ('Experiment 2') and the heterogeneous ('Experiment 1') porous medium packing. In both experiments, quasi steady-state conditions were reached after about four pore volumes of oxygen-depleted water had been flushed through the system.

The calculated cumulative oxygen masses (Fig. 6.8a), based on Eqn. 6.1, are very similar for 'Experiment 1' (heterogeneous porous medium packing) and 'Experiment 2' (homogeneous) because the theoretical oxygen fluxes across the interface differ just slightly between the two cases (see Table 6.3). Moreover, at quasi steady state the oxygen flux for the experiment comprising the heterogeneous porous medium packing is about seven times higher than the mass flux for the homogeneous case. Thus, also the cumulative oxygen mass supplied to the aqueous phase differs by a factor of seven at a specific point in time. Considerably more oxygen is supplied across the unsaturated/saturated interface when a coarse-material inclusion is present near the water table.

Figure 6.8b presents the excess mass of oxygen supplied to the aqueous phase solely due to the rise of the water table; the quasi steady-state dispersive mass flux across the unsaturated/ saturated interface (as well as a possible continuous supply of oxygen from entrapped gas due to the air passage between the unsaturated zone and the dewatered coarse lens) is not considered in the value of EM_{O2}. The two graphs in Fig. 6.8b are very similar to each other and approximately the same amount of oxygen is supplied to the oxygen-depleted water under the constrictions stated above (i.e., only the temporary supply of oxygen from entrapped air is considered). This suggests that, in both experiments, gas partitioning between the aqueous and gaseous phases plays an important role for mass transfer of oxygen in the capillary fringe. However, we have to consider additional 'sources' of oxygen mass in 'Experiment 1' (heterogeneous case), which contribute to the excess mass of oxygen supplied to the system.

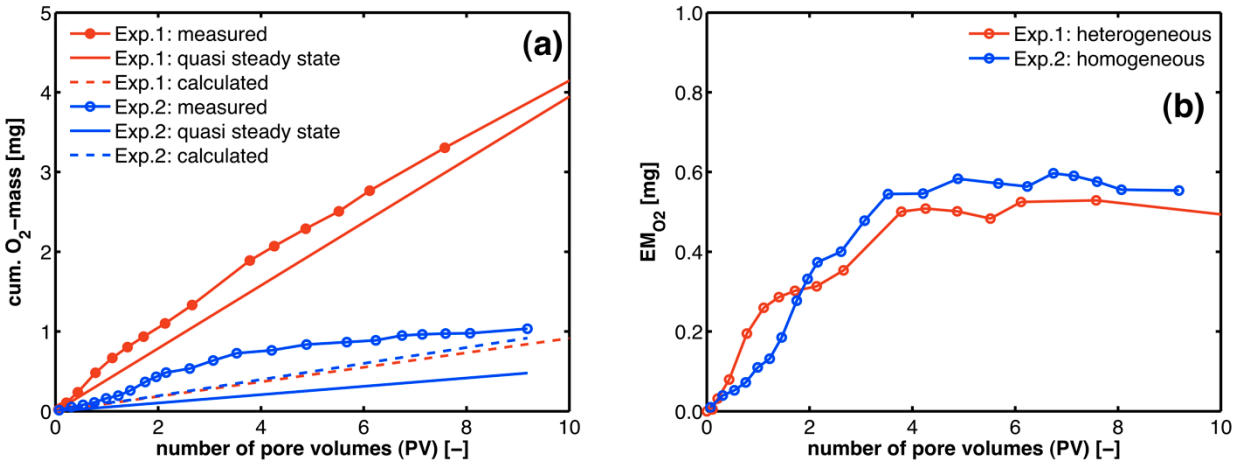

Fig. 6.8. Impact of a homogeneous ('Exp. 2') and a heterogeneous ('Exp. 1') porous medium packing on oxygen transfer. 0 PV denotes the start of the rise in the water table. (a) Cumulative oxygen mass supplied to the aqueous phase across the unsaturated/saturated interface; (b) Excess mass of oxygen supplied to the system solely due to the rise of the water table (Eqn. 6.5).

During the first pore volume after having increased the height of the water table, significantly more oxygen mass was supplied to the aqueous phase in the heterogeneous system (0.24 mg)

compared to the homogeneous case (0.11 mg). The additional supply of oxygen, for the system comprising the heterogeneous porous medium packing, can be partially explained by the reinjected volume of the air-equilibrated and, thus, oxygen-containing tracer solution (accounts for ~0.08 mg of oxygen mass, see Fig. 6.3c); the other part comes (~0.05 mg) from the air-equilibrated water that had been previously trapped in the fine material overlying the coarse lens. The contribution from these 'sources' diminishes after one pore volume. Therefore, the actual oxygen mass supplied to the heterogeneous system solely due to gas partitioning between the aqueous and gaseous phases is lower than in the homogeneous case. We already accounted for the continuous supply of oxygen from air present in the coarse lens by measuring the quasi steady-state oxygen flux in the effluent of the flow-through chamber. As a result, in 'Experiment 1', a lower volume of entrapped air is responsible for the temporary dissolution of oxygen in the aqueous phase than in the homogeneous case. In the homogeneous case, a larger amount of gas entrapped in small air pockets is not replenished by atmospheric oxygen.

6.5 Summary and Conclusions

The presence of a coarse-material inclusion in the direct vicinity of the water table affects flow conditions and, hence, the vertical distribution of equivalent aqueous oxygen concentration across the capillary fringe. Since transverse vertical dispersion controls the mixing of dissolved reaction partners at a plume's fringes under steady-state conditions (Thornton et al., 2001; Schürmann et al., 2003; Rahman et al., 2005; Cirpka et al., 2006), enhanced mixing considerably affects reactive transport and the length of a contaminant plume (e.g., Bauer et al., 2008). Mass fluxes measured at (quasi) steady state were compared to a similar case comprising a homogeneous porous medium packing. We observed significantly higher values of total oxygen flux across the unsaturated/saturated interface in the heterogeneous case. In fact, mixing was considerably enhanced when the coarse-material inclusion was fully water-saturated. In case the coarse lens was dewatered, also continuous gas partitioning between the aqueous and gaseous phases contributed to the measured oxygen flux in the effluent.

During the lowering of the water table, the coarse lens acted as a capillary barrier, i.e., higher values of water content were present in the fine material overlying the coarse lens. This water became air-equilibrated over time and presented an additional 'source' of oxygen supplied to the aqueous phase during the increase in water table elevation. Moreover, the water table fluctuation led to pronounced entrapment of air in the coarse lens since capillary rise in the fine material was faster. Gas partitioning between the aqueous and gaseous phases was shown to be instrumental for mass transfer in the capillary fringe. The existence of air passages between the unsaturated

zone and larger air pockets in the water-saturated domain are advantageous for continuous supply of oxygen to groundwater.

We anticipate that the porous medium characteristics, the geometry (e.g., the surface/volume ratio) and the location of a coarse-material inclusion may considerably affect measured oxygen fluxes in groundwater. In fact, the volume of entrapped air below the water table increases with either a rise in the difference in air entry pressure between the coarse lens and the surrounding sediment matrix, or an increase in the uniformity of grain size of the coarse sediment (Dunn, 2005). Besides, the entrapment of air below and of water above the water table are related to the vertical connectivity of zones of coarse material within a surrounding finer matrix. A higher surface/volume ratio may lead to faster dissolution of oxygen into oxygen-depleted groundwater.

Presence of dissolved oxygen both above and below the water table impacts redox conditions in the capillary fringe region, thus, possibly affecting all biogeochemical reactions that occur in this zone. Additionally, mixing-limited chemical reactions are affected indirectly by physical heterogeneities due to their impact on the spread and mixing of dissolved species (Dentz et al., 2011).

Acknowledgement

This study was funded by the DFG (German Research Foundation) through the Research Group FOR 831 ‘Dynamic Capillary Fringes – A Multidisciplinary Approach’ (grant GR971/22-1).

References

Atkins, P.W., 1990. Physical Chemistry. Oxford University Press, Oxford.

Barber, C., Davis, G.B. and Farrington, P., 1990. Sources and sinks for dissolved oxygen in groundwater in an unconfined sand aquifer, Western Australia. *In* Barto-Kyriakidis, A., Farrell, L. (Eds.) Geochemistry of Gaseous Elements and Compounds. Theophrastus Publications, Athens, pp. 353-368.

Barth, J.A.C., Kappler, A., Piepenbrink, M., Werth, C.J., Regenspurg, S., Semprini, L., Slater, G.F., Schüth, C. and Grathwohl, P., 2005. New challenges in biogeochemical gradient research. EOS, 86: 44 1 November 2005.

Bauer, R.D., Maloszewski, P., Zhang, Y., Meckenstock, R.U. and Griebler, C., 2008. Mixing-controlled biodegradation in a toluene plume – Results from two-dimensional laboratory experiments. Journal of Contaminant Hydrology, 96: 150-168.

Bear, J. and Cheng, A.H.-D., 2010. Modeling groundwater flow and contaminant transport, 23rd Volume, Springer, New York.

Berkowitz et al., 2004. Impact of the capillary fringe on local flow, chemical migration, and microbiology. Vadose Zone Journal, 3: 534-548.

Chiogna, G., Eberhardt, C., Grathwohl, P., Cirpka, O.A. and Rolle, M., 2010. Evidence of compound dependent hydrodynamic and (hydro)mechanical transverse dispersion with multi-tracer laboratory experiments. Environmental Science and Technology, 44(2): 688-693, doi: 10.1021/es9023964.

Cirpka, O.A. and Kitanidis, P.K., 2001. Transport of volatile compounds in porous media in the presence of a trapped gas phase. Journal of Contaminant Hydrology, 49(3-4): 263-285.

Cirpka, O.A., 2002. Choice of dispersion coefficients in reactive transport calculations on smoothed fields. Journal of Contaminant Hydrology, 58: 261-282.

Cirpka, O.A., Olsson, Å., Ju, Q., Rahman, M.A. and Grathwohl, P., 2006. Determination of transverse dispersion coefficients from reactive plume lengths. Ground Water, 44: 212-221.

Cussler, E.L., 2009. Diffusion: Mass transfer in fluid systems, 3rd ed., Cambridge University Press, New York.

Dentz, M., Le Borgne, T., Englert, A. and Bijeljic, B., 2011. Mixing, spreading and reaction in heterogeneous media: A brief review. Journal of Contaminant Hydrology, 120-121: 1-17, doi: 10.1016/j.jconhyd.2010.05.002.

Dunn, A.M. and Silliman, S.E., 2003. Air and water entrapment in the vicinity of the water table. Ground Water, 41(6): 729-734.

Dunn, A.M., 2005. Air and LNAPL entrapment in the partially saturated fringe: Laboratory and numerical investigations. University of Notre Dame, Dissertation, 116 p.

Eberhardt, C., Finkel, M. and Linke, C., 2001. Verbundvorhaben VEGAS, Entwicklung bioaktiver Sorptionsbarrieren zur in situ Abstromsanierung, Abschlussbericht BMBF02WT914/0.

Fetter, C.W., 2001. Applied Hydrogeology, 4th ed., Upper Saddle River, New Jersey: Prentice Hall.

Fry, V.A., Istok, J.D., Semprini, L., O'Reilly, K.T. and Buschek, T.E., 1995. Retardation of dissolved oxygen due to a trapped gas phase in porous media. Ground Water 33(3): 391-398.

Fry, V.A., Selker, J.S. and Gorelick, S.M., 1997. Experimental investigations of trapping oxygen gas in saturated porous media for in situ bioremediation. Water Resources Research, 33(12): 2687-2696.

Haberer, C.M., Rolle, M., Liu, S., Cirpka, O.A. and Grathwohl, P., 2011. A high-resolution non-invasive approach to quantify oxygen transport across the capillary fringe and within the underlying groundwater. Journal of Contaminant Hydrology, 122(1-4): 26-39, doi: 10.1016/j.jconhyd.2010.10.006.

Haberer, C.M., Rolle, M., Cirpka, O.A. and Grathwohl, P., 2012. Oxygen transfer in a fluctuating capillary fringe. Vadose Zone Journal, 11(3), doi: 10.2136/vzj2011.0056.

Haberer, C.M., Cirpka, O.A., Rolle, M. and Grathwohl, P., 2013. Experimental sensitivity analysis of oxygen transfer in the capillary fringe. Ground Water, doi: 10.1111/gwat.12028.

Kerfoot, H.B., 1994. In situ determination of the rate of unassisted degradation of saturated-zone hydrocarbon contamination. Journal of the Air and Waste Management Association, 44: 877-880.

Kitanidis, P.K., 1994. The concept of the dilution index. Water Resources Research, 30: 2011-2026.

Klenk, I.D. and Grathwohl, P., 2002. Transverse vertical dispersion in groundwater and the capillary fringe. Journal of Contaminant Hydrology, 58(1-2): 111-128.

Liu, S., 2008. Mass transfer of oxygen across the capillary fringe. Doctoral Thesis, Institute for Geoscience, University of Tübingen.

Maier, U. and Grathwohl, P., 2005. Natural attenuation in the unsaturated zone and shallow groundwater: Coupled modeling of vapor phase diffusion, biogeochemical processes and transport across the capillary fringe. *In* Nützmann, G., Viotti, P., Aagard, P. (Eds.) Reactive transport in soil and groundwater. Springer Verlag, pp. 141-155.

Orlob, G.T. and Radhakrishna, G.N., 1958. The effect of entrapped gases on the hydraulic characteristics of porous media. Transactions, American Geophysical Union, 39. 648-659.

Papafotiou, A., 2008. Numerical investigations of the role of hysteresis in heterogeneous two-phase flow systems. Doctoral Thesis, University of Stuttgart, Institute of Hydraulic Engineering.

Rahman, M.A., Jose, S.C., Nowak, W. and Cirpka, O.A., 2005. Experiments on vertical transverse mixing in a large-scale heterogeneous model aquifer. Journal of Contaminant Hydrology, 80: 130-148.

Rolle, M., Eberhardt, C., Chiogna, G., Cirpka, O.A. and Grathwohl, P., 2009. Enhancement of dilution and transverse mixing in porous media: Experiments and model-based interpretation. Journal of Contaminant Hydrology, 110: 130-142.

Ronen, D., Scher, H. and Blunt, M., 1997. On the structure and flow processes in the capillary fringe of phreatic aquifers. Transport in Porous Media, 28: 159-180.

Rudolph, N., Esser, H.G., Carminati, A., Moradi, A.B., Hilger, A., Kardjilov, N., Nagl, S. and Oswald, S.E., 2012. Dynamic oxygen mapping in the root zone by fluorescence dye imaging combined with neutron radiography. Journal of Soils and Sediments, 12: 63-74, doi: 10.1007/s11368-011-0407-7.

Schürmann, A., Schroth, M.H., Saurer, M., Bernasconi, S.M. and Zeyer, J., 2003. Nitrate-consuming processes in a petroleum-contaminated aquifer quantified using push-pull tests combined with 15N isotope and acetylene-inhibition methods. Journal of Contaminant Hydrology, 66: 59-77.

Silliman, S.E., Berkowitz, B., Simunek, J. and van Genuchten, M.Th., 2002. Fluid flow and solute migration within the capillary fringe. Ground Water, 40(1): 76-84.

Thornton, S.F., Quigley, S., Spence, M.J., Banwart, S.A., Bottrell, S. and Lerner, D.N., 2001. Processes controlling the distribution and natural attenuation of dissolved phenolic compounds in a deep sandstone aquifer. Journal of Contaminant Hydrology, 53: 233-267.

Williams, M.D. and Oostrom, M., 2000. Oxygenation of anoxic water in a fluctuating water table system: An experimental and numerical study. Journal of Hydrology, 230: 70-85.

Zilch, K., Diederichs, C.J., Katzenbach, R., 2002. Handbuch für Bauingenieure: Technik, Organisation und Wirtschaftlichkeit – Fachwissen in einer Hand. Springer, Berlin, ISBN: 3-540-65760-6.

7. Synopsis and Outlook

This thesis' objectives focused on the investigation of oxygen transfer across the capillary fringe and, especially, on studying the impact of a fluctuating water table on the supply of oxygen to oxygen-depleted groundwater. The quasi two-dimensional flow-through laboratory experiments were mostly carried out in homogeneous porous media with uniform grain sizes. A non-invasive optode technique, to measure oxygen concentrations, was applied. Based on this method, vertical concentration profiles, resulting from the mass transfer of oxygen from the atmosphere into the aqueous phase, were obtained at high spatial resolution at distinct cross-sections along the horizontal groundwater flow direction. Additional mass flux measurements in the effluent of the flow-through chamber were used to quantify the effectiveness of the mass transfer processes under the respective boundary conditions applied. We considered two principal mechanisms for the mass transfer of oxygen across and within the capillary fringe:

- the vertical transport of oxygen from the capillary fringe's upper limit into the water-saturated zone by diffusion along oxygen concentration gradients
- the vertical movement of the water table and the capillary fringe over time resulting, e.g., in the dissolution of oxygen from entrapped gas in the oxygen-depleted groundwater.

7.1 Conclusions

In the following, we give an overview on the different studies performed as well as on the conclusions that were drawn:

Mass Transfer within the Saturated Zone and across the Capillary Fringe. Under the same experimental conditions and at steady state, values of transverse vertical dispersion were found to be the same with regard to oxygen transfer within the saturated zone and across the capillary fringe. This clearly indicates the limitation of oxygen transfer in the aqueous phase and, thus, steep concentration gradients may exist in the region of the capillary fringe. The capillary fringe is, therefore, not different from other regions in aquifers, if strong microbial activity is attributed to regions where steep concentration gradients exist and similar hydraulic conditions apply.

Different Dynamics of the Water Table Fluctuation. (i) Single Rise or Lowering of the Water Table. Partitioning of oxygen between the aqueous and the gaseous phases was identified to be important for the medium term supply of oxygen to oxygen-depleted groundwater. The effect diminished after passage of several pore volumes of water, since no further oxygen could be supplied from the entrapped gas. In case of rapid lowering of the water table, we argued that the

effect of specific yield led to increased oxygen fluxes in the effluent of the flow-through chamber. *(ii) Long-term Fluctuating Water Table.* Provided that the downward movement of the water table is fast (compared with horizontal flow) and the dissolution of oxygen from entrapped gas has not diminished yet, oxygen can travel deep into the saturated zone. In our case, this was reasoned by the effects of specific yield and advective flow in vertical direction, resulting in an increase in penetration depth during drainage. We concluded that the dynamics of the fluctuating water table may considerably affect the supply of oxygen to the oxygen-depleted groundwater, especially in shallow unconfined aquifers.

Influence of Different Parameters on Oxygen Dissolution from Entrapped Air. We performed an experimental sensitivity analysis to investigate the effect of the horizontal flow velocity, the average grain diameter, as well as the magnitude and the speed of the water table rise on oxygen supply to the aqueous phase, following an imbibition event. All parameters investigated were found to have a significant effect. Particularly relevant were the magnitude of the water table fluctuation and the grain size of the porous medium. In fact, different amounts of oxygen were dissolved from entrapped air depending on the dynamics of the water table fluctuations, the specific properties of the porous medium, and the flow conditions applied. We suggest that the simultaneous measurement of water contents across the capillary fringe would provide additional information on the physical and geochemical processes in this zone.

Investigating the Effect of a Heterogeneous Porous Medium Packing. Gas partitioning between the aqueous and the gaseous phases has been shown to be pivotal for the medium term supply of oxygen to the upper region of the aquifer. Therefore, we also studied the impact of a coarse-material inclusion, embedded in finer porous material, on oxygen transfer across and within the capillary fringe. The presence of a coarse-material inclusion led to the deformation of the flow field and, thus, the vertical oxygen distribution. Mass transfer across the capillary fringe was considerably enhanced under steady-state conditions and pronounced gas entrapment occurred in the coarse lens, due to the change in water table elevation. A continuous supply of oxygen into deeper zones of the saturated zone was observed, due to the existence of a vertical air passage between the unsaturated zone and entrapped gas present in the coarse-material inclusion. Enhanced mixing and the transport of oxygen into deeper zones of the aquifer may influence the redox conditions and, thus, many (bio-)geochemical reactions in this interface region (e.g., Hanstein et al., 1999; Yadav and Hassanizadeh, 2011; Jost et al., 2011).

This work provided deeper insight into the relation between flow, porous medium properties, and the mass transfer of volatile compounds across and within the capillary fringe. However, new problems arose and open questions remain, some of which are summarized in the following section.

7.1.1 New Problems and Open Questions

- To date, the impact of an entrapped gaseous phase on transverse vertical dispersion remains undetermined. In order to tackle this problem, further investigations have to be completed, e.g., by performing flow-through laboratory experiments similar to the ones presented in this study and measuring vertical profiles of water content as well as equivalent aqueous oxygen concentration.

  → Is transverse vertical dispersion enhanced due to the presence of entrapped gas (more tortuous flow paths in the quasi-saturated zone) or rather decreased (reduced relative permeability in the quasi-saturated zone), when compared with mass transfer in the fully water-saturated case? Do different regimes exist, where one effect dominates over the other?

- The vertical distribution of microbial strains in the capillary fringe depends not only on the environmental conditions present (water content, availability of electron donors and acceptors, soil properties), but also on the specific microbial metabolism (aerobic or anaerobic strain) and the physical properties (e.g., cell size and shape, hydrophobicity, surface charge, motility) (e.g., Jost et al., 2010). In a field study, Anneser (2008) observed changes in the distribution of biotic and abiotic gradients, which were associated with the shift in the vertical position of a BTEX plume caused by a change in the height of the water table. The adaptation of microbial strains to the dynamic change in environmental conditions, due to a fluctuating water table, may impact biodegradation and, thus, natural attenuation of a contaminant plume located in the capillary fringe region (Dobson et al., 2007).

  → Which are the processes that control the adaptation of microbial strains to the dynamic changes in environmental conditions (e.g., the time period over which the water table fluctuation occurs, the mobility of the microorganisms or sporulation)?

- Microorganisms can form extra-polymeric substance (EPS) that may impact the soil surface properties, the interfacial tension, and the hydraulic conditions present in the capillary fringe region (e.g., Henry and Smith, 2002 and 2003), therefore back-linking the biological activity to the hydraulic processes.

  → What is the effect of EPS-formation and/or surfactant-induced flow phenomena on mass transfer across and within the capillary fringe?

- A fluctuating water table and/or the presence of heterogeneities are expected to affect reactive transport in the capillary fringe.

  → Looking at the dynamics of the system, which role do different types of chemical reaction play (e.g., kinetic vs. instantaneous, precipitation, redox-reaction)? How does entrapped air affect reactive transport within the quasi-saturated zone?

7.2 Outlook

The discussion above illustrates the complexity of this topic, where we studied the mass transfer of oxygen across and within the capillary fringe. Transfer of volatile compounds across the capillary fringe occurs in both directions, i.e., from the porous medium surface to the aquifer (Russo et al., 1989) and from the aquifer to the gas phase. Moreover, due to changes in water table elevation, compounds sorbed to the porous medium matrix in the unsaturated zone possibly dissolve into groundwater. Additionally, dissolved compounds, such as anions and cations, can be transported into the unsaturated zone.

The variations in water content in a fluctuating capillary fringe may influence the redox state and, thus, the environmental conditions in this transition zone. For instance, the formation of gley soils in wetland areas results from both the transport of dissolved iron and manganese into the unsaturated zone as well as changing redox conditions. Whereas anaerobic, reducing environments lead to the dissolution of iron and manganese, the presence of oxidizing agents (e.g., dissolved oxygen) lead to the oxidation and the subsequent precipitation of these compounds, e.g., in the capillary fringe area. Grover et al. (2007) conducted column experiments with a fluctuating water table, where they observed two sets of iron bands: red oxidized bands (ferrihydrite and/or possibly lepidocrocite) were formed at the upper extent of the capillary fringe, whereas black bands (magnetite and/or green rust) formed below the oxidized iron bands.

As iron is a common constituent in soils and groundwater, the iron cycle in the subsurface plays a significant role in determining the environmental fate of many organic and inorganic pollutants. For instance, the interaction with iron minerals is crucial for the migration of arsenic (a known carcinogen and mutagen) in groundwater. Arsenic contaminations represent a serious problem in many regions of the world (e.g., Bangladesh, Vietnam, Cambodia, Argentina etc.), where elevated concentrations of arsenic in groundwater have the potential to impact 90 million people (Smedley and Kinniburgh, 2002; Smedley, 2003). The aquifer redox conditions are of primary importance to determine the fate of arsenic. In fact, under oxic conditions, arsenic in groundwater is removed from solution by adsorption to or co-precipitation with ferric oxyhydroxide (Hering and Kneebone, 2002; Stollenwerk, 2003).

The foregoing discussion points out the importance to investigate reactive transport (i.e., redox reactions involving oxygen as a reactant) within the capillary fringe. At steady state, reactive transport in the capillary fringe should not differ from reactive mass transport in the saturated zone if the transition zone between the unsaturated and the saturated zone is very narrow and a trapped gaseous phase is not present (Haberer et al., 2011). Water table fluctuations are expected to significantly influence the flow field as well as ongoing reactions, e.g., because of associated changes of the interface between the saturated and the unsaturated zone, but also due to gas inclusions in coarse sand lenses (potentially increasing dispersion and, thus, mixing of reaction partners).

References

Anneser, B., 2008. Spatial and temporal dynamics of biogeochemical gradients in a tar oil-contaminated porous aquifer – biodegradation processes revealed by high-resolution measurements. Dissertation, University of Tübingen, Institute for Geoscience, 140 p.

Dobson, R., Schroth, M.H. and Zeyer, J., 2007. Effect of water-table fluctuation on dissolution and biodegradation of a multi-component, light nonaqueous-phase liquid. Journal of Contaminant Hydrology, 94, 235-248.

Grover, D., Baham, J.E., Dragila, M.I., 2007. Precipitation of iron minerals in porous media. AGU fall meeting, abstract, H23D-1616.

Haberer, C.M., Rolle, M., Liu, S., Cirpka, O.A., Grathwohl, P., 2011. A high-resolution non-invasive approach to quantify oxygen transport across the capillary fringe and within the underlying groundwater. Journal of Contaminant Hydrology, 122(1-4): 26-39, doi: 10.1016/j.jconhyd.2010.10.006.

Hanstein, P., Jungbauer, H., Melzer, R., 1999. Biologische In-situ-Sanierung durch Eingabe von reinem Sauerstoff in das Grundwasser. TerraTech – Zeitschrift für Altlasten und Bodenschutz, 2: 46-48.

Henry, E.J., Smith, J.E., 2002. The effect of surface-active solutes on water flow and contaminant transport in variably saturated porous media with capillary fringe effects. Journal of Contaminant Hydrology, 56: 247-270.

Henry, E.J., Smith, J.E., 2003. Surfactant-induced flow phenomena in the vadose zone: A review of data and numerical modeling. Vadose Zone Journal, 2: 154-167.

Hering, J.G., Kneebone, P.E., 2002. Biogeochemical controls on arsenic occurrence and mobility in water supplies. *In* Environmental Chemistry of Arsenic. Ed. Frankenberger, W.T. Jr., Marcel Dekker New York, 7: 155-181.

Jost, D., Winter, J., Gallert, C., 2010. Distribution of aerobic motile and non-motile bacteria within the capillary fringe of silica sand. Water Research, 44: 1279-1287. doi: 10.1016/j.watres.2010.01.001.

Jost, D., Winter, J. and Gallert, C., 2011. Water and oxygen dependence of *Pseudomonas putida* growing in silica sand capillary fringes. Vadose Zone Journal, 10(2): 532-540, doi: 10.2136/vzj2010.0092.

Russo, D., Jury, W.A., Butters, G.L., 1989. Numerical analysis of solute transport during transient irrigation: 1. The effect of hysteresis and profile heterogeneity. Water Resources Research, 25: 2109-2118.

Smedley, P.L., 2003. Arsenic in groundwater – South and East Asia. *In* Arsenic in Groundwater. Eds. Welch, A.H., Stollenwerk, K.G., Kluwer Academic Publishers Boston, 179-209.

Smedley, P.L., Kinniburgh, D.G., 2002. A review of the source, behaviour and distribution of arsenic in natural waters. Applied Geochemistry, 17: 517-568.

Stollenwerk, K.G., 2003. Geochemical processes controlling transport of arsenic in groundwater: A review of adsorption. *In* Arsenic in Groundwater. Eds. Welch, A.H., Stollenwerk, K.G., Kluwer Academic Publishers Boston, 67-100.

Yadav, B.K., Hassanizadeh, S.M., 2011. An overview of biodegradation of LNAPLs in coastal (semi)-arid environment. Water Air Soil Pollution, 220(1-4): 225-239.

A. Appendix

A.1 Conservative Mass Transfer across the Capillary Fringe

In the following, the detailed derivation of the two basic equations used in this work to describe mass transfer across the unsaturated/saturated interface under steady-state conditions is given. First, we present the analytical solution to Fick's second law in 1-D in order to describe the vertical distribution of a volatile compound across the capillary fringe. This result is then the starting point for deriving the mass flux across the unsaturated/saturated interface.

The derivation outlined below is based on the penetration theory for mass transfer as suggested by Higbie in 1935 (see section 2.3.2.2). The key assumption in this theory is that the interfacial region is imagined to be a very thick film continuously generated by flow. Mass transfer involves diffusion into this film and the interfacial concentration in the liquid is assumed to be in equilibrium with that in the gaseous phase (Cussler, 2009).

A.1.1 Vertical Concentration Distribution of a Volatile Compound

Similar to the dissolution of NAPL pools (Hunt et al., 1988; Johnson and Pankow, 1992; Grathwohl, 1997; Eberhardt and Grathwohl, 2002), mass transfer of a volatile compound across the capillary fringe can be treated as diffusion into a semi-infinite domain. The capillary fringe is assumed to represent an upward extension of the fully water-saturated zone (e.g., Liu, 2010; Haberer et al., 2011) and the water-saturated thickness is considered much larger than the diffusion length. Diffusion into a semi-infinite domain is given by Fick's second law in 1-D:

$$\frac{\partial C}{\partial t} = D_t \frac{\partial^2 C}{\partial z^2} \tag{A.1}$$

in which C [M L^{-3}] denotes the aqueous concentration of the volatile compound and t [T] is time. The transverse vertical dispersion coefficient, D_t [L^2 T^{-1}], is assumed constant. z [L] represents the vertical coordinate, with the origin at the upper limit of the capillary fringe, pointing downward.

By replacing t in Eqn. A.1 by x/v_a the above transient case in 1-D can be applied to a two-dimensional case at steady state:

$$v_a \frac{\partial C}{\partial x} = D_t \frac{\partial^2 C}{\partial z^2} \tag{A.2}$$

where x [L] and v_a [L T^{-1}] denote the coordinate and the seepage velocity in horizontal direction, respectively.

Rearranging A.2 yields:

$$\frac{\partial C}{\partial x} = \frac{D_t}{v_a}\frac{\partial^2 C}{\partial z^2} \text{ in which } \frac{D_t}{v_a} = \lambda \tag{A.3}$$

In the present case, the following boundary conditions apply:

$C = C_{bg}$ at x = 0 m for 0 m < z < ∞

$C = C_0$ at z = 0 m for x > 0 m

$C = C_{bg}$ at z → ∞ for x > 0 m

in which C_{bg} [M L^{-3}] is the background concentration of the volatile compound in the aqueous phase and C_0 [M L^{-3}] represents the concentration at the air/water interface.

To solve the partial differential equation above, stated as Eqn. A.3, the 'method of combination of variables' is applied (Boltzmann, 1894; Liu, 2008). The aim of this procedure is to combine two independent variables (here x and z) to produce only one independent variable (here η). The combined variable of x and z is expected to be:

$$\eta = \frac{z}{\sqrt{4\lambda x}} \tag{A.4}$$

In doing so, we convert Eqn. A.3 into an ordinary differential equation (ODE):

1. Find an expression in η to replace $\frac{\partial C}{\partial x}$:

$$\begin{aligned}\frac{\partial C}{\partial x} = \frac{\partial C}{\partial \eta}\frac{\partial \eta}{\partial x} = \frac{\partial C}{\partial \eta}\frac{\partial}{\partial x}\left[\frac{z}{\sqrt{4\lambda x}}\right] = \frac{\partial C}{\partial \eta}\frac{z}{\sqrt{4\lambda}}\left[-\frac{1}{2}\frac{1}{x^{3/2}}\right] \\ = -\frac{\partial C}{\partial \eta}\frac{z}{\sqrt{4\lambda x}}\frac{1}{2x} = -\frac{\partial C}{\partial \eta}\frac{\eta}{2x}\end{aligned} \tag{A.5}$$

2. Find an expression in η to replace $\frac{\partial^2 C}{\partial z^2}$:

$$\frac{\partial C}{\partial z} = \frac{\partial C}{\partial \eta}\frac{\partial \eta}{\partial z} = \frac{\partial C}{\partial \eta}\frac{\partial}{\partial z}\left[\frac{z}{\sqrt{4\lambda x}}\right] = \frac{\partial C}{\partial \eta}\frac{1}{\sqrt{4\lambda x}} = \frac{\eta}{z}\frac{\partial C}{\partial \eta} \tag{A.6}$$

$$\begin{aligned}\frac{\partial^2 C}{\partial z^2} = \frac{\partial}{\partial z}\left[\frac{\partial C}{\partial \eta}\frac{1}{\sqrt{4\lambda x}}\right] = \frac{\partial C}{\partial \eta}\frac{\partial}{\partial z}\left[\frac{1}{\sqrt{4\lambda x}}\right] + \frac{\partial}{\partial \eta}\left[\frac{\partial C}{\partial \eta}\frac{1}{\sqrt{4\lambda x}}\right]\frac{\partial \eta}{\partial z} \\ = \frac{\partial}{\partial \eta}\left[\frac{\partial C}{\partial \eta}\frac{1}{\sqrt{4\lambda x}}\right]\frac{\partial \eta}{\partial z} = \frac{\partial^2 C}{\partial \eta^2}\frac{1}{4\lambda x}\end{aligned} \tag{A.7}$$

Replacing Eqns. A.5 and A.6 in Eqn. A.3 yields:

$$\frac{\partial C}{\partial x} = \lambda \frac{\partial^2 C}{\partial z^2} \rightarrow -\frac{\partial C}{\partial \eta}\frac{\eta}{2x} = \lambda \frac{\partial^2 C}{\partial \eta^2}\frac{1}{4\lambda x} \tag{A.8}$$

and simplifying:

$$\frac{\partial^2 C}{\partial \eta^2} + 2\eta \frac{\partial C}{\partial \eta} = 0 \tag{A.9}$$

The transformed boundary conditions are:

$C = C_{bg}$ at η → ∞

$C = C_0$ at η = 0

$C = C_{bg}$ at η → ∞

Equation A.9 is a 2nd order ODE in η and can be solved by reduction of order. Thus, $\varphi = \frac{\partial C}{\partial \eta}$:

$$\frac{\partial \varphi}{\partial \eta} + 2\eta\varphi = 0 \rightarrow \frac{\partial \varphi}{\varphi} = -2\eta\partial\eta \tag{A.10}$$

Integrate, $\int \frac{\partial \varphi}{\varphi} = -\int 2\eta\partial\eta \rightarrow \ln\varphi = -\eta^2 + C_1^* \rightarrow \frac{\partial C}{\partial \eta} = \varphi = C_1 e^{-\eta^2}$

in which C_1^* and C_1 are constants of integration.

$$\frac{\partial C}{\partial \eta} = C_1 e^{-\eta^2} \rightarrow \partial C = C_1 e^{-\eta^2}\partial\eta \tag{A.11}$$

Further integration leads to:

$$C = C_1 \int_0^\eta e^{-\eta^2}\partial\eta + C_2 \tag{A.12}$$

Applying the 2nd boundary condition (i.e., $\eta = 0$: $C = C_0$) yields, $C_2 = C_0$. Consideration of the 1st/3rd boundary condition (i.e., $\eta \rightarrow \infty$: $C = C_{bg}$) results in:

$$C_{bg} = C_1 \int_0^\infty e^{-\eta^2}\partial\eta + C_0 = C_1 \frac{\sqrt{\pi}}{2} + C_0 \rightarrow C_1 = \left(C_{bg} - C_0\right)\frac{2}{\sqrt{\pi}} \tag{A.13}$$

Replacing the constants of integration, C_1 and C_2, in Eqn. A.12:

$$C = \left(C_{bg} - C_0\right)\frac{2}{\sqrt{\pi}}\int_0^\eta e^{-\eta^2}\partial\eta + C_0 \tag{A.14}$$

in which $\frac{2}{\sqrt{\pi}}\int_0^\eta e^{-\eta^2}\partial\eta = erf(\eta)$.

Thus,

$$C = \left(C_{bg} - C_0\right) erf\left(\eta\right) + C_0 \tag{A.15}$$

Substituting $erf\left(\eta\right) = 1 - erfc\left(\eta\right)$ in Eqn. A.15

$$\begin{aligned} C &= \left(C_{bg} - C_0\right)\left[1 - erfc\left(\eta\right)\right] + C_0 = \left(C_{bg} - C_0\right) - \left(C_{bg} - C_0\right) erfc\left(\eta\right) + C_0 \\ &= C_{bg} - \left(C_{bg} - C_0\right) erfc\left(\eta\right) \end{aligned} \tag{A.16}$$

and replacing η and λ yields:

$$C = C_{bg} - \left(C_{bg} - C_0\right) erfc\left(\frac{z}{\sqrt{4\lambda x}}\right) = C_{bg} - \left(C_{bg} - C_0\right) erfc\left(\frac{z}{\sqrt{4\frac{D_t}{v_a}x}}\right) \tag{A.17}$$

Rearranging Eqn. A.17 leads to the final equation to describe the vertical distribution of a volatile compound across the capillary fringe at steady state:

$$C_{norm}(x,z) = \frac{C - C_{bg}}{C_0 - C_{bg}} = erfc\left(\frac{z}{2\sqrt{D_t \frac{x}{v_a}}}\right) \tag{A.18}$$

in which C_{norm} [-] is the normalized concentration of the compound of interest.

A.1.2 Mass Flux across the Unsaturated/Saturated Interface

To quantify the mass flux, F [M L^{-2} T^{-1}], across the interface (i.e., at z = 0), the derivative of Eqn. A.17 is combined with Fick's first law for a porous medium (see also Cussler, 2009):

$$F = -\phi D_t \frac{\partial C}{\partial z} \tag{A.19}$$

The porosity, ϕ [-], appears in Eqn. A.19 since the dispersive mass transfer can occur only through the pore space.

Equation A.19 can be rewritten as:

$$F = \left(C_0 - C_{bg}\right)\phi\sqrt{D_t \frac{v_a}{x}\frac{1}{\pi}} e^{-\left(\frac{z}{2\sqrt{D_t \frac{x}{v_a}}}\right)^2} \tag{A.20}$$

which is the mass flux density at specified values of x and z. The mass flux density decreases with increasing values of z.

A useful limit is the flux across the interface at $z = 0$:

$$F\big|_{z=0} = \left(C_0 - C_{bg}\right)\phi\sqrt{D_t \frac{v_a}{x}\frac{1}{\pi}} \tag{A.21}$$

Equation A.21 is the mass flux density across the interface at a specific value of x. Integrating the mass flux density over the interfacial area leads to:

$$\dot{m} = \int_0^L \int_0^W F\big|_{z=0}\, dy dx = \left(C_0 - C_{bg}\right) 2\phi W \sqrt{D_t L v_a \frac{1}{\pi}} \tag{A.22}$$

in which $\dot{m}$ [M T^{-1}] is the total mass flux across the interface between the saturated and the unsaturated zone. L [L] and W [-] define the length and the width of the interfacial area between the unsaturated and the saturated zone.

The averaged mass flux per unit interfacial area gives:

$$\frac{\dot{m}}{WL} = \left(C_0 - C_{bg}\right) 2\phi \sqrt{D_t \frac{v_a}{L}\frac{1}{\pi}} \tag{A.23}$$

In Eqn. A.23 the mass transfer coefficient, k [L T^{-1}], is included:

$$k = 2\phi\sqrt{D_t \frac{v_a}{L}\frac{1}{\pi}} \tag{A.24}$$

The mass transfer coefficient is the rate constant for moving one species from the boundary, here the interface between the unsaturated and the saturated zone, into the bulk of the aqueous phase (Cussler, 2009). It refers to a 'lumped-parameter model', which requires the assumption that changes in concentration are limited to that small part of the system's volume near its boundaries.

References

Boltzmann, L., 1894. Zur Integration der Diffusionsgleichung bei variable Diffusionskoeffizienten. Annalen der Physik, 289(13): 959-964.

Cussler, E.L., 2009. Diffusion: Mass transfer in fluid systems, 3rd ed., Cambridge University Press.

Eberhardt, C. and Grathwohl, P., 2002. Time scales of pollutants dissolution from complex organic mixtures: blobs and pools. Journal of Contaminant Hydrology, 59: 45-66.

Grathwohl, P., 1997. Gefährdung des Grundwassers durch Freisetzung organischer Schadstoffe: Methoden zur Berechnung der in-situ Schadstoffkonzentration. Grundwasser – Zeitschrift der Fachsektion Hydrogeologie, 4: 157-166.

Haberer, C.M., Rolle, M., Liu, S., Cirpka, O.A., Grathwohl, P., 2011. A high-resolution non-invasive approach to quantify oxygen transport across the capillary fringe and within the underlying groundwater. Journal of Contaminant Hydrology, 122(1-4): 26-39, doi: 10.1016/j.jconhyd.2010.10.006.

Higbie, R., 1935. The rate of absorption of a purge gas into a still liquid during short periods of exposure. Transactions of the American Institute of Chemical Engineering, 31: 365-389.

Hunt, J.R., Sitar, N. and Udell, K.S., 1988. Non-aqueous phase liquid transport and cleanup, 1. Analysis of mechanisms. Water Resources Research, 24: 1247-1258.

Johnson, R.L. and Pankow, J.F., 1992. Dissolution of dense chlorinated solvents into groundwater, 2: Source functions of pools of solvent. Environmental Science and Technology, 26: 896-901.

Liu, S., 2008. Mass transfer of oxygen across the capillary fringe. Doctoral Thesis, Institute for Geoscience, University of Tübingen, 58 p.

A.2 Movies (for full functionality please open in Adobe Reader)

- ‘Movie 1’: Plotting of isochrones to visualize the flow field

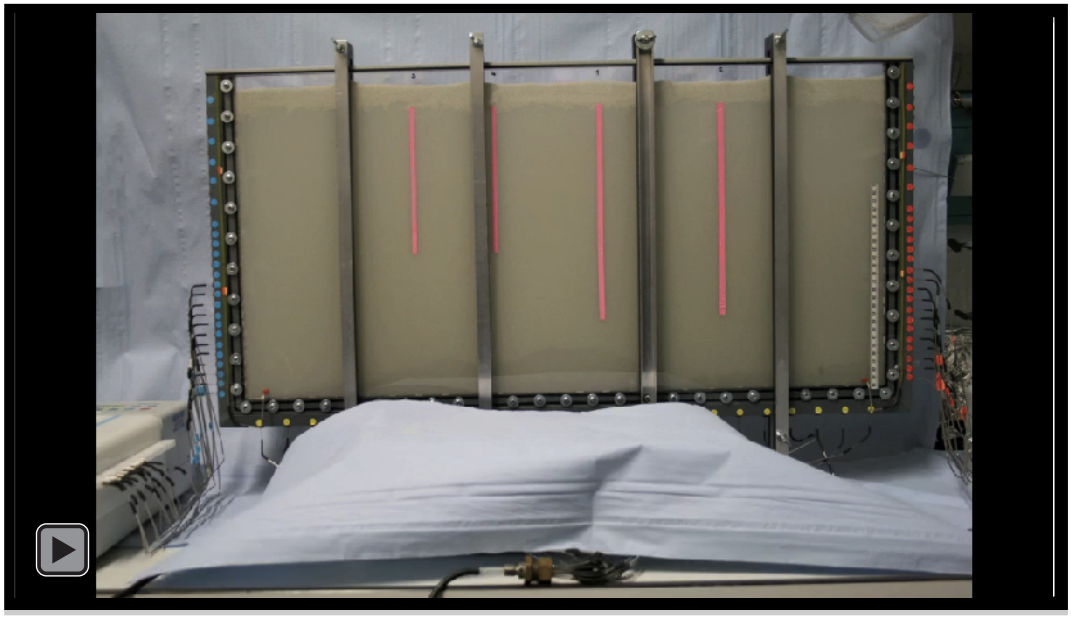

- ‘Movie 2’: Tracer experiment in a heterogeneous porous medium packing